AN ABSTRACT OF THE DISSERTATION OF

John Doucette for the degree of Doctor of Philosophy in Geology presented on March 2, 2000. Title: A Petrochemical Study of the Mount Fubilan Intrusion and Associated Ore Bodies, Papua New Guinea.

Redacted for Privacy

Abstract approved: _____
Cyrus W. Field

The Mount Fubilan Intrusion is part of a geologically young hypabyssal stock in the Star Mountains of Papua New Guinea. This stock was mapped as the Ok Tedi Intrusive Complex and divided into four separate bodies: the Mount Fubilan, Sydney Intrusion, Kalgoorlie, and Ningi Intrusions. Hydrothermal fluids caused alteration of the Mount Fubilan, and parts of the other intrusions, to potassic and propylitic mineral assemblages and deposited gold and copper.

This investigation documents similarities and differences between the least-altered intrusive rocks of the complex and those that have undergone potassic metasomatism. The study involved detailed petrographic examination of more than two hundred thin-sections, major-oxide and trace element chemistry, and microprobe analyses of individual minerals. The magmas that crystallized to form the stock are shown to be intermediate in composition between andesite and latite. They were quartz-saturated, metaluminous, weakly iron-rich, and crystallized under oxidizing conditions. The principal mineral phases in the least-altered intrusive rocks are andesine, pyroxene, orthoclase, and quartz. The accessory mineral suite in least-altered rocks includes biotite, sphene, apatite, magnetite, and zircon.

Hornblende is present in a few samples Magmatic pyroxene is diopsidic in composition; hornblendes is edenitic; and biotite is annitic. Potassic alteration has converted andesine to orthoclase, or mixtures of albite and orthoclase, ferromagnesian minerals to hydrothermal biotite, sphene to rutile, and magnetite to pyrite and chalcopyrite. Hydrothermal biotite is phlogopitic in composition. Gold and copper were concentrated in the zone of potassic alteration.

The mineralogical transformation of the intrusive rocks of the Mount Fubilan and associated intrusions was caused by the infiltration of hydrothermal fluids that deposited potassium, gold, and copper and that leached and removed virtually all other rock constituents. Leached components were transported away from the zone of potassic alteration and deposited in peripheral parts of the intrusive complex to form propylites, endoskarn, and massive replacement bodies or removed from the system entirely.

The Mount Fubilan intrusion was closely similar in chemistry and mineralogy to the other intrusions of the complex prior to alteration. Petrochemical differences between the Mount Fubilan Intrusion and the other intrusions were produced entirely by hydrothermal alteration.

A Petrochemical Study of the Mount Fubilan Intrusion and Associated Ore Bodies, Papua New Guinea

by

John Doucette

A DISSERTATION

submitted to

Oregon State University

in partial fulfillment of
the requirements for the
degree of

Doctor of Philosophy

Presented March 2, 2000
Commencement June 2000

Doctor of Philosophy dissertation of John Doucette presented on March 2, 2000

APPROVED:

Redacted for Privacy

Major Professor, representing Geology

Redacted for Privacy

Chair of Department of Geosciences

Redacted for Privacy

Dean of Graduate School

I understand that my thesis will become part of the permanent collection of Oregon State University libraries. My signature below authorizes release of my thesis to any reader upon request.

Redacted for Privacy

John Doucette, Author

Acknowledgements

First, I would like to thank my major professor Dr. Cyrus W. Field. His perseverence in reading round after round of crudely written manuscript is greatly appreciated. He also contributed materially in numerous discussions and arranged funding for part of the analyses. Discussions with the other Geosciences Department members of my committee (Dr. Ed Taylor, Dr. Roger Nielsen, and Dr Jon Kimerling) also helped in my understanding of petrography and GIS mapping. I would also to thank my graduate representative Dr. Jim Lundy for his participation in committee meetings and the preliminary and final oral examinations.

I would particularly like to thank Joe Seegars who originally hired me to work at Ok Tedi. Rod Jones provided me with the loan of the entire Ok Tedi thin-section collection. Dr. Willard Lacey and Dr Peter Fookes encouraged me to continue my education while I was still employed at Ok Tedi. Help in the collection of samples and other field data by Jonathan Kepa, David Masani, David Maniger, James Yahman, Kurasim Kaifoyeng, Pius Haptamsok, Pumat Diban, Casey Kripe, Nick Hombohori, and Pineas Sep is greatly appreciated. I would also like to thank several hundred Papua New Guineans who made my time at Ok Tedi memorable. Marshall Himes of BHP was helpful in arranging for my field visit in 1994 and for Ok Tedi's purchase of several petrographic and microprobe reports the proceeds from which helped fund the project.

Dr. Robert Stewart of Massey University in New Zealand provided helpful suggestions relating to igneous petrography during his sabbatical stay at Oregon State and later by mail and e-mail. Petrographic discussions with Dr. Alexi Ariskin and Dr. Stanislaus Aleksandrov also proved helpful.

Several individuals provided computer programs that simplified data analysis. In particular I would like to thank Dr. T.S. Ercit for his program for calculations of mineral formulas using microprobe data. Helpful suggestions in mineral and petrographic systematics made by various members of the granite research network use group were extremely helpful. Nancy Dick helped with grammar and punctuation in several chapters.

I would also like to thank several individuals who provided safe havens and encouragement during the writing stage. Among these are Bob Doucette, my mother Marci O'Connor, Christine Jarosz, Matt and Becky Freid, and Ralph Mulhollen,.

Table Of Contents

	Page
Introduction	1
Purpose	5
Nomenclature	8
Geologic Setting	19
Regional Geology	19
Local Geology	24
Sedimentary Rocks	24
Intrusive Rocks	27
Massive Ores and Skarns	36
Petrography and Lithology	44
Methods	48
Physical Properties	50
Mineralogy	68
Feldspar	71
Pyroxene	89
Amphibole	99
Biotite	106
Quartz	120
Groundmass	125
Accessory Minerals - Magmatic Association	126
Other Alteration Minerals	140
Ore Minerals	153
Clay Minerals	160
Limonite	164
Modal Classification	147

Table of Contents (Continued)

	Page
Whole Rock Chemistry	173
Star Mountains Regional Data	173
Ok Tedi Data	174
Normative Mineralogy	187
Silica Variation	193
Alumina Variation	205
Chemical Classification	215
Q'-ANOR Method	216
Total Alkali-Silica Method	221
Igneous Rock Series	228
Iron Content and Oxidation State	238
Volatiles	246
Trace Elements	251
Rare Earth Elements	251
Rubidium and Strontium	259
Gold and Copper	261
Continuity of Alteration in Zone of Potassic Alteration	276

Table of Contents (Continued)

Metasomatic Gains and Losses 288

Least-Altered Rocks of Sydney, Kalgoorlie, and Ningi Intrusions 308

Potassically-Altered Rocks 311

Discussion 316

Classification of Intrusive Rocks 316

Conditions of Magmatic Crystallization and Hydrothermal Mineralization 327

Summary and Conclusions 351

Bibliography 352

List of Figures

Figure		Page
1	Location of the Ok Tedi copper-gold porphyry deposit and the Ok Tedi Intrusive Complex on the island of New Guinea	2
2	Location of the Ok Tedi mine and the town of Tabubil with respect to the Ok Tedi River. Ok is a local word that means river.	9
3	Creeks, named locations, roads, and mine buildings in the vicinity of the Ok Tedi mine.	10
4	Shows configuration of the open pit at Ok Tedi as at January, 1994. Selected benches are identified by elevation.	12
5	Classification diagram similar to that used for the classification of igneous rocks by early workers at Ok Tedi. After Bateman (1963).	14
6	IUGS classification diagrams for (A) volcanic and (B) plutonic rocks. These diagrams were designed to be used for modal analyses (from Le Maitre and others, 1989).	15
7	Total alkali-silica (TAS) diagram for classification of volcanic rocks using chemical analyses (Le Maitre and others, 1989).	17
8	Simplified outline of the tectonic provinces of Papua New Guinea. Redrawn from Bain (1973) and Jacques and Robinson (1977).	20
9	Intrusions and sedimentary formations of the Star Mountains area. Simplified from Arnold and Griffin, 1978.	23
10	Sedimentary rocks of the Ok Tedi mine area. Simplified from Arnold, Griffin, and Hodge (1979).	25
11	Locations of major intrusions that have been postulated to comprise the Ok Tedi Intrusive Complex. Simplified from Arnold, Griffin, and Hodge (1979).	28
12	Location of major occurrences of massive magnetite, massive sulfide, and skarn in the area of the Ok Tedi Intrusive Complex. Simplified from Arnold, Griffin, and Hodge (1979).	40

List of Figures (Continued)

Figure		Page
13	Generalized morphology of the two major types of massive ores at Ok Tedi (redrawn from Bamford and others, 1972:. (A) flat-lying type. This example is of the Sulphide Creek "skarn." (B) Steep-dipping type. This example is of the Gold Coast skarn.	41
14	Locations of the petrographic samples of suite 1. The samples are identified by name in Plate 2.	45
15	Locations of the petrographic samples of suite 2. The samples are identified by name in Plate 3.	46
16	Map showing the distribution of porphyritic and phaneritic textures in samples from petrographic suites 1 and 2. The samples are identified by name in Plates 2 and 3.	47
17	Two examples of least-altered feldspar porphyry. These specimens consist predominantly of minerals formed by magmatic processes and display only traces of the minerals typical of propylitic alteration (actinolite, epidote, chlorite).	52
18	Two examples of intensely altered porphyry	54
19	Two examples of feldspar-hornblende porphyry (A-D) and three examples of texturally destroyed rock with pseudomorphs of hydrothermal biotite after magmatic pyroxene, hornblende, or magmatic biotite (E-H). All of the rocks shown have undergone intense potassic alteration.	57
20	Two examples of samples with phaneritic texture and with andesine and feldspar. These specimens are only weakly altered. They contain only traces of epidote, fibrous amphibole, or other minerals characteristic of propylitic alteration.	60
21	Two samples with phaneritic texture and that consist of albite and potassium feldspar. Extreme potassium feldspar and clay alteration. The only ferromagnesian mineral present is hydrothermal biotite.	63
22	Plot of specific gravity versus void space (porosity).	69

List of Figures (Continued)

Figure		Page
	Ab-Or-An diagram of feldspars from least altered rock (i.e. samples with andesine-potassium feldspar association).	
23	Ab-Or-An diagram of feldspars from least altered rock (i.e. samples with andesine-potassium feldspar association).	75
24	Ab-Or-An diagram of feldspars from potassically altered rock (i.e. samples with albite-potassium feldspar association).	76
25	Examples of albite twinning and oscillatory zoning in plagioclase feldspar.	79
26	Example of resorption surfaces within a crystal of plagioclase feldspar (A-B). Photomicrographs of magmatic potassium feldspar in some of the least altered rocks from the Ok Tedi Intrusive Complex (C-F). Mantles of magmatic potassium feldspar on crystals of plagioclase feldspar (G-H).	82
27	Rinds of hydrothermal potassium feldspar on plagioclase feldspar (A-D). Near total replacement of plagioclase feldspar by potassium feldspar (F-G).	86
28	Examples of pyroxene in andesine-potassium feldspar porphyries and phanerites.	90
29	Examples of pyroxene in andesine-potassium feldspar porphyries and phanerites.	94
30	Mg-Fe-Ca plots. (A) classification of pyroxenes, (B) analyses of pyroxenes from unaltered samples, (C) analyses of pyroxene in garnet-bearing sample.	96
31	Examples of amphiboles in rocks from the Ok Tedi Intrusive Complex.	100
32	Analytical data of hornblende and actinolite plotted on the classification diagram of Leake (1978).	105
33	Examples of magmatic and hydrothermal biotite.	108
34	Examples of hydrothermal biotite.	111

List of Figures (Continued)

Figure		Page
35	Biotite classification scheme based on the end-member biotites: annite, phlogopite, eastonite, and siderophyllite (Speer, 1984; and Guidotti, 1984).	116
36	Ternary plot of FeO^* (total iron as FeO), Al_2O_3, and MgO. Shown on this plot are empirically derived fields of biotites co-existing with muscovite or topaz (I), biotites existing alone(II), and biotites coexisting with pyroxene or hornblende (III). Modified from Nockolds (1947).	119
37	Map showing distribution of magmatic and hydrothermal biotite in samples from the Ok Tedi Intrusive Complex.	121
38	Examples of quartz in phanerites of the Ok Tedi Intrusive Complex and examples of fluid inclusions in quartz.	122
39	Photomicrographs of sphene (A-D) and pseudomorphs of rutile after sphene (E-H).	127
40	Map showing distribution of sphene in the altered and unaltered intrusive rocks of the Ok Tedi Intrusive Complex.	130
41	Photomicrographs of apatite, zircon, and magnetite	133
42	Ternary diagrams illustrating compositions of magmatic magnetite, ilmenite, and mixtures thereof.	139
43	Photomicrographs of epidote and garnet.	142
44	Ternary plot of Grossularite-Andradite-Spessartine +Almandine for garnets from the Ok Tedi Mine area.	147
45	Ternary diagram illustrating composition of rutile.	150
46	Photomicrographs of hydrothermal magnetite.	151
47	Ternary diagram illustrating the composition of hydrothermal magnetite.	156
48	Photomicrographs of pyrite, chalcopyrite, and chalcocite.	158

List of Figures (Continued)

Figure		Page
49	Ternary diagram illustrating the compositions of pyrite, chalcopyrite, bornite(?), and chalcocite-covellite.	162
50	QAP modal classification of unaltered and weakly altered intrusive rocks from the Ok Tedi Intrusive Complex, and the IUGS fields for the classification of igneous rocks (after Streckeisen, 1979).	166
51	QAP modal classification for altered intrusive rocks from the Ok Tedi Intrusive Complex, and the IUGS fields for the classification of igneous rocks (after Streckeisen, 1979). Arrow shows direction of alteration.	167
52	Location map for samples of Katchan (1982). Also shown are rock textures and normative ferromagnesian minerals	177
53	Location map for samples collected by Kepa and analyzed by Mason (1993). Also shown are rock textures and normative ferromagnesian minerals.	178
54	Location map for diamond drill core (DDH) samples collected in 1994 (Suite 2). Also shown by symbols are the rock textures and normative ferromagnesian minerals.	182
55	Location map for surface samples collected in 1994 (Suite 2). Also shown by symbols are rock textures and normative ferromagnesian minerals.	183
56	Collar locations of reverse-circulation drill hole samples.	188
57	Map showing the spatial variation in normative anorthite content for samples of intrusive rock from the Ok Tedi Intrusive Complex.	191
58	Silica variation diagrams for samples from the Star Mountains region.	195
59	Silica variation diagrams for samples from the Sydney Intrusion. Trend lines based on regional variations.	198

List of Figures (Continued)

Figure		Page
60	Silica variation diagrams for samples from the Fubilan Intrusion. Trend lines based on regional variations.	199
61	Silica variation diagrams for samples from the Kalgoorlie Intrusion. Trend lines based on regional variations.	201
62	Silica variation diagrams for samples from the Ningi Intrusion. Trend lines based on regional variations	202
63	Silica variation diagrams for reverse-circulation drill cuttings from the Fubilan Intrusion. Trend lines based on regional variations.	204
64	Alumina variation diagram for samples from the Star Mountains region. Line (a-a') is regression line calculated from the data portrayed.	207
65	Alumina variation diagram for samples from the Sydney Intrusion. Line (a-a') is regression line for data from the Star Mountains region. Circle (b) is area of least-altered/unaltered rocks from the Ok Tedi Intrusive Complex.	208
66	Alumina variation diagram for samples from the Fubilan Intrusion. Line (a-a') is regression line for data from the Star Mountains region. Circle (b) is area of least-altered and unaltered rocks from the Ok Tedi Intrusive Complex.	210
67	Alumina variation diagram for samples from the Kalgoorlie Intrusion. Line (a-a') is regression line for data from the Star Mountains region. Circle (b) is area of least-altered and unaltered rocks from the Ok Tedi Intrusive Complex	211
68	Alumina variation diagram for samples from the Ningi Intrusion. Line (a-a') is regression line for data from the Star Mountains region. Circle (b) is area of least-altered/unaltered rocks from the Ok Tedi Intrusive Complex.	213
69	Q'-ANOR diagram for samples of volcanic and plutonic rocks (undifferentiated) from the Star Mountains region	218

List of Figures (Continued)

Figure		Page
70	Q'-ANOR diagram for samples of phaneritic rocks from the Ok Tedi Intrusive Complex: (A) Sydney Intrusion, (B) Fubilan Intrusion, (C) Kalgoorlie Intrusion, (D) Ningi Intrusion.	220
71	Total alkali-silica diagram: (A) Shows the subdivision of the root names basaltic trachyandesite and trachyandesite, (B) shows the designation of fields as silica-oversaturated (O), saturated (S), and undersaturated (U).	223
72	Total alkali-silica diagram with data from volcanic and plutonic rocks of the Star Mountains region. Also shown is a trend line (a-a') calculated from this data.	225
73	Total alkali-silica diagrams for the Ok Tedi Intrusive Complex. Each diagram also has the trend line (a-a') calculated from all volcanic and plutonic rocks of the Star Mountains region and an elliptical area (b) occupied by data from the least-altered samples.	226
74	Peacock diagrams for data from: (A) Star Mountains region, (B) Sydney Intrusion, (C) Kalgoorlie Intrusion, and (D) Ningi Intrusion.	230
75	Peacock diagrams showing data for altered and unaltered samples from the Ok Tedi Intrusive Complex: (A) unaltered and least-altered, (B and C) intermediate alteration, and (D) extremely altered.	232
76	Irvine and Baragar classification diagram for alkaline and subalkaline volcanic rocks: (A) samples from Star Mountains region, (B) samples from Sydney Intrusion, and (C) samples from Kalgoorlie and Ningi Intrusions.	234
77	AFM diagrams with unaltered samples from: A. Star Mountains region, B. Sydney Intrusion, and C. Kalgoorlie and Ningi Intrusions. Also shown in each diagram is the curve used by Irvine and Baragar (1971) to separate fields of calc-alkaline from tholeiitic rocks.	236

List of Figures (Continued)

Figure		Page
78	Binary plot of K_2O versus SiO_2 with fields of high, medium and low potassium volcanic rocks (LeMaitre, 1989). A. Star Mountains region, B. Sydney Intrusion, C. Kalgoorlie and Ningi Intrusions.	237
79	Diagrams illustrating the iron content and the ratio of ferric to ferrous iron in rocks of the Ok Tedi Intrusive Complex: (A) Plot of FeO^*/MgO versus SiO_2 for igneous rocks of the Star Mountains region (modified from Keith and others, 1991), (B) FeO^*/MgO versus SiO_2 for intrusive rocks of the Ok Tedi Intrusive Complex, (C) Total iron as Fe^* versus An content of normative plagioclase feldspar for rocks of the Ok Tedi Intrusive complex, (D) Plot of the ratio of ferric to ferrous iron versus An content of normative plagioclase feldspar for intrusive rocks of the Ok Tedi Intrusive complex. Ellipses a and b in C and D represent samples with normative andesine (a)or oligoclase (b).	239
80	Plot of $\log f_{O2}$ versus temperature for mineral assemblages commonly used as oxygen buffers in petrologic experiments. The equations for these reactions are also listed above. (Modified from Buddington and Lindsley, 1964; and Dilles, 1987).	243
81	Plot of LOI (loss on ignition) versus the sum of the volatile phases H_2O, S, and F.	247
82	Plot of S versus SiO_2 for samples from reverse-circulation drill holes.	249
83	Map showing the distribution of fluorine values in the intrusive rocks of the Ok Tedi Intrusive Complex.	250
84	Map showing location of samples of Papua New Guinea andesites analyzed by Johnson, 1982.	254
85	Rare-earth element plots for samples of andesite from the Papua New Guinea area (Johnson, 1982). (A) Group one. (B) Group two.	256

List of Figures (Continued)

Figure		Page
86	Rare-earth element plots for samples from the Ok Tedi Intrusive Complex. A. Least-altered or unaltered, B. Potassic alteration.	257
87	Plot of rubidium versus strontium in samples of Ok Tedi intrusive rock with: (A) normative andesine, (B) normative oligoclase, and (C) normative albite.	260
88	Example of a normal distribution - K_2O contents of samples from the potassically altered Mt. Fubilan Intrusion: (A) Histogram, (B) Curve derived from the histogram in A.	264
89	Normal-probability plot for K_2O contents of samples of rotary drill cuttings samples from the Mt. Fubilan Intrusion.	271
90	Example of a log-normal distribution - Au contents of samples from blast-hole drill cuttings: (A) Histogram, (B) Curve derived from the histogram in A.	267
91	Log-probability plot for Au contents of samples from blast-hole drill cuttings.	268
92	Log-probability plots of gold in: A. reverse circulation drill cuttings and diamond drill core, and B. blast hole cuttings grouped as to their content of sulfide minerals (S), limonite (X), or mixtures of sulfide minerals and limonite (M).	271
93	Log-probability plots of copper in: (A) reverse circulation drill cuttings and diamond drill core, and (B) blast hole cuttings grouped as to their content of sulfide minerals (S), limonite (X), or mixtures of sulfide minerals and limonite (M).	273
94	Silica-variation diagrams for gold and copper in samples of rotary drill cuttings from the Fubilan Intrusion.	275
95	Plan view of part of the Mount Fubilan Intrusion contoured for K_2O content. The map is for a planned bench at 1753 meters elevation. Circle symbols show locations of composite samples.	279

List of Figures (Continued)

Figure		Page
96	Map showing the locations of reverse-circulation rotary drill holes shown in Figures 97-99.	280
97	Lithic and selective chemical summary log of drill hole RC 1990.	282
98	Lithic and selective chemical summary log of drill hole RC 2099.	284
99	Lithic and selective chemical summary log of drill hole RC 1988.	286
100	Approximate locations of the samples included in this discussion of hydrothermal gains and losses.	
101	Isocon diagrams comparing major oxide (A) and trace-elements concentrations (B) of reference sample DDH 340-166.1, a phanerite from the Sydney Intrusion, and a sample of unaltered rock with porphyritic texture (DDH 331-218.5) from the Sydney Intrusion. Filled symbols comprise the rare-earth elements, TiO_2, Y, and Zr.	300
102	Isocon diagrams comparing major oxide (A) and trace-elements concentrations (B) of reference sample DDH 340-166.1, a phanerite from the Sydney Intrusion, and a sample of least-altered rock with phaneritic texture (DDH 356-166.5) from the Ningi Intrusion. Filled symbols comprise the rare-earth elements, TiO_2, Y, and Zr.	301
103	Isocon diagrams comparing major oxide concentrations and Y and Zr contents of reference sample DDH 340-166.1, a phanerite from the Sydney Intrusion, and two samples of least-altered rock with phaneritic texture from the Kalgoorlie Intrusion: (A) DDH 319-276.1, and (B) DDH 319-339.3 Filled symbols comprise TiO_2, Y, and Zr.	302

List of Figures (Continued)

Figure		Page
104	Isocon diagrams comparing major oxide (A) and trace-elements concentrations (B) of reference sample DDH 340-166.1, a phanerite from the Sydney Intrusion, and a sample of potassically-altered rock with porphyritic texture (DDH 321-263.1) from the Fubilan Intrusion. Filled symbols comprise the rare-earth elements, TiO_2, Y, and Zr.	303
105	Isocon diagrams comparing major oxide (A) and trace-elements concentrations of reference sample DDH 340-166.5, a phanerite from the Sydney Intrusion, and a sample of potassically-altered rock with porphyritic texture (JDD-94-04) from the Fubilan Intrusion. Filled symbols comprise the rare-earth elements, TiO_2, Y, and Zr.	304
106	Isocon diagrams comparing major oxide (A) and trace-elements concentrations of reference sample DDH 340-166.1, a phanerite from the Sydney Intrusion, and a sample of extremely potassically-altered rock with porphyritic texture (DDH 302-69) from the Sydney Intrusion. Filled symbols comprise the rare-earth elements, TiO_2, Y, and Zr.	305
107	Classification diagrams for the least-altered phanerites from the Sydney intrusion: (A) modal QAP, (B) normative Q'A'P' , (C) Q'-ANOR diagram of Streckeisen and Le Maitre (1979), and (D) TAS diagram of Middlemost (1994).	318
108	Classification diagrams for a sample of least-altered porphyry from the Sydney intrusion. (A) normative Q'A'P', (B) Q'-ANOR diagram of Streckeisen and Le Maitre (1979), and (C) TAS diagram of Le Bas and others (1986).	319
109	Comparison of 2023 samples of andesite and 83 of (quartz) latite from the IGBA database of Brändle and Nagy (1995) on the (A) Q'A'P', (B) Q'-ANOR (Streckeisen, and Le Maitre, 1979), and (C) TAS (Le Bas and others, 1986) classification diagrams.	

List of Figures (Continued)

Figure		Page
110	Comparison of 25 samples of (quartz) monzodiorite on the (A) Q'A'P', (B) Q'-ANOR (Streckeisen, and Le Maitre, 1979), and (C) TAS (Middlemost 1994). classification diagrams.	325
111	Isotherms (°C) on the Ca pyroxene solvus surface projected onto the pyroxene quadrilateral (Kretz, 1982). Microprobe-determined compositions for the magmatic pyroxenes of the Ok Tedi Intrusive Complex form a cluster near, and on, the 700°C isotherm.	331
112	Diagram summarizing possible oxygen and sulfur fugacities during magmatic crystallization and hydrothermal alteration at Ok Tedi. Included are projections from f_{O2} versus f_{S2} at 450 and 700°C into a temperature versus f_{O2} diagram, f_{O2} and temperature estimates of the exsolution of ilmenite from magnetite, oxygen buffers, and a line representing the stability of H2S versus SO2.	334
113	Diagram showing the equimolal solubility of H2O as a function of pressure in four types of silicate melts: (1) basalt (1100°C), (2) andesite (1100°C), (3) albite, (700-870°C), and (4) Li-pegmatite (660-720°C). Redrawn from Burnham (1979). The stippled area indicates the range of pressures inferred for the crystallization of the Ok Tedi magmas.	339
114	Temperature versus pressure plot showing the liquidus curves for given amounts of H_2O (solid lines), H_2O solubility curves (broadly dashed lines), and the water-saturated solidus for the system Qz-Ab-Or-H_2O (eutectic and minimum granitic compositions). Redrawn from Holtz and Johannes (1994). The stippled are indicates the range of pressure inferred for the crystallization of the Ok Tedi magmas.	340

List of Figures (Continued)

Figure		Page
115	Activity-activity diagrams showing the fields of stability of silicate minerals as a function of the ratios of potassium to hydrogen versus sodium to hydrogen for the range of temperatures that may have prevailed during potassic alteration at Ok Tedi. Redrawn from Bowers and others, 1984).	347
116	Paragenetic diagram summarizing the inferred sequence of formation of magmatic and hydrothermal minerals and water in the Ok Tedi Intrusive Complex. Solid lines - temperatures calculated from geothermometers. Dashed lines - temperatures inferred from the relationships of individual minerals to coexisting phases in thin-sections. Dotted lines - speculative and projections from better constrained relationships.	349

List of Tables

Table		Page
1	Radiometric ages of rocks from the Ok Tedi Intrusive Complex (Page, 1975).	35
2	Grades of the various types of ore from the Ok Tedi porphyry copper deposit.	38
3	Representative electron-beam microprobe analyses of feldspar.	73
4	Representative electron-beam microprobe analyses of pyroxene.	95
5	Representative electron-beam microprobe analyses of amphibole.	104
6	Representative electron-beam microprobe analyses of biotite	115
7	Representative electron-beam microprobe analyses of sphene.	131
8	Representative electron-beam microprobe analyses of magnetite and ilmenite	137
9	Electron-beam microprobe analyses of epidote.	145
10	Representative electron-beam microprobe analyses of garnet.	146
11	Electron-beam microprobe analyses of rutile.	149
12	Electron-beam microprobe analyses of hydrothermal magnetite.	154
13	Representative analyses of pyrite, chalcopyrite, chalcocite and bornite.	161
14	Petrographic and chemical features of samples from Katchan (1982).	175
15	Petrographic and chemical features of samples collected by Kepa and analyzed by Mason (1993).	179
16	Petrographic and chemical features of diamond drill core (DDH) and surface samples collected in 1994 (Suite 2).	184

List of Tables (Continued)

Table		Page
17	Summary of the normative anorthite (An) contents of samples from the Sydney, Fubilan, Kalgoorlie, and Ningi Intrusions	190
18	Regression equation and parameters for Star Mountains regional trend lines given in Figures 55 to 60.	196
19	Comparison of the normalizing factors commonly used for REE plots by different researchers. Those of Clarke (unpublished) were used herein.	253
20	Gold (in ppm) and copper (in weight percent) contents of samples of intrusive rock collected from the Ok Tedi Intrusive complex in 1994.	262
21	Summary statistics for gold and copper data from diamond drill hole (DDH), reverse circulation (RC), and blast hole (BH) samples. Also includes statistical values for samples listed in Table 20.	270
22	Geochemical data for the rock samples used to estimate hydrothermal gains and losses. Major oxides in weight percent, all other elements are listed in ppm.	291
23	Gains and losses of elements and oxides at constant volume in least-altered and altered samples compared to reference sample DDH 340-166.56.	295
24	Gains and losses of elements and oxides at constant Al_2O_3 in least-altered and altered samples compared to reference sample DDH 340-166.56.	297
25	Gains and losses of elements and oxides at constant REE, TiO_2, Zr, and Y in least-altered and altered samples compared to reference sample DDH 340-166.5.	306

List of Tables (Continued)

Table		Page
26	Major and trace element compositions, and normative and modal mineral assemblages of a sample with phaneritic texture compared to a sample with porphyritic texture. The two samples are nearly identical in chemical composition despite having different textures.	320
27	Calculated temperatures (°C) of formation of coexisting plagioclase and potassium feldspars in selected samples from the Sydney, Kalgoorlie, Ningi, and Fubilan Intrusions. The temperatures were calculated using equations from Elkins and Grove (1990).	332
28	Total aluminum (Al^{tot}) cations per 23 oxygen atoms from microprobe analyses of crystals of hornblende in samples DDH 356-166.5 and DDH 351-313.2 and estimates of crystallization pressures in kilobars.	336

List of Appendices

Appendix		
1	Geographic coordinates for samples used in petrographic and chemical analyses	on cd
2	Modal data for suite one petrographic analyses	on cd
3	Modal data for suite two petrographic analyses	on cd
4	Microprobe analyses of feldspars	on cd
5	Microprobe analyses of pyroxenes	on cd
6	Microprobe analyses of amphiboles	on cd
7	Microprobe analyses of biotites	on cd
8	Microprobe analyses of sphene	on cd
9	Microprobe analyses of magmatic magnetite and ilmenite	on cd
10	Microprobe analyses of garnet	on cd
11	Microprobe analyses of sulfide ore minerals	on cd
12	Major-oxide chemistry, XRF-determined trace elements, and normative mineralogy of samples from the Ok Tedi Intrusive Complex	on cd
12	Instrumental Neutron Activation (INAA) Analyses	on cd
14	Inductively Coupled Plasma Spectroscopy (ICP) Analyses	on cd

List of Plates

Plate		
1	Simplified geologic map of the Ok Tedi Intrusive Complex, Papua New Guinea.	in pocket
2	Approximate locations for thin-section samples used in first suite of petrographic analyses.	in pocket
3	Approximate locations for thin-section samples used in second suite of petrographic analyses.	in pocket

A Petrochemical Study of the Mount Fubilan Intrusion and Associated Ore Bodies, Papua New Guinea

Introduction

The Ok Tedi porphyry-type deposit of Papua New Guinea is a major source of copper and gold ore. The deposit has been mined from an open pit located at the former site of Mt. Fubilan in the Star Mountains near the border between Papua New Guinea and Irian Jaya (Figure 1) since May of 1984.

The area surrounding the Ok Tedi mine consists of rugged mountains, fast running rivers, and dense rain forest vegetation. Average rainfall varies from 300 to 400 inches per year. The area was described as a "geographic hell" by an early explorer and very little exploration of the area had been done before the discovery of the Mt. Fubilan deposit by geologists of Kennecott Copper Corporation in 1968. Kennecott gave up the property in 1975 despite the fact that a successful exploration program had outlined significant ore because of an inability to come to an agreement on tax structure and infrastructure funding with the fledgling government of the newly independent country.

Having failed to come to an agreement with Kennecott and realizing that the country could ill afford the loss of the potential revenue that could come from a world-class copper mine, the government of Papua New Guinea brought together a

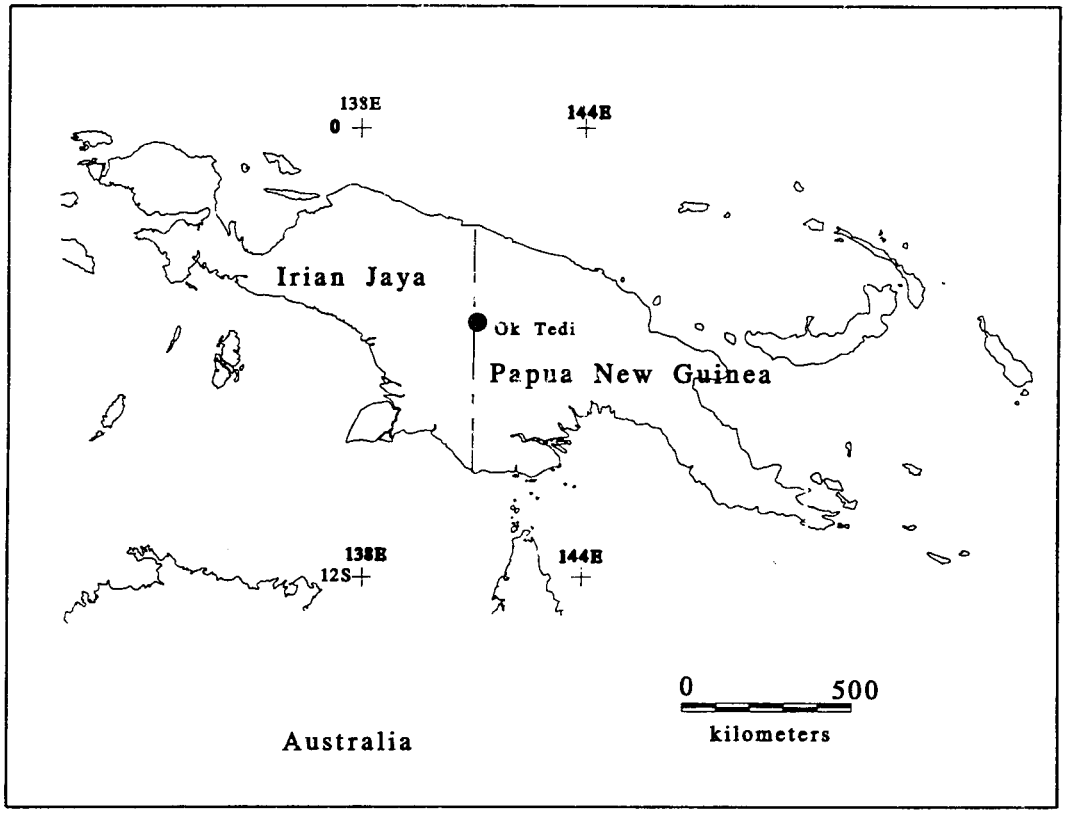

Figure 1: Location of the Ok Tedi copper-gold porphyry deposit and the Ok Tedi Intrusive Complex on the island of New Guinea.

group of consulting firms for feasibility studies. These studies suggested that not only could such a mine be constructed but that the gold present in the leached capping could result in an early cash flow to help pay for construction. The government then sought out and brought together a consortium consisting of the large Australian mining company Broken Hill Proprietary (BHP), an American oil company (AMOCO), and three German companies to develop and mine the deposit. The mine was put in production after an enormous job involving the construction of an infrastructure including: a mill and processing center, a town (Tabubil) to house mine employees, a hydro-electric power station, a 200 kilometer pipeline and road to the river port of Kiunga, and ore-drying and barge loading facilities at Kiunga. The cost of capitalization exceeded 1.4 billion US dollars.

The deposit was developed in a three-phase program: 1) mining of leached surficial rock and processing gold-rich ore by a cyanide leach circuit (May, 1984 to April, 1987), 2) separate mining of sulfide copper ore and leached gold ore and processing these ores using separate gold-leach and copper-floatation circuits (April 1987 to October 1988), and 3) concurrent mining of sulfide copper ore and gold ore and removal of both metals in two parallel flotation circuits (October 1988 to present). Metal concentrates are shipped from the recovery plant at Folomian via pipeline to Kiunga where they are loaded on barges for an 800 kilometer trip to the mouth of the Fly River in the Gulf of Papua. At that point the ore concentrates are transferred to sea-going vessels and delivered to smelters in Japan, Germany,

Finland, South Korea, and the Philippines. The mine has been in production continuously since May of 1984 except for a few idle periods brought on by landslides or disputes with labor unions or local landowners. Production in 1995 resulted in 614,000 tonnes of concentrates containing 213,000 tonnes of copper, 482,000 ounces of gold, and 914,000 ounces of silver (BHP Fact Sheet, 1996). In 1989 the Ok Tedi mine provided 42 percent of Papua New Guinea's export income (The Star, July, 1990).

The Ok Tedi ore deposit differs from that of other large copper porphyries in having significant quantities of gold. It was the gold that made it possible to begin mining of leached ore and it is the gold that turns this otherwise intermediate size copper ore body into a world-class deposit.

Purpose

I began this study to follow up on my earlier work at Ok Tedi from July 1987 to December 1990. I was employed by Ok Tedi Mining Limited (OTML) to be involved in the development of "skarn" orebodies and to train local geologists in matters relating to skarns and ore geology. In fulfilling this job I examined intrusive rock cuttings from many thousands of meters of reverse-circulation rotary- and blast-drill holes. I also supervised the logging of hundreds of meters of diamond drill core. Together with these duties I reviewed all available published and unpublished reports that described the mineralogy and petrology of the Ok Tedi Intrusive Complex. I found that over 20 petrographic names had been assigned to the igneous rocks of the complex; and all in an area of only about 7 square kilometers. I also engaged in many hours of heated discussions with fellow geologists concerning appropriate techniques used to map and log the igneous rocks. The work of many different staff and contract personnel over the mine life of about 25 years would likely lead to unnecessary variations in host rock terminology. One purpose of this study was to investigate the compositional diversity of these igneous rocks, and to determine if the many names assigned to these rocks were valid.

The Ok Tedi Intrusive Complex is ideal for such a petrographic and petrochemical study because the igneous rocks and the ores hosted by these rocks

are very young. The Ok Tedi deposit is the youngest (1-3 my) of the porphyry copper deposits to produce ore, and according to Harayama (1992) the Ok Tedi Intrusive Complex is one of the youngest exposed plutons on Earth. The deposit differs from most Cordilleran porphyry copper deposits by having substantial amounts of gold in addition to copper. The alteration associated with mineralization has transformed, by alkali metasomatism, rocks of originally quartz andesite composition to those of alkali feldspar trachyte. The intrusive complex, therefore, offers information relevant to the study of igneous petrology, ore deposits, and metasomatic replacement.

The chief purpose of this study is, therefore, to provide a precise characterization of the intrusive complex, to document the metasomatic transformation of the Mt. Fubilan porphyry, and to evaluate methods of field identification for the igneous rocks of the Ok Tedi Intrusive Complex. In addition, the data obtained in this study are used to address several important geological questions. These include: (1) are the variously named intrusive bodies at Ok Tedi the end products of different magma batches or do they represent different parts of the same magma that have undergone dissimilar crystallization histories; (2) what were the pressures, temperatures, and depths of intrusion; (3) are the hypogene ores of magmatic or hydrothermal origin; (4) what were the depositional pressures and temperatures of ore and hydrothermal mineral assemblages; and (5) what were the

compositions of the hydrothermal fluids that caused the wallrock alteration and that most likely deposited the ore minerals.

Nomenclature

The terminology used to refer to geographic locations near the Ok Tedi ore deposit and the classification scheme used to define the plutonic and volcanic rocks therein are discussed in this section.

The Ok Tedi deposit (141° 8' 14" east longitude and 5°12' 27" south latitude) and the company formed to mine the ore deposit were named after the Ok Tedi, which is a small river about 7 kilometers to the east as shown in Figure 2. "Ok" is a local world that means river. The mine is south of the Ok Gilor, a tributary of the Ok Tedi, and north of Ok Mani. The deposit forms the core of Mt. Fubilan. Bamford and others (1972), and other authors, also refer to it as the Mt. Fubilan deposit. The Ok Tedi Intrusive Complex includes a group of contiguous intrusions in the Mt. Fubilan area (Arnold and Fitzgerald, 1977).

Informal location names that were given to a number of survey stations and helicopter pads and that will be referred to throughout this dissertation are shown in Figure 3. Most of these locations are named after places that the early explorationists would rather have been than at Ok Tedi.

Geologic, engineering, survey, and maintenance offices and the workshop used to service heavy equipment were located at Vancouver (Figure 3) prior to a major landslide in 1989. The geologic, engineering, and survey offices were relocated to Taranaki after the slide; and the maintenance offices and shops to an

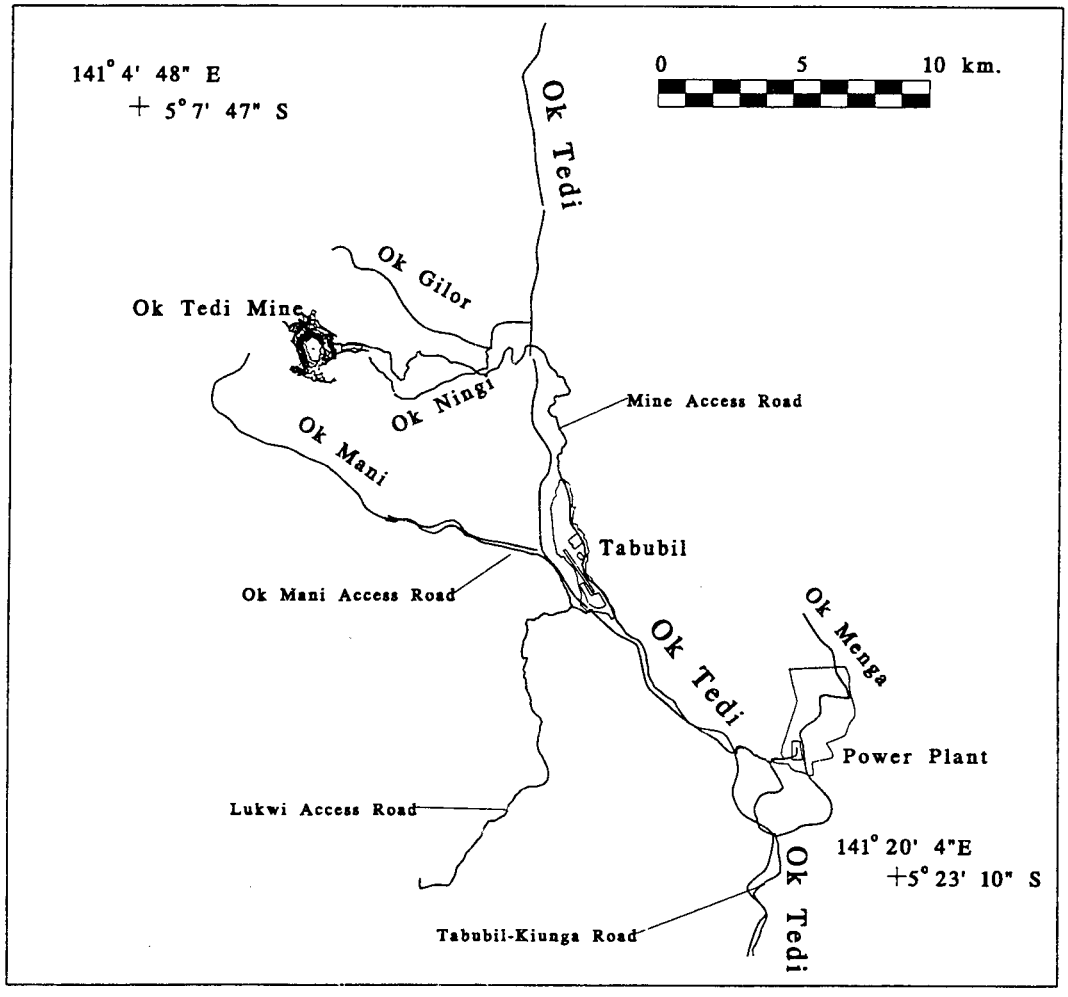

Figure 2: Location of the Ok Tedi mine and the town of Tabubil with respect to the Ok Tedi River. Ok is a local word that means river.

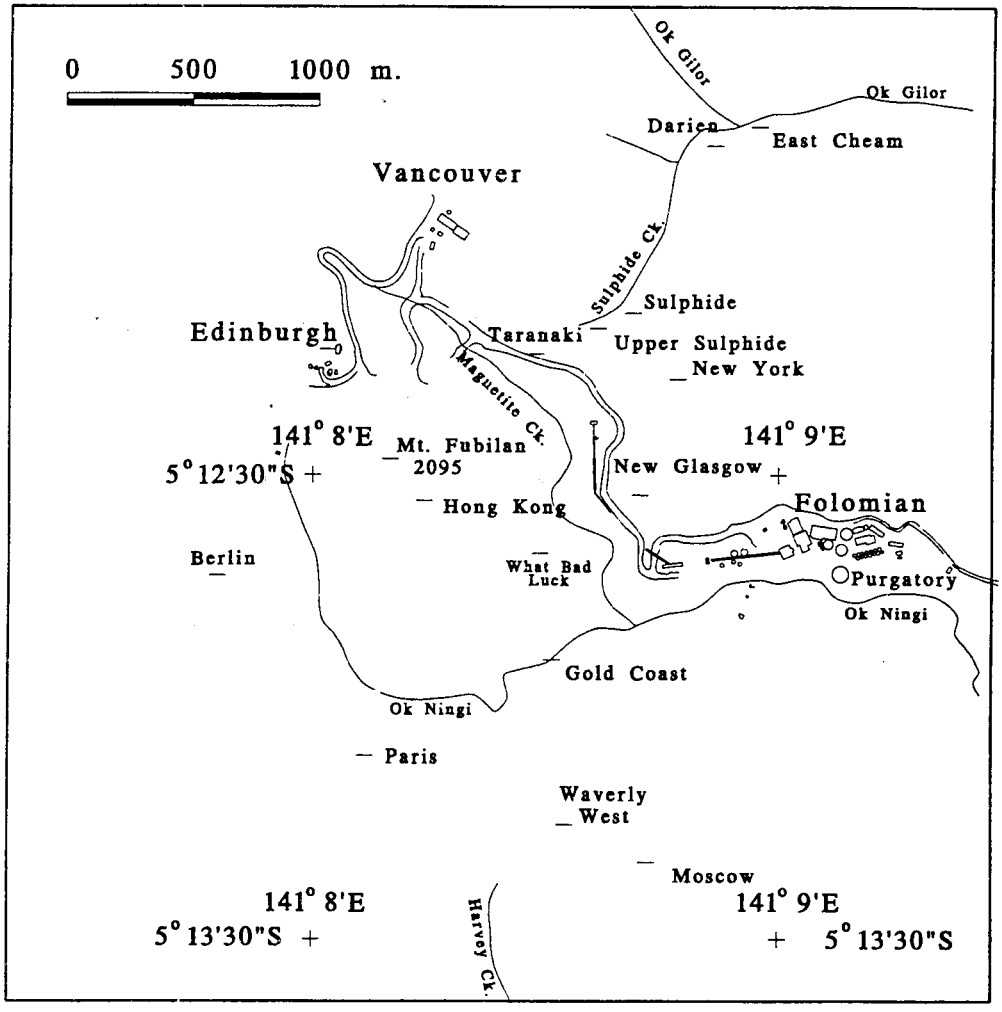

Figure 3: Creeks, named locations, roads, and mine buildings in the vicinity of the Ok Tedi mine.

area between Folomian and New Glasgow. Folomian is the site of the grinding mills and flotation plants that process the ore from the open pit (Figure 3). It is also the site of chemical and metallurgical laboratories, messing facilities, and a medical clinic.

A geology core shed and sample preparation area, a gold pilot plant, a mess for feeding workers, and training offices were located at Edinburgh (Figure 3) until about the end of 1988 when this area was mined and the facilities were relocated. Currently the core shed is at Vancouver, the gold pilot plant is no longer in existence, the training offices and mess are at Taranaki, and sample preparation is done by the chemistry group at Folomian. Limestone is quarried from the Darai Limestone at Edinburgh. This limestone is used for sheeting haul roads inside and outside the pit.

The configuration of the open-pit at Ok Tedi in January 1994 is shown in Figure 4 as are the altitudes (in meters) of selected benches.

The scheme used to name the igneous rocks of the Ok Tedi Intrusive Complex consists of two parts. The first part is the field name used for logging core or mapping exposures. The names used for field identification of igneous rocks are based on texture. They are aphanite, porphyry, and phanerite. These names can be modified to include information about mineralogy that can be seen in hand specimen or thin-section (e.g. feldspar porphyry). The second part is the formal name, given herein as those of the International Union of Geosciences

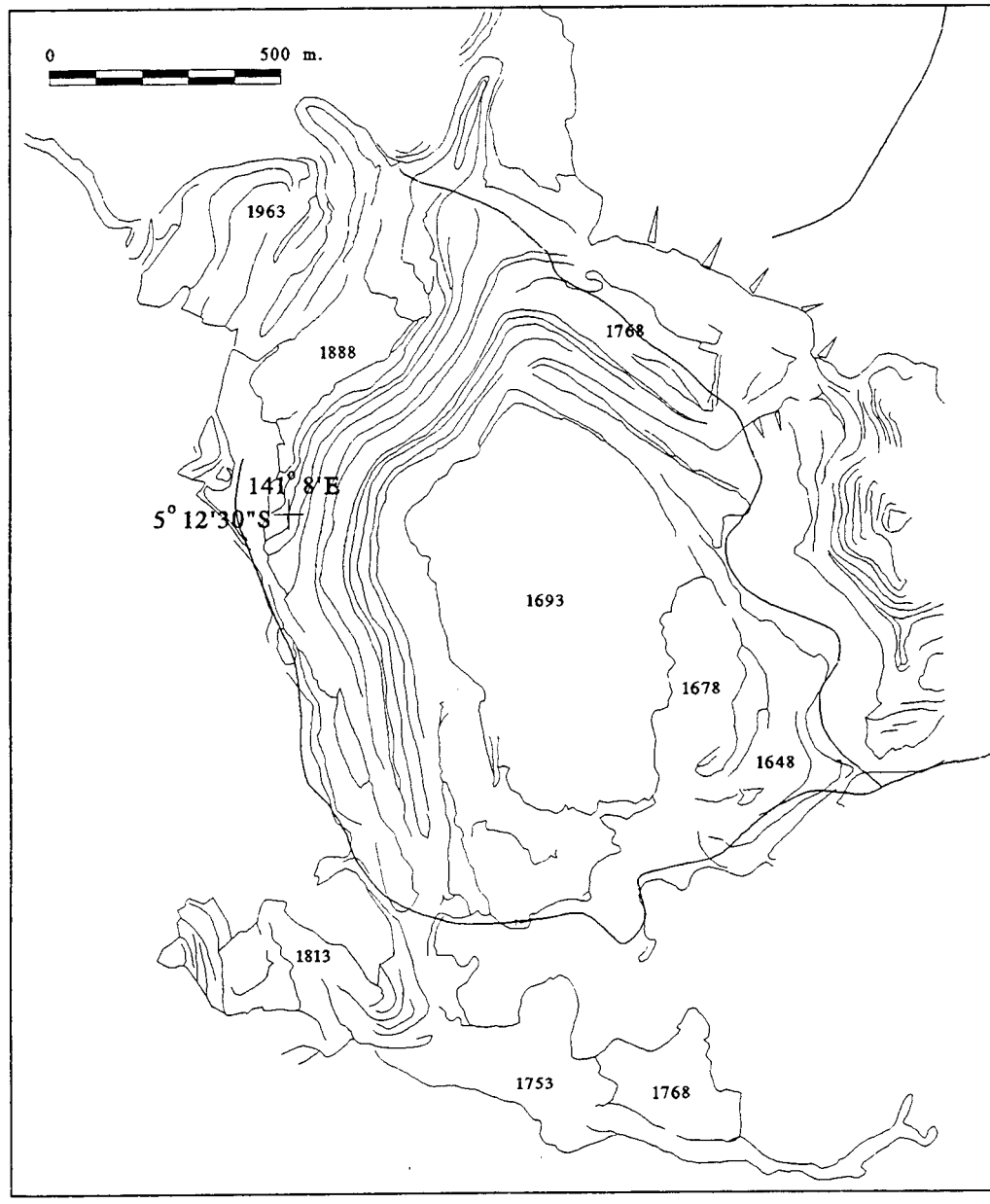

Figure 4: Shows configuration of the open pit at Ok Tedi as at January, 1994. Selected benches are identified by elevation.

(I.U.G.S.; Le Maitre and others, 1989). These names depend on the identification of the ratios of quartz, and plagioclase and potassium feldspars. The formal names can also be modified by attaching a mineral name prefix as an adjectival modifier (e.g. hornblende monzodiorite).

Previous authors such as Ayers and Bamford (1976, revised 1987) used a classification scheme of plutonic rocks similar to that of Bateman and others (1963). This scheme was superseded by that of the I.U.G.S. (Le Maitre and others, 1989). A few differences between the schemes are important in reference to the intrusive rocks of the Ok Tedi Intrusive Complex. The most important difference is the topology of the fields on the quartz-alkali feldspar-plagioclase feldspar (QAP) diagrams of Bateman (Figure 5) and of the I.U.G.S. (Figure 6). Samples formerly classified as diorite according to the older scheme are now termed monzodiorite and quartz monzodiorite by the new scheme. The fields for granodiorite and quartz monzonite are smaller on the I.U.G.S. diagram than on the Bateman diagram; and many rocks that would have earlier been termed quartz monzonite would now be called granite. In addition to these differences, the term "syenodiorite", used in previous studies does not appear either in the Bateman or newer I.U.G.S. classification. Johannsen (1931) defined syenodiorite as a plutonic rock of composition intermediate between syenite and diorite. Because this term is applicable to a wide range of plutonic compositions and therefore is ambiguous, it is not used in this study except in reference to earlier investigations.

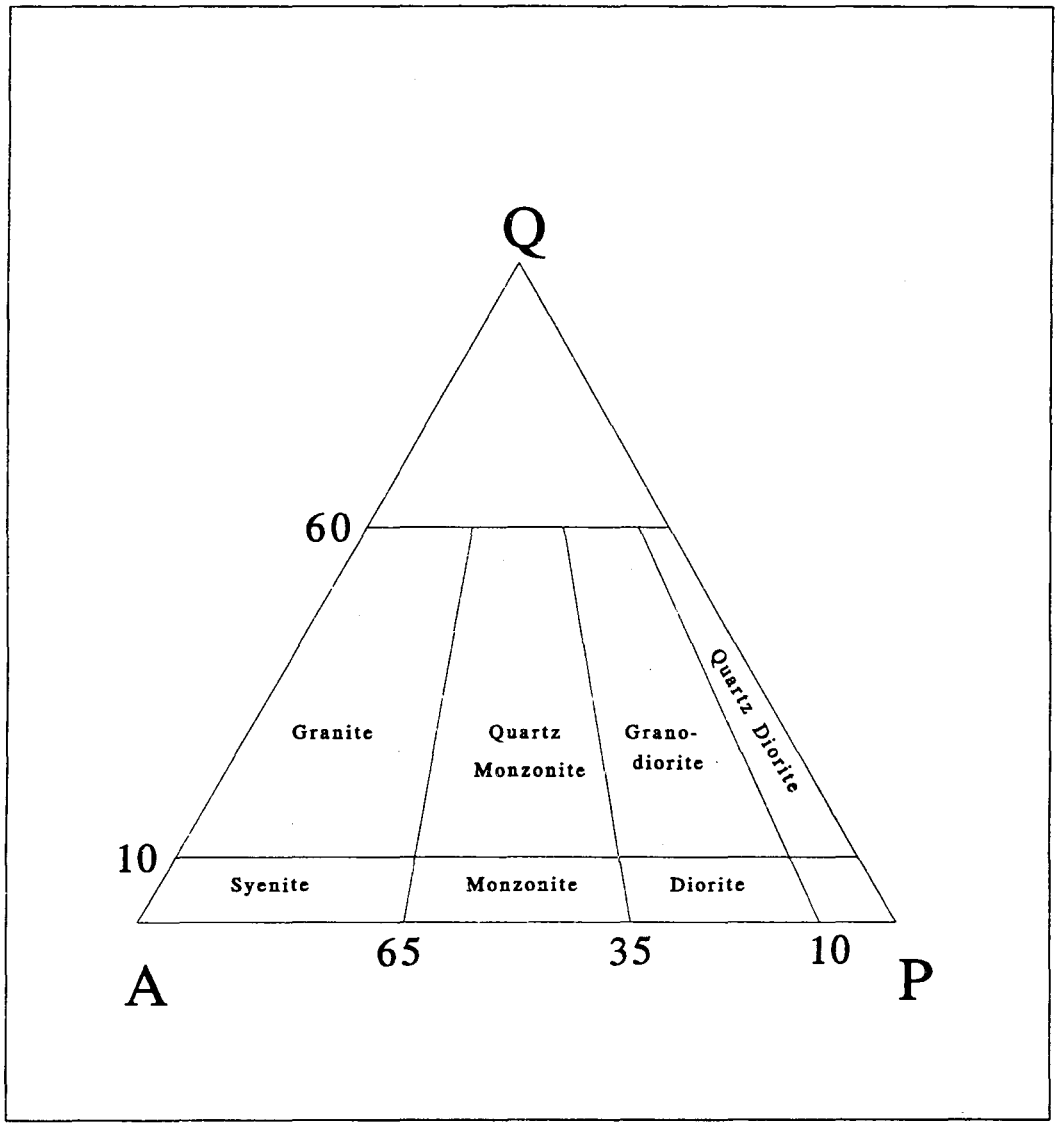

Figure 5: Classification diagram similar to that used for the classification of igneous rocks by early workers at Ok Tedi. After Bateman (1963).

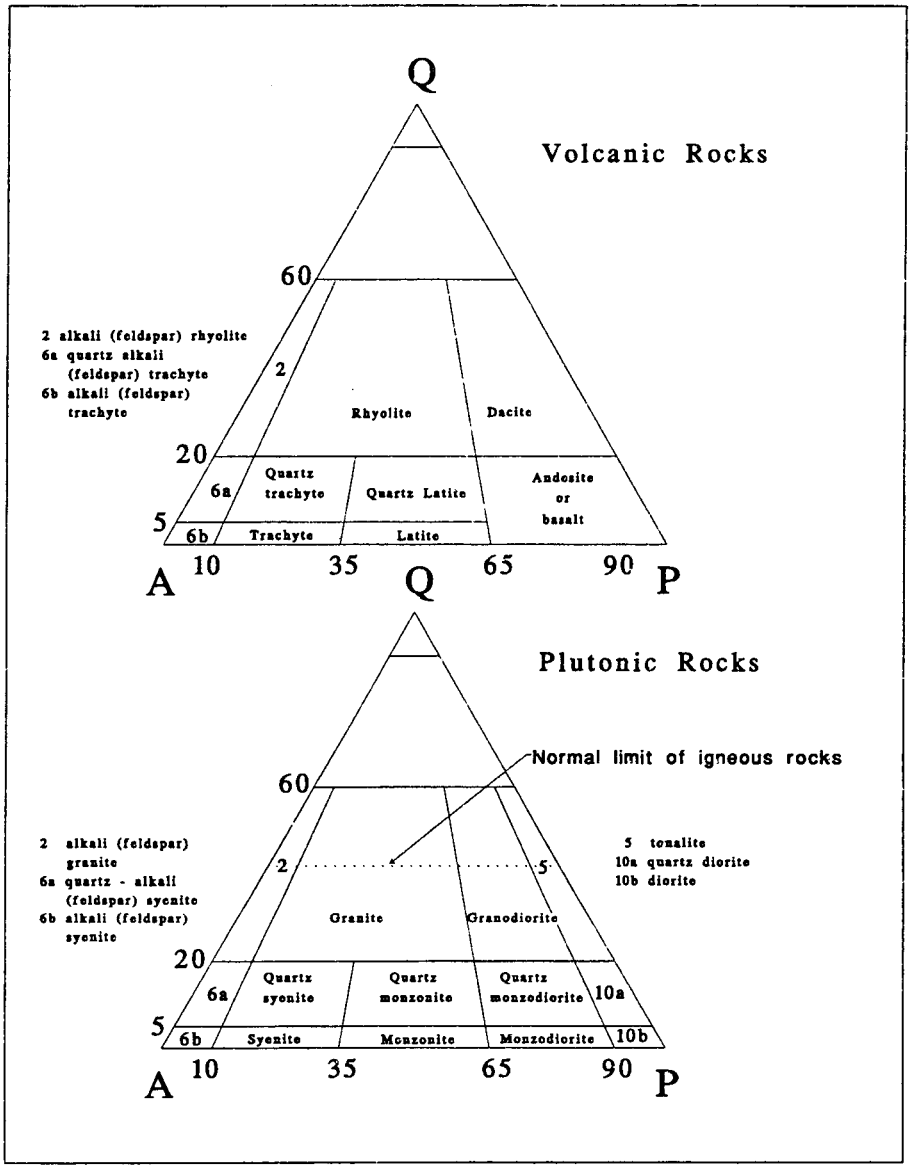

Figure 6: IUGS classification diagrams for (A) volcanic and (B) plutonic rocks. These diagrams were designed to be used for modal analyses (from Le Maitre and others, 1989).

Use of the I.U.G.S. classification of igneous rocks first requires a decision as to whether to use "volcanic" or "plutonic" names. This decision is made on the basis of texture. Aphanitic (finely crystalline or glassy) rocks are given volcanic names; phaneritic (medium to coarsely crystalline rocks) are given plutonic names. Porphyries, however, were not discussed in the naming procedures of the IUGS. The convention used in this study is to assign volcanic rock names to porphyries with aphanitic groundmass and plutonic names to rocks in which porphyritic crystals are imbedded in phaneritic groundmass.

The I.U.G.S. recommends naming phaneritic rocks by means of modal petrographic analyses and volcanic rocks using major oxide chemical analyses -- specifically the total alkali-silica (TAS - Figure 7) diagram of LeBas and others (1986). The commission considered the use of modal [sic, normative?] minerals calculated from chemical analyses for the classification of volcanic rocks (Le Maitre and others, 1989). They rejected this method, however, because of difficulties in making such calculations and in the reliability of the results. These problems are not as acute today because of the ease of doing the calculations on personal computers and the availability of programs that calculate normative minerals. In addition, my experience with making modal estimates using visual or point counter methods leads me to believe that reliable modal analyses are extremely difficult to make particularly by less experienced petrographers. Therefore, in this study, the assignment of formal petrographic names is made from

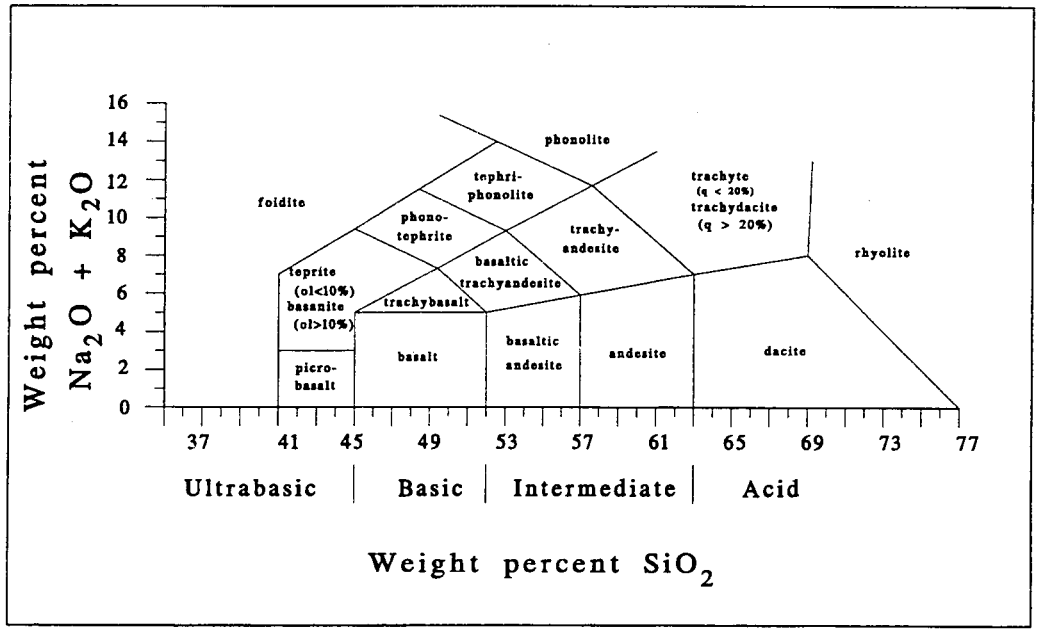

Figure 7: Total alkali-silica (TAS) diagram for classification of volcanic rocks using chemical analyses (Le Maitre and others, 1989).

chemical criteria including normative minerals and the total alkali-silica classification. For comparison, however, many rock samples are also classified using the results of modal analyses using the point counter method.

Three digit computer codes were assigned to all samples of drill core at Ok Tedi. The codes correspond to formal petrographic names. Because of the changes in terminology over the years and because of the differing abilities of the geologists who have done the logging, it is difficult to be certain that rocks of any given code are similar to any others having the same code. For this reason, I believe that all samples should first be classified using the above field names. Accordingly, I have given field names to all rock samples; whereas I have only assigned formal petrographic names to those that were chemically analyzed.

Three terms - magmatic, relict magmatic, and hydrothermal - that will be used repeatedly throughout this dissertation have been defined by Lanier, Folsom, and Cone (1978) as follows:

> "The term magmatic followed by a mineral name infers that the mineral was derived from a magma and has undergone no appreciable alteration. The term relict magmatic is used for a mineral of magmatic origin which has undergone exchange reactions with hydrothermal fluids but which closely retains its original crystal outline. ... The term hydrothermal preceding a mineral name means that the mineral was formed by replacing a preexisting mineral by the action of hydrothermal fluids."

GEOLOGIC SETTING

In summarizing the regional geology of the Ok Tedi Intrusive Complex it is necessary to point out to readers unfamiliar with the area that the island of New Guinea (about 833,700 square kilometers) is larger than the combined states of California, Oregon, and Washington (about 826,000 sq. km.). The large area involved, the diversity of geologic features, and the unexplored condition of much of the area require, therefore, that the following discussion be extremely generalized.

Regional Geology

The island of New Guinea consists of the leading edge of the Australian continental plate and a series of 32 or more tectono-stratigraphic terrains (Pigram and Davies, 1987). These terrains have been accreted onto the edge of the continental plate since Eocene time. Some of the terrains have continental affinities and probably represent displaced parts of continental crust, whereas others have island arc origins (Pigram and Davies, 1987).

A simplified outline of the principal tectonic provinces of Papua New Guinea is given in Figure 8 (modified from Bain, 1973; and Jacques and Robinson, 1977). These provinces consist of the Fly platform and three WNW-ESE trending geologic belts; the Papuan Fold Belt, the New Guinea Mobile Belt, and a belt of

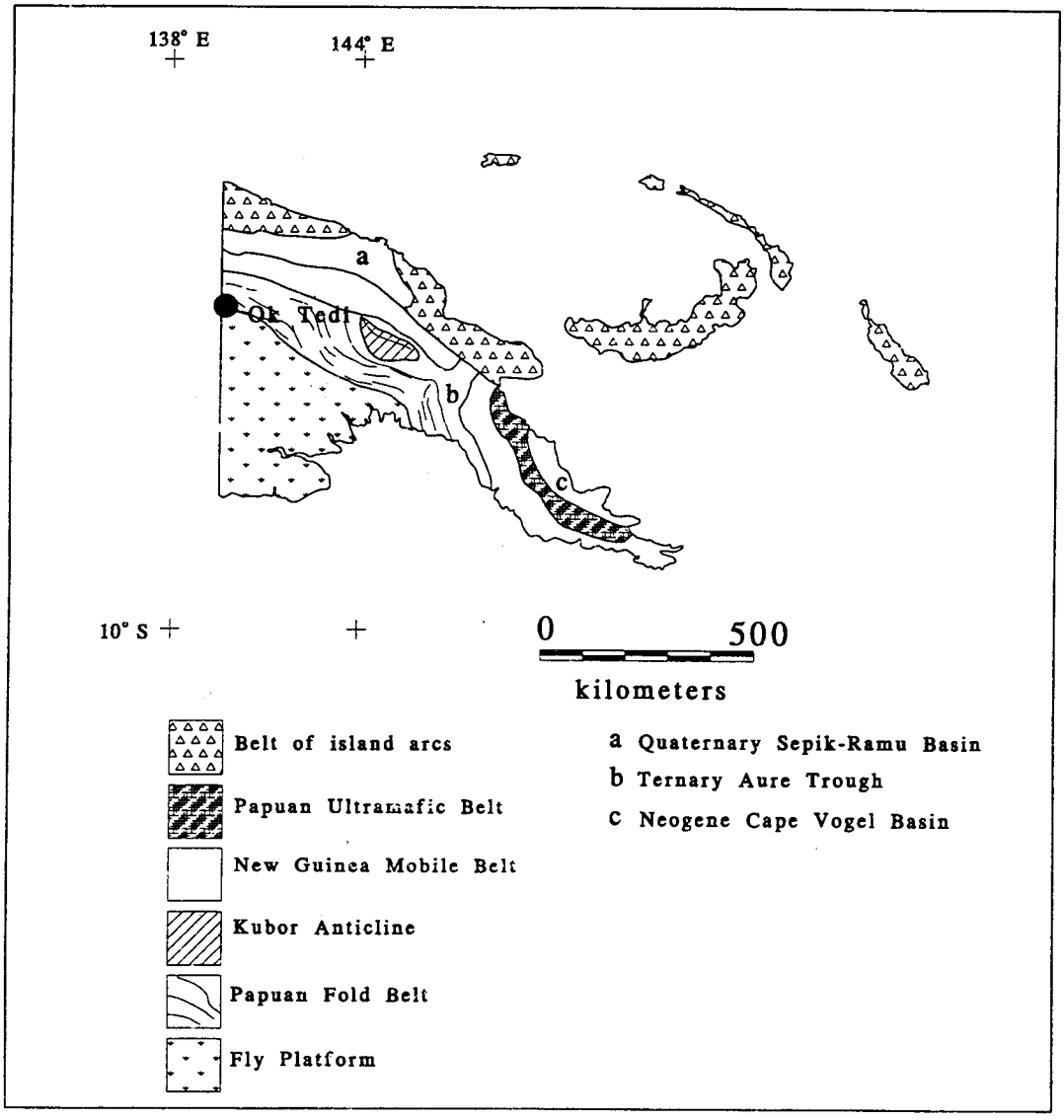

Figure 8: Simplified outline of the tectonic provinces of Papua New Guinea. Redrawn from Bain (1973) and Jacques and Robinson (1977).

former island arcs (Abers and McCaffrey, 1988). In addition to these tectonic elements, three sedimentary basins are shown in Figure 8: the Sepic-Ramu Basin of Quaternary age, the Aure Trough of Tertiary age, and the Cape Vogel Basin of Neogene age.

The Fly Platform consists of a crystalline basement of pre-Mesozoic age overlain by approximately flat-lying sandstones and limestones of Cenozoic age and sedimentary and volcanic rocks of Quaternary age (Bain, 1973). The Fly Platform is a stable platform or foreland basin. It has only weak folds and faults compared to the other structural provinces of Papua New Guinea.

North of the Fly Platform is a the Papuan Fold Belt. This is an area of subparallel folds and faults that forms a transition between the Fly Platform to the south and the New Guinea Mobile Belt to the north. The Papuan Fold Belt includes a 100 to 5000 meter sequence of marine clastic sedimentary rocks of Mesozoic age; a thin sequence of older Tertiary siltstone, limestone, and calcareous sandstone; and a thick (200-1500 meter) sequence of shelf limestone overlain by marine and terrestrial clastic rocks of younger Tertiary age. One of the anticlines within the fold belt, the Kubor Anticline, is shown in Figure 8. This anticline is important to the understanding of the regional geology because it includes the north and easternmost exposures of crystalline basement rock.

The New Guinea Mobile Belt, which according to Bain (1973) includes the Papuan Ultramafic belt, is 50 to 100 kilometers wide and 1600 kilometers long. It

contains most of the major high-angle faults, and intrusive, ultramafic, and metamorphic rocks of Mesozoic or younger age in Papua New Guinea. The belt includes deep water sedimentary rocks, volcanic rocks, and ultramafic intrusives. Ophiolites are present throughout the belt (Abers and McCaffrey, 1988). The mobile belt may be a former section of ocean basin closed by tectonic forces.

North of the New Guinea Mobile Belt are portions of island arcs and oceanic crust that have been accreted onto the leading edge of the Australian continental plate.

The Ok Tedi Intrusive Complex is located on the south flank of a major structure, the Mueller Anticline, near the southern margin of the New Guinea Fold Belt. This anticline is about 150 km by 50 km in size and is unique to the Papuan Foldbelt in that it exposes an entire stratigraphic sequence of sedimentary rocks that range from Pliocene and Pleistocene age at the top of the section to basement rocks of Permian and Triassic age at the bottom (Hill, 1989).

Arnold and Griffin (1978), Mason and McDonald (1978), and Griffin (1983) discussed plutonic and volcanic rocks at several locations within the Star Mountains. Those closest to the Ok Tedi mine are shown in Figure 9 and include the Antares, Ok Tedi, and Mt. Ian intrusive complexes; intrusive stocks at Tifalmin; and several smaller intrusive masses.

Page and McDougall (1972) and Page (1975) have performed radiometric age determinations on samples from a number of these igneous centers. Biotite

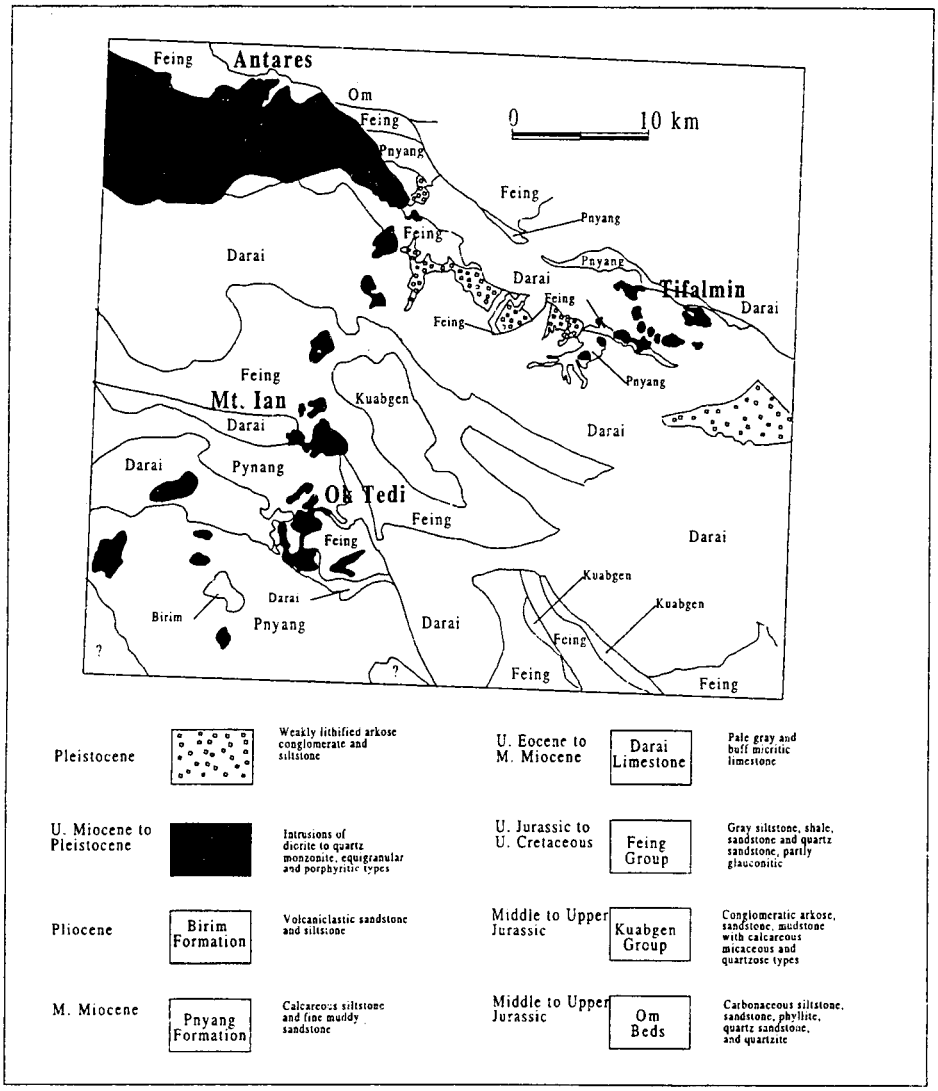

Figure 9: Intrusions and sedimentary formations of the Star Mountains area. Simplified from Arnold and Griffin, 1978.

ages of rocks from the Antares complex range from 2.4 to 6.9 million years (Ma); ages based on hornblendes from the same area range from 4.9 to 5.9 Ma Three biotite ages from the Mount Ian complex range from 1.7 to 1.9 Ma, whereas one hornblende analysis gave an age of 12.9 Ma. Five whole rock dates from the Tifalmin area range from 3.4 to 12 Ma.

Local Geology

The ore deposits of the Ok Tedi deposit are hosted primarily by igneous rocks. However, additional high grade rock also is present as massive ores hosted by sedimentary rock and as disseminated mineralization associated with potassic alteration of sedimentary siltstones and sandstones of a thermal aureole that surrounds the intrusive complex.

Sedimentary Rocks

Sedimentary siliciclastic and carbonate rocks surround the Ok Tedi Intrusive Complex and are the hosts into which the magmas intruded (Figure 10). These sedimentary rocks range from Cretaceous to middle Miocene in age. They have been subdivided into three rock groups based on lithology and regional stratigraphy. They are, according to Bamford and others (1972), composed of a lower unit of intercalated siltstones and sandstones, a middle unit of relatively pure limestone, and an upper unit of siltstones and sandstones. These units correspond

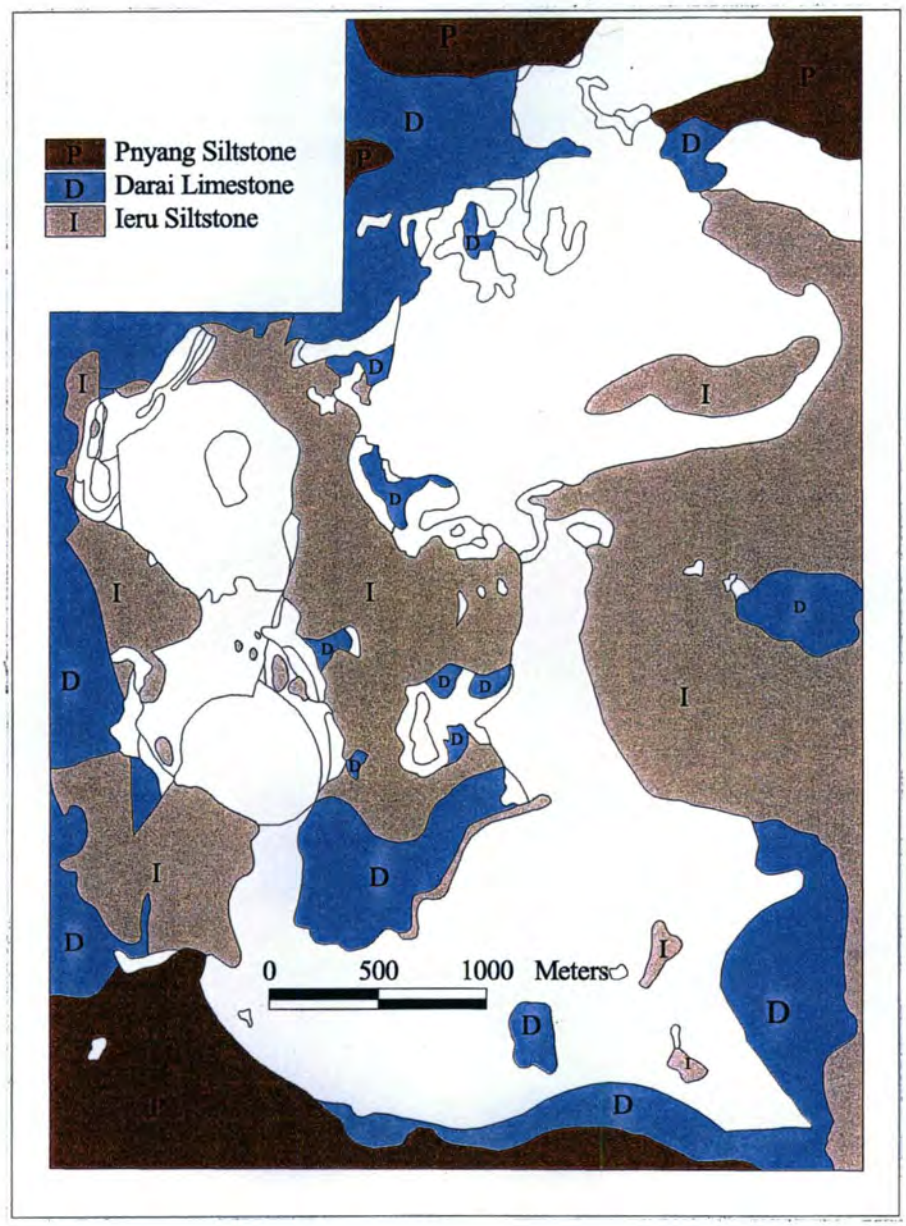

Figure 10: Sedimentary rocks of the Ok Tedi mine area. Simplified from Arnold, Griffin, and Hodge (1979).

to the Ieru Formation, the Dari Limestone, and the Pnyang Formation, respectively, as depicted in Figure 10.

The Ieru Formation is a part of the Feing Group; it is of Jurassic to late Cretaceous age (Arnold and Griffin, 1978) but may be as young as Paleocene or early Eocene in places (Davies and Norvick, 1974). The Feing Group conformably overlies the Jurassic Kuabgen Group. It is paraconformably overlain by the Darai Limestone.

The Feing Group includes the Toro Sandstone and the Ieru Formation. The Toro Sandstone is the older of the two and consists of clean partly glauconitic sandstones; the Ieru Formation is composed of gray or gray-green fine-grained sandstones, siltstones, and mudstones.

The Darai Limestone consists of massive to thick-bedded carbonates. It is late Eocene to middle Miocene in age. The formation varies from about 500 to 1300 meters in thickness, but is significantly thinner (about 240 meters) in the Mt. Fubilan area (Davies and Norvick, 1974).

The Pnyang Formation consists of soft gray calcareous mudstones and siltstones with minor limestone interbeds (Davies and Norvick, 1974). It is middle Miocene in age (Hill, 1989). The Pnyang Formation is locally about 1000 meters in thickness, but increases to the west of the Ok Tedi mine area (Fookes and others, 1991).

Contacts between the Ieru Formation and the Darai limestone at many, if not most, locations in the Mt. Fubilan area are along a system of low angle faults that have been called the Purgatory Thrust (Bamford and others, 1972; Ayers and Bamford, 1976, revised 1987; and Arnold, Griffin, and Hodge, 1979). This same fault system has recently been called the Taranaki Thrust (Hearn, 1995). Zones of crushed, shattered and sheared rock, and clay within the thrust faults attain thicknesses of several centimeters to 15 meters (Katchan, 1982). These cataclastic horizons are the hosts to massive ores at several locations in the Ok Tedi Mine area.

Intrusive Rocks

The igneous rocks of the Ok Tedi Intrusive Complex describe a roughly U-shaped pattern on geologic maps (Figure 11) of the area surrounding Mt. Fubilan. The complex has been subdivided into "separate intrusions" based on contacts purportedly observed from drill core and outcrops. Detailed mapping has been centered on the western-most portions of the exposed intrusive rocks and very little geologic work has been done on the southern and eastern portions. This bias is reflected in the fact that the western-most part of the complex has been subdivided into at least three intrusions (Mt. Fubilan, Kalgoorlie, and Ningi - Figure 11), whereas the remainder of the complex has been lumped together as "undifferentiated Sydney intrusion."

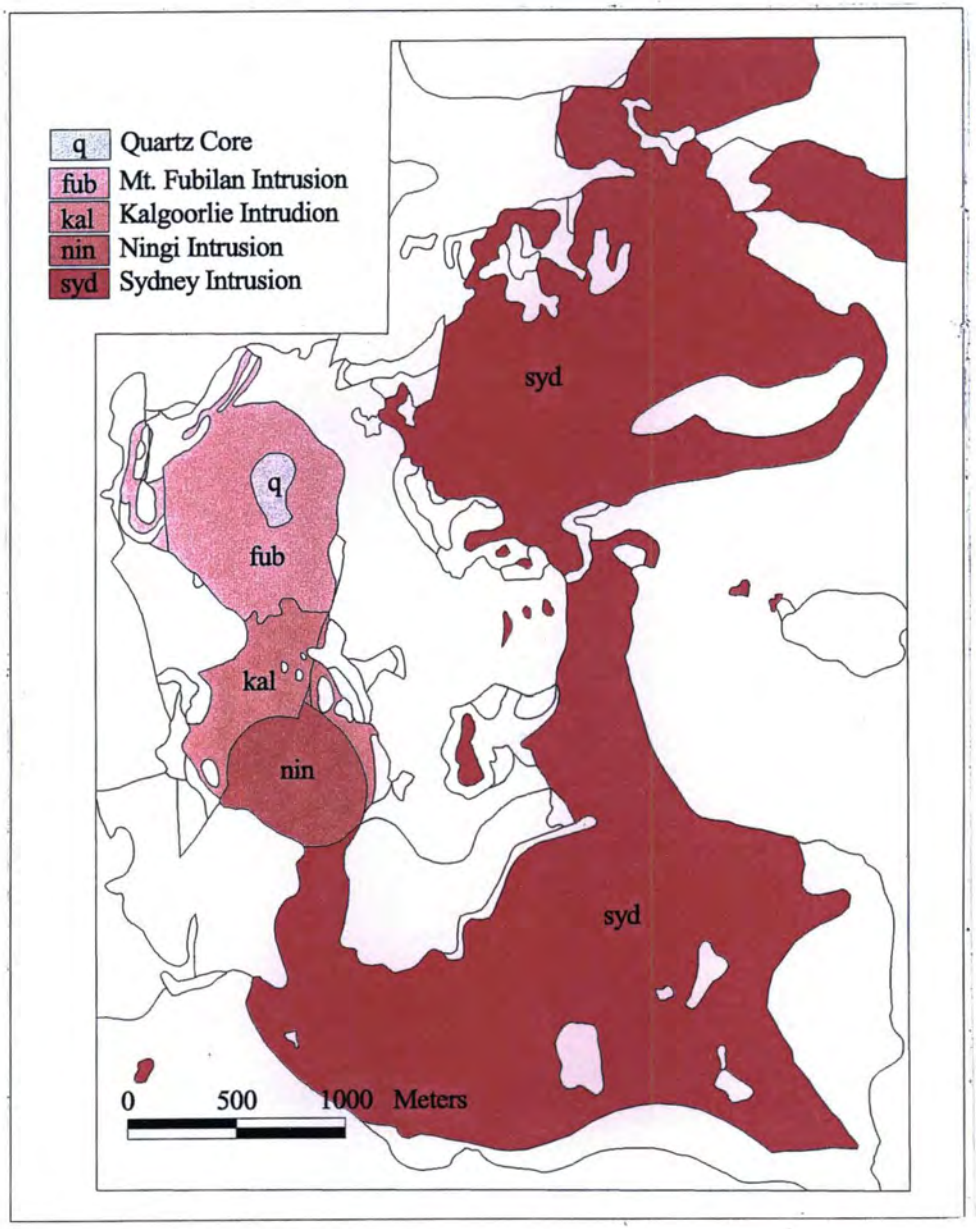

Figure 11: Locations of major intrusions that have been postulated to comprise the Ok Tedi Intrusive Complex. Simplified from Arnold, Griffin, and Hodge (1979).

It is likely that the metasedimentary rocks present between the east, south, and west exposures of intrusive rock constitute a single roof pendant. If this interpretation is correct, then the overall shape of the intrusive complex may be circular to oval and it may form a continuous body from east to west beneath the roof pendant.

Mt. Fubilan Intrusion

In plan view the Mt. Fubilan intrusion is an approximately circular body about 1000 m. in diameter and in three dimensions it appears to have the configuration of a vertical cylinder or stock (Bamford and others, 1972). The intrusion is largely confined to the perimeter of the mountain for which it was named. It is bounded by the Ieru formation on the north, east, and west and by the Kalgoorlie intrusion on the south. This intrusion is porphyritic in texture. It was classified as quartz latite porphyry by Bamford and others (1972), whereas Arnold and Fitzgerald (1977), and Arnold, Griffin, and Hodge (1979) considered it to consist of quartz monzonite porphyry and monzonite porphyry.

Bamford and others (1972) have described the rocks of the Mt. Fubilan intrusion as consisting mainly of phenocrysts of feldspar set in a groundmass of quartz, feldspar, and biotite. They observed that the anorthite content of the plagioclase feldspars ranged from An_5 to An_{20} percent which contrasted markedly to the range of An_{25} to An_{50} for other intrusions of the complex. These authors also

observed the presence of hydrothermal biotite, replacements of plagioclase feldspar by alkali feldspar, and pseudomorphs of hydrothermal micas after primary magmatic pyroxene and hornblende. Arnold and Fitzgerald (1977) have also noted the presence of accessory apatite and, in some specimens, sphene.

A prominent feature of the Mt. Fubilan intrusion is a central plug-like core composed of a stockwork of quartz veins and veinlets, a feature referred to as the "quartz core" (Figure 11). Prior to the commencement of mining the quartz core had surface dimensions of about 180 by 120 meters, was elongated in a northerly direction, and had a vertical extent of more than 300 meters. The quartz veins and veinlets that comprise the stockwork vary in density from relatively sparse at the outer margins of the "quartz core" to as much as 100 percent of the rock at the center.

Breccias, which have been characterized as "intrusive" and "intrusion" types, form discontinuous pods along contacts between the Fubilan intrusion and host Ieru Formation (Bamford and others, 1972). Arnold and Fitzgerald (1977) suggest that intrusive breccia "dykes" are present throughout the Fubilan stock and that they make up 10 to 20 volume percent of the intrusion. Clasts within these breccias include: siltstones and metasiltstones, intrusive rocks with porphyritic and phaneritic textures, massive magnetite and massive sulfide, skarn, magnetite-quartz-apatite rock, and sphalerite-tremolite rock. Clast-type varies with position in

the Mt. Fubilan stock. Siltstone clasts are more common near the outer portions of the stock. Clasts of phaneritic intrusive rock are also present.

Xenoliths, predominantly of siltstone, are found at several locations within the Fubilan intrusion, but are most common near contacts between the intrusive rock and the Ieru Formation. According to Arnold and Fitzgerald (1977) infrequent dikes of hornblende porphyry and microgranite cut across the Mt. Fubilan intrusion.

Ayres and Bamford (1976; revised 1987) have noted a plug-like body of coarse-grained monzonite in the center of the Fubilan stock which they designated the Bonn intrusion. They suggested that this intrusive mass may be either a part of the "Southern" intrusion, a roof pendant, or a large plutonic xenolith. Arnold and Fitzgerald (1977) confirmed the presence of this body in the subsurface, but were unable to define its shape or extent. Several of the thin-sections of intrusive rock that I examined have phaneritic textures and come from the area fringing the quartz core. These may represent the Bonn Intrusion but this feature was not specifically sought out in my time at Ok Tedi and not enough evidence can be garnered from the few available thin-sections to confirm or deny the existence of this intrusion.

Kalgoorlie Intrusion

The Kalgoorlie intrusion is bounded on the north by the Mt. Fubilan stock and to the south by the Ningi porphyry. It is in contact on the east and west with the

Ieru Formation except at the Gold Coast where the contact is with limestones of the Darai Formation. The contact between the Kalgoorlie intrusion and the Ningi intrusion is not well defined by geologic mapping.

The Kalgoorlie intrusion is shown as monzonite on the geologic map of Bamford and others (1972). It was referred to as clinopyroxene-diorite by Mason (1975), whereas Arnold and Fitzgerald (1977) considered it to be composed of monzodiorite, quartz monzodiorite, and quartz monzonite. Rocks of the Kalgoorlie stock were described as subporphyritic to equigranular in texture by Arnold and Fitzgerald (1977). The plagioclase feldspar, in these rocks, is andesine in composition. The most common mafic mineral in rocks of the Kalgoorlie stock is pale green clinopyroxene; green hornblende and magmatic biotite were noted in some samples. Arnold and Fitzgerald (1977) commented on the presence of a particular type of clay that occurs in the rocks of the Kalgoorlie intrusion. This clay is described as forming discrete translucent patches with complete to mottled isotropism and appears to be secondary after mafic magmatic minerals. These authors interpreted this clay to have formed under mesogene or hypogene conditions rather than from supergene alteration, because it occurred at depth in otherwise fresh rock. Laboratory analyses of these clays (by Goode and Gilbert, 1976) indicated them to be montomorillonitic (smectites).

Katchan (1982) provided a good description of the intrusive rocks associated with skarn in the Gold Coast area. He characterized the area as being

part of the Sydney intrusion. It is, however located within the boundary of the Kalgoorlie intrusion as shown in the geologic maps of Arnold and Fitzgerald (1977). His dissertation included petrochemical information about the igneous rocks and their constituent minerals. He noted that his samples ranged over seven fields of the I.U.G.S. classification diagram and that the greatest density of samples was in the monzonite domain. However, he chose, to refer to the intrusive rocks using the term "monzodiorite". His data were portrayed on Harker variation diagrams and the ternary I.U.G.S. classification diagram. Microprobe analyses of feldspars, biotites, amphiboles, and pyroxenes were used to identify the magmatic pyroxenes as salite, magmatic amphiboles as edenite or magnesian hornblende, alteration amphiboles as actinolite and actinolitic hornblende, and the hydrothermal micas as phlogopitic.

Ningi Intrusion

The Ningi intrusion includes all intrusive rocks from the south boundary of the Kalgoorlie stock to the location of the Southern Dumps. Intrusive rocks south of the waste dumps have not been studied in detail so the southern boundary of this intrusion is unknown. Arnold and Fitzgerald (1977) and Arnold, Griffin, and Hodge (1979) described the rocks of the Ningi intrusion as altered and unaltered monzonite and quartz monzonite porphyries that were identical in appearance and mineralogy to the rocks of the Mt. Fubilan intrusion.

Undifferentiated Sydney Intrusion

The extent of intrusive rocks assigned to the Sydney intrusion has changed with additional information. Originally all intrusive rocks except for those of the Fubilan stock were considered to be Sydney Intrusion. It was subdivided into the Kalgoorlie, Ningi, and undifferentiated Sydney intrusions by further mapping including that of Arnold and Fitzgerald (1977). The undifferentiated part of the Sydney intrusion is shown as monzonite, syenodiorite, and diorite by Bamford and others (1972).

Age

Conventional K-Ar radiometric age determinations of samples of igneous rock from the Ok Tedi Intrusive Complex (Page and McDougall, 1972; Page, 1975) are listed in Table 1. Samples taken from the Sydney intrusion at Harvey Creek yielded K-Ar whole rock ages of 2.2 to 3 Ma, biotite ages of 1.1 to 1.5 Ma, and one hornblende age of 3.1 Ma. Samples taken from the Mt. Fubilan intrusion at Hong Kong yielded whole rocks ages of 1.1 to 1.2 Ma and one biotite age of 1.1 Ma. Radiometric dates derived from rocks of the Sydney intrusion were believed to represent unaltered phases and thus the results were considered to be emplacement ages. In contrast, Page and McDougall (1972), suggested that the radiometric ages

Sample	Intrusion	Location	K_2O wt. percent	Ages in million years Whole rock	Biotite	Hornblende
72-198	Sydney	Harvey Ck.	3.03	2.2	1.1	
72-199	Sydney	Harvey Ck.	2.99	2.5	1.2	
72-200	Sydney	Harvey Ck.	2.99	2.4	1.6	
72-201	Sydney	Harvey Ck.	2.99	2.5	1.5	
72-215	Sydney	Harvey Ck.				3.1
72-216	Sydney	Harvey Ck.	2.88	3.0		
72-202	Sydney	Harvey Ck.			1.4	
3010	Fubilan	Hong Kong	8.72	1.1		
6009	Fubilan	Hong Kong	4.53	1.2		
6012	Fubilan	Hong Kong	6.26	1.2		
6013	Fubilan	Hong Kong	5.86	1.2	1.1	

Table 1: Radiometric ages of rocks from the Ok Tedi Intrusive Complex (Page, 1975).

of rocks from the Mt. Fubilan intrusion indicated the age of hydrothermal alteration and not that of magma crystallization.

Alteration

Hydrothermal alteration has changed the mineralogy of most plutonic rocks of the area, but intense alteration is confined to the Mt. Fubilan stock and parts of the Ningi porphyry. In these locations potassic alteration is the dominant assemblage and is manifest by the presence of abundant secondary potassium feldspar, albite, and phlogopitic biotite. Importantly, the copper and gold ores mined at Ok Tedi are found in the rocks modified by potassic alteration. Low-intensity propylitic alteration is present in the rocks of the Kalgoorlie intrusion and throughout the "undifferentiated Sydney intrusion." This alteration type is characterized by the presence of actinolite, epidote, calcite, garnet, and, rarely, chlorite. Argillic alteration is associated with supergene alteration of the Fubilan stock, and was common in the leached capping that was removed during the initial phase of mining Au-rich ore.

Massive Ores and Skarns

Massive amounts of magnetite, pyrite, pyrrhotite, marcasite, chalcopyrite and chalcocite are present at several locations. These are the occurrences which

lead to the discovery of the Ok Tedi deposit and they collectively contained more than 50 million tonnes of ore. Gossans developed on these ores in the near surface environment by supergene processes. Skarns are also present, but these to date are of secondary importance in terms of contained metal and volume. All of these ores have generally been lumped together as "skarn" in scientific publications about Ok Tedi and in published ore reserve estimates. Here a distinction is made between: (1) massive ores which have specific gravities greater than 3.25 and which consist of 90 percent, or more, mixtures of magnetite and sulfide minerals with little or no associated skarn calc-silicates and (2) skarn characterized by the presence of garnet, pyroxene, or hydrous calcium aluminosilicates.

A review of typical ore grades of the main categories of ores at Ok Tedi is given in Table 2, The data in the table indicate the value of the categories of ore and the reasons for distinguishing between types. The massive ores, because of the high grade and high density, are considerably move valuable per truck-load than the porphyry or skarn ores. One cubic meter of sulfide porphyry ore contains, on average, 1.5 grams of gold and 2.5 kilograms of copper whereas an equivalent volume of magnetite-sulfide ore has 10.3 grams of gold and 11.7 kilograms of copper.

	Au	Cu	S.G.
	grams/tonne	wt. percent	
	Porphyry Ore		
Sulfide	0.61	1.01	
Mixed	0.50	0.72	2.49
Oxide	0.57	0.13	
	Skarn Ore		
	0.95	1.10	2.70
	Massive Ore		
Magnetite	1.48	1.27	3.93
Magnetite-Sulfide	2.92	3.33	3.52
Sulfide	1.89	2.88	3.93
Gosan	1.89	1.49	2.99

Table 2: Grades of the various types of ore from the Ok Tedi porphyry copper deposit.

The locations of major occurrences of massive ores (magnetite and/or sulfide) and skarns are portrayed in Figure 12. Some of the massive ores are associated with significant volumes of skarn (Gold Coast and Paris), but others (Edinburgh, New Glasgow, Sulphide Creek) do not contain important amounts of the typical skarn minerals (garnet, clinopyroxene).

The massive ore bodies at Ok Tedi are manifest in two contrasting styles based on morphology (Katchan, 1982; Duncan, 1972). One type is flat-lying in orientation and sheet-like or tabular in shape as shown in Figure 13A. The other type, shown in Figure 13B, consists of tabular or pipe-like bodies that dip steeply. Massive ore bodies of the flat-lying type appear to be controlled in location by the Purgatory (Taranaki) system of thrust faults. They are localized where thrust faults have juxtaposed Darai limestone over Ieru siltstone. Massive ore bodies that have steep dips may have formed by open space filling and replacement in zones of structurally broken rock such as within intrusive or contact breccias.

Massive ores at Ok Tedi are manifest in two contrasting styles based on morphology (Katchan, 1982; Duncan, 1972). One type is flat-lying in orientation and sheet-like or tabular in shape (Figure 13A). The other type occurs as tabular or pipe-like bodies that dip steeply (Figure 13B). Massive ore bodies of the flat-lying type appear to be controlled in location by the Purgatory (Taranaki) system of thrust faults. They are localized where thrust faults have juxtaposed Darai

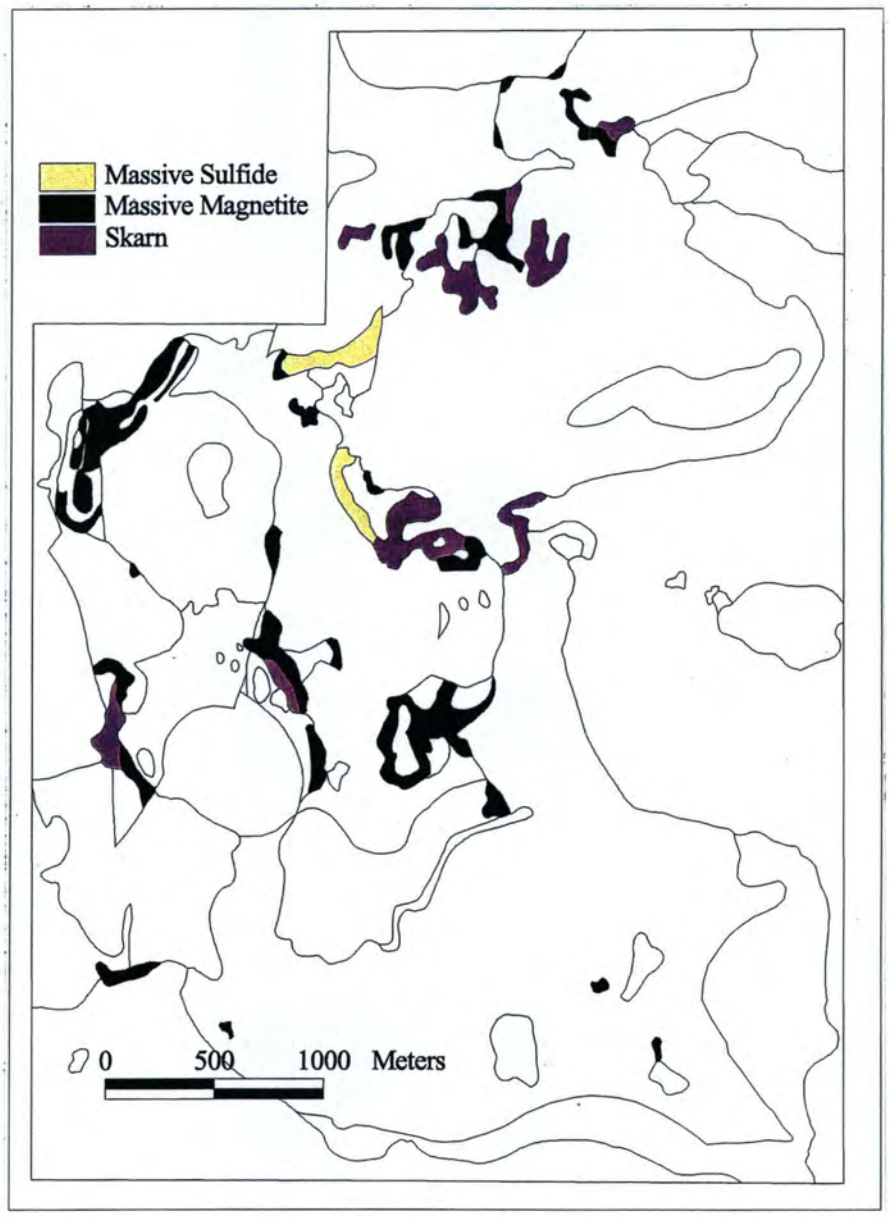

Figure 12: Location of major occurrences of massive magnetite, massive sulfide, and skarn in the area of the Ok Tedi Intrusive Complex. Simplified from Arnold, Griffin, and Hodge (1979).

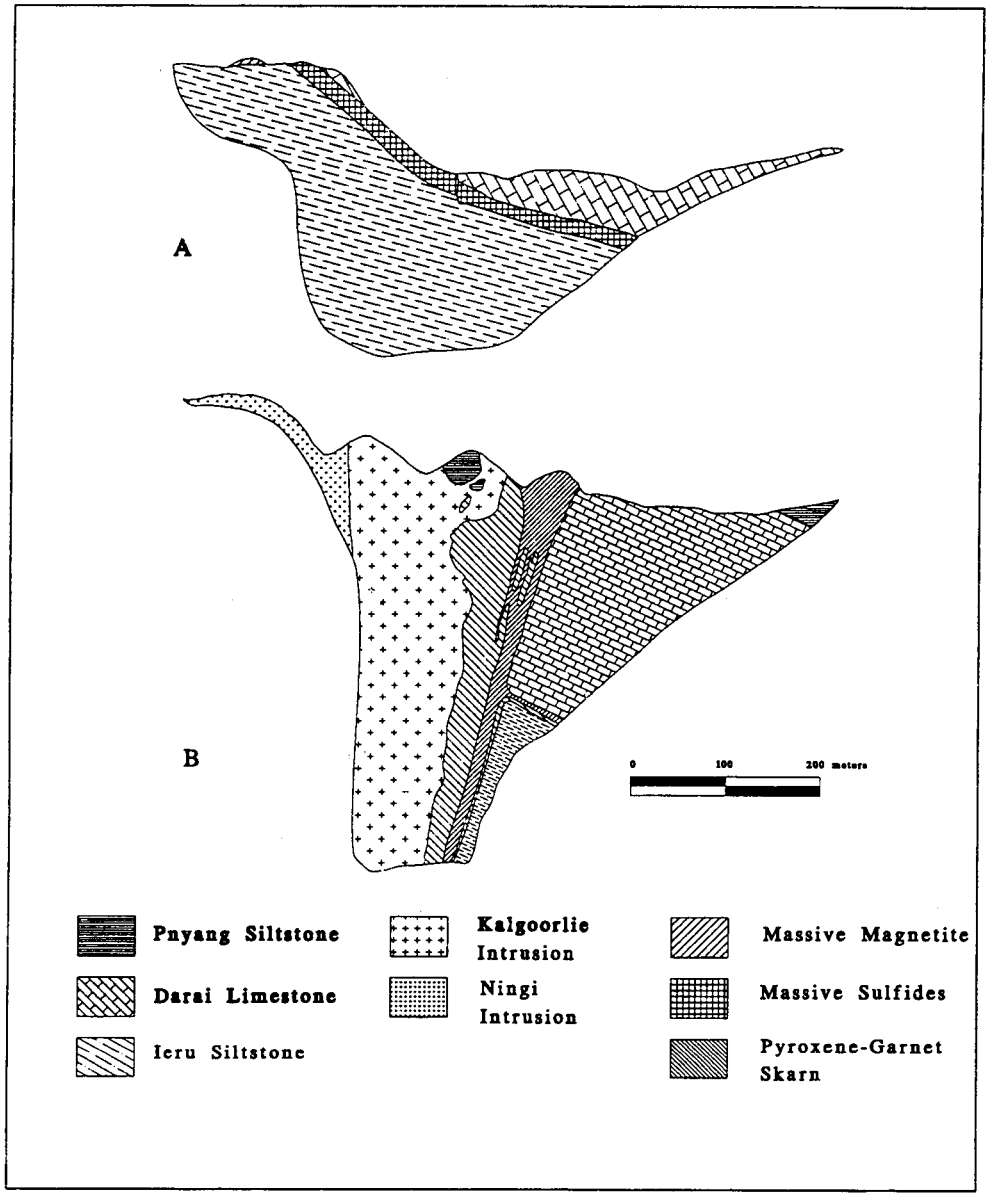

Figure 13: Generalized morphology of the two major types of massive ores at Ok Tedi (redrawn from Bamford and others, 1972: (A) flat-lying type. This example is of the Sulphide Creek "skarn." (B) Steep-dipping type. This example is of the Gold Coast skarn.

limestone over Ieru siltstone. Massive ore bodies that have steep dips may have formed by open space filling and replacement in zones of structurally broken rock such as within intrusive or contact breccias.

True skarns (as opposed to massive ores) are present in the Mt. Fubilan area at Paris, the Gold Coast, and Darien-East Cheam. Katchan (1982) noted that most of the skarns at Ok Tedi were endoskarns. Skarns formed from carbonate rocks (exoskarns) of the Darai Formation are difficult to locate or document; perhaps because the stratigraphic level at which the Ok Tedi Intrusive Complex is exposed today is largely within the Ieru Formation and most of the rocks that were above the Ieru have since been removed by erosion.

Garnets of grandite (grossular and andradite) composition and clinopyroxene of diopside-hedenbergitic composition are the dominant minerals in the Ok Tedi skarns. Retrograde assemblages of actinolite and epidote have replaced the earlier garnet-clinopyroxene skarns locally, and scapolite was noted in samples from a few locations.

Katchan (1982) and Duncan (1972) documented the presence of a spatial sequence of metasomatic zones in the Ok Tedi "skarns." The generalized sequence as developed by these authors consist of: 1) intrusion ± secondary biotite; 2) intrusion with montmorillonite alteration; 3) weak skarn alteration (called periskarn by Duncan, 1972); and followed by successive zones of 4) clinopyroxene; 5) garnet; 6) magnetite; and 7) marble or siltstone.

Duncan (1972) noted that "the planar nature of the magnetite limestone contact and the development of calc-silicate rocks on the intrusive side of the magnetite is in direct contrast to the 'porphyry-skarn' models based on deposits in the southwestern U.S. (Rose, 1970)."

Petrography and Lithology

Detailed petrographic examinations of standard thin- and polished-thin sections have been performed on 200 samples of porphyry and phanerite from the Ok Tedi Intrusive Complex. These samples collectively represent rocks of the Mount Fubilan, Kalgoorlie, and Ningi Intrusions (Bamford, 1972; Arnold, Griffin, and Hodge, 1979; and Arnold and Fitzgerald, 1977), and a part of the undifferentiated Sydney Intrusion (New Glasgow, New York, and Darien-East Cheam areas). The approximate locations of these samples are given on Plates 2 and 3, and Figures 14 and 15. The distribution of textural types is given in Figure 16.

All of the thin-sections described in this chapter are from intrusive rocks but many of the sample locations fall within the boundaries of sedimentary or metasomatic rocks as shown in Plate 1 (after Arnold, Griffin, and Hodge, 1979). This apparent inconsistency is due to the fact that the geologic boundaries shown are a two-dimensional representation of surface outcrops as mapped prior to 1976. Most of the samples, however, come from drill core and therefore from structural positions below the outcrops shown in Plate 1. Others come from areas where surface outcrops have been removed as part of the mining process and, therefore, from rock units that were not exposed at the time the maps were made. In addition it is important for the reader to keep in mind the fact that two samples that appear

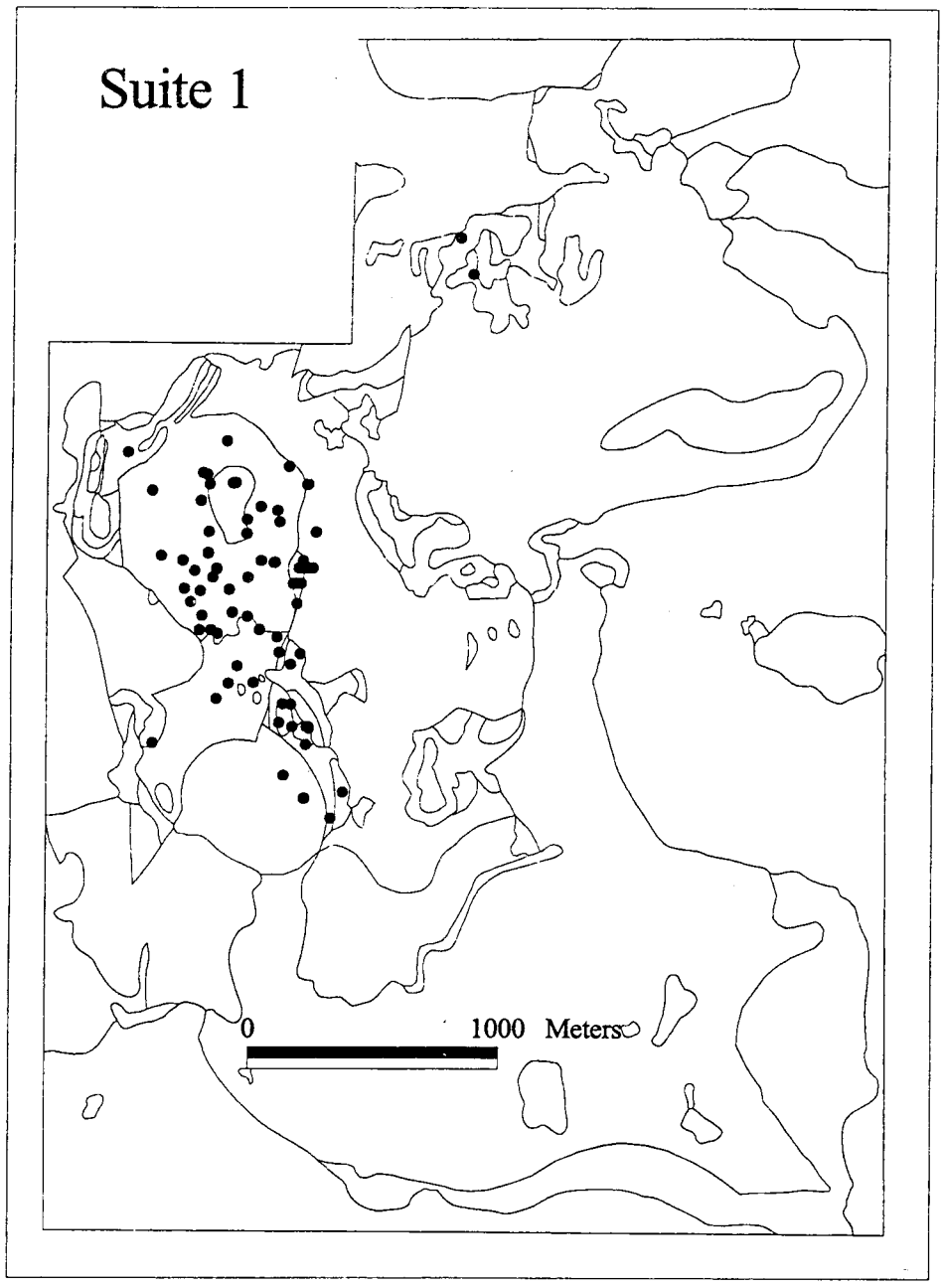

Figure 14: Locations of the petrographic samples of suite 1. The samples are identified by name in Plate 2.

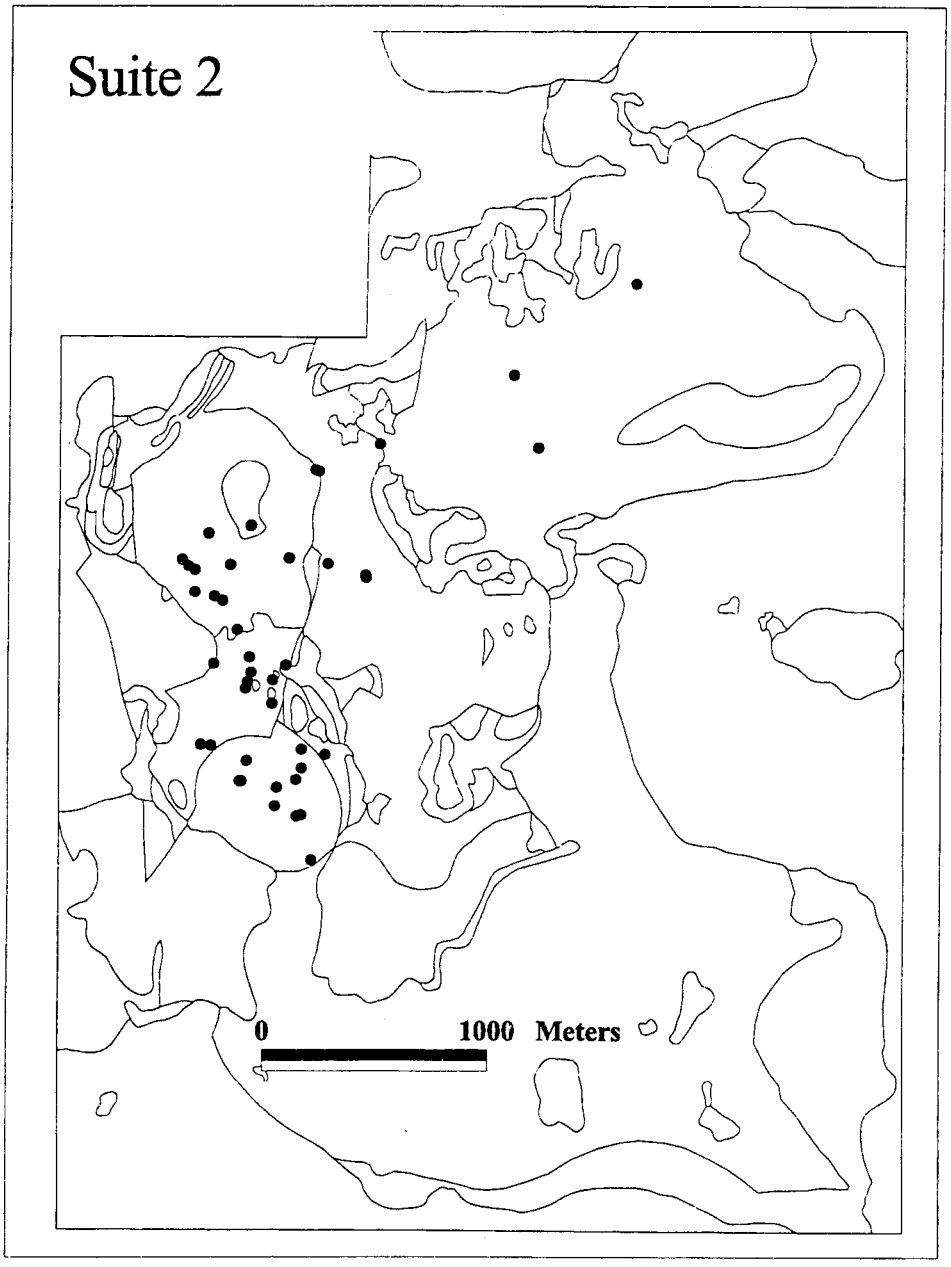

Figure 15: Locations of the petrographic samples of suite 2. The samples are identified by name in Plate 3.

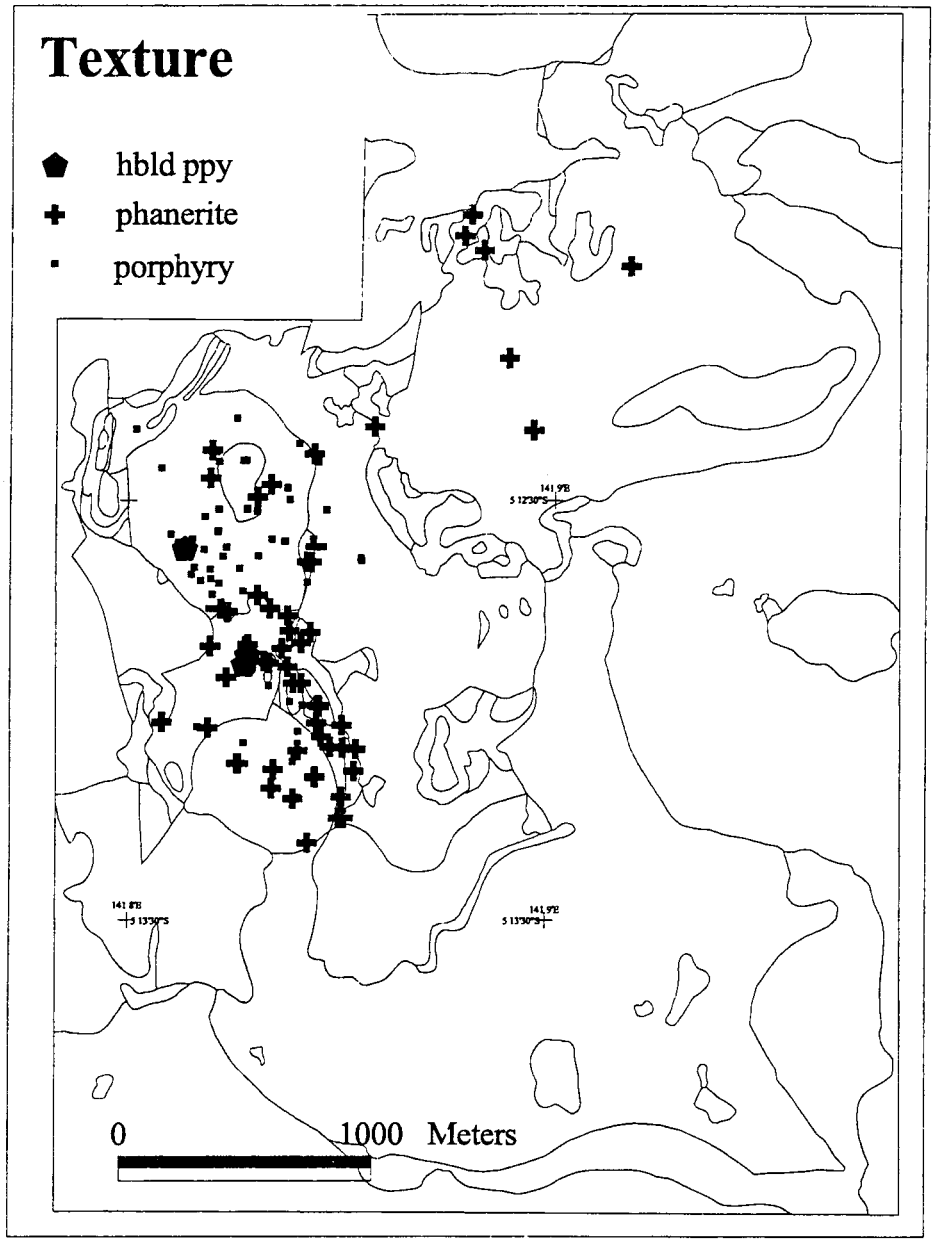

Figure 16: Map showing the distribution of porphyritic and phaneritic textures in samples from petrographic suites 1 and 2. The samples are identified by name in Plates 2 and 3.

to be in close proximity on a two-dimensional map may be separated by as much as two or three hundred meters in elevation. A list of the geographic coordinates for each sample (including northing, easting, and elevation) is given as Appendix 1.

Methods

A total of 410 thin- and polished thin-sections from the Ok Tedi Mine and adjacent areas were available for petrographic analyses. One hundred fifty four of the sections chosen for detailed examinations were selected from this collection. Another 46 polished thin-sections were selected from samples that I collected in 1994.

A photographic inventory of all thin-sections was prepared. The photographs portray the entire useable surface of the thin-sections. These photographs were used in conjunction with microscopy to select from all available samples those for later use in detailed analyses. The samples that were examined in detail, and that are discussed in this chapter, include phanerites and porphyries. Thin-sections of skarn, breccia, contact rocks, siltstone, and marble were not examined in detail. Samples in which the original textures were completely obliterated by clay, or other supergene minerals were also omitted from the examination set.

Detailed examinations included estimating mineral abundances, preparing lists of mineralogical and textural features, and making photomicrographs of

characteristic or unusual features. Estimations of mineral abundances were obtained by the point-counter method, and approximately one thousand points were counted in each thin section.

The petrographic analyses were done in two stages. The first stage was largely completed before my field work in January 1994. The suite of 154 thin-sections examined in this stage came from the thin-section collection of Ok Tedi Mining Limited and included samples taken from the beginning of exploration in 1969 to 1991. Hand specimens were not available for these samples. Modal data from this suite of samples are given in Appendix 2 and their locations are given in Figure 14.

The second stage of analyses included a suite of 46 polished thin-sections made from the samples that I collected in January of 1994. Modal data from this suite of samples is given in Appendix 3 and sample locations in Figure 15. The samples taken in this stage included sufficient material to provide thin-sections, archival hand specimens, and pulps for chemical analyses. This was necessary to insure that all microscopic and chemical analyses could be referred back to hand specimens representative of the actual rock samples. It was also important that chemical analyses be performed on precisely those samples that were examined using petrographic methods.

Petrographic and chemical study of the second stage also differs from the first stage by having been done in conjunction with microprobe analyses. This

approach was useful because I originally had found it difficult to optically distinguish between much of the plagioclase and potassium feldspar with any degree of confidence. It was also difficult to distinguish hornblende from pyroxene in most samples. These problems were caused by the fact that many crystals of plagioclase feldspar have oscillatory zones but lack albite twins, and because the optical properties of the hornblendes and pyroxenes in the samples from Ok Tedi are remarkably similar as both have olive-green pleochroism. The microprobe analyses alleviated these problems considerably, but not completely.

Reflected light microscopy was also used in petrographic studies of the polished thin-sections of the second stage to determine the identities and abundances of the opaque minerals. This had been impossible previously because the thin-sections of the first suite had cover slips.

Physical Properties

The physical properties that characterize the intrusive rocks from Ok Tedi are discussed here. These properties are: 1) texture, 2) grain-size, 3) color, 4) hardness, and 5) density.

All thin-sections examined in this study have porphyritic or phaneritic textures. The primary textures of a few samples could not be identified because of intense hydrothermal alteration. However, the primary texture of most samples could be readily distinguished, regardless of alteration intensity because

metasomatism took place by pseudomorphic replacements which seldom blurred textural or mineralogical relationships between phenocrysts and groundmass in porphyries or between adjacent crystals in phanerites.

Porphyritic textures are well-displayed in hand specimens characterized by intermediate to strong alteration, but are difficult to distinguish in the least altered porphyries. Phaneritic textures are difficult to distinguish in all samples. In contrast, primary textures are easily identified in thin-sections.

Two types of porphyritic intrusions were noted. Examples of the most common type, feldspar porphyry, are given as Figures 17 and 18. Hornblende porphyry as shown in Figures 19A-D is less common and apparently restricted to dikes. Hornblende porphyries also contain phenocrysts of feldspar but these do not stand out prominently in hand specimens. The crystals of hornblende in all available samples of the hornblende porphyry have been altered to biotite. Accordingly, these rocks in their present altered state are not strictly "hornblende porphyries."

Samples with phaneritic texture include some in which most crystals of feldspar are subhedral or euhedral as shown in Figure 20 and other samples in which most crystals of feldspar are subhedral or anhedral as shown in Figure 21. Phaneritic rocks with euhedral crystals typically contain more plagioclase feldspar than potassium feldspar. Conversely, most phanerites with subhedral or anhedral

Figure 17: Two examples of least-altered feldspar porphyry. These specimens consist predominantly of minerals formed by magmatic processes and display only traces of the minerals typical of propylitic alteration (actinolite, epidote, chlorite).

A. Rock slab. The porphyritic texture is difficult to see. Thin fractures with bleached selvedges cut across the slab. DDH 331-218.5. The surface portrayed is about 3 x 6 cm. in size.

B. Photograph of thin-section in polarized light. Phenocrysts of feldspar and pyroxene in aphanitic groundmass. Nearly the entire surface area of the thin-section is portrayed (about 2.4 x 3.6 cm.). DDH 331-21.8.5.

C. Photomicrograph displaying euhedral to subhedral phenocrysts of feldspar, pyroxene, and magnetite (white) in aphanitic to aplitic groundmass. DDH 331-218.5 The field of view is about 3 x 4 mm. Reflected light.

D. Same area of thin-section DDH 331-218.5 shown in C. The phenocrysts of feldspar are white, black, and gray in color; pyroxenes are red or orange; and magnetite is black. The field of view is about 3 x 4 mm. Crossed-polar light.

E. Rock slab. The porphyritic texture is easily visible in this specimen. Two thin fractures with associated limonite stains can be seen in the extreme right of the slab. DDH 464-9. The slab is about 3.8 x 8 cm in size.

F. Photograph of thin-section in polarized light. Phenocrysts of feldspar (white), void spaces (black), and fracture controlled limonite (orangish brown). DDH 464-9. Nearly the entire surface of the thin-section (about 2.4 x 3.3 cm.) is portrayed.

G. Subhedral to euhedral phenocrysts of feldspar (white), hornblende (green), magnetite (black) and sphene (crystals in center and lower right corner of photograph) in aphanitic groundmass. DDH 464-9. The field of view is about 4.2 x 6.5 mm. Plane-polarized light.

H. Same area of thin-section DDH 464-9 as in G. Crossed-polar light. The field of view is about 4.2 x 6.5 mm.

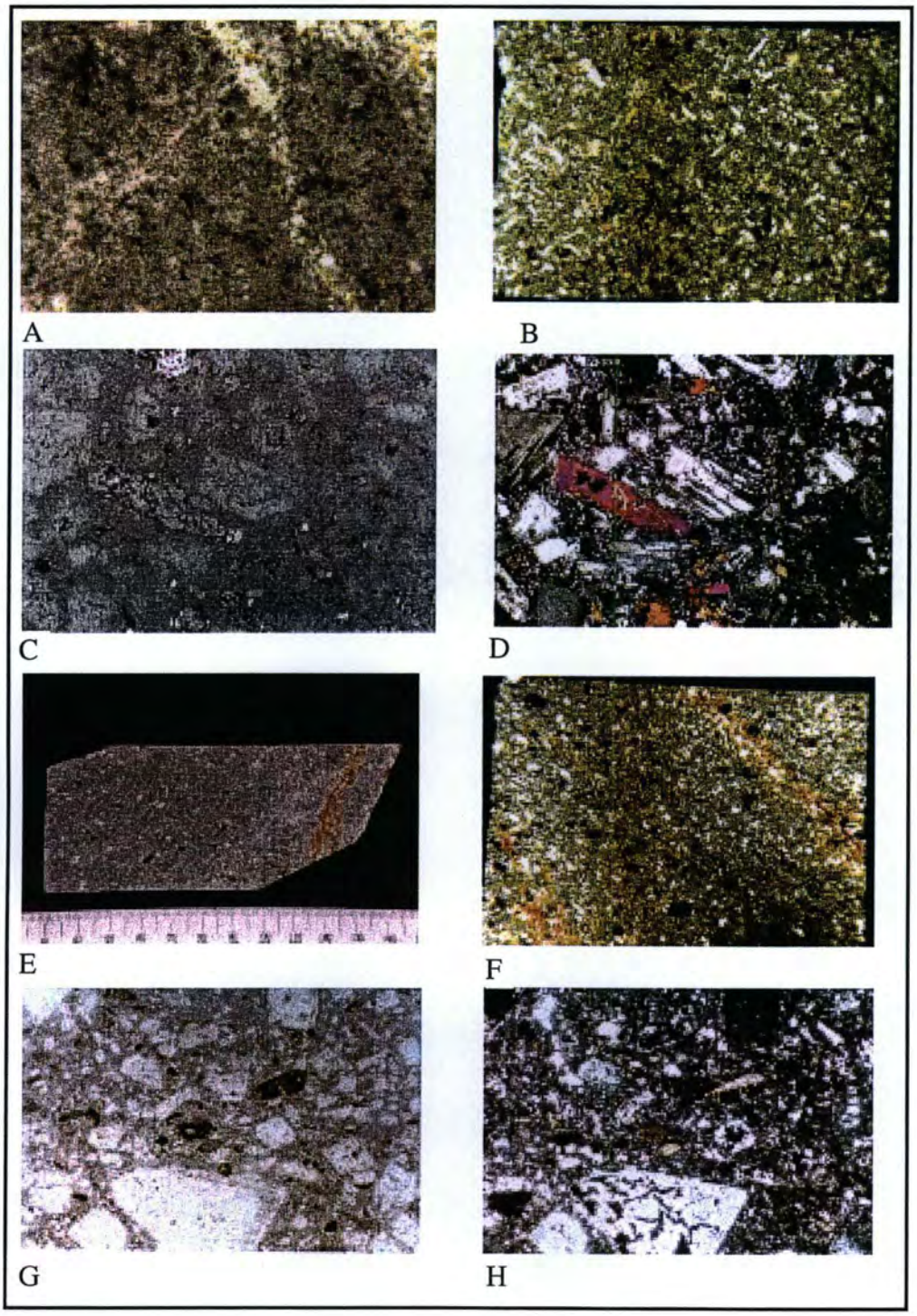

Figure 17 continued.

Figure 18: Two examples of intensely altered porphyry. These rocks have undergone strong potassic alteration.

A. Rock slab. The specimen displays easily noted porphyry texture consisting of white to pinkish gray phenocrysts of feldspar and black pseudomorphs of magnetite in the sites of previous existing ferromagnesian minerals. The right end of the slab is bluish-black in color due to finely disseminated hydrothermal magnetite. JDD-94-07. The slab is about 3 x 10 cm. in size.

B. Photograph of thin-section in polarized light. Phenocrysts of feldspar (white and gray) and hydrothermal biotite (orange) in aphanitic groundmass. Field of view is about 2.6 x 3.5 cm. JDD-94-07.

C. Photomicrograph of thin-section JDD-94-07. Subhedral to euhedral phenocrysts of potassium feldspar and albite. Also visible are several patches of anhedral hydrothermal biotite (particularly in lower right of photograph). The field of view is about 4.7 x 6.4 mm. Plane-polar light

D. Photomicrograph of same area of thin-section JDD-94-07 shown in C. The crystals of potassium feldspar are gray and white. Albite is can be recognized by its twinning lamallae. Crossed-polar light.

E. Rock slab. This specimen represents the most intense potassium feldspar alteration found at Ok Tedi. The rock surface is strongly pitted with void spaces and is weakly stained by limonite and manganese oxide(?). The surface shown in the photograph is about 3.5 x 5.5 cm. in size. DDH 302-69.

F. Photograph of thin-section in polarized light. Phenocrysts of feldspar (white and gray) and void spaces (black) surrounded by aphanitic groundmass. The entire surface area of the thin-section (about 2.5 x 3.6 cm.) is shown. DDH 302-69.

G. Photomicrograph of thin-section DDH 302-69. Phenocrysts of potassium feldspar in aphanitic groundmass. The surface of the thin section is pitted with void spaces (white). The field of view is about 4 x 6.3 mm. Plane-polar light.

Figure 18 continued.

H. Photomicrograph of the same area of thin-section DDH 302-69 shown in G. Subhedral to anhedral phenocrysts of potassium feldspar (gray and white) set in aphanitic groundmass. Noteworthy is the absence of phenocrysts displaying albite twins. Crossed-polar light.

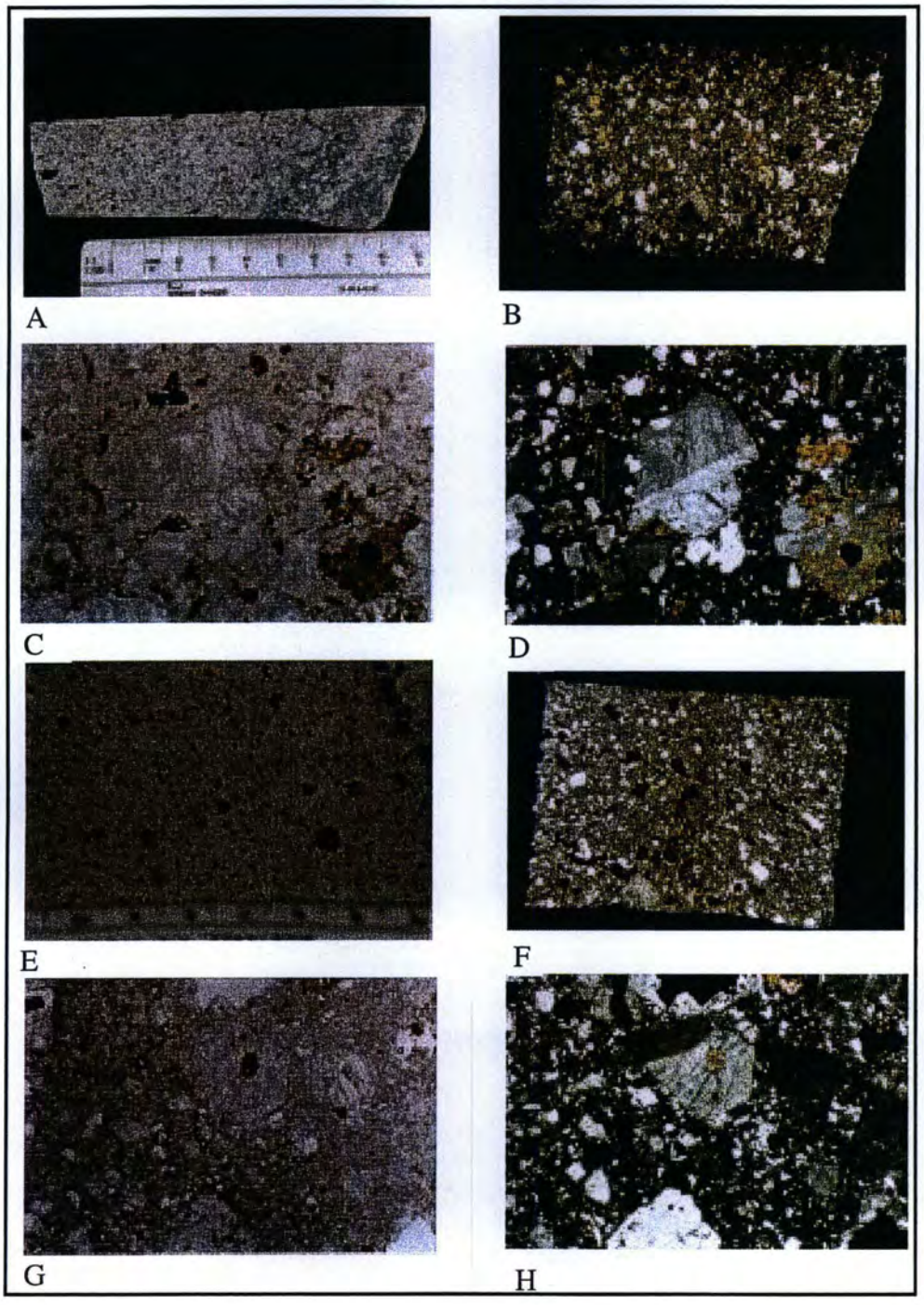

Figure 18 continued.

Figure 19: Two examples of feldspar-hornblende porphyry (A-D) and three examples of texturally destroyed rock with pseudomorphs of hydrothermal biotite after magmatic pyroxene, hornblende, or magmatic biotite (E-H). All of the rocks shown have undergone intense potassic alteration.

A Two rock slabs. One is about 7 x 7 cm. and the other 6 x 6 cm in size. Conspicuous phenocrysts of biotite after hornblende can be seen on the surface of both slabs. These phenocrysts attain diameters of about 0.5 cm. JDD-94-05.

B. Photograph of thin-section in polarized light. Phenocrysts of feldspar (white) and hydrothermal biotite pseudomorphs after hornblende are suspended in an aplitic groundmass of potassium feldspar and albite. The entire surface of the thin-section (about 2.3 x 4.5 cm.) is shown. JDD-94-05.

C. Rock slab. Porphyry with conspicuous phenocrysts of hydrothermal biotite after hornblende (black). JDD-94-19. The slab is about 4.5 x 7.4 cm. in size.

D. Photograph of thin-section in polarized light. Phenocrysts of feldspar (white) and biotite (orange) and void spaces (black) are visible in the photograph. JDD-94-19. Nearly the entire surface of the thin-section (about 2.2 x 4.2 cm.) is portrayed.

E. Two rock slabs. Porphyry with hydrothermal biotite pseudomorphs after magmatic ferromagnesian minerals. The identity of the original ferromagnesian mineral(s) are equivocal. The slabs are nearly white in color due to bleaching caused by hydrothermal alteration. DDH 302-125.15.

F. Rock slab. Porphyry with hydrothermal biotite pseudomorphs after magmatic ferromagnesian minerals. This rock is stained green by malachite and chrysocolla. A fracture with bleached selvedges can be seen cutting vertically across the middle of the slab. DDH 305-56.2.

G. Rock slab. Porphyry with hydrothermal pseudomorphs after magmatic pyroxene(?). The rock has been bleached by the alteration process. The slab is about 4 x 5 cm in size. JDD-94-01.

Figure 19 continued.

H. Photograph of thin-section in polarized light. The section is mottled with orange biotite after pyroxene(?) and associated limonite and smectite(?). The thin-section is about 2.5 x 3.5 cm. in size. JDD-94-01.

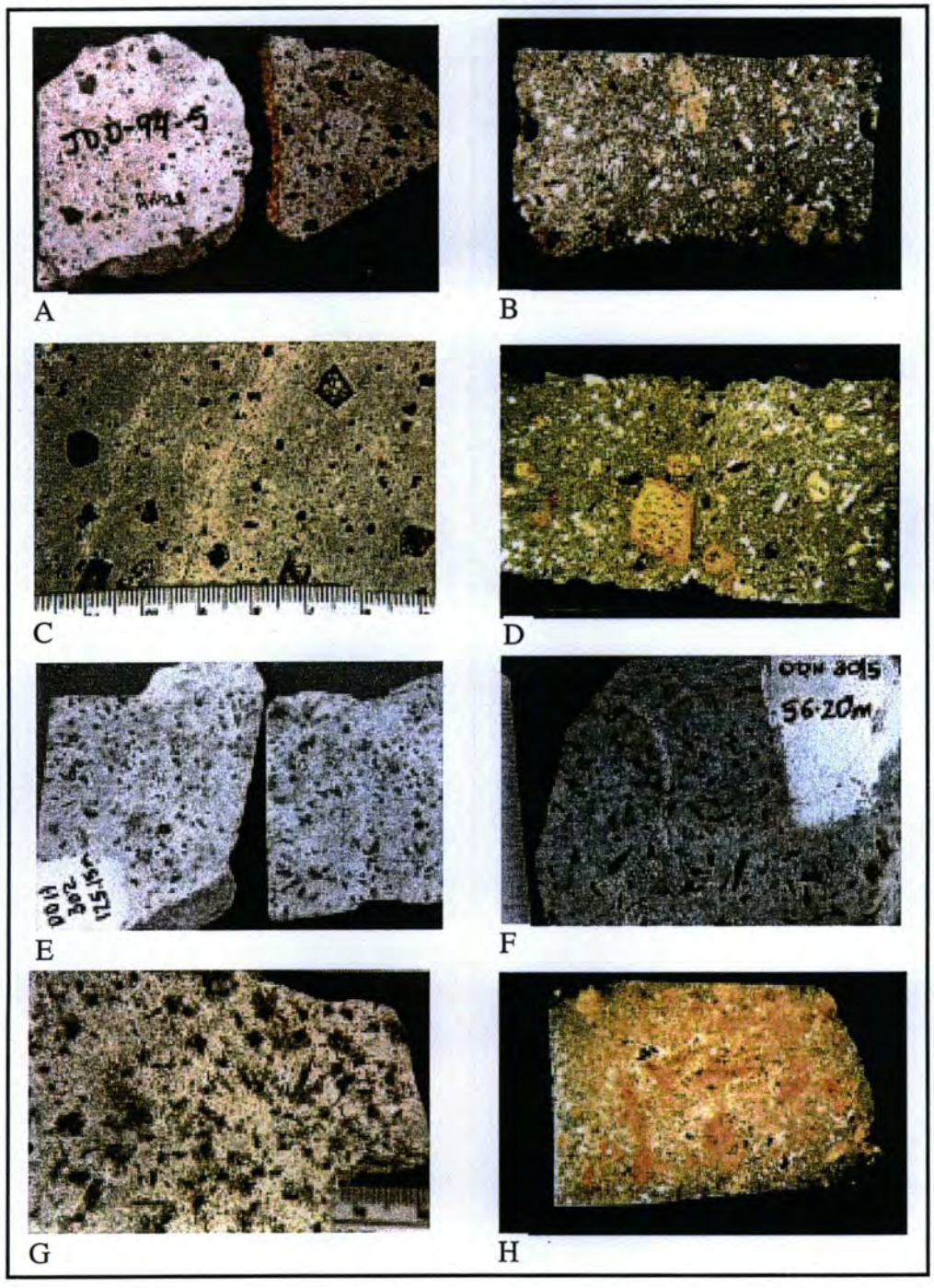

Figure 19 continued.

Figure 20: Two examples of samples with phaneritic texture and with andesine and potassium feldspar. These specimens are only weakly altered. They contain only traces of epidote, fibrous amphibole, or other minerals characteristic of propylitic alteration.

A. Rock slab. Subhedral to euhedral green crystals of pyroxene stand out against a background of plagioclase and potassium feldspar (gray). The rock surface is about 3.3 x 5.6 cm. in size. DDH 340-166.1

B. Photograph of thin-section in polarized light. Crystals of subhedral to euhedral feldspar (black, white, and gray), pyroxene (orange), and biotite (also orange) can be recognized. The entire surface area of the thin-section (about 2.3 x 3.8 cm.) is shown. DDH 340-166.1

C. Photomicrograph of thin-section DDH 340 -166.1. The sample consists mainly of plagioclase feldspar. One crystal of euhedral biotite is in the center of the photograph. Small subhedral phenocrysts of pyroxene and magnetite are scattered throughout. The field of view is about 4 x 6 mm. Plane-polar light.

D. Photomicrograph of the same area of thin-section DDH 340-166.1 shown in C. The subhedral to euhedral crystals of feldspar are andesine in composition. Small inconspicuous crystals of pyroxene are scattered throughout the photograph (blues and greens). Crossed polarizers.

E. Two rock slabs of phanerites which consist mainly of feldspar (light colors) speckled by pyroxene (dark colors). The surface of one of the slabs is about 6.5 x 6.5 cm; the other is about 2.2 x 5.5 cm. DDH 342-84.5

F. Photograph of thin-section in polarized light. The thin-section displays well developed phaneritic texture consisting predominantly of crystals of plagioclase and potassium feldspar (gray, black, and white) with lesser amounts of ferromagnesian minerals (orange). The entire surface of the thin-section (about 2.5 x 3.3 cm) is portrayed. DDH 342-84.5.

G. Photomicrograph of thin-section DDH 342-84.5. Subhedral to euhedral crystals of plagioclase and potassium feldspar, biotite (one

Figure 20 continued.

crystal near the center of the photograph), pyroxene (greenish gray, high relief), and magnetite (black). The crystals of orthoclase have frosted appearance and are gray in color whereas those of plagioclase feldspar have smooth surfaces and are white in color. The field of view is about 4 x 6 mm. Plane-polarized light.

H. Photomicrograph of the same area of thin-section DDH 342-84.5 shown in G. Crystals of plagioclase feldspar display albite twinning. Crystals of pyroxene are orange, red, and blue in color. Crossed-polar light.

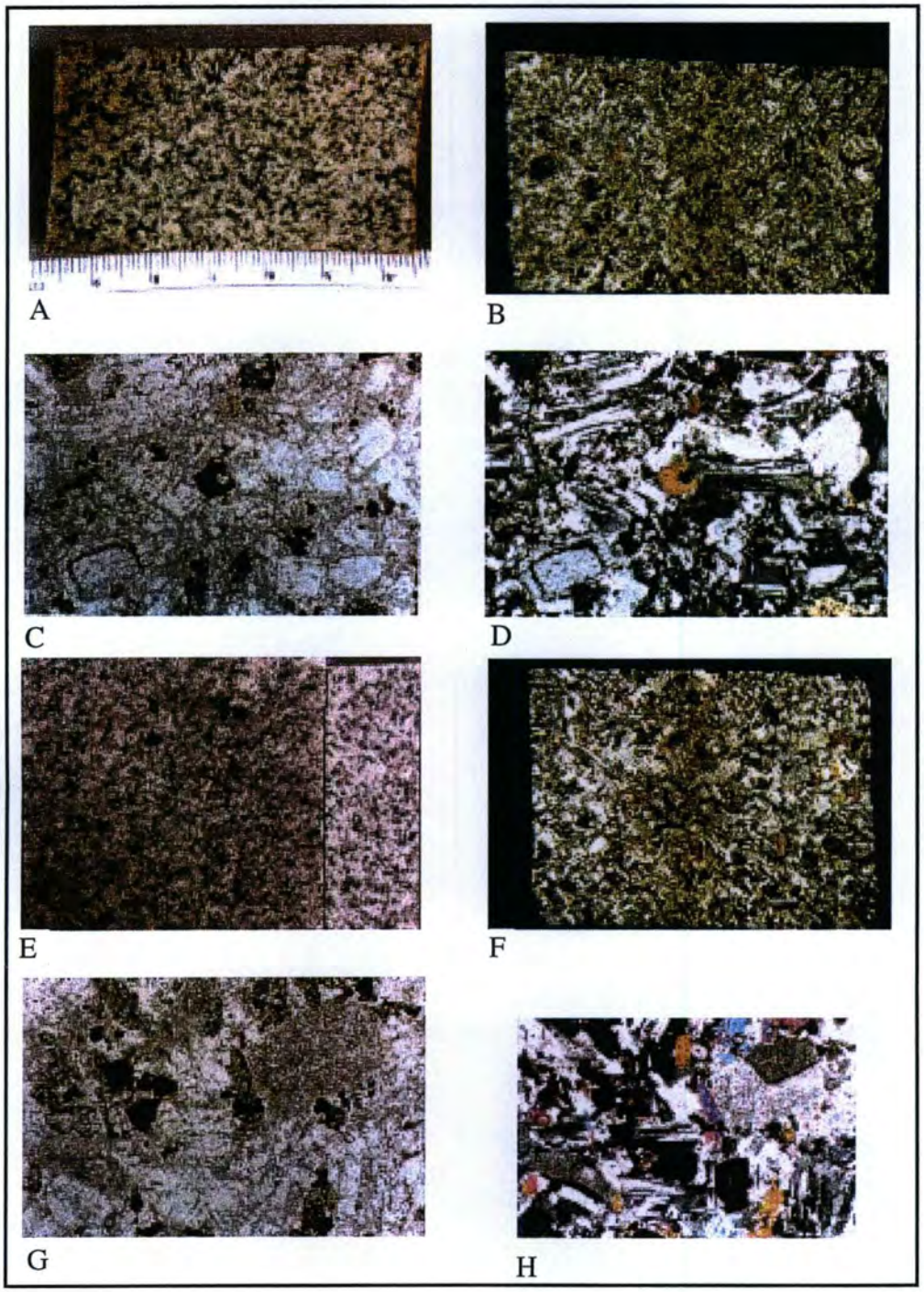

Figure 20 continued.

Figure 21: Two samples with phaneritic texture and that consist of albite and potassium feldspar. Extreme potassium feldspar and clay alteration. The only ferromagnesian mineral present is hydrothermal biotite.

A. Rock slab. The surface is pitted with pores in sites where ferromagnesian mineral existed prior to hydrothermal alteration. Black crystals of magnetite are scattered throughout the rock. The slab is about 2.8 x 5.5 mm. in size. DDH 407-257.6.

B. Photograph of thin-section in polarized light. Crystals of anhedral to subhedral potassium feldspar. The black areas are pores. Scattered anhedral crystals of hydrothermal biotite (orange). The surface is about 3.7 x 2.5 cm in size. DDH 407-257.6.

C. Photomicrograph of thin-section DDH 407-257.6. Anhedral crystals of potassium feldspar and interstitial quartz. The field of view is about 4 x 6 mm. Plane-polar light.

D. Photomicrograph of the same area of DDH 407-257.6 shown in C. The interstitial quartz can be more readily recognized in this photograph, which was taken with crossed polarizers, than in Figure 19C. Several anhedral crystals of hydrothermal biotite (orange) are visible.

E. Rock slab with heavily pitted surface (dark elongate areas). The pits contain hydrothermal biotite and crystalline quartz and mark the sites of that ferromagnesian minerals occupied prior to alteration. The orange mottling is localized in areas of clay altered feldspar. The slab is about 3.5 x 5.5 cm. in size. JDD-94-14.

F. Photograph of thin-section in polarized light. Sample consists predominantly of anhedral crystals of potassium feldspar and quartz. Lesser amounts of albite are present but not easily recognized. Black areas are void spaces. The thin-section is about 2.5 x 3.8 cm. in size. JDD-94-14.

G. Photomicrograph of thin-section JDD-94-14. Anhedral potassium feldspar (frosted surface) and interstitial quartz (smooth surface). Rectangular, T-shaped crystal near the center of the photograph is albite. The field of view is about 3 x 4.3 mm. Reflected light.

Figure 21 continued.

H. Photomicrograph of the same area of thin-section JDD-94-14 shown in G. Faint twinning can be seen two crystals of albite. Anhedral hydrothermal biotite (orange). Crossed-polar light.

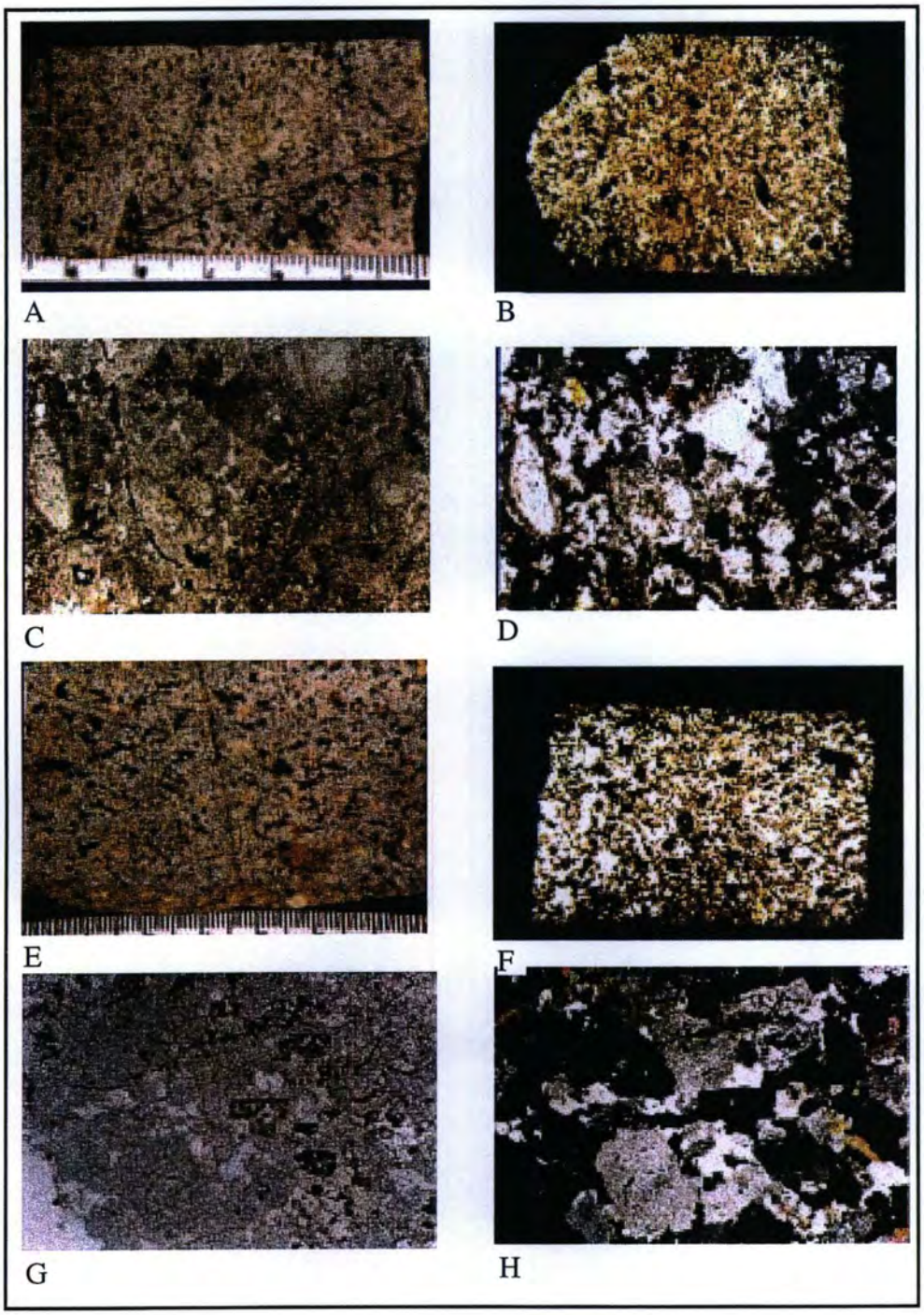

Figure 21 continued.

texture contain more potassium feldspar than plagioclase feldspar. This difference is caused by differences in petrogenesis - the samples with more euhedral crystals are of magmatic origin whereas those with more anhedral crystals have a metasomatic origin.

Phaneritic rocks from the Ok Tedi Intrusive Complex are medium in grain size (1 to 5 mm) as are phenocrysts in the plagioclase and hornblende porphyries. Samples of phanerites and plagioclase porphyries consist mostly of feldspar and this mineral is commonly the largest mineral present (the largest measured was about 7 mm in length).

Samples of fresh or propylitically altered phanerites or porphyries are dark to medium greenish gray in color because of the large abundance of their component ferromagnesian minerals. In contrast, samples that have undergone strong potassium feldspar or clay alteration are pale pinkish and yellowish gray to white because their dark-colored ferromagnesian minerals have been totally destroyed or hydrothermally altered to lighter colored phlogopite or clay and because of the overall bleaching effect caused by the conversion of plagioclase to potassium feldspar (± clay). Limonite stains were developed during supergene alteration and surface weathering and these stains have modified the color of many rock samples (chiefly to brown, orange, yellow, and red colors).

Almost all samples from the Fubilan intrusion have porphyry textures (Figure 16). Exceptions to this generalization include several samples from near

the contact with the Kalgoorlie intrusion, a few from near the southeast boundary of the Fubilan intrusion near its contact with the Ieru Formation, and four from areas near the quartz core (Bonn intrusion?).

Thin-sections from the Kalgoorlie and Ningi intrusions include a mix of phanerite and porphyry textures (Figure 16). In fact, it is difficult to characterize either of these intrusions as dominantly phaneritic or porphyritic based on the sample collections.

Samples from the Sydney intrusion come from only a portion of the rock mapped under this name (Figure 16). They were taken from the New York and Darien/East Cheam areas. All but one of the samples have phaneritic textures. One sample from DDH-331 has a porphyritic texture. It was collected at depth in a diamond drill hole beneath rocks with similar mineralogy but having a phaneritic texture.

Exposures in the upper levels of the Mount Fubilan Intrusion were incompetent (soft) as a consequence of tropical weathering. Early mining by free-digging with bulldozers was thus possible. The bedrock increased in strength and hardness with increasing depth in the deposit, however, and drilling and blasting became necessary when the top 50 or 100 meters of had been removed. Most clay-altered intrusive rocks are very friable and can be easily broken by hand. In contrast, those that are unaltered or that have been subjected to propylitic or

potassic alteration are hard and competent except were structural shattering or surficial weathering has occurred.

Igneous rocks from the Ok Tedi Intrusive Complex, and their metasomatically altered equivalents, vary in specific gravity (SG) from 2.23 for those strongly altered by potassium metasomatism to 2.70 for unaltered samples and those affected by propylitic alteration. Endoskarns, characterized by the presence of garnet or veinlets of magnetite, are typically denser than 2.70.

Because the rocks that have undergone strong alkali metasomatism consist almost entirely of albite (SG = 2.60) and potassium feldspar (SG = 2.5 to 2.6), it is unlikely that SG's below about 2.5 can be obtained simply by the observed mineralogical changes imposed by hydrothermal alteration. A plot of the specific gravities of the rock samples versus the percentage of void-space observed in thin-sections (determined by point counter analyses) is shown in Figure 22. The specific gravities of the samples exhibit a well-defined inverse correlation r = 0.68) with the amount of inferred void space. Accordingly, the decrease in specific gravity of the intensely altered rock samples is interpreted to reflect an increase in porosity rather than a decrease in densities of the constituent minerals.

Mineralogy

Plagioclase and potassium feldspar are the most abundant minerals in all of the intrusive rocks at Ok Tedi. This is as true for hydrothermally altered intrusions

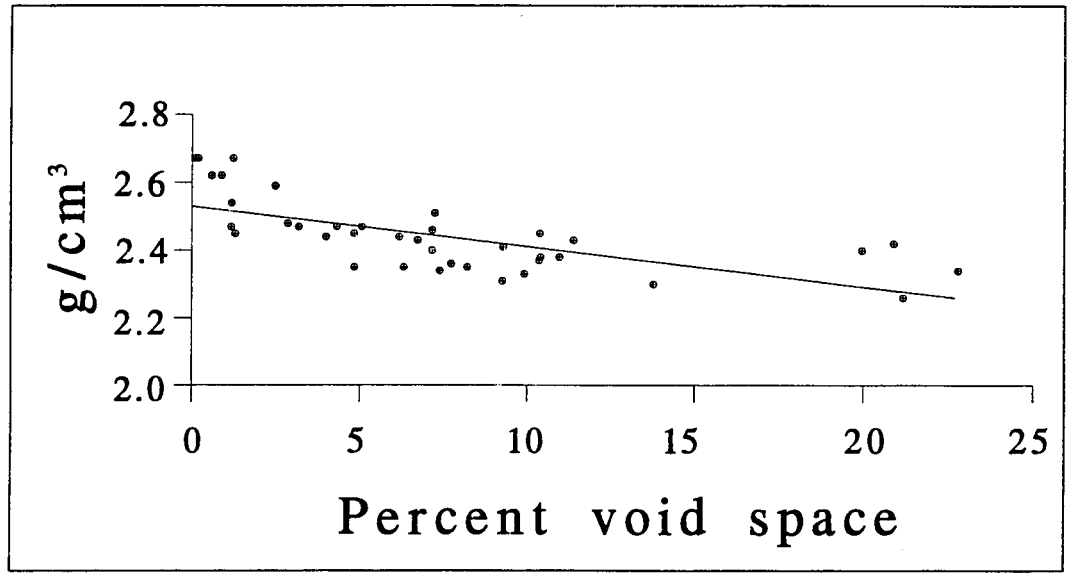

Figure 22: Plot of specific gravity versus void space (porosity).

as it is for unaltered rock. The feldspars comprise up to 80 volume percent, or more, of the phanerites and probably are similar in abundance in the porphyries. Pyroxene is the next most abundant mineral, comprising as much as nine volume percent, in most samples of unaltered rock but it is not present in rocks affected by potassic alteration. Hornblende is present in rocks from the Kalgoorlie, Ningi, and Sydney intrusions. Where present it never exceeds five volume percent in feldspar porphyry or rocks with phaneritic texture. It is a major constituent of hornblende porphyry dikes that cut the Fubilan and Kalgoorlie intrusions, but these are volumetrically insignificant. Quartz is a minor constituent in most thin-sections of unaltered rock. Its forms anhedral interstitial crystals in phanerites and is sparse as a phenocryst phase in porphyries. Veinlets with quartz as the major infilling gangue mineral cut across many samples and exposures of phanerite and porphyry. These veinlets are most abundant in and surrounding the quartz core. Magmatic biotite is common in many unaltered rocks with phaneritic and porphyritic texture. Relict magmatic biotite and finely crystalline aggregates of hydrothermal biotite are present in rocks that have undergone potassic alteration. Magnetite and sphene are common accessory minerals in unaltered intrusive rock as well as in propylitically altered rock, whereas various associations of chalcopyrite, pyrite, chalcocite, marcasite, pyrrhotite, bornite, molybdenite, and rutile are typically present in altered equivalents. Hydrothermal magnetite and sphene were noted in a few samples that have undergone potassic alteration, but, in general, these minerals do not seem to be

a part of the process of potassic alteration. They may have been deposited in an earlier or later stage of hydrothermal alteration than the alkali feldspars and biotite. Apatite and zircon are present in both altered and unaltered host rocks.

Mineral assemblages indicative of propylitic, potassic, and argillic alteration are common at Ok Tedi and in both suites of thin-sections examined as part of this study. Propylitic alteration is characterized by the presence of epidote, calcite, actinolite, and chlorite. One or more of these minerals are present in many samples from the Kalgoorlie, Ningi, and Sydney Intrusions but are rare, or entirely lacking, in the Fubilan Intrusion. Potassic alteration is typified by potassium feldspar and/or hydrothermal biotite. Virtually all rocks of the Fubilan Intrusion have been subjected to potassium feldspar alteration and most also contain hydrothermal biotite either as pseudomorphs after ferromagnesian minerals, disseminations, or in veinlets. In addition, potassic alteration is present locally within the Kalgoorlie and Ningi intrusions. Argillic alteration is also found at many locations. It is typically manifest as smectite in the propylitically altered rock and as halloysite in areas of potassic alteration. Samples with strong argillic alteration were not used in detailed petrographic examinations.

Feldspar

The thin sections chosen for detailed microscopy and microprobe analyses included samples with diverse textures and mineral assemblages. In terms of

feldspar assemblages, however, most samples fall into one of two major types: (1) igneous rocks that are unaltered or weakly altered, and (2) igneous rocks that have undergone moderate to strong potassium metasomatism. Rocks that are characterized by strong propylitic or endoskarn alteration, although certainly present at Ok Tedi, are relatively rare and were not selected for detailed study.

Six hundred seventy-three microprobe analyses were done on the feldspars in 21 polished thin-sections. Representative analyses are given in Table 3. The entire sets of analyses are given in Appendix 4. The chemical compositions obtained for the plagioclase feldspars in these rocks clearly indicate the mineralogical differences between rocks with andesine and those with albite. The least altered rocks contain plagioclase feldspars with microprobe determined compositions that range from anorthite to albite but with most analyses falling in the range from calcic-andesine to calcic-oligoclase (Figure 23). The plagioclase feldspars in rocks that have undergone potassic alteration range from sodic-oligoclase to near end-member albite in composition (Figure 24). In contrast to the strong chemical differences in plagioclase feldspars in rocks of magmatic and metasomatic origin, the potassium feldspar in magmatic assemblages is not significantly different in composition from that in rocks that have undergone

DDH No.	302	319	319	331	340	342	342	344	351	356	356	407	458	459
Depth m.	69	314.7	319.3	218.5	166.1	84.5	141	16	313.2	166.5	190	257.8	151.8	102.9
Plagioclase Feldspar														
Analyses		34	21	62	24	84	10	44	20	8	6	7	71	31
SiO_2		67.76	58.09	54.43	56.57	57.11	56.11	56.92	57.63	61.00	59.79	63.48	60.60	58.59
Al_2O_3		20.09	25.97	27.45	27.05	26.32	26.93	26.65	23.70	24.58	25.26	21.97	24.46	24.35
FeO		0.13	0.29	0.40	0.02	0.03	0.41	0.35	0.07	0.38	0.46	0.25	0.26	0.36
MgO		0.00	0.01	0.19	0.01	0.01	0.02	0.02	1.36	0.00	0.00	0.01	0.01	0.01
CaO		0.48	7.54	10.30	8.99	8.13	9.18	8.47	9.37	6.07	6.80	2.87	5.81	6.59
Na_2O		10.94	6.90	5.39	5.94	6.34	5.73	6.07	6.09	7.63	7.12	9.27	7.66	7.20
K_2O		0.36	0.31	0.29	0.45	0.58	0.42	0.77	0.31	0.40	0.38	0.60	0.53	0.53
SrO		0.00	0.00	0.00	0.00	0.00	0.00		0.00	0.01	0.00	0.00	0.00	0.00
BaO		0.01	0.05	0.04	0.03	0.06	0.03	0.09	0.03	0.04	0.02	0.07	0.05	0.02
Total		99.77	99.16	98.50	99.07	98.58	98.84	99.34	98.57	100.09	99.81	98.51	99.39	97.67
Ab		95.6	61.3	47.9	53.0	56.5	51.7	53.9	54.1	67.8	64.0	82.4	68.3	64.7
Or		2.1	1.8	1.7	2.7	3.4	2.5	4.6	1.8	2.3	2.3	3.5	3.1	3.1
An		2.3	37.0	50.4	44.3	40.1	45.8	41.5	44.1	29.9	33.8	14.1	28.6	32.2
Potassium Feldspar														
Analyses	18	13	1	4	5	8	2	8	7	4	1	10	3	14
SiO_2	65.10	64.70	62.76	62.59	63.83	62.51	63.38	63.24	64.13	65.31	61.73	62.98	66.59	63.96
Al_2O_3	18.94	18.99	20.04	19.48	18.92	19.34	18.51	19.52	19.10	18.84	18.42	19.29	18.56	18.79
FeO	0.08	0.07	0.26	0.18	0.02	0.02	0.14	0.21	0.02	0.20	4.14	0.15	0.18	0.12
MgO	0.00	0.00	0.00	0.01	0.01	0.01	0.00	0.01	0.00	0.00	0.04	0.00	0.01	0.00
CaO	0.04	0.06	0.85	0.34	0.24	0.51	0.07	0.28	0.17	0.10	0.51	0.18	0.52	0.09
Na_2O	2.32	2.43	2.08	2.79	1.86	2.91	1.07	3.69	2.21	2.40	3.28	3.15	3.61	1.92
K_2O	13.49	13.22	12.49	11.46	13.73	11.70	14.83	10.39	13.18	13.22	10.62	11.38	10.16	13.87
SrO	0.00	0.00	0.00	0.00	0.00	0.00	0.00		0.00	0.00	0.00	0.00	0.00	0.00
BaO	0.18	0.25	1.17	1.89	0.40	0.74	0.19	1.16	0.39	0.11	0.11	1.22	0.13	0.38
Total	100.15	99.72	99.65	98.72	99.01	97.73	98.18	98.48	99.21	100.18	98.85	98.35	99.76	99.13
Ab	20.68	21.72	19.32	26.51	16.84	26.67	9.85	34.68	20.16	21.57	31.12	29.67	34.28	17.28
Or	79.11	77.99	76.34	71.69	81.92	70.72	89.80	63.90	78.96	77.94	66.23	69.36	62.96	82.29
An	0.22	0.28	4.34	1.80	1.23	2.61	0.36	1.43	0.88	0.49	2.65	0.98	2.76	0.44

Table 3: Representative electron-beam analyses of feldspar.

Sample	JDD-94-03	JDD-94-04	JDD-94-05	JDD-94-07	JDD-94-11	JDD-94-12	JDD-94-14
				Plagioclase Feldspar			
Analyses	12	7	23	31	18	7	6
SiO_2	66.94	65.53	66.03	66.76	66.50	58.79	63.43
Al_2O_3	20.33	19.49	20.82	20.08	20.31	25.22	22.49
FeO	0.10	0.47	0.06	0.10	0.04	0.25	0.18
MgO	0.00	0.00	0.00	0.01	0.01	0.01	0.01
CaO	0.69	0.40	1.28	0.67	1.12	7.41	3.33
Na_2O	10.74	10.53	9.96	10.56	10.26	6.56	9.13
K_2O	0.36	0.31	0.98	0.32	0.33	0.40	0.39
SrO	0.00	0.00	0.00	0.00	0.00	0.00	0.00
BaO	0.01	0.00	0.01	0.01	0.01	0.02	0.01
Total	99.18	96.74	99.14	98.50	98.59	98.66	98.97
Ab	94.55	96.11	88.01	94.82	92.46	60.26	81.37
Or	2.08	1.83	5.75	1.89	1.97	2.41	2.27
An	3.36	2.07	6.24	3.30	5.57	37.33	16.37
				Potassium Feldspar			
Analyses	1	5	3	3	1		10
SiO_2	64.56	62.71	64.52	63.80	63.63		63.67
Al_2O_3	18.89	18.39	19.33	18.41	18.60		18.73
FeO	0.06	0.45	0.06	0.11	0.01		0.17
MgO	0.00	0.01	0.01	0.01	0.00		0.00
CaO	0.00	0.03	0.30	0.02	0.00		0.02
Na_2O	2.24	2.31	2.71	1.61	1.12		1.77
K_2O	13.76	12.91	12.56	14.23	15.17		14.05
SrO	0.00	0.00	0.00	0.00	0.00		0.00
BaO	0.03	0.35	0.16	0.09	0.13		0.33
Total	99.54	97.15	99.64	98.28	98.66		98.73
Ab	19.82	21.35	24.49	14.65	10.12		16.01
Or	80.18	78.49	74.02	85.25	89.88		83.88
An	0.00	0.16	1.49	0.10	0.00		0.11

Table 3 continued.

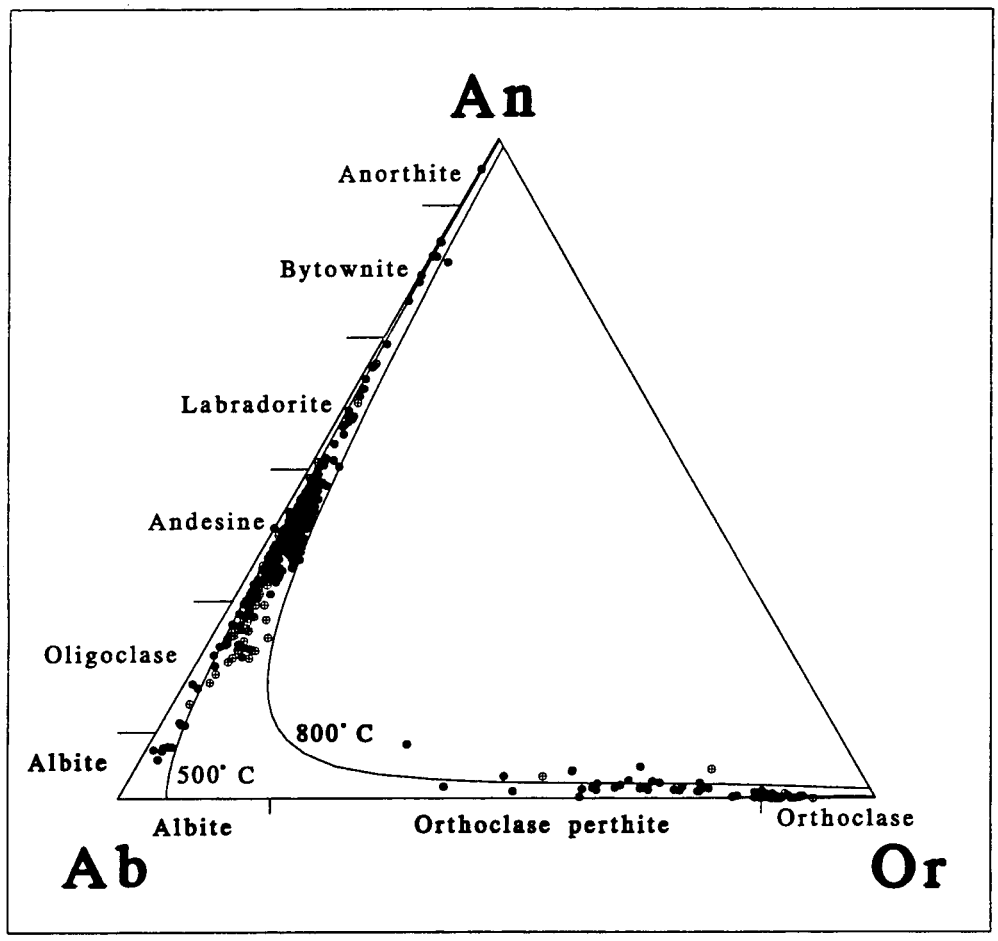

Figure 23: Ab-Or-An diagram of feldspars from least altered rock (i.e. samples with andesine-potassium feldspar association).

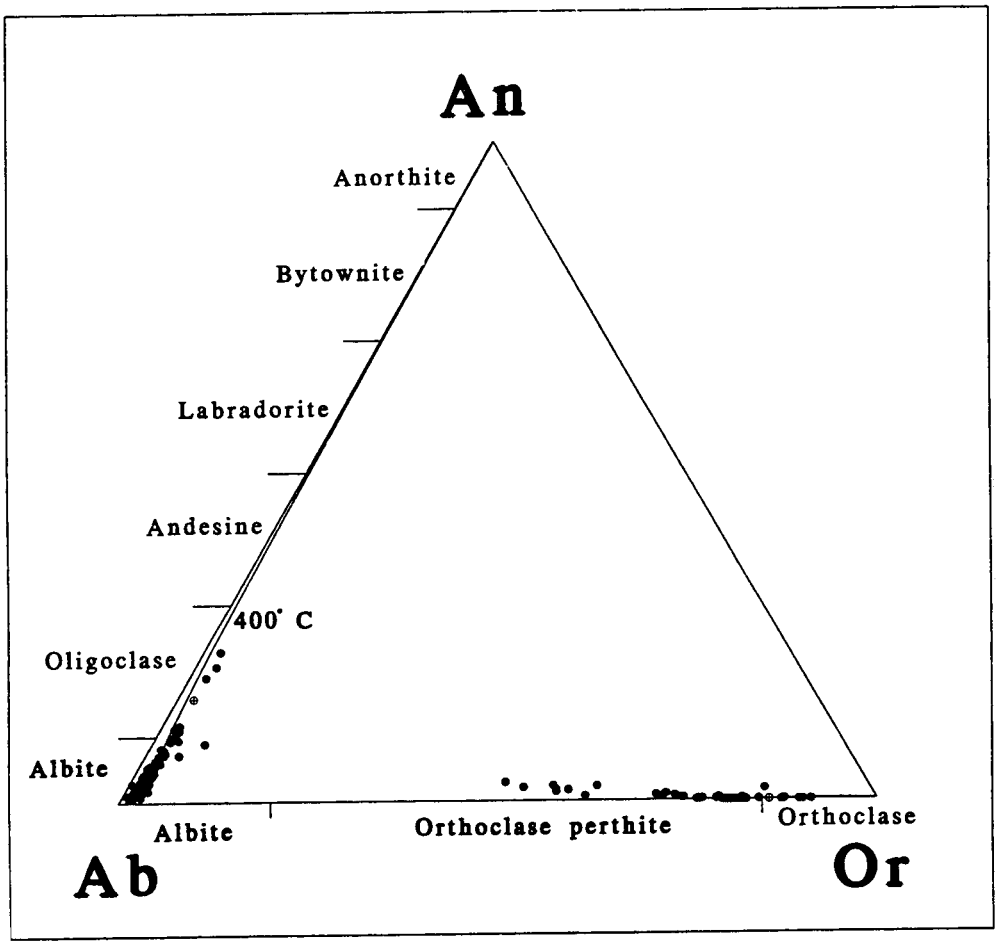

Figure 24: Ab-Or-An diagram of feldspars from potassically altered rock (i.e. samples with albite-potassium feldspar association).

potassium metasomatism. Potassium feldspar ranges in composition from Or_{90} to Or_{50} when in association with either andesine or albite (Figures 23 and 24).

Temperature curves based on calculations using the SOLVCALC program of Wen and Nekvasil (1994) are shown on these Figures 23 and 24. The curves shown on each diagram were calculated using analytical data (Ab-Or-An contents) of coexisting plagioclase and potassium feldspars. A pressure of one kilobar was assumed but the positions of the curves were not found to be strongly dependant on pressure. The curves chosen probably represent reasonable ranges of temperatures for primary magmatic crystallization (andesine-potassium feldspar) and hydrothermal alteration (albite-potassium feldspar). The compositions of feldspars of andesine-potassium feldspar association fall between the curves for 500 and 800° C and represent the temperatures of magma solidification. The feldspars in the plot of albite-potassium feldspar association were formed at temperatures below 400° C. Curves for temperatures below 350° C were not calculated because the method used is not considered to be accurate at these temperatures.

Feldspar displays a spectacular diversity in texture and internal structure in the unaltered igneous rocks of the Ok Tedi Intrusive Complex and their altered equivalents. Specific features that merit elaboration include: twins, growth zones, synnuesis, resorption, crystal shapes, replacement textures, and inclusions. The crystals of feldspar in phanerites and the phenocrysts in porphyries range in longest

dimension from about one to three mm on average and attain lengths of approximately 7 mm in a few of the examined thin-sections

Albite twinning is characteristic of plagioclase feldspars and is present in all but the most potassically altered rocks. Most crystals with albite twins display many narrow and sharply defined lamellae when viewed in cross-polarized light (Figures 25A and B); others show only a few lamellae that are diffuse in detail (Figure 25C) and yet others are defined by two sets of lamellae that are oriented nearly perpendicular to one another (Figure 25D). All feldspars that have lamellae are called "polysynthetically twinned feldspar" in point counter analyses and are listed as "PST feldspar in Appendices 2 and 3."

Plagioclase feldspars with oscillatory zones are equal, or greater, in abundance than those with albite twins in many thin sections. Many zoned crystals display concentric patterns of zones (Figures 25E-H) that go to extinction sequentially from rim to core as the microscope stage is rotated between crossed polarizing filters. Others with oscillatory zones have more complex extinction patterns. All crystals of plagioclase with oscillatory zoning are described in petrographic examinations as "CZ (concentrically zoned) feldspar" and are listed as such in Appendix 3 (this category was not counted separately in Suite 1 analyses).

Crystals of plagioclase feldspar with twins are not significantly different in composition from those with oscillatory zones. The average anorthite content of

Figure 25: Examples of albite twinning and oscillatory zoning in plagioclase feldspar.

A. Elongate phenocryst of plagioclase feldspar with narrow and sharply defined albite twins. The field of view is about 2 x 3.2 mm. Crossed-polar light. DDH 318-246.7

B. Rectangular phenocryst of plagioclase feldspar with narrow and sharply defined albite twins. The field of view is about 1.6 x 2 mm. Crossed-polar light. DDH 303-350.55

C Phenocryst of plagioclase feldspar with broad and diffuse albite twins. The field of view is about 1.0 x 1.6 mm. Crossed-polar light. DDH 316-314.7

D. Phenocryst of plagioclase feldspar which displays two directions of albite twins that are oriented nearly 90 degrees to each other. The field of view is about 0.8 x 1.2 mm. Crossed-polar light. DDH 356-190

E. Diffuse oscillatory zones in crystal of plagioclase feldspar. Only a few zones can be seen. The field of view is about 0. 7 x 1.0 mm. Crossed-polar light. DDH 356-166.5

F. Oscillatory zones in crystal of plagioclase feldspar. Many zones can be seen in this crystal. The zones are roughly concentric in orientation. The field of view is about 0.4 x 0.6 mm. Crossed-polar light. DDH 342-84.5

G. Oscillatory zones and synnuesis twinning in crystal of plagioclase feldspar. The twinning pattern includes a broad central zone surrounded by a narrow peripheral area with multiple zones. The field of view is about 0.7 x 1.0 mm. Crossed-polar light. DDH 331-218.5

H. Multiple oscillatory zones in crystal of plagioclase feldspar. The crystal is about 1.3 x 2 mm in size. DDH 342-84.5.

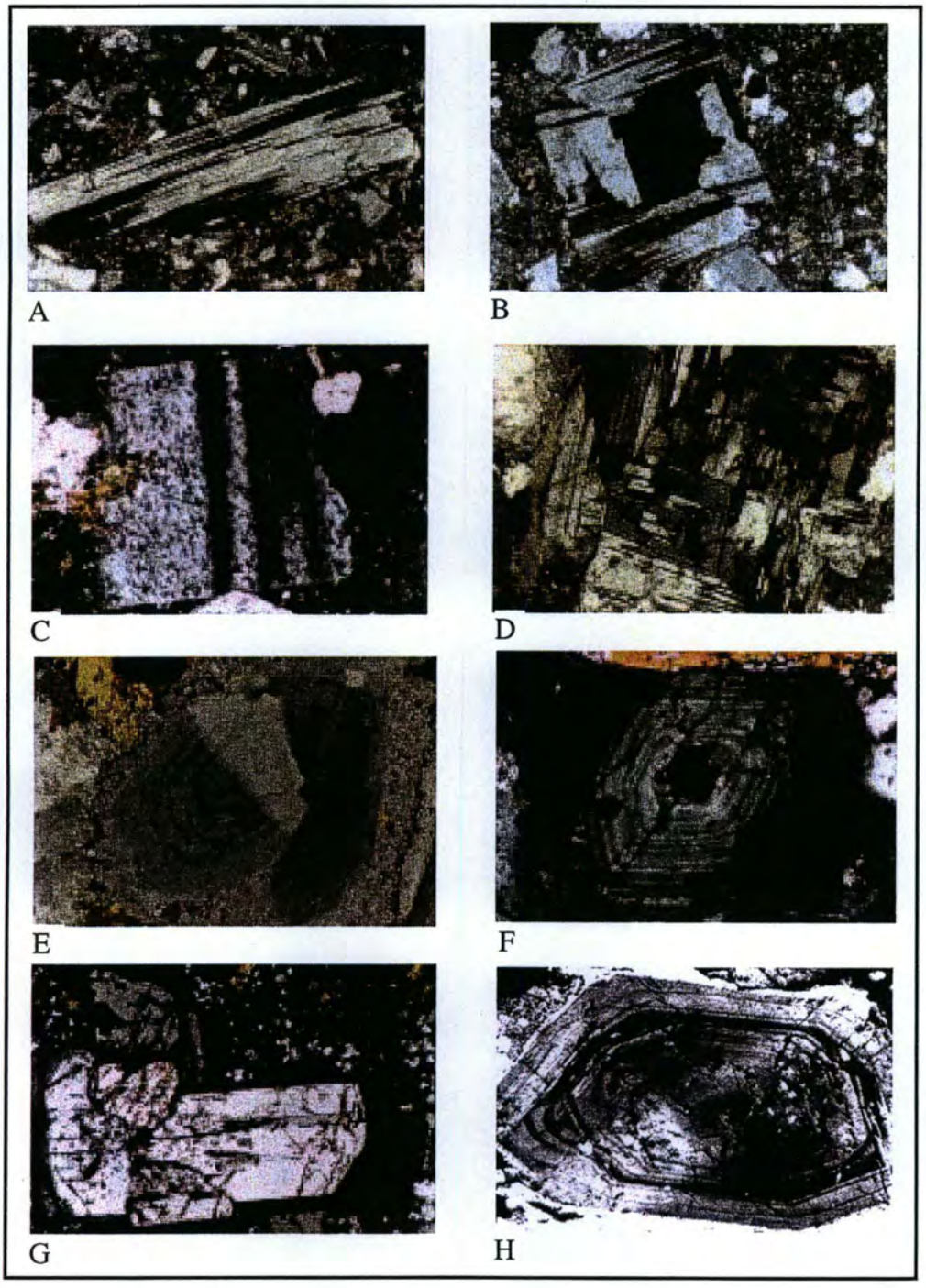

Figure 25 continued.

both twinned and zoned crystals from unaltered or weakly propylitically altered phanerites and porphyries is about An_{40} whereas that of the crystals in porphyries that have undergone strong potassic alteration is about $An_{2.5}$ (not enough analyses were available from potassically altered phanerites for comparison).

Many crystals of plagioclase feldspar exhibit complex growth patterns. Glomerocrysts consisting of synnuesis twins (Vogt, 1921; Vance, 1969) and other forms of crystal coalescence are common. An example, shown in Figures 26A and B, consists of two intergrown phenocrysts of plagioclase feldspar. One phenocryst has two internal resorption surfaces indicating that it had at least three periods of growth, and that it was resorbed at least twice (A and B in Figure 26B).

Potassium feldspar is a common mineral component in thin-sections of porphyritic and phaneritic texture. It is generally subhedral to euhedral in shape in the least altered rocks and in those that have undergone propylitic alteration. A typical example of euhedral potassium feldspar from a sample of phanerite is shown in Figure 26C. Pseudomorphs of potassium feldspar after plagioclase feldspar are characteristic of the rocks that have undergone potassic alteration and these commonly reproduce the subhedral or euhedral shapes of their magmatic plagioclase precursors. In contrast, a few samples of potassically altered phanerites from the Kalgoorlie and Ningi intrusions were found to consist mainly of anhedral crystals of potassium feldspar (Figures 21C and D, and 21G-H).

Figure 26: Example of resorption surfaces within a crystal of plagioclase feldspar (A-B). Photomicrographs of magmatic potassium feldspar in some of the least altered rocks from the Ok Tedi Intrusive Complex (C-F). Mantles of magmatic potassium feldspar on crystals of plagioclase feldspar (G-H).

A. Photomicrograph of two crystals of plagioclase feldspar joined along a common face. One of these has two internal resorption boundaries dividing it into three growth sectors (A, B, C Figure 26B). The outermost of these has a thin oscillatory zone at its outer edge Crossed-polar light. The crystal cluster is about 1.6 x 2.2 mm. in size. DDH 319-339.3

B. Sketch of the crystals of plagioclase feldspar shown in A. DDH 319-339.3

C. Euhedral crystal of potassium feldspar in an andesine-potassium feldspar phanerite. The crystal shows the typical frosted surface and uniform gray color of potassium feldspar. Several subhedral or euhedral crystals of pyroxene abut against the crystal. The field of view is about 1.7 x 2.2 mm. Crossed-polar light. DDH 342-84.5.

D. Poikilitic texture. Chadacrysts of pyroxene and plagioclase feldspar enclosed in oikocryst of potassium feldspar. This texture is magmatic in origin. The field of view is about 3 x 5 mm. Crossed-polar light. Ok Tedi 1009.

E Large single crystal of potassium feldspar. This crystal is among the largest found in suites 1 and 2 of petrographic analyses. Growth zones approximately parallel to the crystals faces can be seen within the crystal. Alternatively this texture may be metasomatic. The field of view is about 4.7 x 7 mm. Plane polar light. DDH 303-243

F Same phenocryst of potassium feldspar shown in E. Crossed-polar light. The crystal contains several inclusions of plagioclase feldspar. These inclusions are aligned along growth zones within the crystal of potassium feldspar or they may represent unreplaced portions of a partly replaced feldspar of metasomatic origin.

G Crystal of plagioclase feldspar overgrown by mantle of potassium feldspar. Both are euhedral in shape and are elongated in the same

direction. This texture is magmatic in origin. The field of view is about 2.4 x 3.5 mm. Crossed-polar light. Ok Tedi 37.

H Crystal of plagioclase feldspar cut perpendicular to its "c" axis. The core of the crystal displays a mottled extinction whereas the rim displays even extinction. It is enclosed by interstitial potassium feldspar on three sides and is in contact with an elongate section of plagioclase on the forth. These minerals are of magmatic origin. The field of view is about 1.4 x 2.0 mm. Crossed-polar light. Ok Tedi 1009.

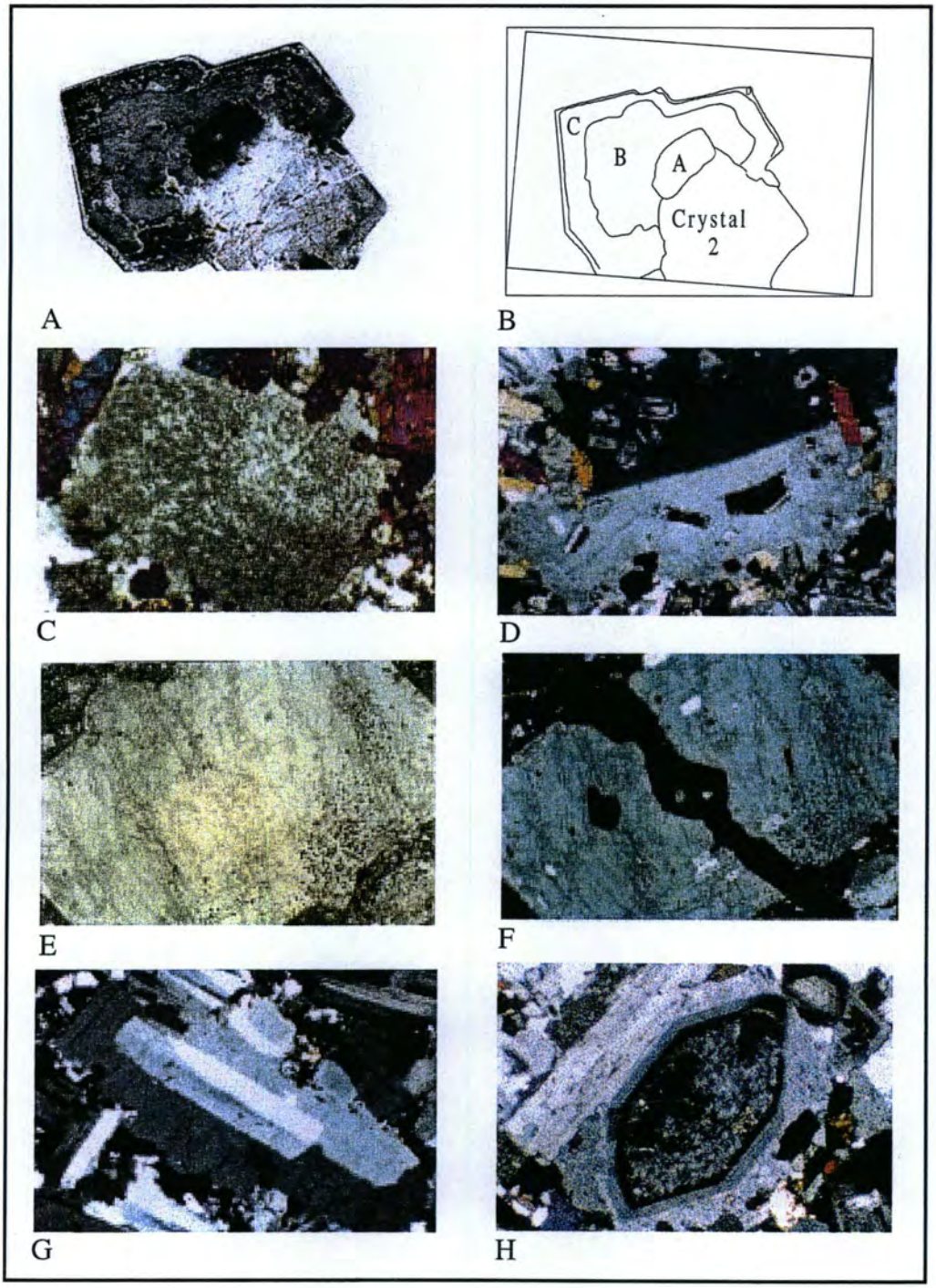

Figure 26 continued.

Poikilitic textures consisting of chadacrysts of plagioclase feldspar and pyroxene enclosed by oikocrysts of potassium feldspar are common in phaneritic rocks. A good example is shown as Fig 26D. Large (> 5mm) crystals of euhedral potassium feldspar with inclusions of plagioclase feldspar that are aligned along internal growth zones are illustrated in Figures 26E and F. This texture suggests that potassium feldspar was actively forming up to the completion of magmatic crystallization or may represent metasomatic replacement.

Crystals of plagioclase feldspar with mantles of potassium feldspar are common in the least altered samples of phaneritic rock (Figures 26G and H). The mantles of potassium feldspar are magmatic in origin and result from the late stage growth of potassium feldspar into the void spaces between earlier formed plagioclase feldspars. In contrast, other examples of plagioclase feldspar with rinds of potassium feldspar are present only in strongly altered rocks. These rinds are not formed by overgrowth but rather by hydrothermal replacement which has progressed from the rims inward. A variety of crystals consisting partly of plagioclase feldspar and partly of potassium feldspar are shown in Figure 27A-D. These crystals represent arrested stages in the pseudomorphic replacement of plagioclase by potassium feldspar. From observations of such textures, it is possible to infer that many crystals of potassium feldspar in potassically altered rock were originally of plagioclase before hydrothermal alteration ensued.

Figure 27: Rinds of hydrothermal potassium feldspar on plagioclase feldspar (A-D). Near total replacement of plagioclase feldspar by potassium feldspar (F-G).

A. Euhedral crystal of plagioclase feldspar in potassically altered porphyry. A thin rind of potassium feldspar has replaced the outer rim of the crystal. The field of view is about 2.3 x 3.4 mm. Crossed-polar light. DDH 318-246.7

B. Three crystals showing varying degrees of replacement. The one on the right displays only a thin rind which does not extend around the entire perimeter of the crystal. Approximately half of the central crystal has been replaced - a central core with ragged outer boundary is surrounded by an outer pseudomorph of potassium feldspar after plagioclase feldspar. Potassium feldspar has nearly entirely replaced the crystal of plagioclase in the lower left part of the photograph - only tiny remnants of plagioclase remain (weak sieve texture). The field of view is about 3.4 x 2.3 mm. Crossed-polar light. DDH 318-246.7

C. Rectangular phenocryst of plagioclase feldspar that has been partly (about two-thirds) replaced by pseudomorphic potassium feldspar. The field of view is about 0.8 x 1.2 mm. Crossed-polar light. DDH 303-243

D. Phenocryst of partly replaced plagioclase feldspar that displays albite twins in its core. The right side of the crystal has either: (1) never been replaced, or (2) been broken subsequent to replacement. The field of view is about 0.7 x 1.0 mm. Crossed-polar light. DDH 318-246.7

E. Mottled replacement texture in plagioclase feldspar. Plagioclase (white) is replaced by potassium feldspar (gray). At some locations (upper left) the potassium feldspar is partly localized by visible fractures; at another location (lower right) potassium feldspar is seeming unrelated to a fracture. The field of view is about 0.8 x 1.2 mm. Crossed-polar light. DDH 318-282.25

F. Advanced replacement of plagioclase by potassium feldspar (black). Only tiny remnants of plagioclase (white; best seen in upper left side of phenocryst) remain. These show similar extinction properties

when the stage is rotated. DDH 316-314.7. The field of view is about 2.5 x 1.7 mm. Crossed-polar light.

G. Advanced replacement of plagioclase by potassium feldspar (dark gray). Tiny remnants as in B are scattered throughout the thin-section. These go to extinction approximately simultaneously as the stage is rotated. The field of view is about 2.3 x 3.4 mm. Crossed-polar light. DDH 302-101.3

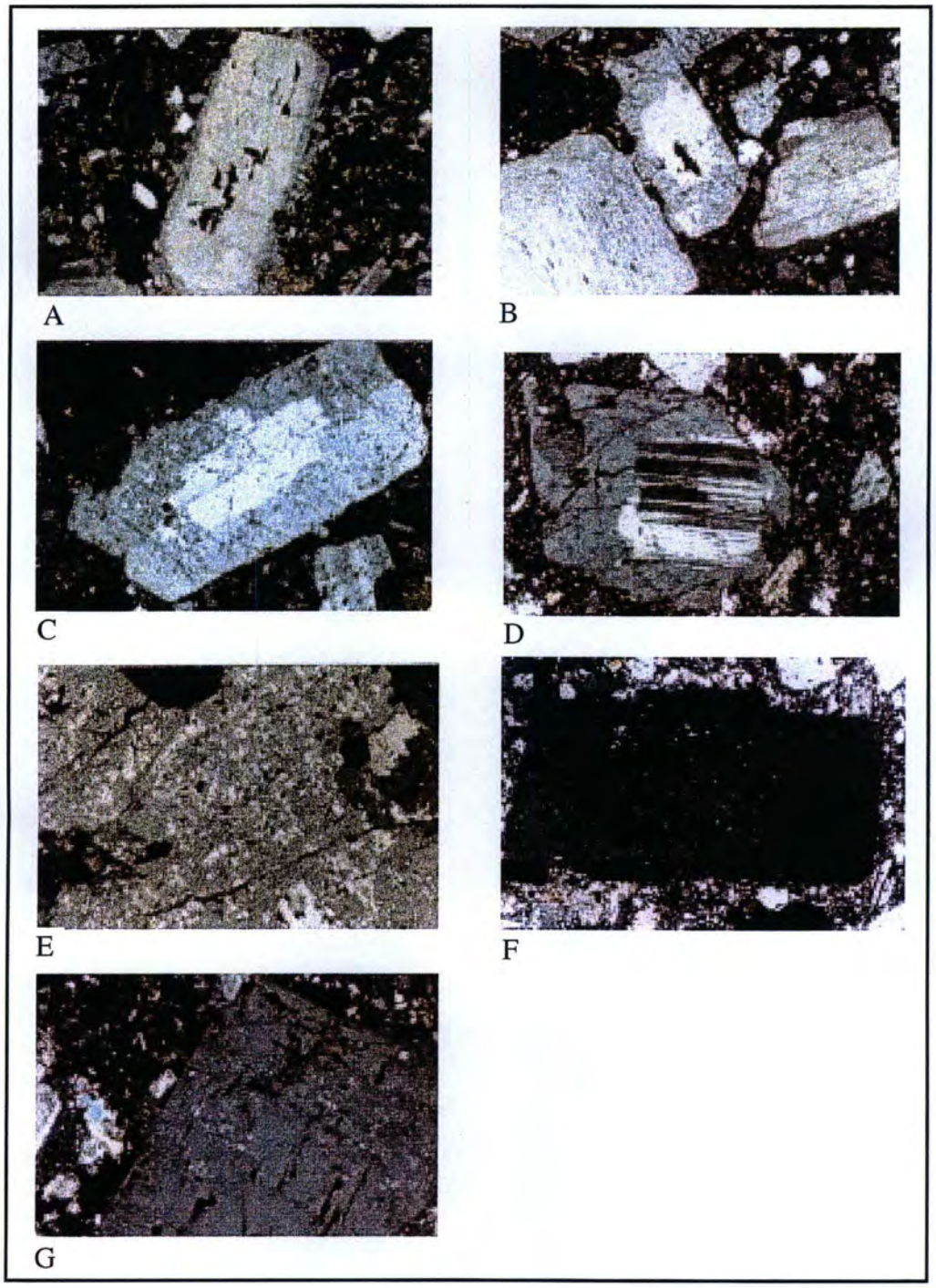

Figure 27 continued.

All varieties of potassium feldspar are counted as "non-polysynthetically twinned feldspar" or "gray feldspar" in point counter analyses and are listed as "NPST feldspar" in Appendices 2 and 3. The average Or contents of potassium feldspar crystals in altered and unaltered porphyries and phanerites range from Or_{73} to Or_{80}.

Where replacement of feldspar is nearly complete, tiny relicts of the original plagioclase host may be completely enveloped by secondary potassium feldspar. This texture is herein referred to as "sieve texture." Feldspars that show this feature superficially appear to be perthitic. However, the plagioclase feldspar relicts are in optical continuity and thus are more likely to be unreplaced remnants from hydrothermal alteration than products of exsolution. Examples of this texture are illustrated in Figures 27E-G.

Pyroxene

Pyroxene is present in thin-sections of unaltered and in propylitically altered intrusive rocks having both porphyritic and phaneritic texture. Crystals of pyroxene are subhedral to euhedral in shape in both textural varieties of the intrusions. Elongate prisms (Figure 28A-D) and octagonal cross-sections are common (Figure 28E-F). The crystals are pale green in color and weakly pleochroic in plane-polarized light. Most display even extinction when viewed between crossed polarizers. Pyroxene accounts for 4 to 10 volume percent of the

Figure 28: Examples of pyroxene in andesine-potassium feldspar porphyries and phanerites.

A. Cluster of two (or more) phenocrysts of pyroxene in sample with porphyritic texture. The pyroxene is green and weakly pleochroic. It contains inclusions of magnetite (black). The field of view is about 3.9 x 5.3 mm. Plane-polar light. DDH 172-221.5

B. Same pyroxenes shown in A. Crossed-polar light. Shows typical interference colors of the pyroxenes in the rocks of the Ok Tedi Intrusive Complex. The field of view is about 3.9 x 5.3 mm. Crossed-polar light. DDH 172-221.5

C. Crystals of pyroxene in a rock with phaneritic texture. Two directions of cleavage can be seen in the equant crystals northwest of the large crystal in the lower left part of the photograph. These cleavages cross at nearly right angles. A stubby crystal of apatite abuts against the lower edge of the large pyroxene in the center of the photograph. Crystals of magnetite abut against, or are included within the pyroxenes. The field of view is about 3.0 x 4.2 mm. Plane-polar light. DDH 74-66

D. Common association of magmatic minerals in a sample of phanerite. Several pyroxenes, including the large central crystal, in juxtaposition with magnetite and feldspar. A single diamond shape crystal of sphene can be seen in the lower center of the photograph. The field of view is about 4 x 6 mm. Plane-polar light. DDH 342-84.5.

E. Eight-sided cross-section through a crystal of pyroxene in a sample of porphyry. The crystal shows the typical cleavage (~87°) of pyroxene and contains two inclusions of magnetite (black). The field of view is about 0.6 x 0.9 mm. Plane-polar light. DDH 172-221.5

F. Same crystal of pyroxene seen in E. Crossed-polar light. DDH 172-221.5

G. Photomicrograph showing the typical spatial distribution and abundance (~13%) of pyroxene in the least-altered phanerites of the Ok Tedi Intrusive Complex. Also shows the typical close spatial

proximity of magnetite and pyroxene. The field of view is about 4.1 x 6.2 mm. Plane-polar light. Ok Tedi 1009.

H. Photomicrograph showing the typical spatial distribution and abundance (~13%) of pyroxene in the least-altered phanerites of the Ok Tedi Intrusive Complex. Also shows the typical close spatial proximity of magnetite and pyroxene. The field of view is about 4 x 6 mm. Plane-polar light. Ok Tedi 1009.

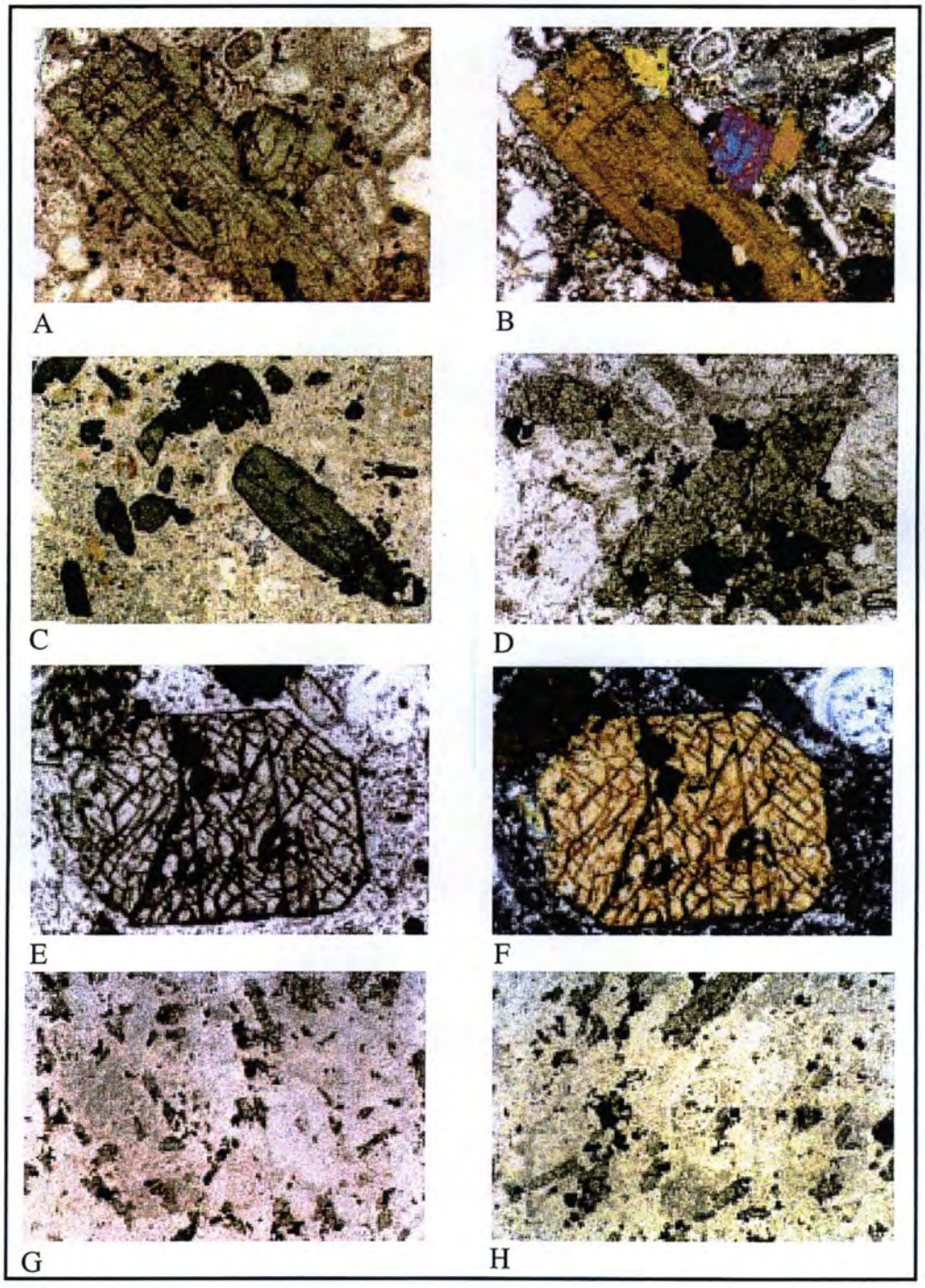

Figure 28 continued.

least-altered rocks. Crystals of pyroxene are commonly juxtaposed against or contain inclusions of magnetite (Figure 28 A-H), apatite, or sphene. They are typically equal in size to the feldspars with which they coexist. The longest dimensions of individual crystals range from less than 1 mm to up to about 5 mm. The relative abundance, crystallinity, and mineralogical relationships of pyroxene to feldspar and magnetite are shown in Figure 28G-H.

A map showing the spatial distribution of pyroxene is given as Figure 29. The map shows that pyroxene is a common mineral phase in the Kalgoorlie, Ningi, and Sydney intrusions, whereas it is rare, or entirely absent, in the Mt. Fubilan intrusion.

One hundred and three microprobe analyses were made of pyroxenes in eight polished thin-sections. Representative analyses are given in Table 4. The entire sets of analyses are given in Appendix 5. Structural formulae for the analyses were calculated using the computer program FORMULA (Ercit, unpublished). The formulae were calculated on the basis of four cations and with all iron treated as FeO. The cation percentages of Mg, Ca, and Fe were plotted on triangular diagrams for classification. The classification scheme used (Figure 30A) is that of the International Mineralogical Association, Committee on New Minerals and Mineral Names, Subcommittee on Pyroxenes (Morimoto and others, 1988). The nomenclature of the Commission is simplified from older classifications and contains fewer names. The Subcommission's recommendations on the use of the

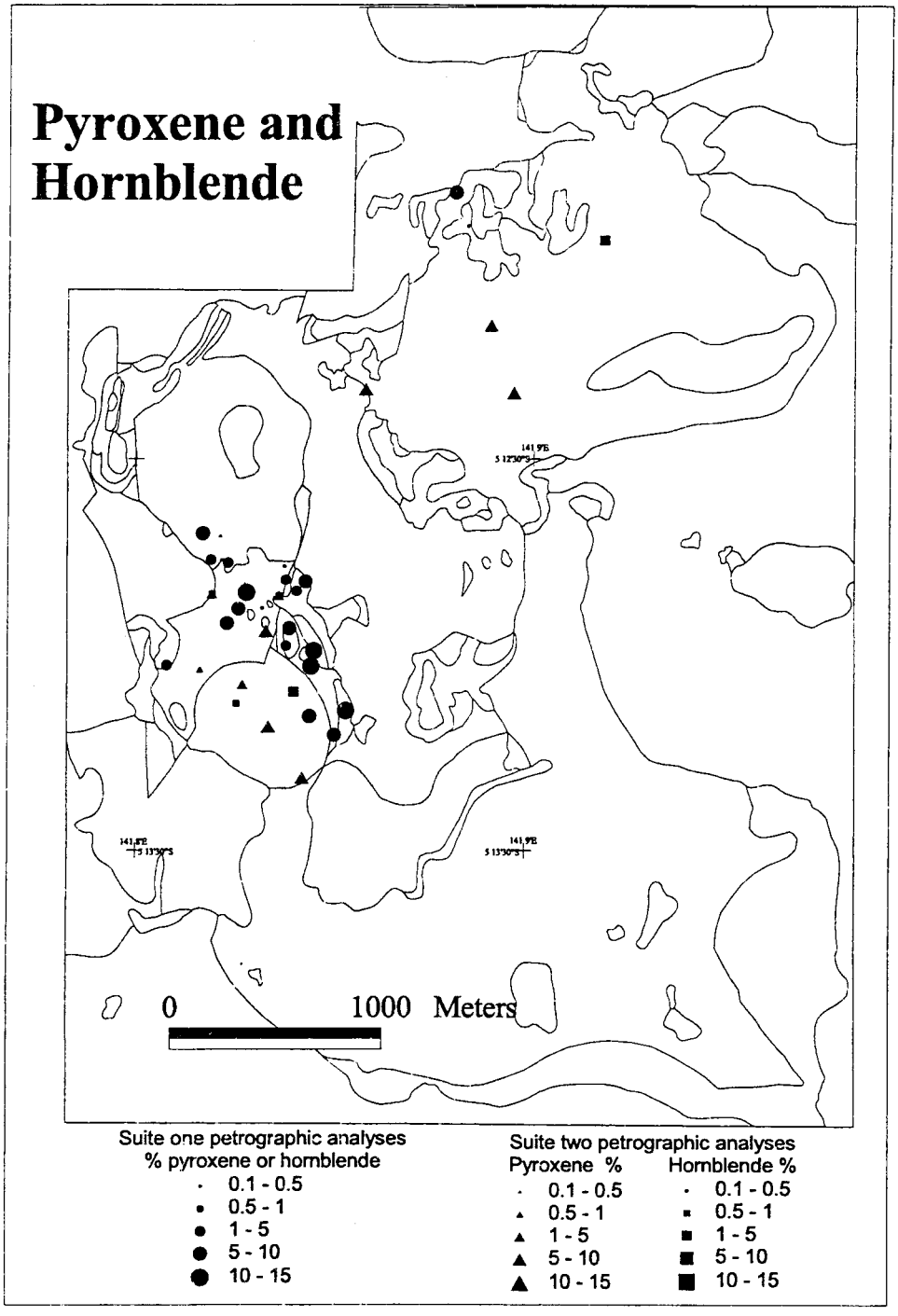

Figure 29: Map showing geographic distribution of hornblende and pyroxene in the Ok Tedi Intrusive Complex.

Sample	319	331	342	351	356	458
	339.3	218.5	84.5	313.2	166.5	151.8
Analyses	13	23	15	19	2	30
SiO_2	53.81	51.15	51.36	52.89	52.04	51.20
TiO_2	0.14	0.30	0.18	0.21	0.34	0.23
Al_2O_3	0.74	1.75	1.25	1.16	1.30	1.66
FeO	7.68	8.90	8.91	8.39	8.14	9.84
MnO	0.48	0.84	0.89	0.79	0.72	0.93
MgO	14.47	13.00	12.98	13.92	13.40	12.29
CaO	23.38	22.20	22.44	22.75	22.94	22.15
Na_2O	0.39	0.48	0.47	0.44	0.56	0.67
K_2O	0.00	0.01	0.00	0.01	0.01	0.01
Cl	0.00	0.00	0.00	0.00	0.04	0.00
F	0.00	0.00	0.00	0.03	0.01	0.00
H_2O	0.00	0.00	0.00	0.00	2.07	0.00
CR_2O_3	0.01	0.00	0.00	0.02	0.00	0.00
TOTAL	101.10	98.64	98.50	100.61	101.55	98.99
			Cation numbers			
Si^{4+}	1.975	1.935	1.948	1.957	1.948	1.94
Ti^{4+}	0.004	0.008	0.005	0.006	0.010	0.01
Al^{3+}	0.032	0.078	0.056	0.051	0.057	0.07
Fe^{2+}	0.236	0.282	0.283	0.260	0.255	0.31
Mn^{2}	0.015	0.027	0.029	0.025	0.023	0.03
Mg^{2}	0.791	0.733	0.734	0.768	0.748	0.69
Ca^{2}	0.919	0.900	0.912	0.902	0.920	0.90
Na	0.028	0.036	0.034	0.032	0.041	0.05
K	0.000	0.000	0.000	0.000	0.000	0.00
Total	4.000	4.000	4.000	3.999	4.000	4.000

Formulae calculated using program of Ercit(unpublished)
Formula contents on a basis of 4 cations

Table 4: Representative electron-beam microprobe analyses of pyroxene.

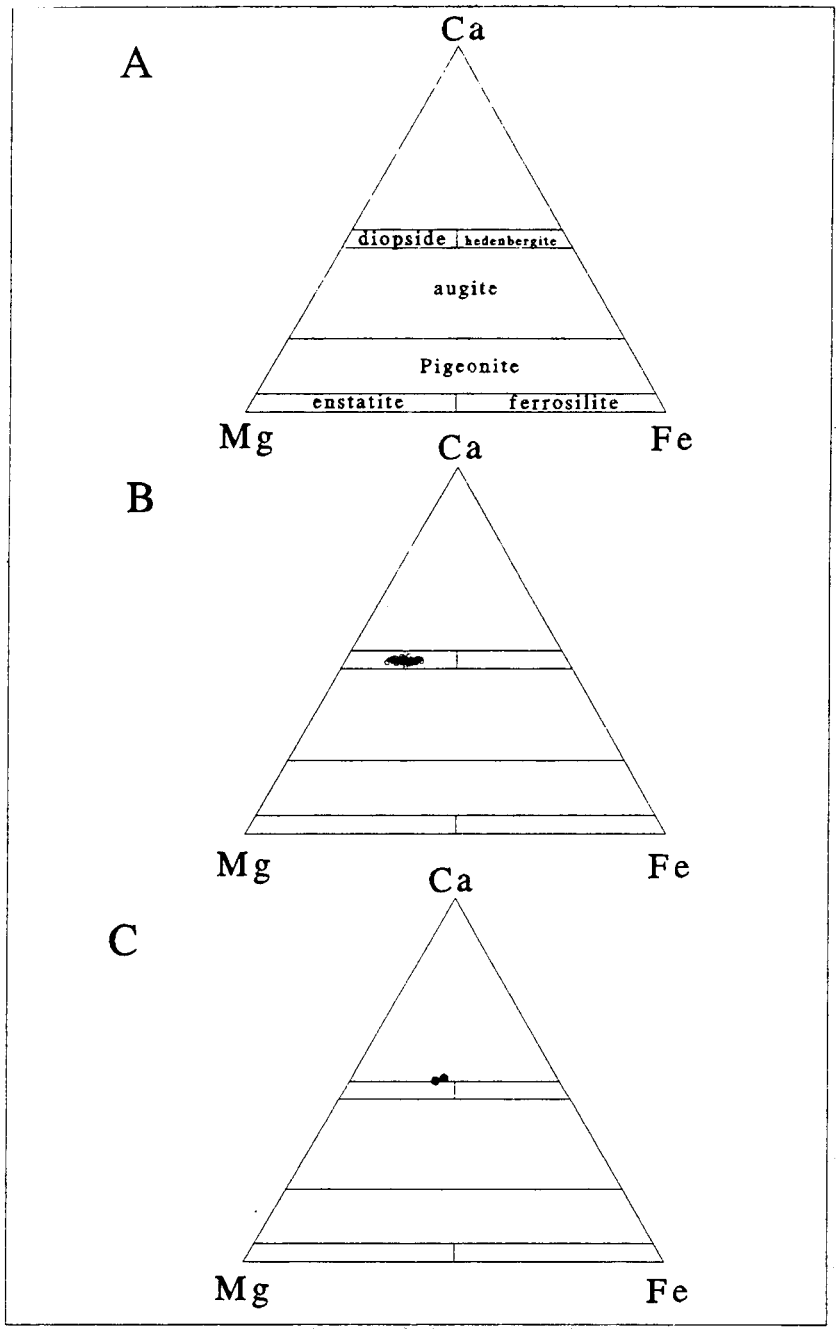

Figure 30: Mg-Fe-Ca plots. (A) classification of pyroxenes, (B) analyses of pyroxenes from unaltered samples, (C) analyses of pyroxene in garnet-bearing sample.

term diopside and the dropping of salite as a mineral name are of particular interest to this study.

All of the analyses of pyroxene (Figure 30B and C) from the analyzed samples fall within the field of diopside as defined by the Commission and include examples that would have been categorized as diopside and as salite under older classifications. The terminology used in this dissertation follows the recommendations of the Subcommittee. The term diopside includes all pyroxenes that would have previously been named salite and diopside. However the term salite should be kept in mind for comparison to pyroxenes in publications that predate the Subcommittee's report or for those that don't follow these recommendations. Two analyses from one thin-section (DDH 459-102.9; Figure 30C) are characterized by higher CaO contents than the others. This thin-section contains garnet and it is possible that the analyses are of metasomatic pyroxene. Katchan (1982) has noted that skarn clinopyroxenes can be distinguished from igneous pyroxenes by slightly higher CaO and lower Na_2O and that they plot above the tie line between diopside and hedenbergite compositions.

Pe-Piper (1984) reported that "recent reviews of orogenic rocks have suggested that the clinopyroxenes in potash-rich rocks may differ from those in lower-K calc-alkali rocks." Whereas augite is characteristic of most calc-alkali rocks, the compositions of clinopyroxenes in potash-rich calc-alkali andesites may extend into the fields of diopside and salite (Ewart, 1982). This is consistent with

an interpretation of the Ok Tedi Intrusive Complex as a part of a high-potassium magma suite.

The average value of Fe/(Fe+Mg) in the analyzed pyroxenes is 0.28. In contrast to hornblende and biotite, the analyzed pyroxenes contain low amounts of fluorine. Typically fluorine abundances are below the detection limits in the analyses of pyroxene whereas hornblende and biotite were each found to contain greater than one percent fluorine.

Pyroxene is not present in thin-sections of samples collected from most mineralized locations within the Mount Fubilan, Kalgoorlie, or Ningi Intrusions. However pseudomorphs of mica or smectite after pyroxene in many samples from these areas attest to the fact that pyroxene was present before alteration occurred. With increasing potassic or argillic alteration the pseudomorphs after pyroxene have been destroyed and neither pyroxene nor its pseudomorphs are observed in rocks dominated by intense alterations of these types.

Although pyroxene is not found in most samples of porphyry that display strong potassic alteration, it was found in a few thin-sections of anhedral metasomatic alkali feldspar phanerite from the Kalgoorlie area. The samples which contain this association may be the periskarns observed by Duncan (1972). The association is unusual, occurring in only a few specimens, and confusing in light of the general antithesis of CaO-rich minerals in the potassic assemblage at Ok Tedi. Further study of rocks of this type is necessary but I was unable to find any samples

during my visit in 1994 and the thin-sections of the first suite of samples (which includes examples of the association) were not suitable for microprobe analyses.

Amphibole

Two distinct types of amphibole are present in the intrusive rocks at Ok Tedi. These are hornblende and actinolite. The hornblende is magmatic in origin, whereas the actinolite formed by replacement of pyroxene in rocks that have undergone propylitic alteration.

Hornblende is strongly subordinate to pyroxene in both suites of samples examined in this study. It was found only in thin-sections of samples from the Kalgoorlie and Ningi Intrusions, and in two thin-sections from one drill hole in the Sydney Intrusion (DDH-331). Hornblende is scarce or absent in rocks that have undergone potassic alteration.

Crystals of hornblende are anhedral to subhedral in shape, and pleochroic from pale green to medium green in color. A few show the two directions of cleavage that are characteristic of amphiboles (Figures 31B, C, and D), but others display only a singe direction or none at all (Figures 31A and B). Some hornblende may have formed by replacement of pyroxene. A possible example of this is depicted in Figures 31E-F where hornblende clearly has enveloped and may have partly replaced magmatic pyroxene.

Figure 31: Examples of amphiboles in rocks from the Ok Tedi Intrusive Complex.

A. Ragged subhedral phenocryst of hornblende in a sample of porphyry. It has been partly replaced by fibrous amphibole. Where intact, the hornblende displays two directions of cleavage. Also shown are a diamond-shaped phenocryst of sphene, two small bits of hornblende (lower right), and small crystals of magnetite at two locations. The field of view is about 0.8 x 1.2 mm. Plane-polar light. DDH 464-9.

B. Same phenocryst of hornblende shown in C. Crossed-polarizers. The field of view is about 0.8 x 1.2 mm. DDH 464-9.

C. Cluster of subhedral or euhedral crystals of hornblende. The larger crystal is oriented such that cleavage directions are not shown whereas the two smaller crystals display two directions of cleavage. The field of view is about 0.7 x 0.9 mm. Plane-polar light. DDH 356-190

D. Anhedral crystal of hornblende in sample of phanerite. The crystal shows the typical dark green color of hornblendes from the Ok Tedi Intrusive Complex. Also shown in the photograph is a crystal of magnetite (black, upper right) and a small part of a crystal of sphene (top center) both of which abut against the which abut against the hornblende. The field of view is about 0.9 x 1.3 mm. Crossed-polar light. DDH 356-166.5

E. Anhedral crystal of hornblende which has overgrown, or replaced, part of an euhedral prism of pyroxene. Two crystals of sphene and two of magnetite abut against the pyroxene and hornblende. The field of view is about 0.7 x 1.0 Plane-polar light. DDH 351-313.2

F. Photomicrograph of the same crystals shown in E but rotated to a different orientation. Crossed-polar light. DDH 351-313.2.

G. Cluster of fibrous amphibole crystals and remnant bits of pyroxene in the site of a magmatic pyroxene. Also present in the photomicrograph are two small crystals of magnetite (black) and one of sphene (upper left). The field of view is about 0.7 x 1 mm. Plane-polar light. JDD-94-12.

Figure 31 continued.

H. Cluster of fibrous amphibole crystals that form a pseudomorph after a pre-existing crystal of a ferromagnesian mineral (probably pyroxene). A crystal of magnetite is partly enclosed by the pseudomorph. This crystal of magnetite contains an inclusion of sphene. The field of view is about 0.7 x 1.0 mm. Plane-polar light. JDD-94-12.

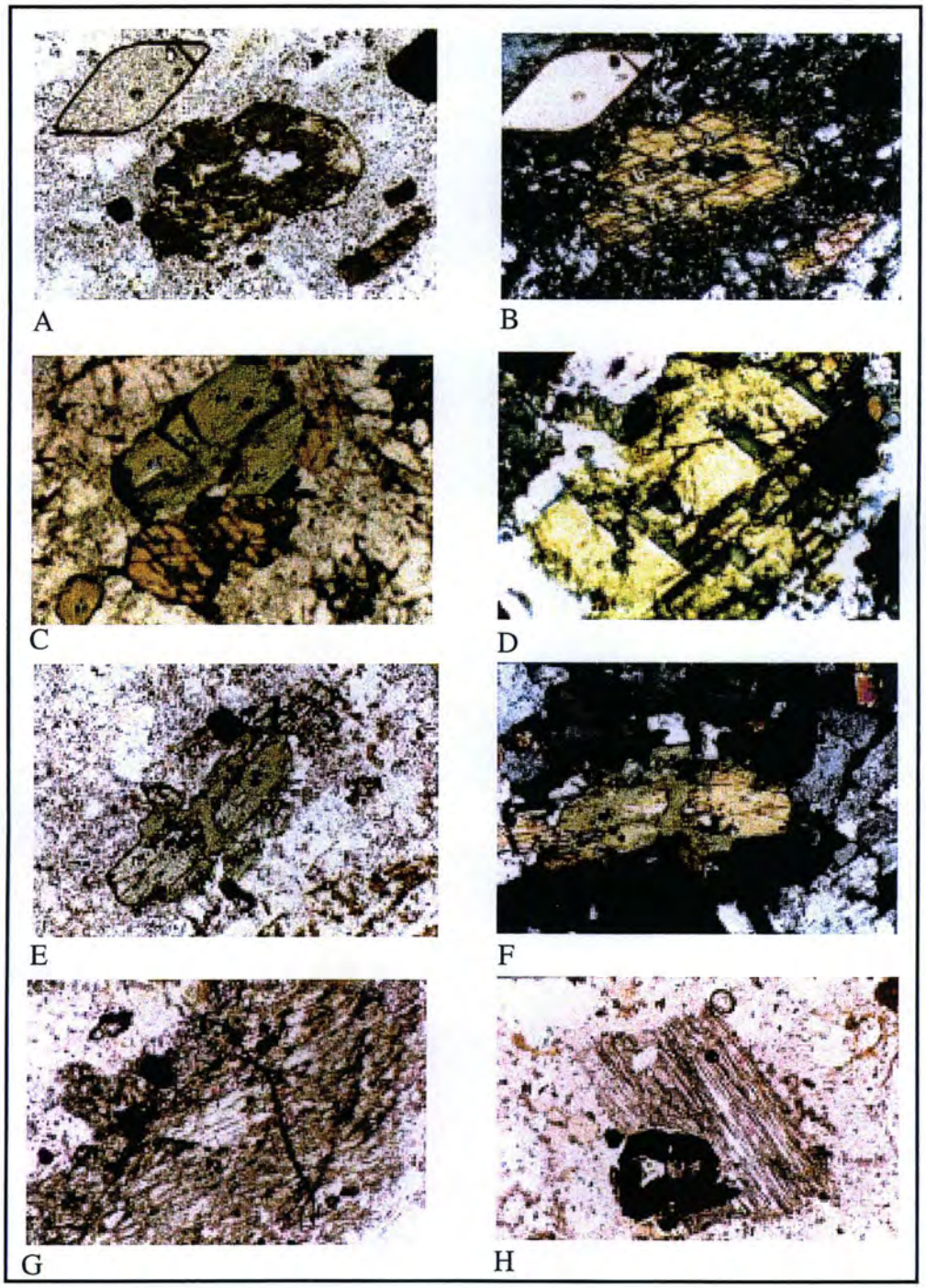

Figure 31 continued.

Actinolite is characterized by fibrous habit and pale green color. Many clusters, or fibre bundles, of actinolite formed by pseudomorphic replacement of magmatic pyroxene, hornblende, and biotite (Figures 31G-H) are present in propylitically altered rocks.

Eighty-seven analyses were made of hornblende and actinolite in five polished thin-sections. Representative analyses are given in Table 5. The entire sets of analyses are given in Appendix 6. Their mineral formulae were calculated using the computer program AMPHIBOL (Richard and Clarke, 1990). This program produces five sets of output based on various assumptions that can be made about the iron and water content of the samples. The mineral names assigned here were taken from the standard calculation method which assumes that all iron is present as Fe^{2+} and on a basis of 23 anions.

All of the analyzed amphiboles from the Ok Tedi Complex are calcic according to the classification scheme of Leake (1978) shown in Figure 32. The hornblendes are edenite in composition (Figure 32A) whereas the actinolites are actinolite or actinolite hornblende (Figure 32B).

Several microprobe analyses of pyroxene were carried out using an amphibole analytical file. These are shown plotted on an amphibole classification diagram in Figure 32C. It can be seen from this figure that the analyzed actinolites are closely similar in chemistry to pyroxene. This similarity supports an

Sample	319	351	351	356	356	356	356	JDD-94-12
	339.3	313.2	313.2	166.5	166.5	190	190	
Analyses	17	27	2	22	1	6	1	13
	actinolite	edenite	actinolite	edenite	actinolite	edenite	actinolite	actinolite
SiO2	51.98	48.39	52.33	49.88	53.04	49.57	51.04	50.69
TiO2	1.20	0.97	0.48	0.75	0.23	0.73	0.51	0.20
Al2O3	3.21	6.02	3.52	5.20	2.95	5.26	3.78	3.49
FeO	10.54	11.50	10.68	10.24	10.83	9.95	9.13	10.49
MnO	0.24	0.50	0.67	0.48	0.28	0.46	0.51	0.35
MgO	17.24	16.32	17.40	17.43	17.89	17.34	16.76	16.66
CaO	12.14	11.65	11.95	11.68	12.00	11.64	14.64	11.46
Na2O	1.01	1.77	1.08	1.88	0.99	1.88	1.29	0.82
K2O	0.29	0.87	0.49	0.81	0.36	0.84	0.61	0.30
Cl	0.07	0.08	0.03	0.08	0.06	0.08	0.05	0.09
F	1.00	1.46	1.28	1.94	0.95	1.83	1.28	1.11
Sub-total	98.92	99.54	99.92	100.36	99.58	99.57	99.60	95.68
-O=Cl,F	0.44	0.69	0.55	0.83	0.41	0.79	0.55	0.49
Total	98.48	98.90	99.38	99.53	99.17	98.78	99.05	95.20
TSi	7.455	7.044	7.465	7.176	7.547	7.175	7.341	7.519
TAl	0.489	0.956	0.535	0.825	0.453	0.825	0.641	0.481
CAl	0.054	0.078	0.058	0.058	0.042	0.072	0.000	0.131
CTi	0.054	0.106	0.052	0.081	0.025	0.080	0.000	0.023
CMg	3.684	3.540	3.700	3.737	3.794	3.741	3.593	3.683
CFe2+	1.130	1.275	1.188	1.124	1.140	1.108	1.098	1.162
CMn	0.001	0.000	0.000	0.000	0.000	0.000	0.062	0.000
CCa	0.077	0.000	0.000	0.000	0.000	0.000	0.247	0.000
BFe2+	0.135	0.125	0.087	0.108	0.149	0.096	0.000	0.140
BMn	0.028	0.062	0.080	0.058	0.034	0.056	0.000	0.044
BCa	1.784	1.809	1.823	1.801	1.817	1.805	2.000	1.805
BNa	0.023	0.004	0.011	0.033	0.000	0.044	0.000	0.011
ACa	0.007	0.007	0.004	0.000	0.012	0.001	0.009	0.016
ANa	0.256	0.495	0.288	0.490	0.273	0.483	0.360	0.225
AK	0.053	0.174	0.089	0.148	0.065	0.156	0.112	0.057
CCl	0.017	0.021	0.008	0.020	0.014	0.020	0.012	0.022
CF	0.454	0.728	0.577	0.881	0.427	0.836	0.582	0.519
Sum Oxygen	23.00	23.00	23.00	23.00	23.00	23.00	23.00	23.00

Formulae calculated using AMPHIBOL (Richard and Clarke, 1990)

Formula contents on a basis of 23 anions

Table 5: Representative electron-beam microprobe analyses of amphibole.

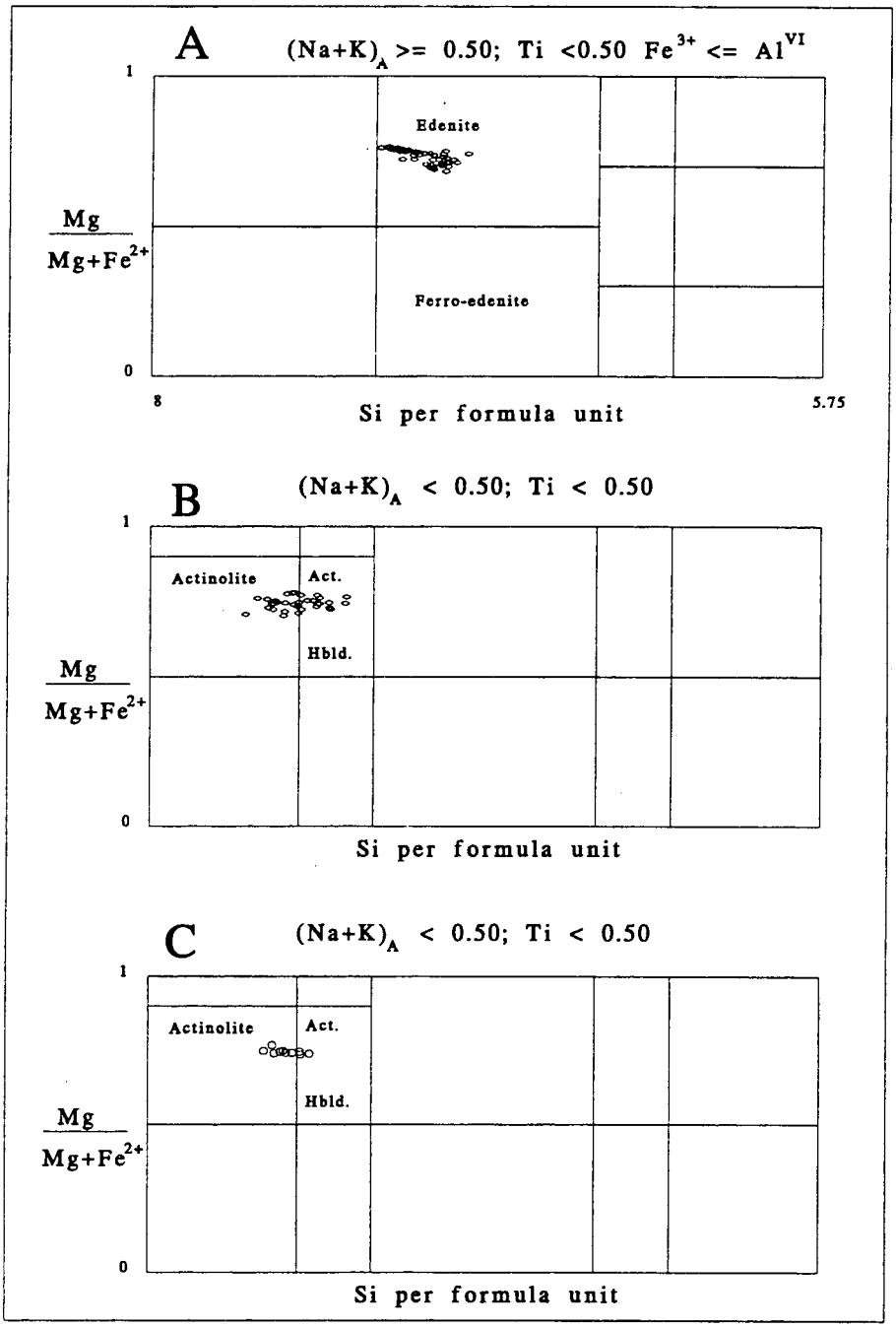

Figure 32: Analytical data of hornblende and actinolite plotted on the classification diagram of Leake (1978).

interpretation that much of the actinolite in rocks from the Ok Tedi complex is derived from magmatic pyroxene by the process of metasomatic replacement.

The average value of the ratio Fe/(Fe+Mg) in this group of amphiboles is 0.26. The average fluorine content of 53 edenites is 1.75 weight percent, of 17 actinolitic hornblendes it is 1.10 percent, and of 13 actinolites it is 1.03 percent. The fluorine content of the magmatic amphiboles is higher than that of the alteration amphiboles.

A map showing the spatial distribution of hornblende is given in Figure 29. Hornblende was found in one drill core sample each of feldspar porphyry and phanerite from the Sydney Intrusion north of Folomian (DDH-331) and in several specimens from the Kalgoorlie and Ningi intrusion. In addition, hornblende was present in dikes of hornblende porphyry in the Mt. Fubilan and Kalgoorlie intrusions before replacement by hydrothermal biotite.

Biotite

Micas of the biotite group that have formed by both magmatic and hydrothermal processes are present in the rocks of the Ok Tedi Intrusive Complex. Ayres and Bamford (1976) recognized three distinct types of biotite that they believed could be distinguished petrographically: (1) dark brown laths and euhedral crystals with textural relationships that suggest they are probably early formed and magmatic in origin; (2) brown to red-brown laths or aggregates that

replace pyroxene or hornblende at many locations; and (3) colorless to light-brown laths which are more phlogopitic in composition and which form veins and replacements. These authors believed that the last two types are of hydrothermal origin.

Magmatic biotite is characterized by euhedral or subhedral shape and even extinction between crossed polarizing filters (Figures 33A-C). It is typically pleochroic from dark brown to pale yellowish brown. Many examples of magmatic biotite display the polygonal shape typical of micas and, in cross-section, parallel planes of exfoliation or cleavage lamellae. Magmatic biotite is commonly associated, or intergrown, with pyroxene, magnetite, apatite, or sphene (Figure 33D).

A crystal of magmatic biotite showing evidence of resorption is shown in Figures 33E and F. The resultant crystal is skeletal in form and is surrounded by a ring of magnetite granules. Resorption surfaces in feldspar were also noted earlier in this chapter.

Hydrothermal biotite displays a wider range of pleochroic colors and crystal shapes than does biotite of magmatic origin. The maximum pleochroic colors include: orange, red, and yellowish brown. The minimum pleochroic color is pale yellowish brown. Most crystals of hydrothermal biotite are ragged in shape and form shreds, flakes, and patchwork aggregates; typical examples are shown in Figures 33 G-H and Figures 34A-B. Many crystals, and crystal clusters, are

Figure 31: Examples of magmatic and hydrothermal biotite.

A. Rectangular subhedral phenocryst of biotite. Shows typical maximum pleochroism (moderate brown). The biotite contains three inclusions of magnetite; a tiny diamond-shaped phenocryst of sphene can be seen along the left upper surface of the biotite; and a small subhedral phenocryst of pyroxene can be seen in the lower right corner of the photomicrograph. The field of view is about 1.7 x 2.5 mm. Plane-polar light. Ok Tedi R15.

B. Typical anhedral flake of magmatic biotite in a sample with phaneritic texture. Contains inclusions of magnetite. Dark brown pleochroism. The field of view is about 0.4 x 0.6 mm. Plane-polar light. DDH 356-166.5

C. Ragged anhedral crystal of magmatic biotite in a sample with phaneritic texture. Contains inclusions of magnetite. Dark brown pleochroism. The field of view is about 0.6 x 0.8 mm. Plane-polar light. DDH 356-166.5

D. Magmatic mineral association of biotite (left, brown), pyroxene (center, pale green), and magnetite (right, black). The field of view is about 0.6 x 0.8 mm. Plane-polar light. DDH 331-218.5

E. Anhedral, partly resorbed, phenocryst in weakly-altered porphyry. This photomicrograph shows the maximum pleochroic color (dark brown) of magmatic biotites from the Ok Tedi Intrusive Complex. The green fibrous mineral at the center is chlorite which has replaced biotite. Two large phenocrysts of magnetite that were partly, or totally, enclosed by the biotite are visible in the center of the photo. Additional small granular crystals of magnetite form a fringe around parts of the perimeter of the biotite. The field of view is about 0.8 x 1.2 mm. Plane-polar light. JDD-94-10

F. The same phenocryst of biotite shown in E. The crystal has been rotated to a position of minimum pleochroism (pale yellow brown). Plane-polar light. JDD-94-10

G. Pseudomorph of hydrothermal biotite after a phenocryst of magmatic ferromagnesian mineral. Identification of the original mineral is no longer possible by visual means. Patchwork texture

Figure 33 continued.

consisting of an aggregate of tiny flakes of biotite and myriad crystals of an opaque mineral. One small crystal of sphene is present just to the left of the larger opaque inclusion. The field of view is about 2 x 3 mm. Plane-polar light. DDH 345-468

H. The same pseudomorph of hydrothermal biotite shown in G. Crossed-polarizers. DDH 345-468

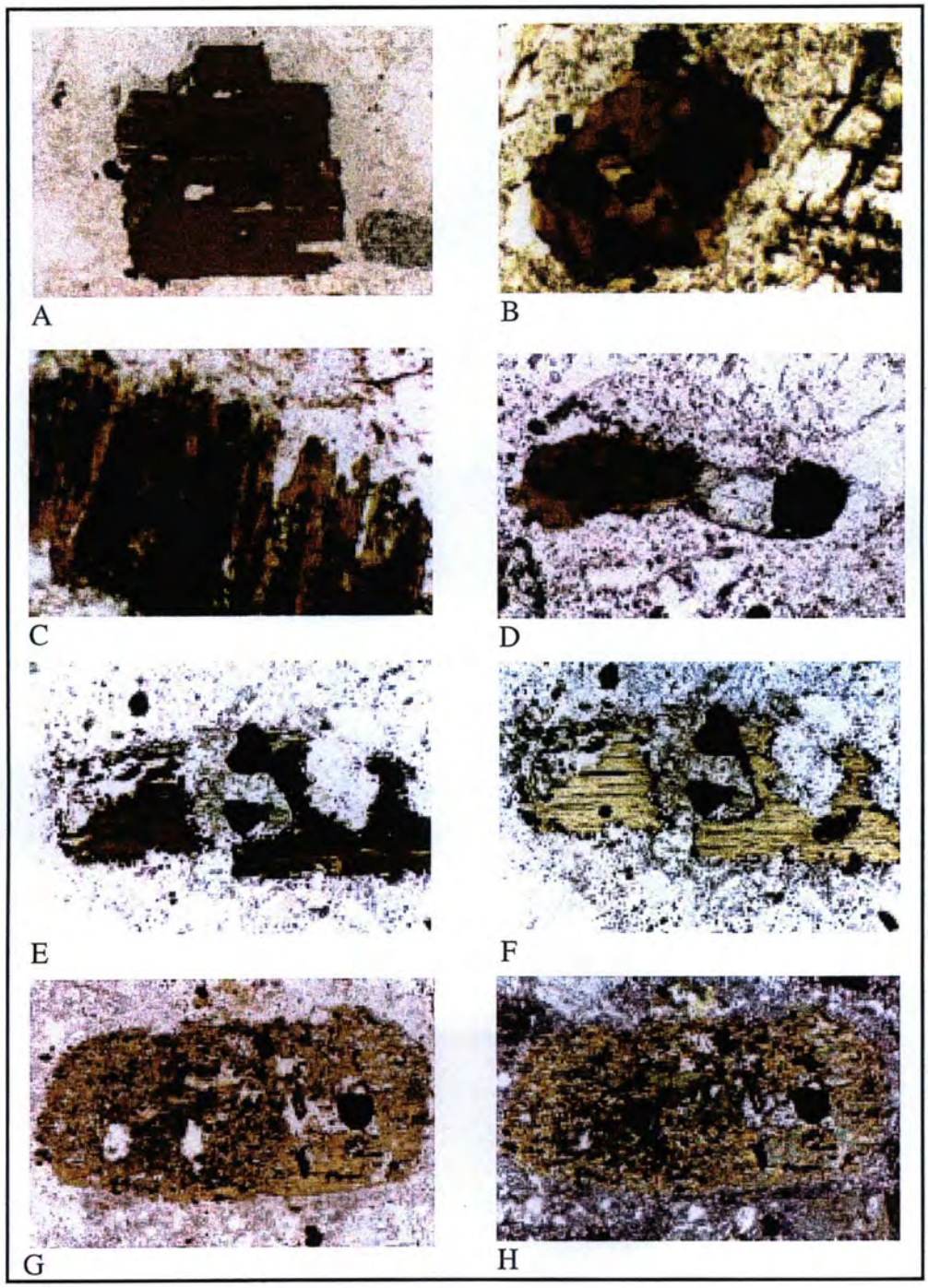

Figure 33 continued.

Figure 34: Examples of hydrothermal biotite.

A. Patchwork aggregate pseudomorph of hydrothermal biotite after a magmatic ferromagnesian mineral. Shows the pale yellow to orange pleochroism typical of hydrothermal biotites from the altered rocks at Ok Tedi. The field of view is about 4.6 x 6.6 mm. Crossed-polar light. DDH 355-382.5

B. Anhedral crystals of hydrothermal biotite in a potassium feldspar-altered phanerite. These crystals show uniform pleochroism and birefringence and are oriented so as to display their maximum pleochroic color (pale orange brown). The field of view is about 0.8 x 1.2 mm. Plane-polar light. JDD-94-14

C. Patchwork aggregate pseudomorph of hydrothermal biotite, quartz, and opaque mineral after a magmatic ferromagnesian mineral. The field of view is about 0.8 x 1.2 mm. Plane-polar light. DDH 345-468

D. Patchwork aggregate pseudomorph of hydrothermal biotite and quartz after a magmatic ferromagnesian mineral. The linear streaks in the quartz (pale yellow) are probably fluid inclusions. A rounded crystal of zircon can be seen in near the center of the right edge of the photograph. The field of view is about 4.5 x 6.7 mm. Crossed-polar light. DDH 345-468

E. Pseudomorph of hydrothermal biotite after a phenocryst of hornblende in hornblende porphyry. The euhedral shape of the original crystal is retained. The secondary biotite has a felted texture. The field of view is about 0.7 x 1.0 mm. Plane-polar light. JDD-94-05

F. The same pseudomorph of hydrothermal biotite after hornblende shown in E. An inclusion of plagioclase feldspar can be seen in the upper right part of the pseudomorph. Crossed-polar light. JDD-94-05

G. Pseudomorph of hydrothermal biotite after hornblende in hornblende porphyry. Shows maximum and minimum pleochroic colors of the hydrothermal biotite (medium orange brown - large crystal; pale yellow brown - smaller crystal included within the

Figure 34 continued.

larger one). The field of view is about 2 x 3 mm. Plane-polar light. JDD-94-05

H. Pseudomorphs of hydrothermal biotite after ferromagnesian minerals in a sample of texturally destroyed rock. The secondary biotite is dark brown in color. Identification of the original magmatic minerals is uncertain. The field of view is about 4 x 6 mm. Plane-polar light. DDH 366-226.5

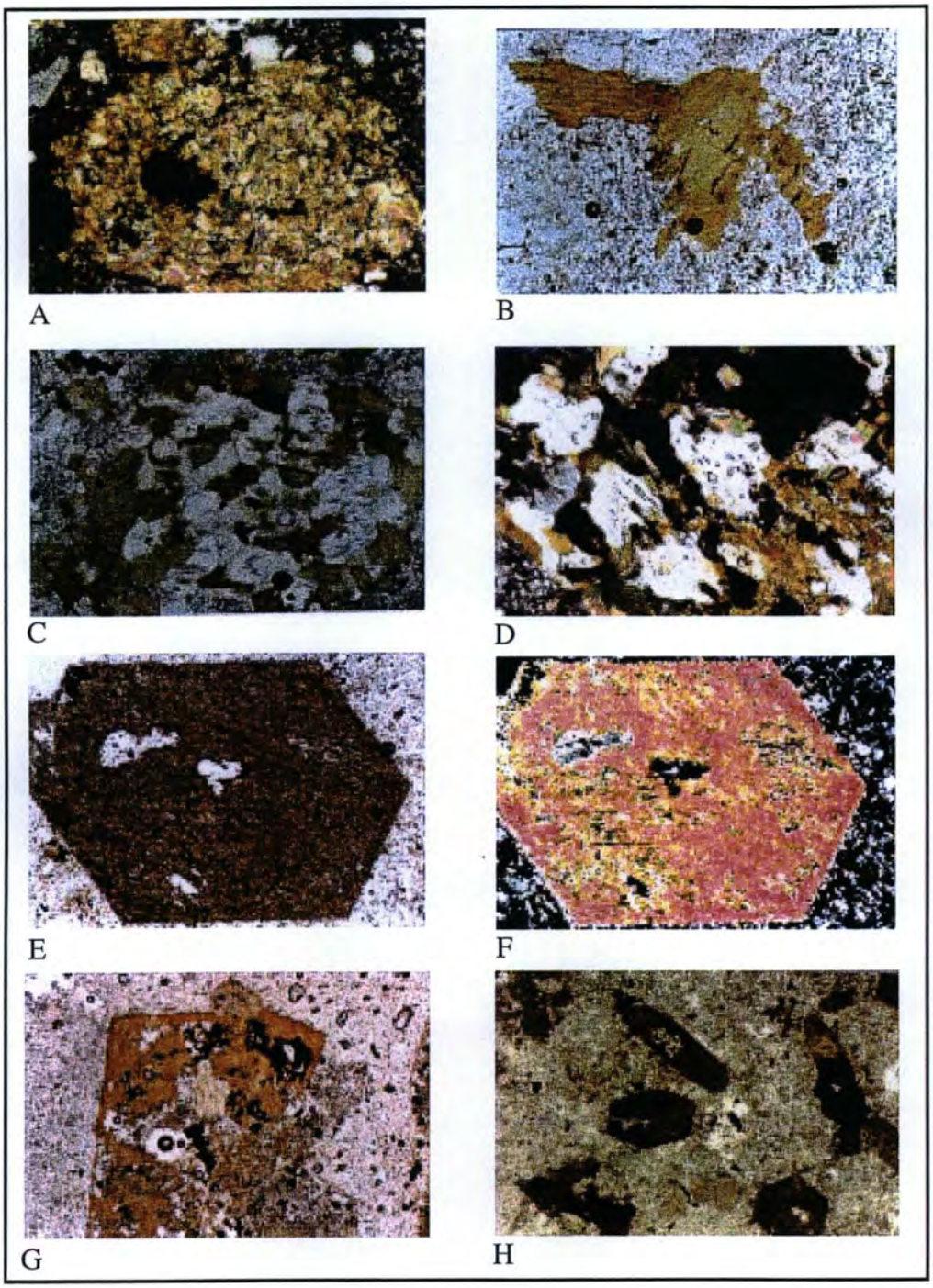

Figure 34 continued.

secondary after earlier mafic minerals (pyroxene, hornblende, or magmatic biotite). Others form along veinlets or at apparently random sites.

Hydrothermal biotite is associated with rutile or quartz in many thin-sections. Intergrowths of biotite and quartz are common and together they form pseudomorphic replacements of earlier ferromagnesian minerals as shown in Figures 34C and D).

Two pseudomorphs of hydrothermal biotite that have replaced hornblende in hornblende porphyry are shown in Figure 34E-G. An example of hydrothermal biotite that has replaced preexisting mafic pyroxene (or hornblende) in a sample of texturally destroyed rock is shown in Figure 34H.

Veinlets and veins of hydrothermal biotite are locally abundant in areas of potassic alteration. Complex mesh-like networks of hydrothermal biotite were also noted in many thin-sections.

Microprobe analyses were made on 58 biotites present as phenocrysts and other crystal forms of mica in six polished thin-sections. Representative analyses are given in Table 6. The entire sets of analyses are given in Appendix 7. These analyses are from both magmatic and hydrothermal biotites.

The compositions of all micas analyzed as part of this dissertation are shown in Figure 35 a compound classification diagram based on the end-member biotite minerals: annite, phlogopite, eastonite, and siderophyllite (Speer, 1984; and Guidotti, 1984). The upper part of the figure is a plot of the ratio Fe/(Fe+Mg)

Sample	356	356	407	458	JDD-94-05	JDD-94-07
	166.5	190	257.8	151.8		
Analyses	15	1	6	7	15	11
	magmatic	magmatic	hydrothermal	magmatic	hydrothermal	hydrothermal
SiO_2	41.65	41.11	40.53	36.63	40.68	40.57
TiO_2	3.00	1.52	1.81	3.58	1.79	2.08
Al_2O_3	13.53	12.48	10.77	13.78	13.67	12.22
FeO	12.53	13.53	12.96	14.75	9.23	12.18
MnO	0.26	0.11	0.08	0.30	0.05	0.05
MgO	14.10	17.33	18.73	15.17	19.76	17.10
CaO	0.17	0.01	0.02	0.01	0.04	0.07
Na_2O	0.98	0.14	0.14	0.23	0.28	0.15
K_2O	9.46	9.83	9.08	9.47	9.87	8.68
F	1.94	2.03	2.57	0.87	3.27	2.37
Cl	0.18	0.11	0.13	0.21	0.10	0.13
CuO	0.00	n.a.	0.04	0.00	0.00	0.03
RbO	0.00	n.a.	0.08	0.00	0.00	0.06
V_2O_5	0.00	n.a.	0.04	0.00	0.00	0.01
$H2O^*$	2.96	3.04	2.75	3.42	2.51	2.80
O=F	-0.82	-0.85	-1.08	-0.37	-1.38	-1.00
O=Cl	-0.04	-0.02	-0.03	-0.05	-0.02	-0.03
Total	99.90	100.37	98.45	98.00	99.84	97.38
Si^{4+}	6.379	6.11	6.073	5.650	5.972	6.157
Ti^{4+}	0.344	0.17	0.204	0.416	0.198	0.237
Al^{3+}	2.443	2.19	1.903	2.506	2.365	2.185
Fe^{2+}	1.599	1.68	1.626	1.905	1.134	1.547
Mn^{2+}	0.033	0.01	0.010	0.039	0.006	0.007
Mg^{2+}	3.202	3.84	4.184	3.484	4.326	3.867
Ca^{2+}	0.028	0.00	0.003	0.001	0.006	0.012
Na^{+}	0.290	0.04	0.039	0.149	0.079	0.043
K^{+}	1.848	1.86	1.737	1.862	1.849	1.681
F^{-}	0.933	0.95	1.219	0.424	1.519	1.135
Cl^{-}	0.048	0.03	0.032	0.056	0.026	0.033
H^{+}	3.019	3.02	2.749	3.520	2.455	2.832
$O2^{-}$	24.061	23.34	22.869	23.806	22.777	23.195
Anion Sum	25.04	24.33	24.12	24.29	24.32	24.36
Formula calculated using program of Ercit (Unpublished) and on a basis of 24 anions						

Table 6: Representative electron-beam microprobe analyses of biotite.

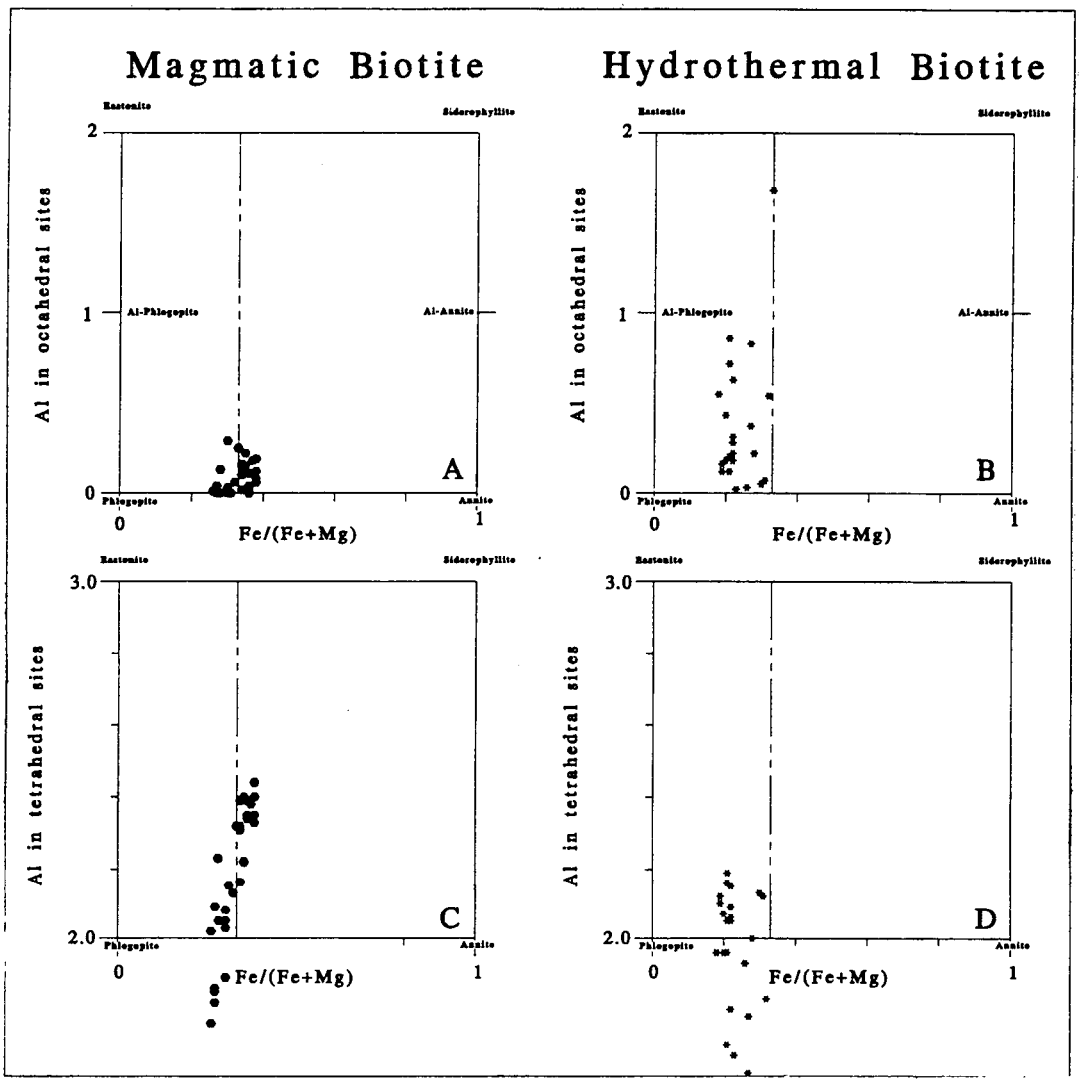

Figure 35: Biotite classification scheme based on the end-member biotites: annite, phlogopite, eastonite, and siderophyllite (Speer, 1984; and Guidotti, 1984).

versus the number of aluminum cations assigned to the octahedral site and the lower plot shows Fe/(Fe+Mg) versus the number of aluminum cations assigned to the tetrahedral site. The analyzed compositions cluster near the vertical dashed line at Fe/(Fe+Mg) = 0.33. This value has been used to distinguish biotite (>0.33) from phlogopite by Mason (October 1993). Magmatic biotite (Figure 35A, B) is characterized by higher Fe/(Fe+Mg) ratios (average=0.33) than hydrothermal biotite (Figure 35C, D; average=0.26). Many of the analyses of magmatic biotite have Fe/(Fe+Mg) ratios lower than 0.33; therefore, this ratio cannot be considered an unequivocal method for distinguishing between igneous and metasomatic biotites. Optical properties are the best criteria for discrimination in this case. The average value of the ratio Fe/(Fe+Mg) for the hydrothermal biotites is 0.26. This value is closely similar to the value of the same ratio for pyroxenes (0.28) and amphiboles (0.26) from the Ok Tedi Intrusive Complex and may indicate that the hydrothermal biotite that was analyzed was formed by pseudomorphic replacement of magmatic pyroxene or hornblende. The values of tetrahedral Al calculated from many analyses of magmatic and hydrothermal biotites plot below the tie-line between phlogopite and annite. These micas can, therefore, probably considered aluminum-poor.

Nockolds (1947) reported that the amount of Al_2O_3 with respect to MgO and FeO^* in biotite mica is dependant on the nature of the other "mafic" minerals associated with it. The Al_2O_3 content is greatest in biotites associated with topaz or

muscovite (Nockolds extended the use of the term *mafic* to include these minerals), intermediate in biotites that are not associated with other "mafic" minerals, and lowest in those associated with hornblende or pyroxene. He noted that the ratio of MgO to FeO^* is not related to the paragenesis but to the degree of differentiation or contamination of the magma from which the biotite crystallized. The amounts of Al_2O_3, MgO, and FeO^* (recalculated to 100 percent) in biotites from the Ok Tedi Intrusive Complex are plotted in Figure 36. This diagram has fields representing the paragenesis of the biotites (from Nockolds, 1947). Almost all of the analyses of biotite from the intrusive rocks at Ok Tedi fall in field of micas that are expected to coexist with pyroxene or hornblende. This is true for both magmatic and hydrothermal biotites. Hydrothermal biotite can be distinguished from magmatic biotite in Figure 36 by having a slightly lower ratio of FeO^* to MgO. Both types have similar Al_2O_3 content but that of hydrothermal biotite is slightly less than that of magmatic biotite. The fact that pyroxene coexists with magmatic biotite in the least-altered intrusive rocks of the Ok Tedi Intrusive Complex is consistent with the Al_2O_3-poor nature of the biotites plotted in Figures 35A and 35B. The amount of Al_2O_3 in hydrothermal biotite also is consistant with its presence in zones of potassic alteration and with the very low amount of sericite (muscovite) in this environment.

The average fluorine content of the magmatic biotite is 1.76 weight percent whereas that of the hydrothermal biotite is 2.81 percent. This suggests that the

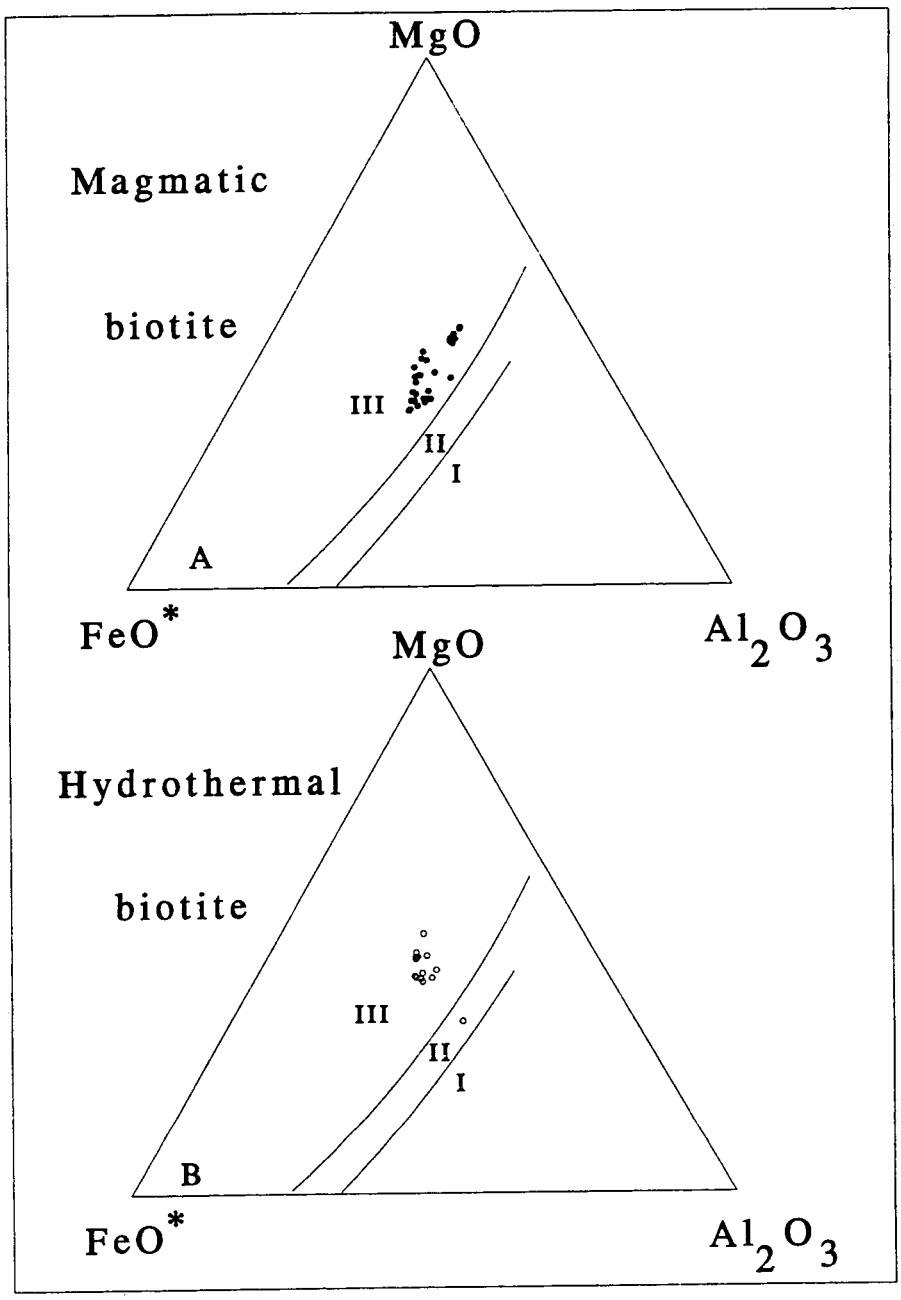

Figure 36: Ternary plot of FeO^* (total iron as FeO), Al_2O_3, and MgO. Shown on this plot are empirically derived fields of biotites co-existing with muscovite or topaz (I), biotites existing alone (II), and biotites coexisting with pyroxene or hornblende (III). Modified from Nockolds (1947).

fluorine content of the hydrothermal fluids may have been higher than that of the magma. TiO_2 averages 3.50 weight percent in magmatic biotite and 2.16 percent in hydrothermal biotite. The average MgO content of magmatic biotite is 15.9 percent whereas that of hydrothermal biotite is 18.5 percent.

A map showing the spatial distribution of magmatic and hydrothermal biotite is given in Figure 37. All, but one, of the thin-sections from the Sydney Intrusion have only magmatic biotite. The remaining sample is from the Darien-East Cheam area and may be from rock associated with skarn alteration. A few thin-sections of samples from the Kalgoorlie and Ningi intrusions contain only magmatic biotite, but most contain either hydrothermal biotite alone or combinations of magmatic and hydrothermal biotite. Thin-sections of all but a few samples from the Mt. Fubilan Intrusion contain hydrothermal biotite exclusively, and this intrusion is the principal host to the Ok Tedi ore deposit.

Quartz

Quartz accounts for an average of 4.5 volume percent in rocks with phaneritic texture. Most quartz is anhedral in shape and is found in the interstices between crystals of feldspar (Figures 38A and B) or crystals of feldspar and pyroxene (Figures 38C-F). The anhedral shape of the quartz and its presence in

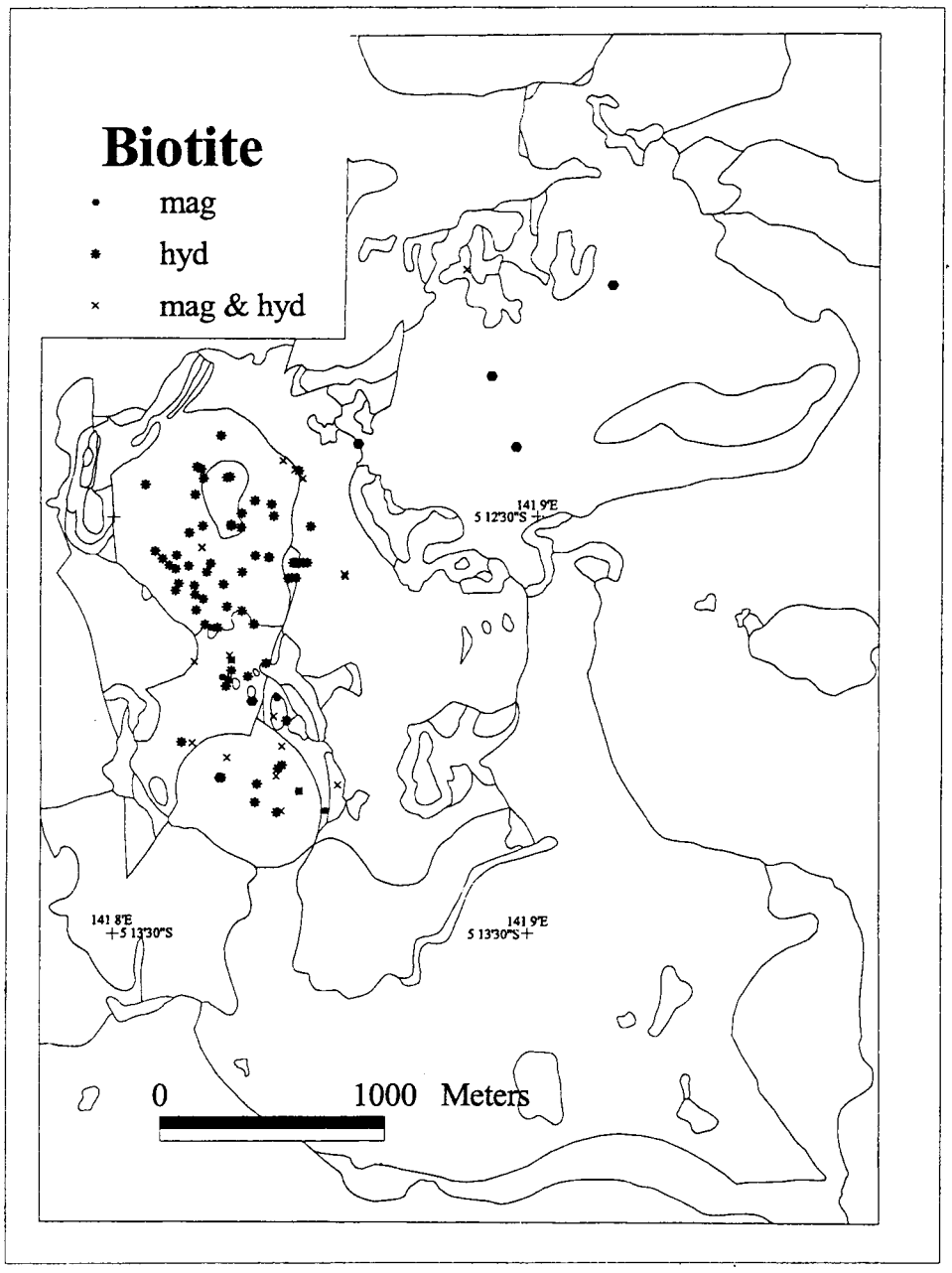

Figure 37: Map showing distribution of magmatic and hydrothermal biotite in samples from the Ok Tedi Intrusive Complex.

Figure 38: Examples of quartz in phanerites of the Ok Tedi Intrusive Complex and examples of fluid inclusions in quartz.

A. Example of interstitial quartz (center) in a phanerite. The quartz was among the last minerals to crystallize and its shape is entirely determined by the surrounding minerals (plagioclase feldspar in this instance). The field of view is about 0.7 x 1.0 mm. Plane-polar light. DDH 344-16.

B. The same interstitial quartz shown in A but here it is shown in crossed-polar light. DDH 344-16.

C. Anhedral interstitial quartz (center, white) and potassium feldspar (frosted texture) in a framework of a pyroxene (left, high relief) and plagioclase feldspar. The field of view is about 0.8 x 1.2 mm. Plane-polar light. TC-02-11.9.

D. The same minerals shown in C but here they are shown in crossed-polar light. The quartz is yellow in this photomicrograph. TC-02-11.9.

E. Anhedral interstitial quartz (center, white) in a framework of plagioclase feldspar and pyroxene (bottom center). Also shown is a cluster of crystals of magnetite and sphene (just left of center), several small crystals of pyroxene, and a one of biotite (lower right) that has been partly altered to chlorite.. The field of view is about 0.8 x 1.2 mm. Plane-polar light. TC-02-11.9.

F. The same minerals shown in E but here it is shown in crossed-polar light. The quartz in yellow in color. TC-02-11.9.

G. Fluid inclusions in quartz. The largest of these have the inverted morphology of doubly terminated crystals. All of them contain at least a bubble of gas and a cube of halite. Other daughter products may be present. Plane-polar light. The field of view is about 0.27 x 0.4 mm. DDH 103-429.

H. Fluid inclusion in quartz. This inclusion is roughly circular in shape. It contains a bubble of gas, a cube of halite, and at least one other daughter mineral. The field of view is about 0.05 x 0.08 mm. Plane-polar light. DDH 165-360.5.

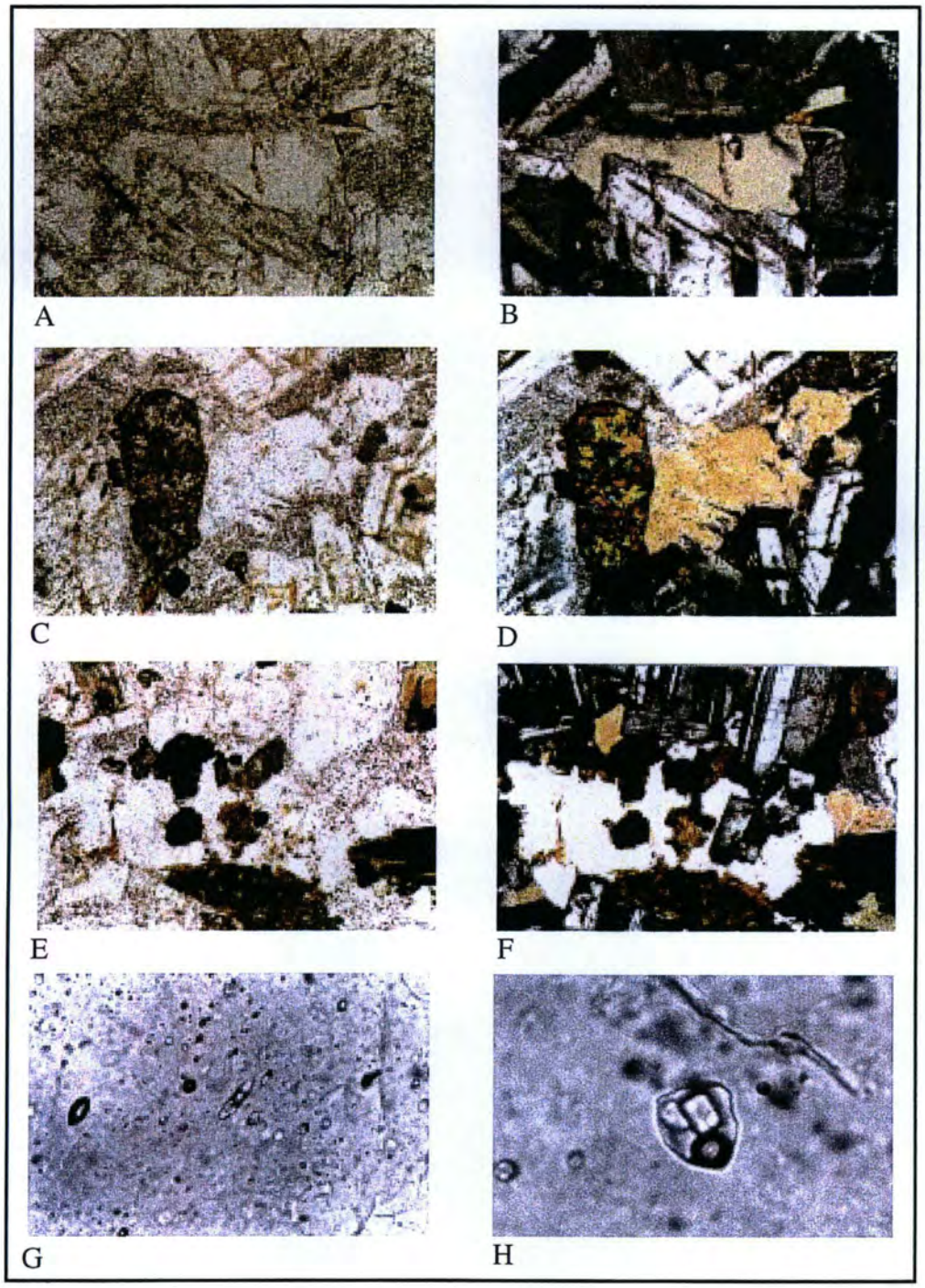

Figure 38 continued.

interstitial sites suggests that it crystallized during a late stage of the solidification of the magmas that formed the phanerites.

Quartz is present as an anhedral phase that is sparsely distributed throughout the groundmass of unaltered porphyries at Ok Tedi. It was noted as a possible phenocryst phase in only a few of the thin-sections of porphyry samples examined as part of this study. However most of these samples consisted of highly altered rock in which quartz may have been part of a veinlet, vug filling, or miarolitic cavity rather than a discrete magmatic crystal. Euhedral crystals of quartz such as the "quartz-eyes" that are found in many other porphyry copper systems are entirely lacking at Ok Tedi.

Many crystals of quartz contain fluid inclusions. Most of the inclusions include multiple phases consisting of a liquid, a gas bubble, and one or more crystal phases. The largest and most common solid phase is invariably a cube of halite (Figures 38G and H). The presence of saline fluid inclusions in unaltered phanerites is significant in that it suggests that a fluid phase was present in the late stages of magma consolidation. Such a saline fluid may have been responsible for the hydrothermal alteration that transformed the mineralogical composition of the intrusive rocks and that deposited the hydrothermal copper and gold of the Ok Tedi deposit. A study by R.W.T. Wilkins (unpublished) of CSIRO Laboratories of Australia has shown that both high-density multiphase liquid inclusions and low-density gas-rich inclusions are common at Ok Tedi; that homogenization

temperatures of the inclusions range from 400° to 650° C; and that the multiphase inclusions contain up to 64 weight percent NaCl + KCl.

Veinlets of quartz are present in both phanerites and porphyries throughout the Ok Tedi Intrusive Complex, but are most common and abundant in and near the quartz core. Within veinlets, the quartz forms anhedral granular mosaics. Fluid inclusions are also common in the vein quartz. Chalcopyrite, pyrite, and (possibly) bornite are common associates of quartz in the veinlets. Limonite as an oxidation product of earlier formed sulfides is also a common associate of quartz in the zone of oxidation.

Quartz also occurs as intergrowths with hydrothermal biotite in sites previously occupied by magmatic pyroxene (possibly also hornblende or biotite.) Fluid inclusions are common in the quartz in these many of these pseudomorphic intergrowths. The quartz in these sites also commonly contains fluid inclusions. Many of these inclusions are elongate and tube-like in shape.

Groundmass

The term *groundmass* is used to describe the finely-crystalline material that forms the matrix for phenocrysts in rocks with porphyritic texture. Groundmass averages about 38 volume percent in samples of porphyry. It consists of fine-grained, generally anhedral, crystals of the same minerals recognized as phenocryst phases such as plagioclase and potassium feldspar, quartz, biotite, pyroxene,

amphibole, magnetite, and others. Feldspar is the dominant mineral of the groundmass in all samples. Although distinguishing the difference between plagioclase and potassium feldspar in the groundmass of unaltered and hydrothermally altered porphyries is difficult, potassium feldspar is dominant in samples from areas of potassic alteration whereas the two feldspars are probably subequal in abundance in unaltered or propylitically altered porphyries. Confirmation of potassium feldspar in groundmass was made possible by using a large number of stained thin-sections in first suite of petrographic samples. The groundmass varies in grain-size from aphanitic to aplitic in porphyries from Ok Tedi.

Groundmass was a counted phase in a few of the phanerites listed in Appendices 2 and 3. Where used in such descriptions of phanerites the term denotes areas of very finely crystalline texture.

Accessory Minerals - Magmatic Association

The accessory minerals of magmatic origin identified in rocks that have been unaffected by subsequent hydrothermal alteration, or that have only undergone only slight modification, are sphene, apatite, zircon, and magnetite.

Most crystals of sphene in the intrusive rocks from Ok Tedi are euhedral in shape. They display the wedge, diamond (Figure 39A), lozenge (Figure 39B-D), and dovetail shapes that are characteristic of this mineral. Sphene is closely

Figure 39: Photomicrographs of sphene (A-D) and pseudomorphs of rutile after sphene (E-H).

A. Diamond-shaped crystal of sphene in phanerite. The crystal is about 0.2 x 0.5 mm. in size. DDH 342-84.5

B. Doubly-terminated lozenge-shaped crystal of sphene in porphyry. The crystal is about 02. x 0.9 mm in size. DDH 331-218.5

C. Euhedral crystal of sphene in phanerite. This crystal contains inclusions of apatite (clear) and magnetite (black). In addition it contains an inclusion of sphene (adjacent to and below apatite). The field of view is about 0.7 x 1.1 mm. Plane-polar light. JDD-94-12

D. The same minerals shown in C but here they are shown in crossed-polar light. JDD-94-12

E Pseudomorph of rutile after sphene in porphyry. The crystal is about 0.4 x 0.8 mm in size. Plane-polar light. DDH 323-308

F. Euhedral crystal of sphene partly pseudomorphed by rutile in a potassium feldspar-altered phanerite. Plane-polar light. The field of view is about 0.3 x 1.1 mm. in size. DDH 464-147.2

G. Euhedral crystal of sphene partly pseudomorphed by rutile in a potassium feldspar-altered phanerite. Plane-polar light. The field of view is about 0.3 x 1.1 mm. DDH 464-147.2

H. Pseudomorph of rutile after sphene in porphyry. Plane-polar light. The field of view is about 0.6 x 0.9 mm. DDH 334-216.2

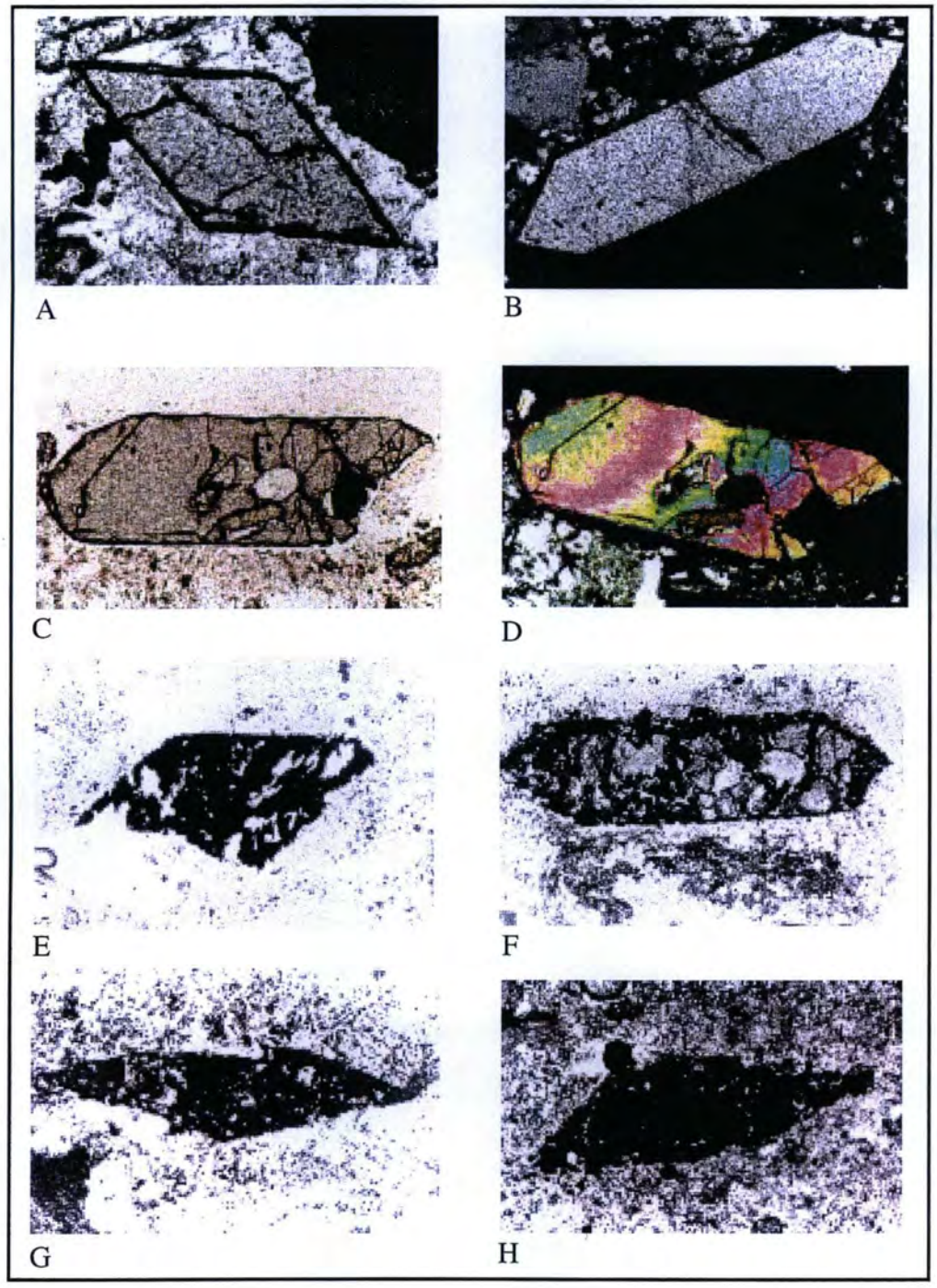

Figure 39 continued.

associated with the mafic minerals (pyroxene, hornblende, and magmatic biotite), apatite, and magnetite. This association is typified by inclusions of sphene in the mafic minerals, ragged growths of sphene on magnetite, and the close physical proximity of sphene to the mafic minerals in samples believed to represent magmatic rock. Inclusions of apatite and magnetite are present in some samples (Figures 39A and B). The common association of sphene with the mafic minerals, apatite, and magnetite as well as as inclusions of these minerals in one another suggests that they formed contemporaneously.

A map showing the distribution of sphene in thin-sections from the Ok Tedi Intrusive Complex is given as Figure 40. The average modal content of sphene in samples that contain either pyroxene or hornblende (and therefore are representative of magmatic assemblages) is 1.04 percent whereas the average in samples which do not contain these minerals (i.e., those with potassic alteration) is 0.13. This suggests that sphene was unstable, and therefore destroyed, in the hydrothermal environment.

Fifteen microprobe analyses were made on crystals of magmatic sphene in three thin sections. Representative analyses are listed in Table 7. The entire sets of analyses are given in Appendix 8. The weight percentages of CaO, TiO_2, and SiO_2 of stoichometric sphene, as calculated from the ideal formula, should be 28.6, 40.8, and 30.65, respectively. The average of these oxides in the fifteen analyses performed are 27.3, 35.9, and 29.9 weight percent, respectively. The measured

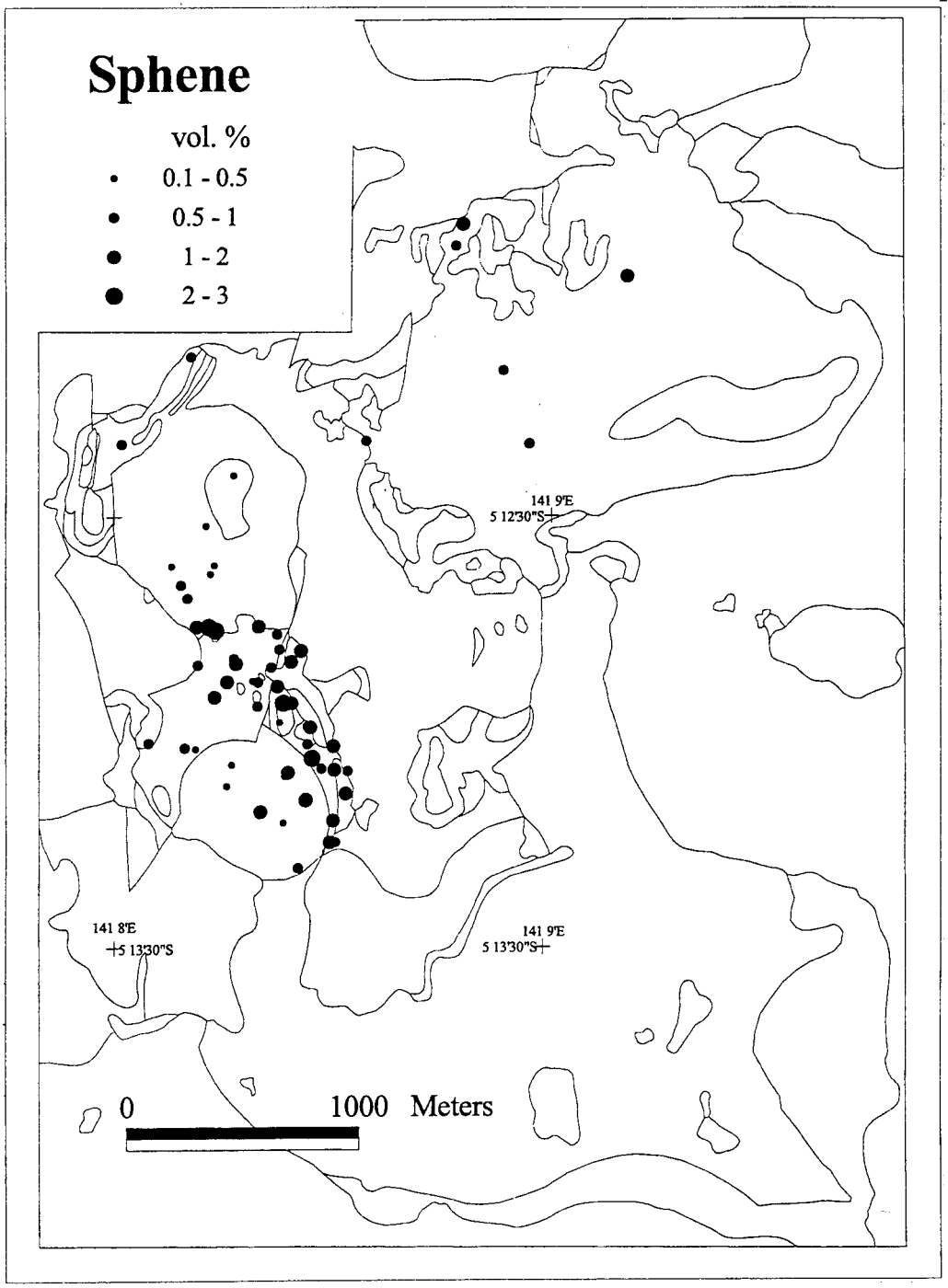

Figure 40: Map showing distribution of sphene in the altered and unaltered intrusive rocks of the Ok Tedi Intrusive Complex.

Sample	331 218.5	356 166.5	356 190
Analyses	4	8	2
SiO_2	29.83	29.99	29.67
TiO_2	36.51	36.12	35.01
Al_2O_3	1.36	1.09	1.16
FeO	1.62	1.87	2.09
MnO	0.19	0.13	0.16
MgO	0.03	0.00	0.04
CaO	27.53	27.62	27.10
Na_2O	0.02	0.03	0.06
K_2O	0.01	0.01	0.03
CL	0.01	0.00	0.02
F	0.41	0.55	0.55
O=CL	0.00	0.00	<0.01
O=F	<0.18	<0.23	<0.23
TOTAL	97.32	97.19	95.63
Si^{4+}	1.00	1.01	1.02
Ti^{4+}	0.92	0.92	0.90
Al^{3+}	0.05	0.04	0.05
Fe^{2+}	0.05	0.05	0.06
Mn^{2+}	0.01	0.00	0.01
Mg^{2+}	0.00	0.00	0.00
Ca^{2+}	0.99	1.00	0.99
Na^{+}	0.00	0.00	0.00
K^{+}	0.00	0.00	0.00
Cl^{-}	0.00	0.00	0.00
F^{-}	0.04	0.06	0.06
O^{2-}	4.96	4.94	4.94

Formula calculated using Program of Ercit and on basis of 5 anions

Table 7: Representative electron-beam analyses of sphene.

values of CaO and SiO_2 are reasonably close to their stoichiometric values but the amount of TiO_2 is low. The analyses contain, besides the expected oxides, an average of 1.2 weight percent Al_2O_3, 1.9 percent FeO, and 0.53 weight percent fluorine. It is likely that some substitution of Fe for Ca(?) and possibly Al, for Ti has taken place, and that the deficiency of TiO_2 can be related to such possible substitutions.

Apatite is present in altered and unaltered phanerites and porphyries from Ok Tedi. It has two distinctly different sizes and habits: 1.) as tiny rod-shaped crystals that are typically less than 0.01 mm in length, and 2.) as stout crystals with circular cross-sections, which are as large as one millimeter in diameter (Figures 41A-C). Apatite was noted in about 20 percent of the thin-sections with porphyry texture and in about 65 percent of those with phaneritic texture. It accounts for about 0.3 volume percent in both the phanerites and porphyries in which it was observed.

Zircon is present in about one-half of all thin-sections that were examined. It is present in phanerites and porphyries. Its abundance is about the same in unaltered intrusions and their counterparts that have been subjected to strong potassic alteration. Zircon accounts for less than 0.1 volume percent in the rocks in which it is found. Most crystals are rounded in shape (Figure 41D) and less than 0.1 mm in diameter. Zircon is found in association with, or is overgrown by

Figure 41: Photomicrographs of apatite, zircon, and magnetite.

A. Stout subhedral crystal of apatite in unaltered phanerite. The field of view is about 0.5 x 0.8 mm. Plane-polar light. DDH 351-313.2.

B. Stout subhedral to euhedral crystal of apatite in porphyry that has undergone weak potassic alteration. The field of view is about 0.4 x 0.6 mm. Plane-polar light. DDH 303-350.55.

C. Stout subhedral crystal of apatite in phanerite that has undergone propylitic alteration. Tiny fluid inclusions are present in the crystal. These inclusions contain bubbles of gas and at least one daughter mineral phase. The field of view is about 0.8 x 1.2 mm. Plane-polar light. JDD-94-12.

D. Rounded crystal of zircon (center) in a pseudomorph of hydrothermal biotite and quartz that has replaced a magmatic ferromagnesian mineral (probably pyroxene). The zircon was an inclusion within the original magmatic mineral. The field of view is about 0.2 x 0.3 mm. Plane-polar light. DDH 345-468.

E. Anhedral crystal of magnetite in a phanerite. This crystal is magmatic in origin. A crystal of sphene is also shown (upper left). The field of view is about 0.7 x 1.0 mm. Plane-polar light. DDH 356-166.5.

F. Common magmatic mineral assemblage in unaltered rocks of the Ok Tedi Intrusive Complex: pyroxene (pale green, lower left center), hornblende (moderate olive green, adjacent to pyroxene), magnetite (black), sphene (top center, adjacent to magnetite). A crystal of apatite (just out of field of view, but shown in Fig. 39A) rounds out the magmatic accessory mineral suite. The field of view is about 0.5 x 0.8 mm. Plane-polar light. DDH 351-313.2.

G. Several phenocrysts of magnetite are shown in this photomicrograph. Two of these abut against a phenocryst of pyroxene. The lower one of these is euhedral in shape; all other magnetite phenocrysts in the photo are subhedral or anhedral. The mineral assemblage is magmatic. The field of view is about 1.3 x 2 mm. Reflected light. DDH 458-151.8.

Figure 41 continued.

H. Typical distribution of magmatic magnetite in a sample of phanerite. Two size populations can be seen: (1) larger crystals many of which abut against crystals of pyroxene, and (2) small crystals that are scattered uniformly throughout the thin-section. The field of view is about 4.0 x 6.4 mm. Plane-polar light. DDH 74-66.

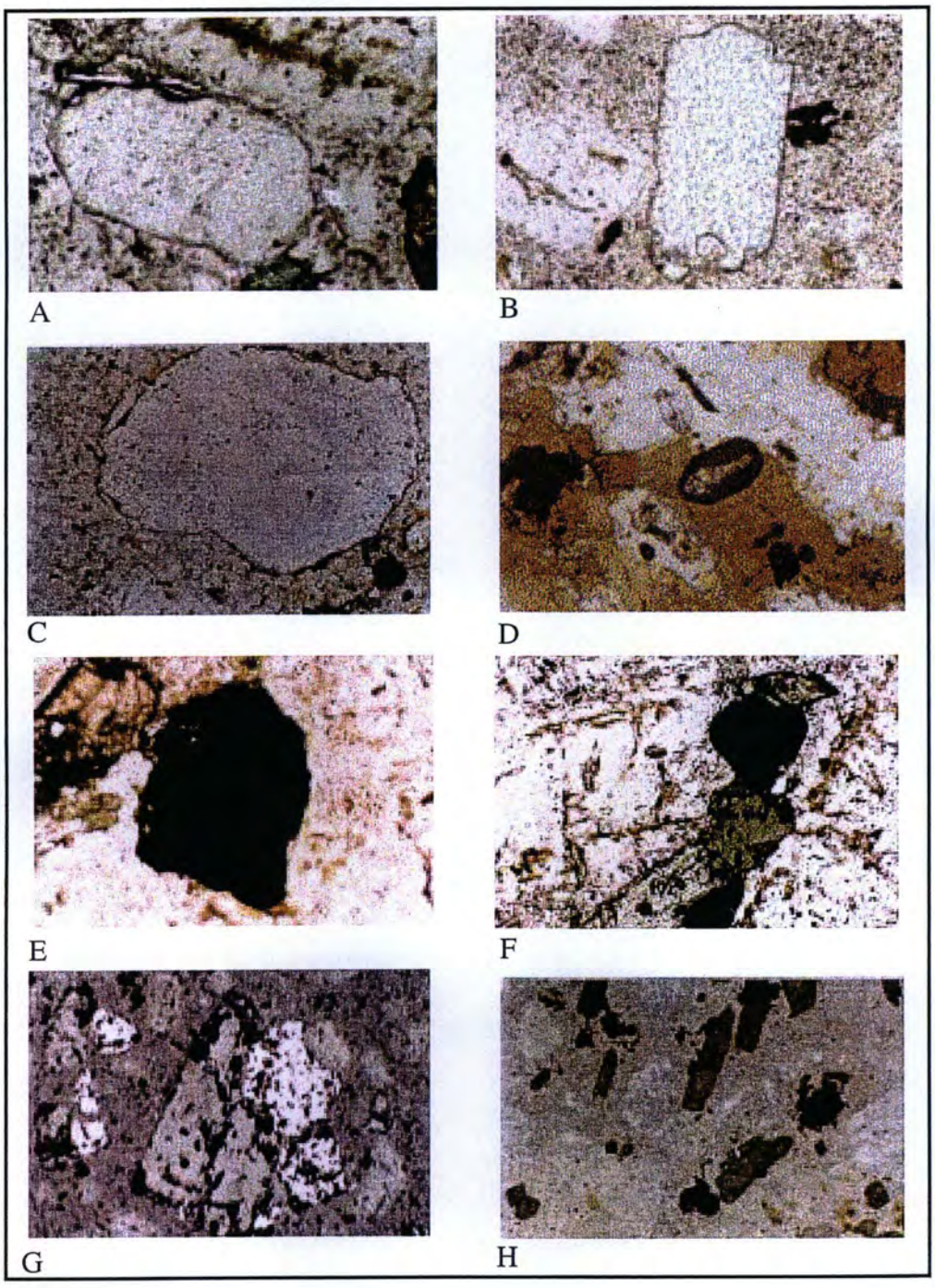

Figure 41 continued.

apatite, magnetite, pyroxene, and magmatic biotite, which suggests an early formation in the paragenetic sequence.

The principal opaque oxide mineral of the least altered intrusive rocks is magnetite. It occurs as cubes and rounded cubes (Figures 41E-G). Exsolution lamellae of ilmenite were observed in the magnetite crystals of a few thin sections. Two size populations are present in many samples: 1.) magnetite granules (larger than 0.1 mm), and 2.) magnetite dust (less than 0.01 mm). Although granules are less abundant in terms of total number of crystals, they are probably much greater in aggregate volume as compared to the dust variety. Magnetite granules form rings around ragged crystals of magmatic biotite in some samples (e.g., Figures 33E and F). These may have originated as oxidation or resorption products of the biotite and, therefore, the result of a magmatic process. Magnetite is present as inclusions in pyroxene, hornblende, biotite, and sphene. Much of the magnetite in samples from Ok Tedi is enveloped by thin fringes of ragged anhedral biotite which suggests that it may have served as a nucleation site for the biotite.

Microprobe analyses were made of magnetite in six thin-sections. Representative analyses of magnetite and ilmenite are listed in Table 8. The entire set of analyses which includes magnetite, ilmenite, and mixtures of magnetite and ilmenite is given in Appendix 9. The results of the analyses are portrayed on ternary diagrams in Figures 42A and B. Many of the analyses plot near $Fe_2O_3 = 69$ weight percent, FeO = 31 weight percent on these diagrams (Figure 42A). Many

Sample	319	331	356	356	458
	339.3	218.5	166.5	190	151.8
	magnetite	magnetite	magnetite	magnetite	magnetite
Analyses	6	8	18	2	37
Fe_2O_3*	67.86	71.24	68.90	67.97	71.45
FeO	30.75	32.16	30.98	30.89	32.17
TiO_2	0.14	0.24	0.40	0.45	0.38
MnO	0.12	0.24	0.28	0.24	0.35
SiO_2	0.03	0.02	0.05	0.02	0.01
Al_2O_3	0.12	0.42	0.16	0.36	0.25
MgO	0.02	0.02	0.05	0.04	0.06
Cr_2O_3	0.03	0.03	0.02	0.01	0.04
V_2O_5	0.00	0.31	0.68	0.66	0.49
NiO	0.02	0.01	0.00	0.00	0.02
CuO	0.00	0.02	0.00	0.00	0.02
ZnO	0.01	0.16	0.00	0.00	0.06
Total	99.1	104.9	101.5	100.6	105.3
Fe^{3+}	15.800	15.606	15.708	15.442	15.493
$Fe2^{+}$	7.956	7.829	7.848	7.799	7.752
Ti	0.033	0.052	0.092	0.102	0.081
Mn	0.033	0.060	0.071	0.060	0.084
Si	0.010	0.006	0.014	0.006	0.004
Al	0.044	0.143	0.057	0.128	0.086
Mg	0.007	0.008	0.023	0.018	0.025
Cr	0.007	0.006	0.005	0.003	0.008
V		0.084	0.188	0.182	0.130
Ni	0.004	0.003		0.000	0.004
Cu		0.005		0.000	0.003
Zn	0.003	0.034		0.000	0.014
Sum Cations	23.90	23.84	24.01	23.74	23.69

* Determined by stoichiometry

Formula contents on a basis of 32 anions

Table 8: Representative electron-beam microprobe analyses of magnetite and ilmenite.

Sample	331	342	458	458	458
	218.5	84.5	151.8	151.8	151.8
	ilmenite	ilmenite	ilmenite	ilmenite	ilmenite
Fe_2O_3 *	6.03	4.72	6.06	5.45	1.25
FeO	30.62	36.51	36.14	36.97	45.05
TiO	46.03	47.18	45.48	45.12	41.87
MnO	15.42	9.38	10.75	10.03	8.31
SiO_2	0.02	0.02	0.05	0.08	0.03
Al_2O_3	0.01	0.00	0.02	0.04	0.17
MgO	0.07	0.09	0.18	0.21	0.89
Cr_2O_3	0.00	0.00	0.02	0.01	0.04
V_2O_5	0.36	0.35	0.31	0.37	0.44
NiO	0.06	0.00	0.00	0.00	0.00
CuO	0.00	0.00	0.01	0.03	0.09
ZnO	0.08	0.24	0.03	0.11	0.03
TOTAL	98.7	98.49	99.05	98.42	98.17
Fe^{3+}	0.118	0.092	0.118	0.107	0.025
Fe^{2+}	0.665	0.792	0.785	0.809	1.012
Ti^{4+}	0.899	0.920	0.888	0.887	0.846
Mn^{2+}	0.339	0.206	0.236	0.222	0.189
Si^{4+}	0.001	0.001	0.001	0.002	0.001
Al^{3+}	0.000	0.000	0.001	0.001	0.005
Mg^{2+}	0.003	0.003	0.007	0.008	0.036
Cr^{3+}	0.000	0.000	0.000	0.000	0.001
V^{5+}	0.006	0.006	0.005	0.006	0.008
Ni^{2+}	0.001	0.000	0.000	0.000	0.000
Cu^{2+}	0.000	0.000	0.000	0.001	0.002
Zn^{2+}	0.002	0.005	0.001	0.002	0.001
Sum cations	2.03	2.02	2.04	2.05	2.13

*Determined by stoichiometry

Formulae calculated using program of Ercit (unpublished)

Formula contents on a basis of 3 anions

Table 8 continued.

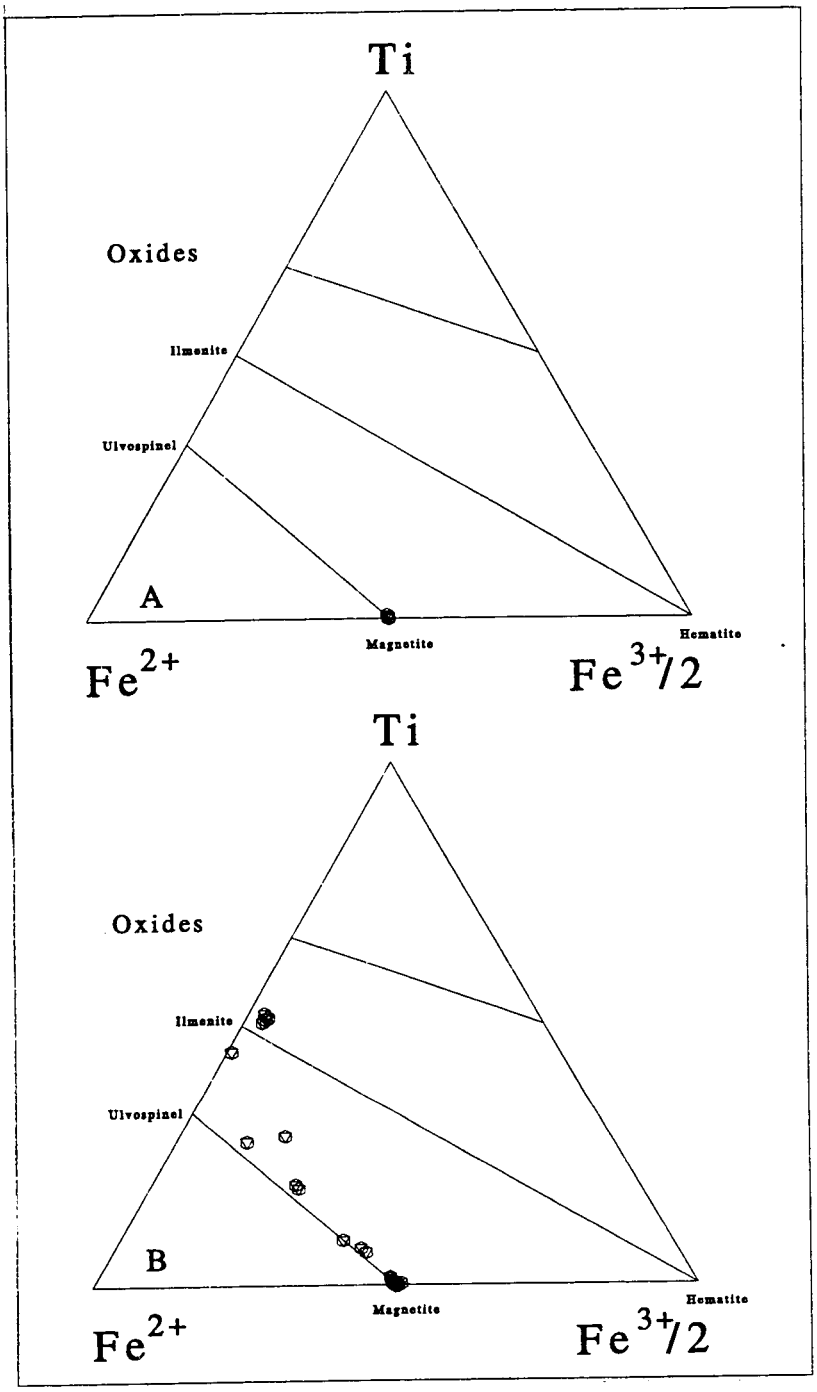

Figure 42: Ternary diagrams illustrating compositions of magmatic magnetite, ilmenite, and mixtures thereof.

other analyses plot between the composition of magnetite and ilmenite (or ulvospinel). This indicates the presence of titanium at the sites that were hit by the electron beam and may indicate the presence, in these locations, of thin exsolution lamellae of ilmenite or concentrations of unexsolved titanium. Still other analyses plot near the composition of ilmenite. These represent the composition of ilmenite lamellae.

Other Alteration Minerals

Alteration minerals that result from propylitic alteration of the intrusive rocks at Ok Tedi are epidote, garnet, clinopyroxene, scapolite(?), and calcite. These are typically found in association with the primary magmatic minerals including pyroxene (and/or hornblende), apatite, magnetite, sphene, zircon, and apatite. The alteration minerals formed by potassic alteration of intrusive rocks are rutile, magnetite, iron-sulfides (pyrite, pyrrhotite, marcasite), and copper-iron sulfides (chalcopyrite, bornite, and idaite). These are not typically found in association with magmatic pyroxene, hornblende, or sphene. These minerals are destroyed as part of the process of potassic alteration. Zircon and apatite can be found in potassically altered rocks and appear to be unaffected by the alteration. Some apatite is formed by hydrothermal alteration at Ok Tedi as suggested by Duncan (1972) and cobbles and boulders of apatite-magnetite have been found in breccias within the Fubilan intrusion. Apatite, however, is generally lower in abundance in rocks that have

undergone strong potassic alteration then in their unaltered counterparts and the P_2O_5 contents of potassically altered rocks are only about one-half of those of unaltered rocks.

Garnet and epidote are both common in samples from the Kalgoorlie, Ningi, and Sydney intrusion. Garnetite and epidotite that formed by wholesale replacement of intrusive rocks can be found in a few locations at Ok Tedi. These alteration minerals are likely the result of extreme propylitic alteration involving additions of calcium, in particular, and possibly of iron. These calc-silicate minerals and assemblages thereof can also be classified as skarns, particularly where the silicate minerals are in association with sulfide and/or oxide minerals. Katchan (1982) and Duncan (1972) suggest that most of the skarn at Ok Tedi is endoskarn and thus formed from intrusive host rocks. I excluded samples of massive garnetite, epidosite, and endoskarn from my detailed petrographic studies.

Epidote is found as partial pseudomorphic replacements of plagioclase feldspar, as an infilling mineral in veinlets (Figure 43A and B), and as disseminated anhedral to subhedral crystals that may have originated by the replacement of earlier-formed minerals or by the filling of void spaces (Figure 43C and D). Katchan (1982) reported that the Sydney Monzodiorite is the host for veinlets of epidote and that these increase in abundance toward bodies of skarn. He listed microprobe analyses of epidote and allanite and noted that epidote rims were found on allanite cores. I performed eight microprobe analyses on epidote in one thin-

Figure 43: Photomicrographs of epidote and garnet.

A. Veinlets of epidote cutting across crystals of plagioclase feldspar in a rock with phaneritic texture. The field of view is about 1.2 x 0.8 mm. Plane-polar light. DDH 342-84.5

B. Same veinlets of epidote shown in A. Crossed-polar light. DDH 342-84.5

C. Subhedral crystal of epidote in a rock with phaneritic texture. The epidote has grown into contact with crystals of feldspar and pyroxene. The crystal displays distinct zones as the microscope is rotated. The field of view is about 1.3 x 2.0 mm. Plane-polar light. DDH 459-102.9

D. The same crystal of epidote as in A. Crossed-polar light. DDH 459-102.9

E. Cluster of high-relief minerals in a phanerite that has undergone weak endoskarn alteration. Crystals of sphene (amber; top left, left center, and center right) and pyroxene (green) are of magmatic origin whereas the anhedral to subhedral garnets (brown, left center) have formed by metasomatic processes. The field of view is about 0.8 x 1.1 mm. Plane-polar light. DDH 342-141

F. Crystal (or cluster of) anhedral to subhedral garnet in a phanerite that has undergone weak endoskarn alteration. [the garnet has probably replaced plagioclase feldspar] The field of view is about 2.8 x 4.2 mm. DDH 459-102.9

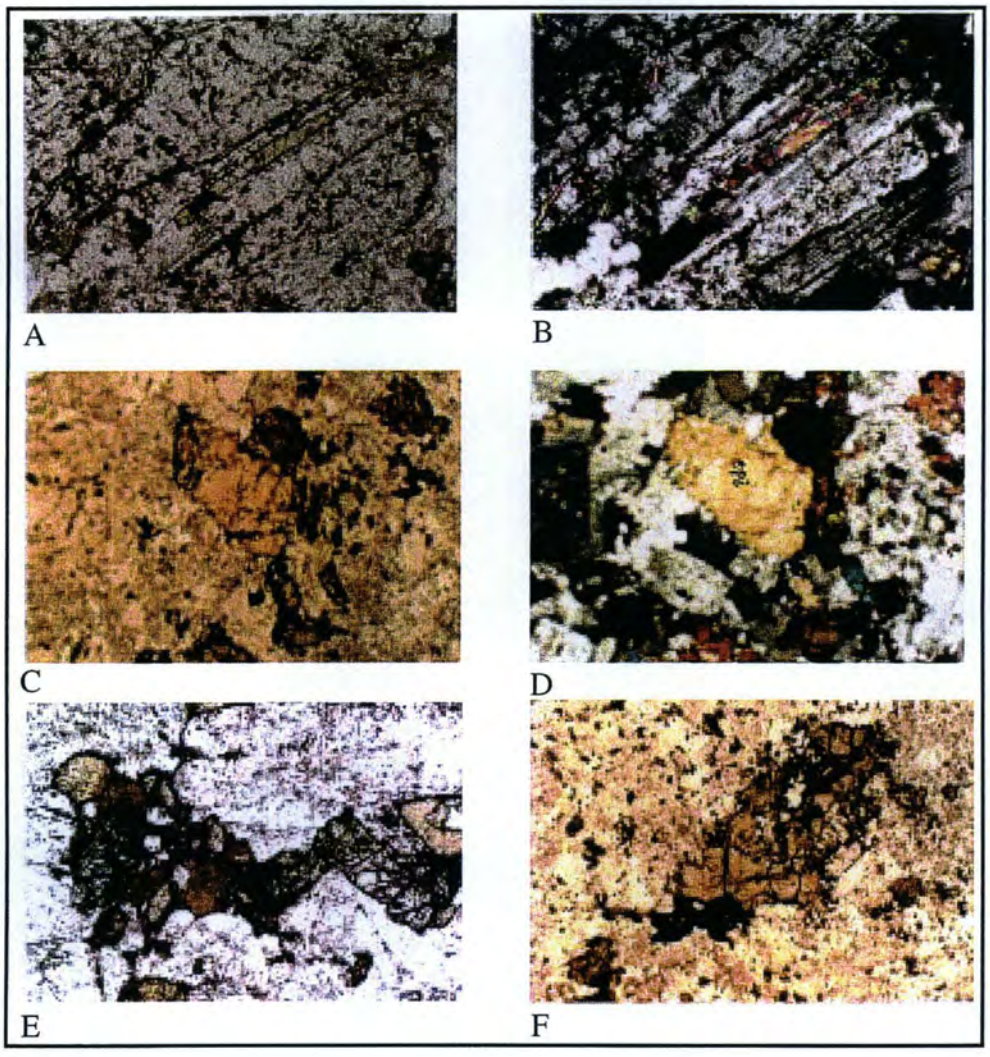

Figure 43 continued.

section as part of my study. The results of these analyses are given in Table 9. Not enough analyses were done to allow any discussion of systematic variation of the composition of epidote, but they conform the petrographic identification of the mineral. Lanthanum and cerium (characteristic of allanite) were not included in the analytical files and may account for the low total oxide percentages. Structural formulae were calculated on the basis of 13 anions (oxygen and fluorine) and with all iron as Fe_2O_3.

Garnet is similar to epidote in spatial distribution and mode of occurrence. It forms veinlets and disseminated crystals (Figures 43E-G) in rocks with propylitic alteration and culminates in abundance as massive garnetite in garnet skarn. It is found in association with the magmatic ferromagnesian minerals in some thin-sections (Figure 43E and F) and by itself in others (Figure 43G). Fifty-one microprobe analyses were performed on disseminated anhedral garnet in two thin-sections (DDH 341-141 and DDH 459-102.9). Representative analyses are given in Table 10; the complete sets are included as Appendix 10. Representative analyses from a set of 155 analyses performed by Lihua Zhang (using the microprobe laboratory at OSU) on one sample of garnet skarn from the Edinburgh area at Ok Tedi are also included in Table 10. All of these analyses are portrayed on Gr-Ad-Sp+Al ternary diagrams in Figure 44. The garnets are all grandite in composition consisting principally of the grossularite and andradite end members. The analyses

	DDH-459-102.9							
Run No.	**24011**	**24012**	**24013**	**24014**	**24018**	**24019**	**24020**	**24021**
SiO_2	35.00	35.03	34.57	34.78	32.98	35.48	36.65	34.77
TiO_2	0.00	0.01	0.05	0.18	0.04	0.04	0.05	0.02
Al_2O_3	23.69	24.33	21.62	21.78	19.70	22.13	21.26	21.38
Cr_2O_3	0.00	0.02	0.00	0.00	0.00	0.02	0.03	0.04
Fe_2O3	11.80	11.19	14.31	13.21	16.26	14.21	15.40	15.18
MnO	0.61	0.33	0.09	0.17	0.23	0.03	0.03	0.05
MgO	0.10	0.05	0.07	0.07	0.02	0.02	0.00	0.01
CaO	22.81	23.13	23.42	23.29	22.67	23.14	23.58	23.44
F	0.24	0.22	0.27	0.34	0.29	0.27	0.25	0.25
H_2O^*	1.69	1.71	1.66	1.62	1.59	1.68	1.72	1.68
O=F	-0.10	-0.09	-0.11	-0.14	-0.12	-0.11	-0.11	-0.11
TOTAL	95.85	95.92	95.94	95.30	93.66	96.90	98.85	96.71
Si^{4+}	2.911	2.902	2.903	2.929	2.869	2.936	2.981	2.903
Ti^{4+}	0.000	0.001	0.003	0.011	0.003	0.002	0.003	0.001
Al^{3+}	2.322	2.376	2.140	2.161	2.019	2.158	2.038	2.104
Cr^{3+}	0.000	0.001	0.000	0.000	0.000	0.001	0.002	0.003
Fe^{3+}	0.738	0.698	0.904	0.837	1.064	0.885	0.943	0.954
Mn	0.043	0.023	0.006	0.012	0.017	0.002	0.002	0.004
Mg	0.012	0.006	0.009	0.009	0.003	0.002	0.000	0.000
Ca	2.032	2.053	2.107	2.101	2.113	2.052	2.055	2.097
F^-	0.630	0.058	0.072	0.091	0.080	0.071	0.064	0.066
Sum cations	8.1	8.1	8.1	8.1	8.1	8.0	8.0	8.1

Calculated using program of Ercit (unpublished)

*Determined by stoichiometry

Contents on a basis of 13 anions ane with all iron as Fe_2O_3

Table 9: Electron-beam microprobe analyses of epidote.

Sample		342-141			459-102.9	
Run No.	24044		24041	24017		24031
	min andradite	Avg. of 16	max andradite	min andradite	Avg. of 16	max andradite
SiO_2	35.35	33.92	33.42	33.96	34.43	34.97
TiO_2	0.47	2.03	2.09	0.20	0.38	0.04
Al_2O_3	6.26	4.85	3.28	10.46	6.79	1.10
Cr_2O_3	0.03	0.02	0.00	0.00	0.01	0.06
Fe_2O3	0.00	0.00	0.00	0.00	0.00	0.00
FeO	20.71	20.77	23.25	14.73	20.39	27.44
MnO	0.37	0.30	0.25	0.86	0.35	0.23
MgO	0.03	0.07	0.03	0.01	0.02	0.02
CaO	32.47	32.41	32.04	33.98	32.48	31.68
F	0.31	0.36	0.33	0.44	0.40	0.32
Total	96.00	94.72	94.69	94.64	95.25	95.85
Uvarovite	0.10	0.06	0.01	0.02	0.05	0.20
Andradite	71.32	79.81	89.96	33.85	69.59	94.19
Pyrope	0.13	0.30	0.15	0.06	0.09	0.10
Spessartine	0.89	0.75	0.63	2.61	0.91	0.57
Grossularite	26.97	19.01	9.26	63.46	27.62	3.24
Almandine	0.59	0.08	0.00	0.00	1.74	1.70

Sample		E03-009	
Run No.	1014		939
	min andradite	Avg. of 156	max andradite
SiO_2	37.92	35.71	34.05
TiO_2	0.04	0.34	2.28
Al_2O_3	16.26	9.40	4.60
Cr_2O_3	0.00	0.01	0.05
Fe_2O3	8.78	17.25	21.92
FeO	0.97	0.74	0.62
MnO	1.36	0.73	0.49
MgO	0.05	0.25	0.00
CaO	34.51	33.58	33.65
F	0.14	0.09	0.00
Total	100.03	98.10	97.66
Uvarovite	0.00	0.03	0.18
Andradite	26.25	56.22	80.22
Pyrope	0.20	0.98	0.00
Spessartine	3.04	1.73	1.22
Grossularite	70.51	40.99	18.38
Almandine	0.00	0.05	0.00

Table 10: Representative electron-beam microprobe analyses of garnet.

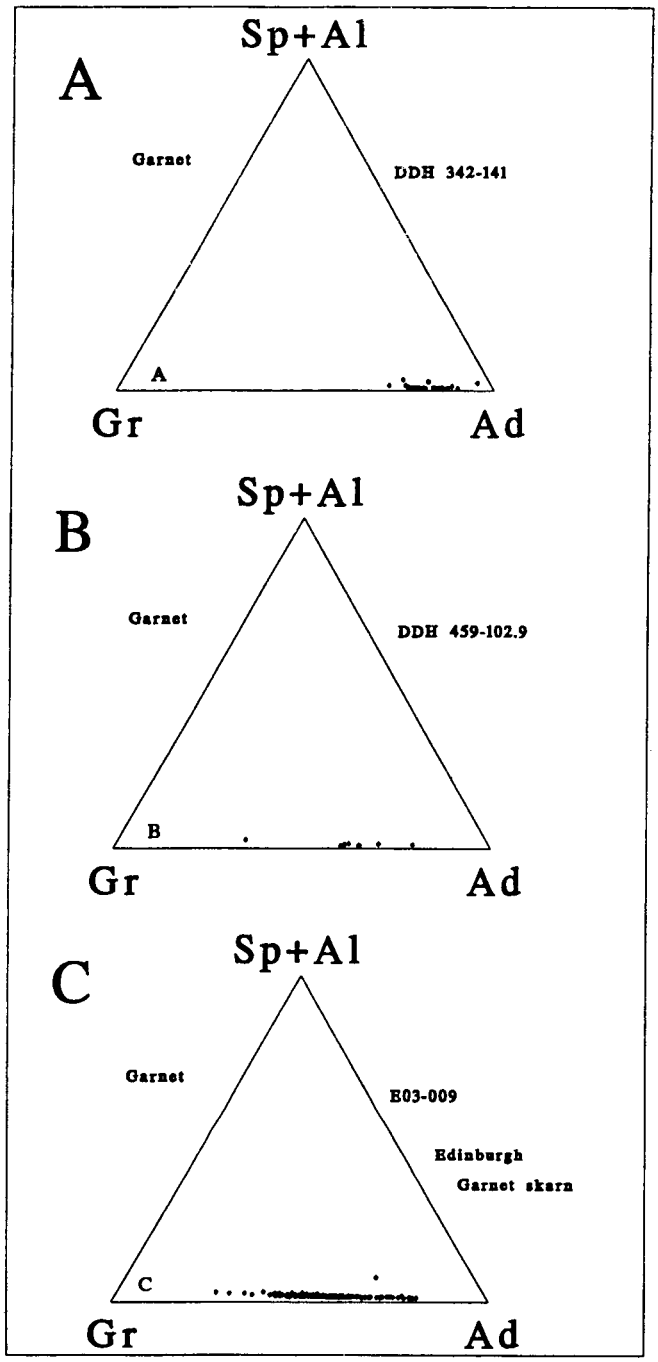

Figure 44: Ternary plot of Grossularite-Andradite-Spessartine +Almandine for garnets from the Ok Tedi Mine area.

from the garnet in DDH 342-141 cluster near the andradite corner of the diagram and range in Ad content from about 71 to 95. Most of the analyses of garnet in DDH 459 fall in the range of Ad_{60-79} but one analysis gave Ad_{35}. The garnet in the sample of garnetite from Edinburgh shows a wide range of Ad content (about 27 to 81) and includes analyses similar to those of both other thin-sections.

The principal oxide mineral in samples that have undergone strong potassic alteration is rutile. Pseudomorphs of rutile after sphene are common in thin-sections from rocks which have undergone strong potassic alteration. Examples are shown in Figures 39E-H. Rutile is also present in the patches of hydrothermal biotite formed from mafic minerals.

Four microprobe analyses were performed on rutile in one thin-section (JDD-94-07). The analyses are given as Table 11. Three of these analyses fall on or near the Ti apex in Figure 45. The remaining analysis falls on the tie-line between Ti and Fe^{2+}. These microprobe analyses confirm the identification of rutile but are insufficient in number to establish any patterns of chemical composition.

Veinlets of hydrothermal magnetite cut across intrusive rocks at several locations within the Ok Tedi intrusive complex. Anhedral clusters of magnetite crystals were observed in one specimen from an area of strong potassium feldspar metasomatism (JDD-94-07; Figure 46). The anhedral shapes of the crystal clusters of hydrothermal magnetite are considerably different from the characteristic cubic

	JDD-94-05		
Sample	**18078**	**18079**	**18081**
FeO*	0.52	0.52	0.65
TiO_2	93.72	93.16	94.09
MnO	0.04	0.00	0.00
SiO2	0.30	0.40	0.08
Al_2O_3	0.04	0.06	0.02
MgO	0.03	0.02	0.04
Cr_2O_3	0.07	0.16	0.07
V_2O_5	1.29	1.17	1.37
NiO	0.00	0.02	0.02
CuO	0.01	0.00	0.04
ZnO	0.01	0.00	0.01
	0.00	0.00	0.00
Total	96.02	95.50	96.40
Fe^{2+}	0.10	0.09	0.12
Ti	15.53	15.44	15.60
Mn	0.01	0.00	0.00
Si	0.07	0.09	0.02
Al	0.01	0.01	0.00
Mg	0.01	0.01	0.01
Cr	0.01	0.03	0.01
V	0.26	0.24	0.28
Ni	0.00	0.00	0.00
Cu	0.00	0.00	0.01
Zn	0.00	0.00	0.00
Sum of cations	16.00	15.91	16.05
* all iron as FeO			
formula contents on the basis of 32 anions			

Table 11: Electron-beam microprobe analyses of rutile.

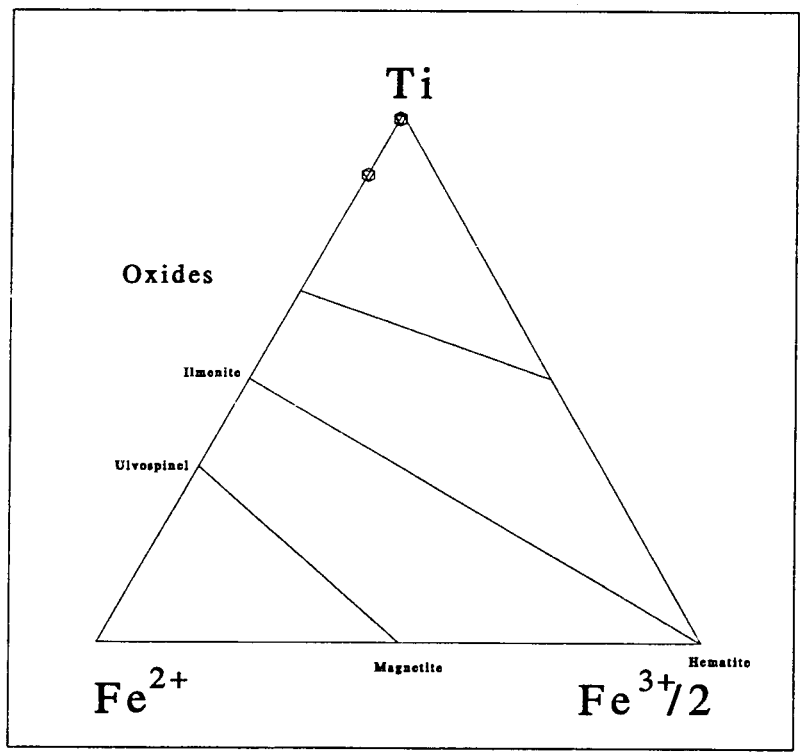

Figure 45: Ternary diagram illustrating composition of rutile.

Figure 46: Photomicrographs of hydrothermal magnetite.

A. Pseudomorph of hydrothermal magnetite that has replaced a pre-existing mineral, probably a crystal of pyroxene, in a potassically altered porphyry. The field of view is about 0.7 x 1.0 mm. Reflected light. JDD-94-07

B. Cluster of hydrothermal opaque minerals in a sample of porphyry from the Fubilan Intrusion. The field of view is about 0.8 x 1.2 mm. Plane-polar light. JDD-94-07

C The same cluster of minerals shown in B. The cluster includes: one crystal of chalcopyrite, two of pyrite, and a pseudomorph of magnetite after a mafic mineral. Reflected light. JDD-94-07

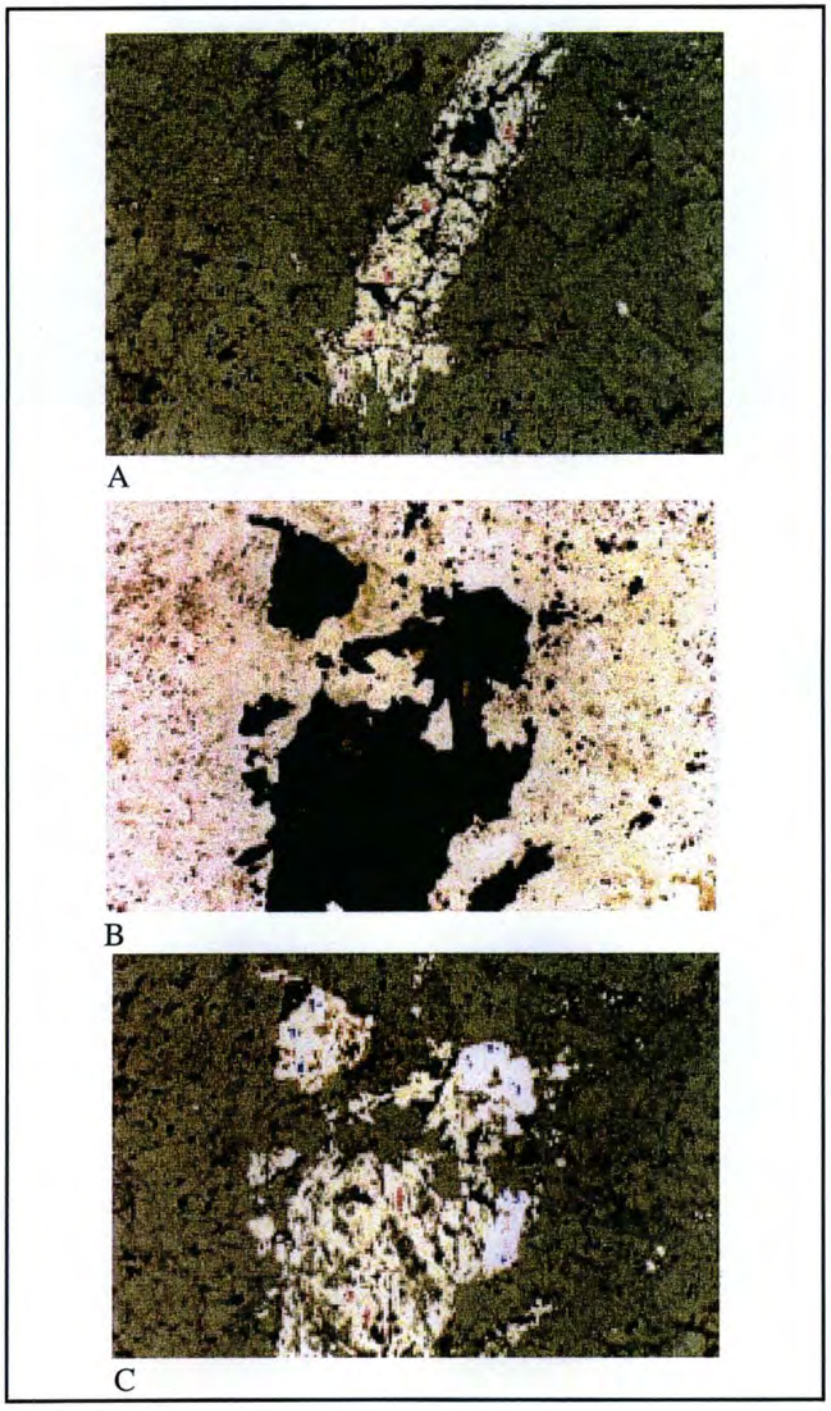

Figure 46 continued.

habit of the magmatic variety. Microprobe analyses of the hydrothermal magnetite are given in Table 12 and are plotted on a ternary diagram (Ti-Fe^{2+}-Fe^{3+}/2) in Figure 47. This magnetite is indistinguishable in composition from that of magnetic origin.

Ore Minerals

The principal ore minerals that are being sent to smelters from the floatation circuits at Ok Tedi are chalcopyrite, bornite, and gold. These minerals form the protore assemblage. Chalcopyrite is ubiquitous in the mineralized zones in porphyry, skarn, and massive ores. Bornite is locally abundant but in not the sample suites of this study. Idaite (a bornite-like mineral) was observed by Radke (unpublished) as an exsolution product in crystals of bornite and chalcopyrite. Chalcocite and covellite were the most abundant secondary copper minerals in the blanket of supergene enrichment and oxidation that was present when mining began. Supergene minerals may still be present in areas near surface contours and in areas of deep oxidation, but most occurrences have been removed by mining. Pyrite is a common gangue mineral and is also the host for finely- granular gold. Pyrrhotite has been reported in association with massive ores (Bamford and others, 1972, Arnold, Griffin, and Hodge, 1979, Katchan, 1982). Marcasite, which may form

	JDD-94-07			
Analysis	**20021**	**20023**	**20024**	**20025**
$Fe_2O_3^*$	66.46	66.68	66.44	67.05
FeO	30.51	28.88	30.32	30.63
TiO_2	0.28	0.21	0.20	0.18
MnO	0.04	0.00	0.00	0.00
SiO_2	0.02	1.40	0.03	0.02
Al_2O_3	0.12	0.21	0.13	0.11
MgO	0.01	0.03	0.02	0.00
Cr_2O_3	0.01	0.00	0.00	0.01
V_2O_5	0.00	0.00	0.00	0.00
NiO	0.00	0.00	0.02	0.00
CuO	n.a.	n.a.	n.a.	n.a.
ZnO	0.00	0.00	0.02	0.00
Total	97.44	97.43	97.18	98.00
Fe^{3+}	15.80	15.86	15.80	15.95
Fe^{2+}	8.06	7.63	8.01	8.09
Ti	0.07	0.05	0.05	0.04
Mn	0.01	0.00	0.00	0.00
Si	0.01	0.44	0.01	0.01
Al	0.05	0.08	0.05	0.04
Mg	0.00	0.02	0.01	0.00
Cr	0.00	0.00	0.00	0.00
V	0.00	0.00	0.00	0.00
Ni	0.00	0.00	0.00	0.00
Cu	0.00	0.00	0.00	0.00
Zn	0.00	0.00	0.00	0.00
Sum of cations	24.00	24.08	23.94	24.13

Table 12: Electron-beam microprobe analyses of hydrothermal magnetite.

	JDD-94-07			
Analysis	**20032**	**20033**	**20035**	**20037**
$Fe_2O_3^*$	66.41	67.00	66.72	66.66
FeO	30.16	30.53	30.47	30.18
TiO_2	0.14	0.13	0.18	0.12
MnO	0.05	0.02	0.02	0.08
SiO_2	0.05	0.02	0.01	0.04
Al_2O_3	0.15	0.17	0.16	0.14
MgO	0.02	0.00	0.03	0.06
Cr_2O_3	0.00	0.00	0.00	0.01
V_2O_5	0.00	0.00	0.00	0.00
NiO	0.01	0.01	0.00	0.00
CuO	n.a.	n.a.	n.a.	n.a.
ZnO	0.01	0.00	0.00	0.00
Total	96.99	97.89	97.58	97.27
Fe^{3+}	15.79	15.93	15.87	15.85
Fe^{2+}	7.97	8.07	8.05	7.98
Ti	0.03	0.03	0.04	0.03
Mn	0.01	0.01	0.00	0.02
Si	0.02	0.01	0.00	0.01
Al	0.05	0.06	0.06	0.05
Mg	0.01	0.00	0.01	0.03
Cr	0.00	0.00	0.00	0.00
V	0.00	0.00	0.00	0.00
Ni	0.00	0.00	0.00	0.00
Cu	0.00	0.00	0.00	0.00
Zn	0.00	0.00	0.00	0.00
Sum of cations	23.89	24.11	24.04	23.97

Table 12 continued.

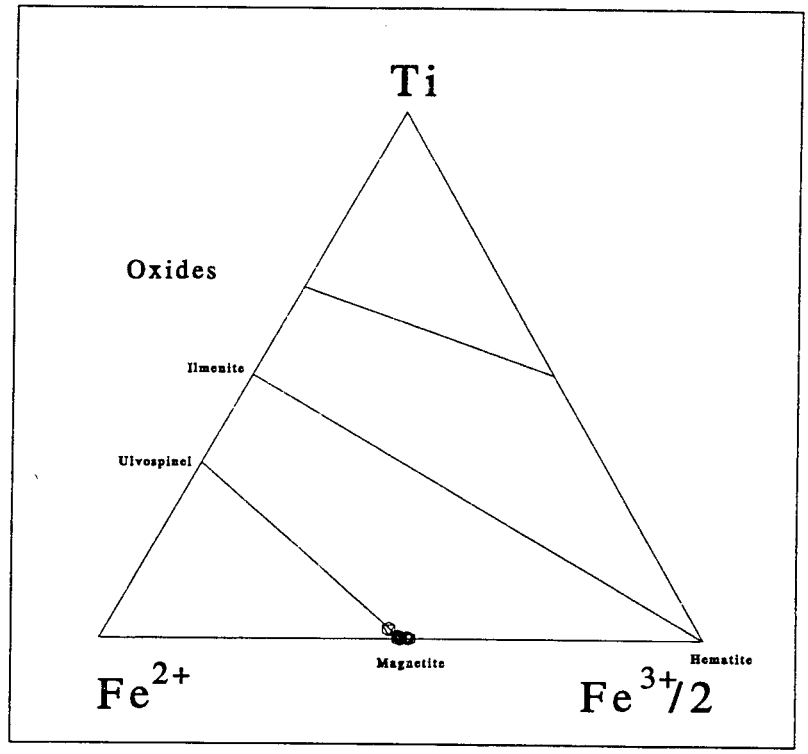

Figure 47: Ternary diagram illustrating the composition of hydrothermal magnetite.

from near-surface alteration of pyrite or pyrrhotite, is present locally. Molybdenite is a minor yet widespread constituent of porphyry ores but not in quantities sufficient to constitute an economic return. Galena and sphalerite have been collected locally. Samples of galena were found at an unknown location (reportedly near Folomian), but apparently peripheral to the ore body. Sphalerite has been noted in a zone of mixed breccia and massive ore in an area of intense potassic alteration near the contact between the Mt. Fubilan Intrusion and the Ieru Siltstone.

The principal copper sulfides are chalcopyrite and bornite. They are most abundant and constitute mineable ore only in rocks affected by potassic alteration. Chalcopyrite and pyrite are also present in veinlets cutting across propylitically altered rock. Photomicrographs illustrating the typical appearance and crystal form of pyrite, chalcopyrite, and chalcocite are illustrated in Figure 48. Many of the crystals of sulfide minerals in these photomicrographs (and in porphyry ore in general) are strikingly similar in appearance, and in geometric relations to the silicate minerals, to magnetite in unaltered intrusive rock. The textural occurrence, distribution, and relationship to associated rock-forming silicates of the disseminated sulfides collectively suggests that most disseminated ore sulfides formed by hydrothermal replacement of magmatic magnetite. Pyrite could have been produced merely by the exchange of sulfur for oxygen in the magnetite crystal structure, whereas he formation of chalcopyrite would require the addition of copper as well as sulfur. Microprobe analyses were performed on pyrite, chalcopyrite, and

Figure 48: Photomicrographs of pyrite, chalcopyrite, and chalcocite.

A. Crystals of chalcopyrite in porphyry from the ore zone in the Mt. Fubilan intrusion. The chalcopyrite (yellow) has been partly replaced from the rims inward by chalcocite (blue). The field of view is about 0.6 x 0.8 mm. Reflected light. JDD-94-04

B. Crystal of chalcopyrite. This crystal has been replaced by chalcocite (blue) around its rim and along fractures. The field of view is about 0.4 x 0.5 mm. Reflected light. JDD-94-04

C. Disseminated crystals of chalcopyrite and pyrite in a sample of porphyry from the ore zone in the Mt. Fubilan Intrusion. The field of view is about 3 x 4 mm. Plane-polar light. JDD-94-04

D. The same crystals of chalcopyrite (yellow) and pyrite (white) shown in C. Reflected light. JDD-94-04

E. Disseminated crystals of chalcopyrite in JDD-94-04. Plane polar light. The field of view is about 0.8 x 1.2 mm. JDD-94-04

F. The same crystals of chalcopyrite shown in E. The crystals of chalcopyrite (yellow and pale blue) are replaced around their rim by chalcocite (moderate blue). Reflected light. JDD-94-04

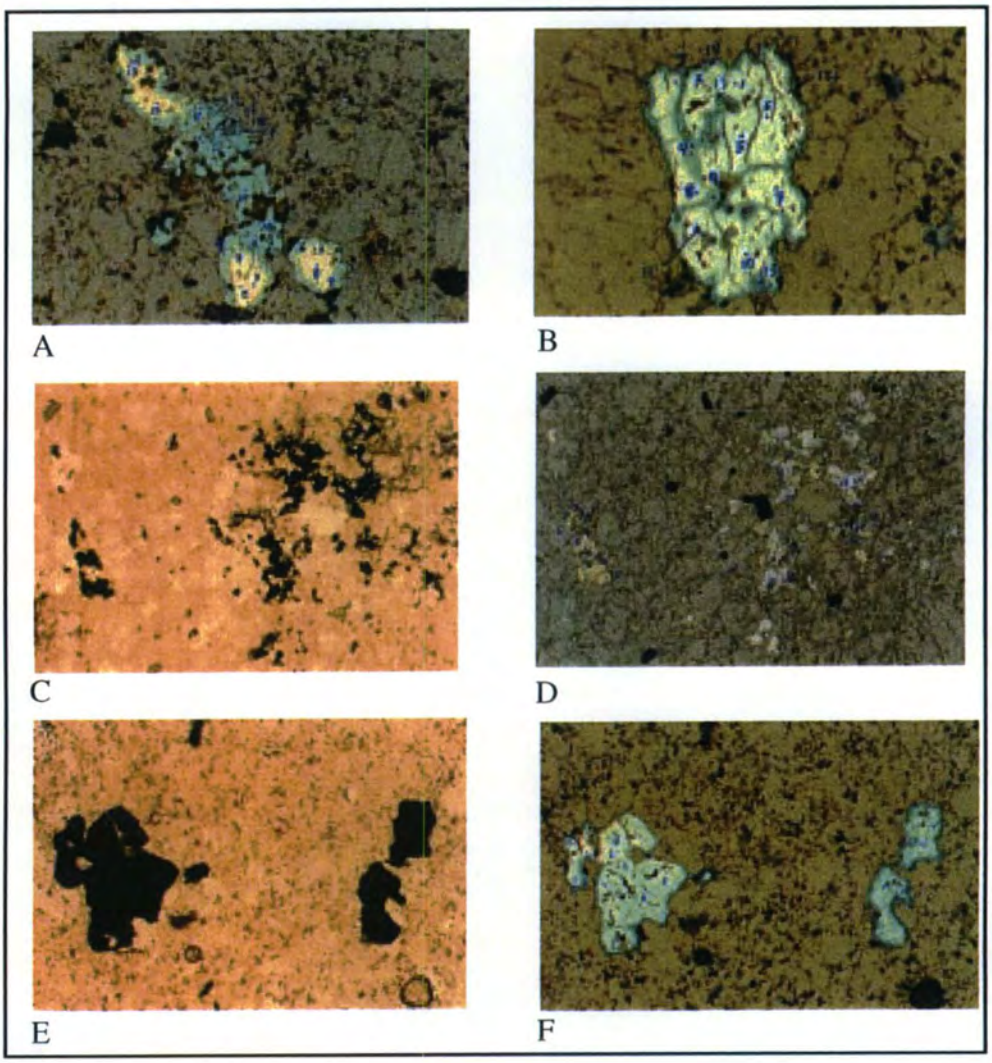

Figure 48 continued.

chalcocite in polished thin-sections. Representative analyses are presented in Table 13; the complete set is given in Appendix 11. Most of these analyses are of nearly pure monomineralic sulfide material. The analyses are portrayed graphically in Figure 49 where symbols representing the analytical compositions of pyrite and chalcopyrite (pentagons) fall at, or immediately adjacent to, their expected compositions (open circles). Chalcocite analyses plot between chalcocite and covellite. Two analyses plot near the expected composition of bornite.

Zinc, silver, platinum, gold, and lead were included in the microprobe analytical files for all sulfide mineral analyses. These elements were not, however, encountered in significant quantities in any of the analyses. Most, in fact, have low values that fall within the expected counting error for the analyses. Although microscopic evidence suggests that some gold is present as inclusions in the sulfide minerals, these results do not contradict the observed microscopic evidence. They do, however, suggest that these elements are not evenly distributed throughout matrices of the sulfide minerals.

Clay minerals

Clay of two general types was observed in thin-sections from the Ok Tedi Intrusive complex. The first type is yellow or yellow-brown in color and waxy in appearance. This type of clay is common in unaltered rock and in rock affected by propylitic alteration. It is most abundant in sites previously occupied by

Sample	459	JDD-94-03	JDD-94-04	JDD-94-07
	102.9			
	Pyrite			
Analyses	7	44	8	8
Fe	46.04	46.02	46.26	45.15
Cu	0.02	0.05	0.11	0.02
Pb	0.77	0.18	0.16	0.17
Zn	0.04	0.01	0.00	0.03
Ag	0.00	0.03	0.01	0.02
Au	0.01	0.01	0.02	0.01
As	0.02	0.03	0.03	0.04
S	53.51	53.21	53.58	53.21
Total	100.41	99.55	100.17	98.63
	Chalcopyrite			
Analyses	5	4	53	7
Fe	29.64	29.33	29.06	29.40
Cu	32.27	31.97	33.48	32.03
Pb	0.59	0.15	0.11	0.52
Zn	0.04	0.04	0.03	0.02
Ag	0.03	0.03	0.02	0.02
Au	0.01	0.00	0.02	0.01
As	0.03	0.01	0.02	0.03
S	34.40	34.27	34.24	34.39
Total	97.01	95.81	96.98	96.43

Sample	JDD-94-04	JDD-94-04
	Chalocite	Bornite
Analyses	16	4
Fe	1.16	2.76
Cu	73.76	64.95
Pb	0.07	0.06
Zn	0.00	0.00
Ag	0.02	0.01
Au	0.02	0.04
As	0.01	0.01
S	23.33	23.15
Total	98.37	90.97

Table 13: Representative analyses of pyrite, chalcopyrite, chalcocite, and bornite.

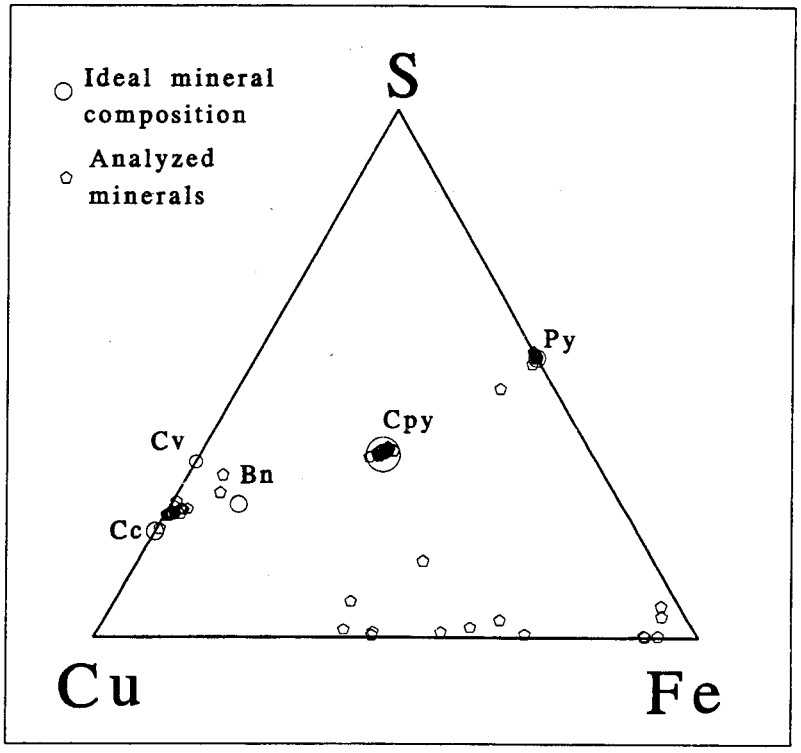

Figure 49: Ternary diagram illustrating the compositions of pyrite, chalcopyrite, bornite(?), and chalcocite-covellite.

ferromagnesian silicate minerals. Many instances show this clay to occupy sites that contain remnant amounts of the ferromagnesian silicates. Presumably this observation provides a similar interpretation for sites which are now completely filled by clay. This clay is referred to as smectite on the basis of petrographic examinations.

The second type of clay is white or gray in color, very fine-grained, and found in the sites of corroded crystals of feldspar. This type of clay is present in rocks that have undergone strong propylitic and potassic alteration. It is most abundant in areas of supergene alteration that are largely coincident with those of intense potassic alteration. White clay is present in local fault structures including one low angle fault that is located between the Vancouver and Edinburgh areas and that is over two meters in thickness. This type of clay was provisionally identified as kaolinite in petrographic studies. It is designated as Qz/Wm/Clay in Appendices 2 and 3 because of the possibility that, in many instances, it was an admixture with very fine-grained drusy quartz or white mica.

Four samples containing these clays were submitted for x-ray diffraction (XRD) analyses. This analytical work confirmed the identity of smectite in samples with yellow waxy clays. Prior analytical work in the exploration and feasibility stages of development (Goode and Gilbert, 1976; Katchan, 1982; Ayres and Bamford, 1976, revised 1987) also found yellowish clays to be smectites

(montmorillonites). The white clays in the samples analyzed were found to be mixtures of illite and halloysite. The identification of smectite in thin-sections is now well-established and can be easily applied in field identification. The identification of the white clays, however, remains more tentative and further analytical work using samples from related locations and alteration types is necessary for positive identification and mineralogical interpretations.

Limonite

Limonite is widely present in the oxide capping of the Ok Tedi deposit as veinlets, fracture-fillings, and pervasive staining of the fractured and altered host rocks. It coats crystal boundaries in the intrusive rocks and grain boundaries in metasiltstones of the Ieru Formation. It has soaked into clayey aggregates that formed as a result of silicate mineral destruction in the zone of oxidation. The limonite has formed by weathering related to surficial oxidation of ferromagnesian minerals in the host rock that was further complicated and enhanced by deposition of iron oxides attendant with the leaching action of sulfuric acid produced by the breakdown of the sulfide minerals, particularly pyrite. Limonite is most abundant where surface waters have pervasively saturated massive ores in which pyrite or pyrrhotite had been the major constituents. Massive sulfides in these bodies have been converted to limonite minerals such as goethite, hematite, and jarosite by supergene alteration and interactions with surface water. Such bodies of massive

limonite are properly termed gossan. However, they have been referred to improperly by miners and some researchers as "skarn." Most of these gossans contain few if any of the common skarn minerals expected such as garnet or pyroxene. The principal pre-oxidation remnants, where they can be found, are usually pyrite and chalcopyrite. Magnetite is also common in the gossans but, unlike the sulfide minerals, it appears to have been stable in the zone of oxidation

Limonite has also formed by the in situ oxidation (rusting) of disseminated crystals of pyrite and chalcopyrite within areas of porphyry-style mineralization in intrusive rock and in the siliciclastic Ieru Formation. Pseudomorphs of limonite after pyrite were common in the leached capping and in the upper part of the zone of supergene enrichment. Limonite is commonly associated with malachite and azurite in porphyry, phanerite, and siltstone hosts. These oxidation minerals are also accompanied by cuprite and native copper at some locations.

Modal Classification

The rock samples from the second suite of petrographic analyses are classified on ternary QAP diagrams in Figures 50 and 51. The samples from the first suite are not portrayed because I do not consider the ratios of alkali to plagioclase feldspar in this suite to be as reliable as those of the second suite. The problem was discussed earlier, but to reiterate, point-counting conducted on the first suite was done before microprobe analyses were made. One of the outcomes of the

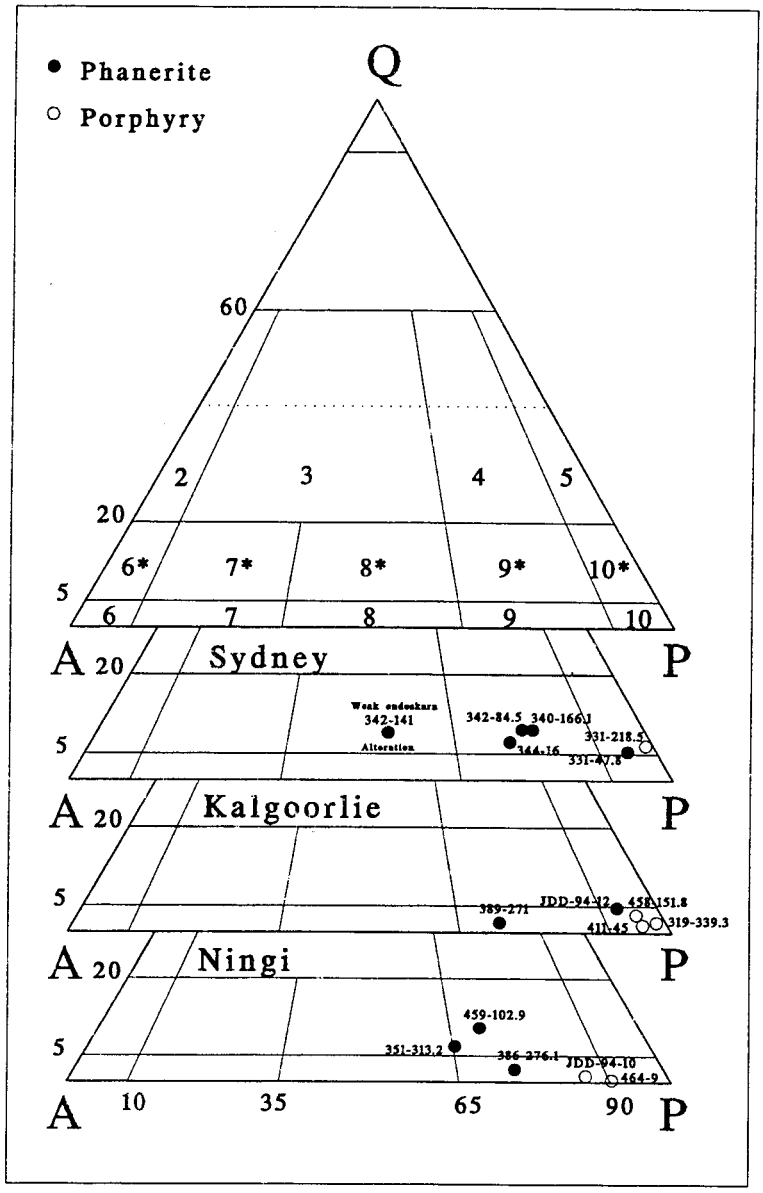

Figure 50: QAP modal classification of unaltered and weakly altered intrusive rocks from the Ok Tedi Intrusive Complex, and the IUGS fields for the classification of igneous rocks (after Streckeisen, 1979).

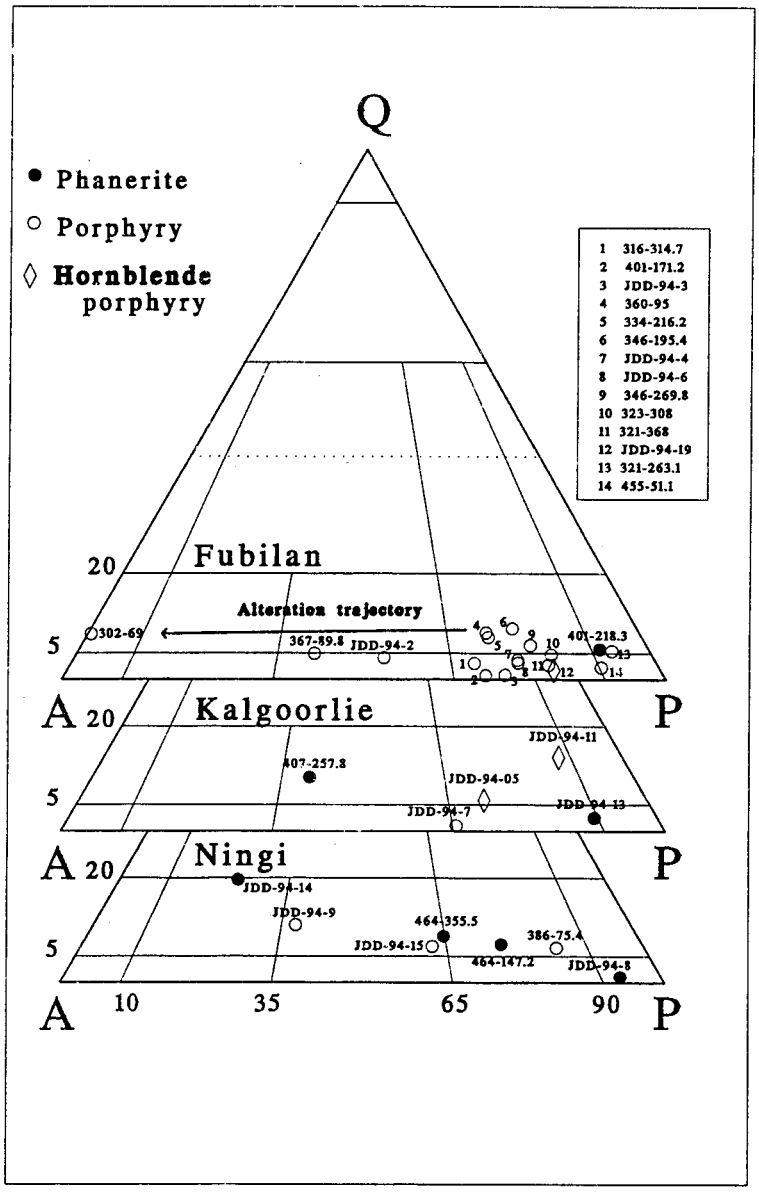

Figure 51: QAP modal classification for altered intrusive rocks from the Ok Tedi Intrusive Complex, and the IUGS fields for the classification of igneous rocks (after Streckeisen, 1979). Arrow shows direction of alteration.

instrumental analyses was the realization that many of the crystals that had been identified as alkali feldspar because they lacked twinning, were in fact plagioclase feldspar. This error caused a bias toward the A (alkali feldspar) component.

The samples portrayed in the accompanying figures are subdivided into two categories: 1) unaltered (or weakly altered, Figure 50), and 2) strongly altered (Figure 51). This distinction is based on the presence or absence of pyroxene (±hornblende). Samples with one or both of these minerals are considered to be unaltered. The figures are further subdivided according to which intrusion the samples are assigned. There are no samples of unaltered rock from the Fubilan Intrusion. Only one sample of altered (texturally-destroyed) intrusive rock is included in the samples from the Sydney Intrusion. This sample was not subjected to petrographic analysis, and it is not portrayed in Figure 51 because it has been changed by alteration to a very fine-grained texture, in which the distinction of quartz and the feldspars is difficult or impossible using a conventional petrographic microscope.

The recommendation of the I.U.G.S. Subcommittee on Igneous Rocks is to name rocks with phaneritic texture using plutonic rock names, and to name those with aphanitic texture using volcanic rock names. The Subcommittee does not make any recommendations for rocks with porphyritic texture. The convention used in this dissertation is to assign plutonic terminology to porphyritic rocks with phaneritic groundmass, and to assign volcanic terminology to those having aphanitic

groundmass. This convention is in agreement with older classifications including that of Shand (1943). The QAP data from rocks with porphyry and phaneritic texture are plotted together on the same ternary diagrams in Figures 50 and 51. The textural varieties are distinguished by symbols: porphyries by unfilled circles, phanerites by filled circles. Samples of hornblende porphyry are depicted as unfilled diamonds.

Three samples of phaneritic rock from the Sydney Intrusion fall in field 9* and are, therefore, quartz monzodiorites (Figure 50). The thin-sections from these samples are among the least-altered encountered in examinations of both suites of petrographic samples. Two samples fall into field 10*. One has phaneritic texture and is classified as quartz diorite; the other has porphyritic texture and is classified as andesite. One sample (DDH 342-141) which contains a minor amount of garnet and is therefore considered to have undergone weak propylitic or endoskarn alteration, is classified as quartz monzonite.

All of the samples from Mount Fubilan are strongly altered and virtually all have porphyritic texture. Most plot in fields of 9 and 9* (andesite) as given in Figure 51. However, two samples fall in field 8 (latite) and one plots near the A-Q join in field 6* (quartz alkali-feldspar trachyte). A thin-section of the latter quartz alkali-feldspar trachyte sample (DDH 302-69) shows the most intense potassium feldspar alteration and the highest K_2O content of any analyzed sample. The samples classified as latite and quartz alkali-feldspar trachyte most likely

crystallized as andesites and were subsequently modified by potassium metasomatism. The names applied to these rocks, and to the others portrayed in Figure 51 imply metasomatic, and not igneous compositions. The example of hornblende porphyry (sample JDD-94-12) was collected from a dike within the Fubilan Intrusion; it plots in field 9 (andesite).

Four of the unaltered rocks from the Kalgoorlie Intrusion (Figure 50) plot in field 10 (andesite or diorite), whereas the fifth (DDH 389-271), a phanerite, plots in field 9 (monzodiorite). Five samples with strong potassic alteration are shown in Figure 51. Two of these are hornblende porphyry (samples JDD-5 and 11). They plot in field 9* and are, therefore, classified as andesites. One sample of feldspar porphyry plots near the boundary between fields 8 and 9. Two samples of phanerite are shown in Figure 51. One of these plots near the boundary between fields 9 and 10 and is a monzodiorite based on modal criteria. The other falls in field 8* (monzonite).

Samples of unaltered phanerite from the Ningi Intrusion plot in fields 9 (quartz monzodiorite) and 9* (monzodiorite). One of the unaltered porphyries occupies field 9 (andesite), the other plots near the boundary between fields 9 and 10 (andesite). Samples of altered rock from this intrusion spread across the QAP diagram from field 10 to near the boundary between fields 7* and 3.

In summary, most of the unaltered samples of phanerites (7 of 10) fall in fields 9 and 9* whereas those with porphyry texture (4 of 5) fall closer to the P apex

within fields 10 or 10*. This reflects the fact that plagioclase feldspar was an early phase in the crystallization sequence and that most of the rocks with porphyry texture were quenched before potassium feldspar was on the solidus, or shortly after it began to form. Presumably, this implies that the groundmass of unaltered samples with porphyry texture has high ratios of potassium to plagioclase feldspar, while most of the strongly altered samples that have porphyry texture fall in field 9 and 9*. Subsequently it will be demonstrated that these samples are metasomatic (quartz) trachytes and (quartz) alkali trachytes when classified using chemical criteria. They should, therefore, fall in fields 7, 7*, 6, and 6*. This discrepancy arises because most of the feldspar in these samples that was counted as plagioclase has An content of less than 5 and is, therefore, technically alkali feldspar and should be part of the A component. In addition, the potassium feldspar which dominates the groundmass in stained samples, and by implication all of the groundmass in potassically-altered rock, was not counted or added to the A component. The displacement of the strongly altered samples of porphyry from near the P apex to fields 9 and 9* results from partial replacement of many of the crystals of plagioclase feldspar by pseudomorphs or rinds of potassium feldspar. Modal analyses of those samples in which potassium feldspar replacement of plagioclase has been exceptionally well developed plot in fields 6*, 8, and 8*.

The mineralogical effects of metasomatic alteration on the feldpars in samples of strongly altered phanerites are more complex. Only one of these samples

(JDD-94-14) show much displacement toward the A apex. The remaining samples from altered phanerites may have undergone albitization of the plagioclase feldspar with but minor pseudomorphic replacement of plagioclase by potassium feldspar. However, many samples with phaneritic texture that were studied as part of the first suite of petrographic analyses display strong alkali-feldspar replacement textures demonstrating that such alteration is common in rocks with phaneritic texture.

Whole Rock Chemistry

Variations in the major and trace element chemistry of samples from the Ok Tedi Intrusive Complex are described in this chapter. These data are used for comparison with other intrusions of the Star Mountains, to classify the rocks, to describe changes that occurred during hydrothermal alteration, and to provide a basic understanding of the petrochemical evolution of the igneous rocks of the Ok Tedi Intrusive Complex.

The data used herein consist of six sets of analyses performed on rocks collected by more than seven different geologists over a period of more than twenty years (Appendices 12). Together, these sets of data provide a good test of the effects of sample selection and analytical uncertainty.

Star Mountains Regional Data

Mason (1975), Ayres and Bamford (1976), and Arnold, Griffin, and Hodge (1979) provided data on the volcanic and plutonic rocks of the Star Mountains area that surrounds the Ok Tedi Intrusive Complex. Collectively, analyses on 49 rock samples taken from the Antares Complex, the Tifalmin Intrusive, the Mount Ian Complex, the Frew Complex, and several small stocks are included in these publications. The samples that were analyzed are of calc-alkaline rocks that range in composition from quartz monzodiorite or monzonite to gabbro. Many of the

samples are relatively unaltered but some are reported to have undergone various degrees of hydrothermal or supergene alteration. The mineralogical descriptions of the rocks from the intrusive centers in the Star Mountains suggest that most are similar to their unaltered counterparts in the Ok Tedi Intrusive Complex. Because of their close geographic proximity, mineralogical similarities, and near equivalency in geologic age, data for the Star Mountains sample suite provide a useful regional background by which to compare the data for samples from the Ok Tedi Intrusive Complex.

Ok Tedi Data

Mason (1975) and Ayres and Bamford (1976, revised 1987) published analyses of 37 samples of intrusive rocks from the Ok Tedi Intrusive Complex. Included in these data are 16 samples from the Mt. Fubilan intrusion, 12 from the Kalgoorlie intrusion, and 9 from unknown locations within the complex. Only the 28 samples from the Mt. Fubilan and Kalgoorlie intrusions will be included in the following discussion.

Katchan (1982) listed major oxide data for ten samples. Eight of these are from the Kalgoorlie intrusion in the Gold Coast Area, one is from a central part of the Kalgoorlie Intrusion, and one is from the Sydney intrusion in the Darien-East Cheam area. All of these samples contain modal pyroxene, hornblende, or both (Table 14). Six of the samples contain modal epidote or garnet in trace quantities.

Kalgoorlie Intrusion

Sample	A/CNK	Modal Minerals Qtz	Pyx	Hbld	Tn	Gar	Epi	Normative An content Plag. Feld.	F-Mag Mineral
029-215.2	0.82	0.10	3.80	1.70	0.07			22.57	di&hy
077-148.7	0.77		12.20	0.80	1.30	0.20		33.47	di&hy
080-197.5	0.79	4.20		10.40	1.20			0.00	di&hy&ol
144-192.1	0.85	1.70	0.30	13.20	1.30			27.39	di&hy
148-138.1	0.74	0.10	9.30	1.20	1.00			36.16	di&hy
161-050	1.38	2.70	2.50	9.20	1.80		0.70	8.75	hy
161-086.7	0.75		7.90	1.20	1.00	1.20		20.82	di&ol
163-119.5	0.75		13.10	0.40	1.30		0.50	37.11	di&ol
163-246.5	0.69		14.70	0.10	0.70		0.10	28.55	di&wo

Sydney Intrusion

Sample	A/CNK	Modal Minerals Qtz	Pyx	Hbld	Tn	Gar	Epi	Normative An content Plag. Feld.	F-Mag Mineral
001-202.1	0.96	8.40		9.20	1.00		1.40	37.72	di&hy

Abbreviations

Qtz	**quartz**	**An**	**anorthite**
Pyx	**pyroxene**	**F-mag**	**ferromagnesian**
Hbld	**hornblende**		
Tn	**sphene**		
Gar	**garnet**		
Epi	**epidote**		

Table 14: Petrographic and chemical features of samples from Katchan (1982).

The locations from which the samples used in Katchan's study were taken are shown in Figure 52.

Jonathan Kepa, a geologist for Ok Tedi Mining Limited, collected samples of intrusive rock from 64 locations within the Mt. Fubilan intrusion and from four locations in the Ningi intrusion in 1993. The approximate locations from which the samples were taken are given in Figure 53. Petrographic and chemical analyses were subsequently performed on these samples by Dr. D. R. Mason of Amdel Laboratories of Australia and these data are summarized in Table 15. Mason classified most of the samples from the Fubilan Intrusion as altered latite porphyry and those from the Ningi as quartz monzonite and latite porphyry (Mason, 1993a, 1993b, 1993c). Twenty of the samples were from the quartz-core or its periphery and these contain veinlets of quartz. Four of the samples contained xenoliths of siltstone; these four samples are not included in the following diagrams.

I collected 56 samples from the Ok Tedi Intrusive Complex in January 1994. Major and trace element analyses were performed on these samples using X-ray fluorescence spectroscopy by Chemex Laboratories. Additional trace elements were obtained by Instrumental Neutron Activation analyses (INAA) from the Triga reactor at Oregon State University and by Inductively Coupled Plasma Spectroscopy by Chemex Laboratories. Included in this group of samples are 24 from the Mt. Fubilan, 19 from the Kalgoorlie, 17 from the Ningi, and nine from the

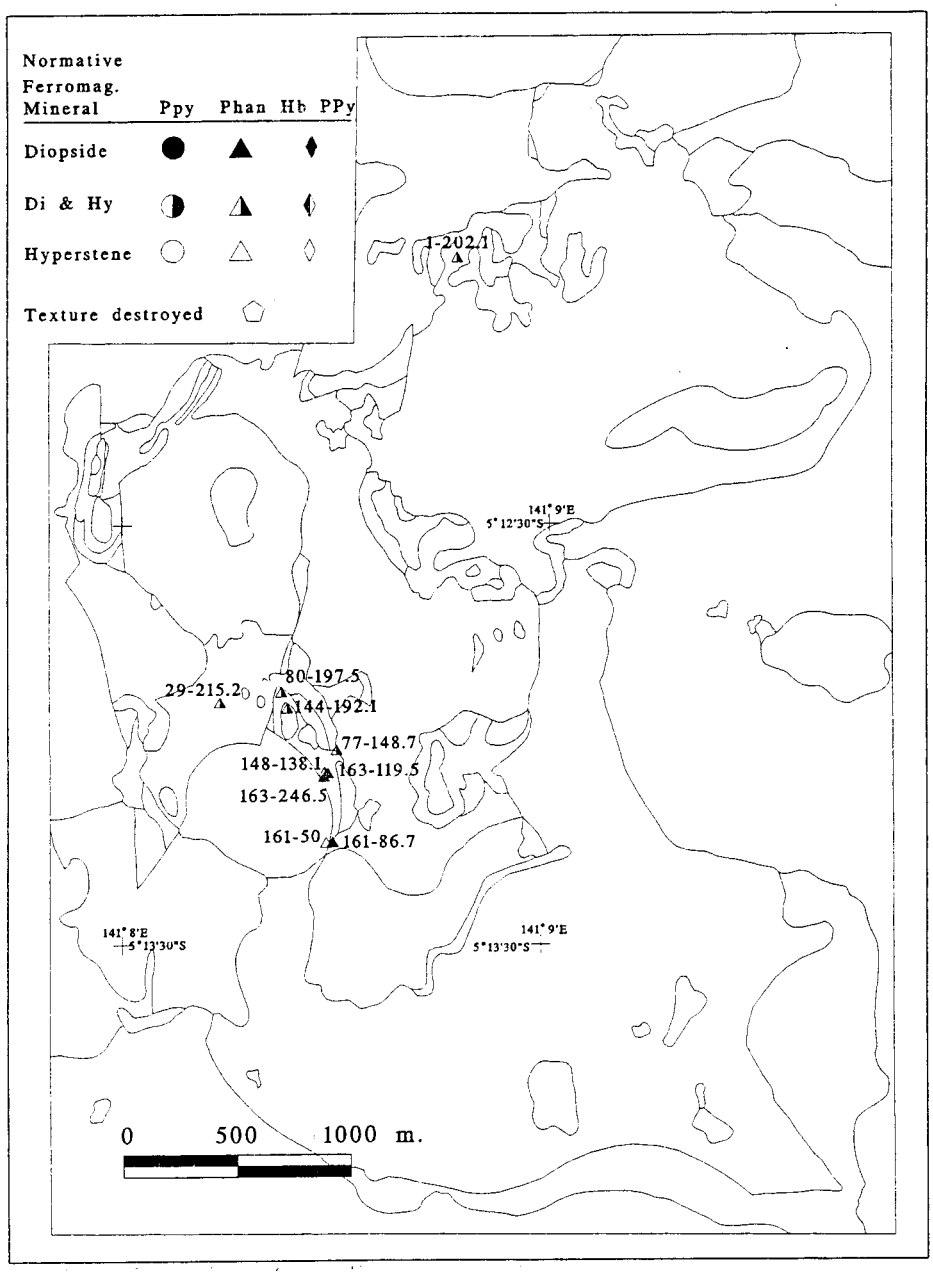

Figure 52: Location map for samples of Katchan (1982). Also indicated are rock textures and normative ferromagnesian minerals.

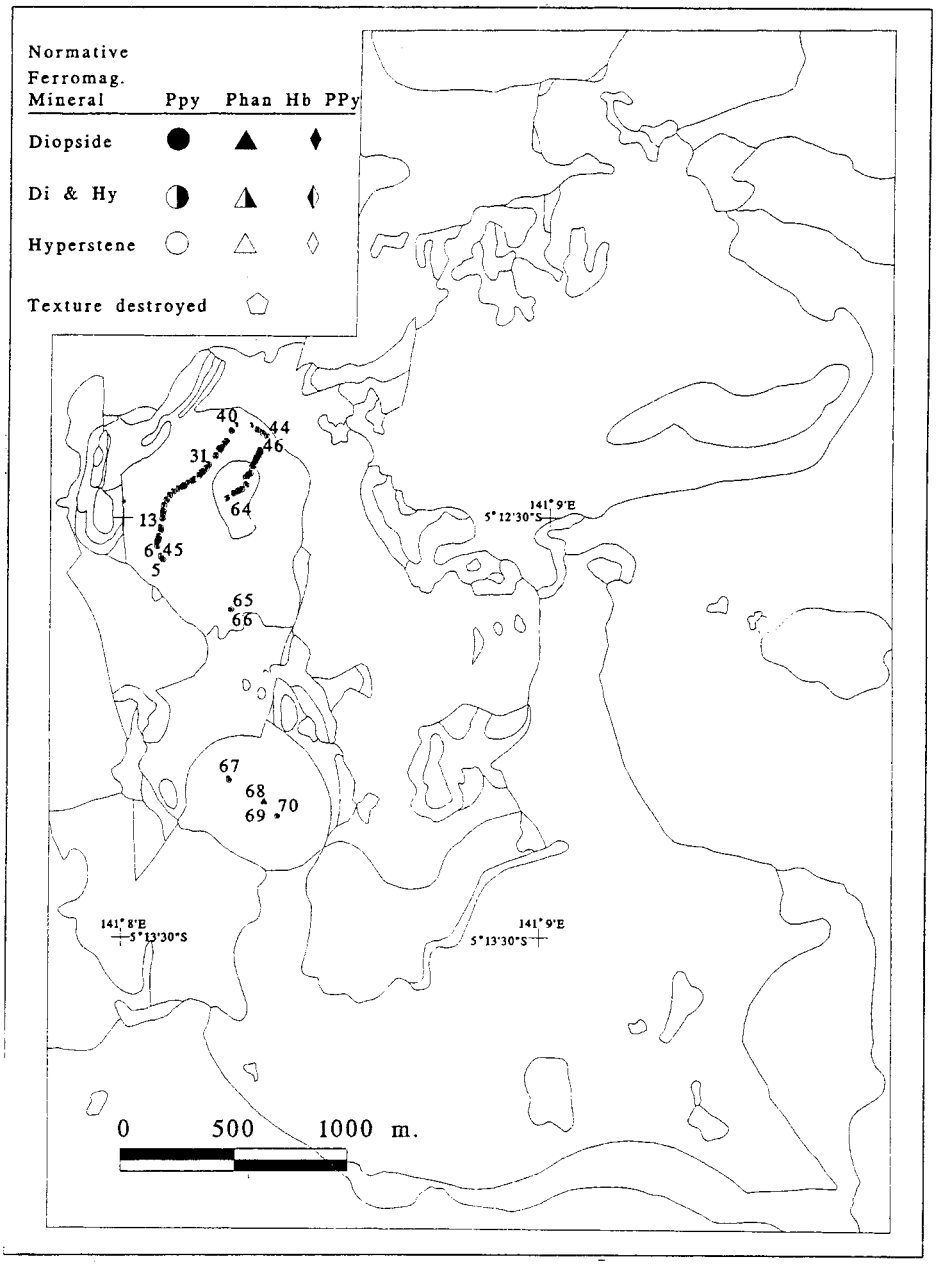

Figure 53: Location map for samples collected by Kepa and analyzed by Mason (1993a,b,c). Also indicated are rock textures and normative ferromagnesian minerals.

Fubilan Porphyry					
		Modal	Normative		
Sample	A/CNK	Biotite	An content Plag. Feld.	F-mag Mineral	Alteration
TS-05	1.16	hyd	5.03	hy	Late-magmatic and clay
TS-06	1.05	hyd	2.31	hy	Potassium metasomatism
TS-07	1.08	ser	1.23	hy	Potassium metasomatism
TS-08	1.20	hyd	3.64	hy	Potassium metasomatism
TS-09	0.99	hyd	0.53	hy	Potassium metasomatism
TS-10	1.13	hyd	5.39	hy	Potassium metasomatism
TS-11	1.04	hyd	1.12	hy	Potassium metasomatism
TS-12	1.08	hyd	1.84	hy	Potassium metasomatism
TS-13	1.30	hyd	2.76	hy	Potassium metasomatism
TS-14	1.04	hyd	4.92	hy	Potassium metasomatism
TS-15	1.12	hyd	8.71	hy	Potassium metasomatism
TS-16	2.49	hyd	5.68	hy	Potassium metasomatism
TS-17	1.10	hyd	10.57	hy	Potassium metasomatism
TS-18	1.07	hyd	2.99	hy	Potassium metasomatism
TS-19	1.13	hyd	3.35	hy	Potassium metasomatism
TS-20	1.12	hyd & mag	10.57	hy	Potassium metasomatism
TS-21	1.22	hyd	10.87	hy	Potassium metasomatism
TS-23	1.12	hyd	8.13	hy	Potassium metasomatism
TS-24	1.16	hyd	10.52	hy	Potassium metasomatism
TS-25	1.14	hyd	6.11	hy	Potassium metasomatism
TS-26	1.17	hyd	6.17	hy	Potassium metasomatism
TS-42	2.86	hyd	0.00	hy	Potassium metasomatism, clay
TS-43	3.43	hyd	0.00	hy	Potassium metasomatism, clay
TS-44	1.34	hyd & mag	2.13	hy	Clay, potassium metasomatism
TS-45	1.18	hyd	7.09	hy	Potassium metasomatism
TS-46	1.18	hyd	8.38	hy	Potassium metasomatism,low grade
TS-47	1.50	hyd	5.85	hy	Potassium metasomatism,moderate grade
TS-48	1.23	mag	9.95	hy	Potassium metasomatism,low grade
TS-49	1.79	hyd	1.24	hy	Potassium metasomatism,high grade
TS-50	1.79	hyd	0.00	hy	Potassium metasomatism,high grade
TS-52	1.14	hyd	8.55	hy	Potassium metasomatism,moderate grade
TS-60	1.19	hyd & mag	12.03	hy	Potassium metasomatism,low to moderate grade
TS-61	1.25	hyd	15.41	hy	Potassium metasomatism,low grade
TS-65	1.10	hyd	4.04	hy	Potassium metasomatism,low grade
TS-66	1.04	hyd	1.44	hy	Potassium metasomatism,low to moderate grade

Table 15: Petrographic and chemical features of samples collected by Kepa and analyzed by Mason (1993a,b,c).

Fubilan Porphyry with Quartz veinlets

Sample	A/CNK	Modal Biotite	Normative An content Plag. Feld.	Normative F-mag Mineral	Alteration
TS-28	1.05	hyd	10.91	hy	Potassium metasomatism
TS-29	1.12	hyd	10.46	hy	Potassium metasomatism
TS-30	1.08	hyd	13.94	hy	Potassium metasomatism
TS-31	1.25	hyd	1.33	hy	Potassium metasomatism
TS-32	1.06	hyd	6.58	hy	Potassium metasomatism
TS-33	1.12	hyd	3.31	hy	Potassium metasomatism
TS-35	1.19	hyd	0.00	hy	Potassium metasomatism
TS-36	1.60	hyd	1.99	hy	Potassium metasomatism, intense
TS-39	1.69	hyd	3.50	hy	Potassium metasomatism
TS-53	1.17	hyd	0.00	hy	Potassium metasomatism
TS-54	1.05	hyd	5.80	hy	Potassium metasomatism, high grade
TS-55	1.15	hyd	0.69	hy	Potassium metasomatism, high grade
TS-56	1.21	hyd	0.00	hy	Potassium metasomatism, high grade
TS-57	1.56	hyd & mag	2.74	hy	Potassium metasomatism, moderate grade
TS-58	1.15	hyd	2.02	hy	Potassium metasomatism, high grade
TS-59	1.08	ser	2.00	-	Potassium metasomatism, intense
TS-62	1.84	hyd	0.00	hy	Potassium metasomatism,low to moderate grade
TS-63	2.32		0.00	-	Oxidized
TS-64	1.66		0.00	-	Potassium metasomatism, high grade

Ningi Intrusion

Sample	A/CNK	Modal Biotite	Normative An content Plag. Feld.	Normative F-mag Mineral	Alteration	Texture
TS-69	1.21	hyd & mag	0.00	hy	Potassium metasomatism, mod.	phanerite
TS-67	1.10	mag	24.81	hy	Propylitic	porphyry
TS-70	1.23	hyd & mag	8.82	hy	Potassium metasomatism, low	porphyry
TS-68	1.13	mag	23.54	hy	Potassium metasomatism, patchy	phanerite

Abbreviations

hyd	hydrothermal	hy	hypersthene
mag	magmatic	An	anorthite
ser	sericite	F-mag	ferromagnesian

Table 15 continued.

Sydney intrusion. Sampled locations are shown in Figures 54 and 55, and the petrochemical features of the samples are summarized in Table 16. All but one of the samples (DDH 401-218.3) from the Mount Fubilan Intrusion are porphyritic in texture and all have undergone potassic (± argillic) alteration. One sample is from a dike of hornblende porphyry (JDD-94-19) that cuts the Fubilan Intrusion and one sample (DDH 366-232.5) is of texturally destroyed rock with pseudomorphs of biotite and pyrite after hornblende or pyroxene. Samples of intrusive rock from the Magnetite Creek area were assigned to the Sydney Intrusion if they had a phaneritic texture and to the Fubilan if they had a porphyritic texture. One sample from this area (JDD-94-01), consisting of texturally destroyed rock with pseudomorphs of biotite and pyrite after pyroxene or hornblende, was assigned to the Sydney Intrusion based on perceived phaneritic texture. The remaining, spatially adjacent, samples were assigned to the Fubilan Intrusion because they have porphyritic textures. Rock samples from the Kalgoorlie Intrusion included the following: five with minor amounts of garnet or epidote (weak endoskarn or propylitic alteration); two samples from a dike of hornblende porphyry; and eight samples of feldspar porphyry and phanerite that range from relatively pristine to highly potassically altered. Most of the samples from the Sydney Intrusion are characterized by primary magmatic mineral assemblages and textures, and with only trace quantities of epidote. One sample (DDH 342-141) has garnet in its mode.

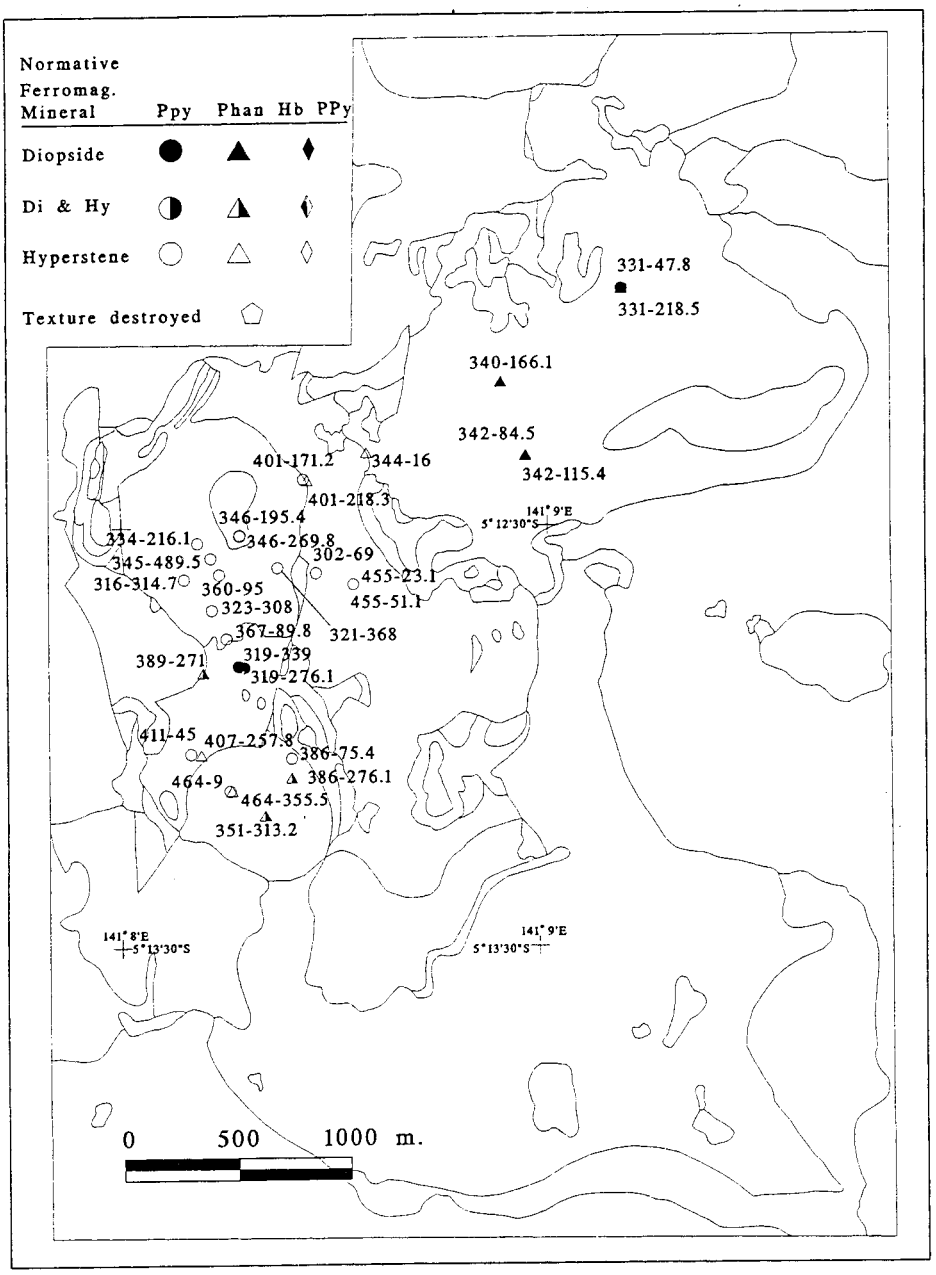

Figure 54: Location map for diamond drill core (DDH) samples collected in 1994 (Suite 2). Also indicated by symbols are rock textures and normative ferromagnesian minerals.

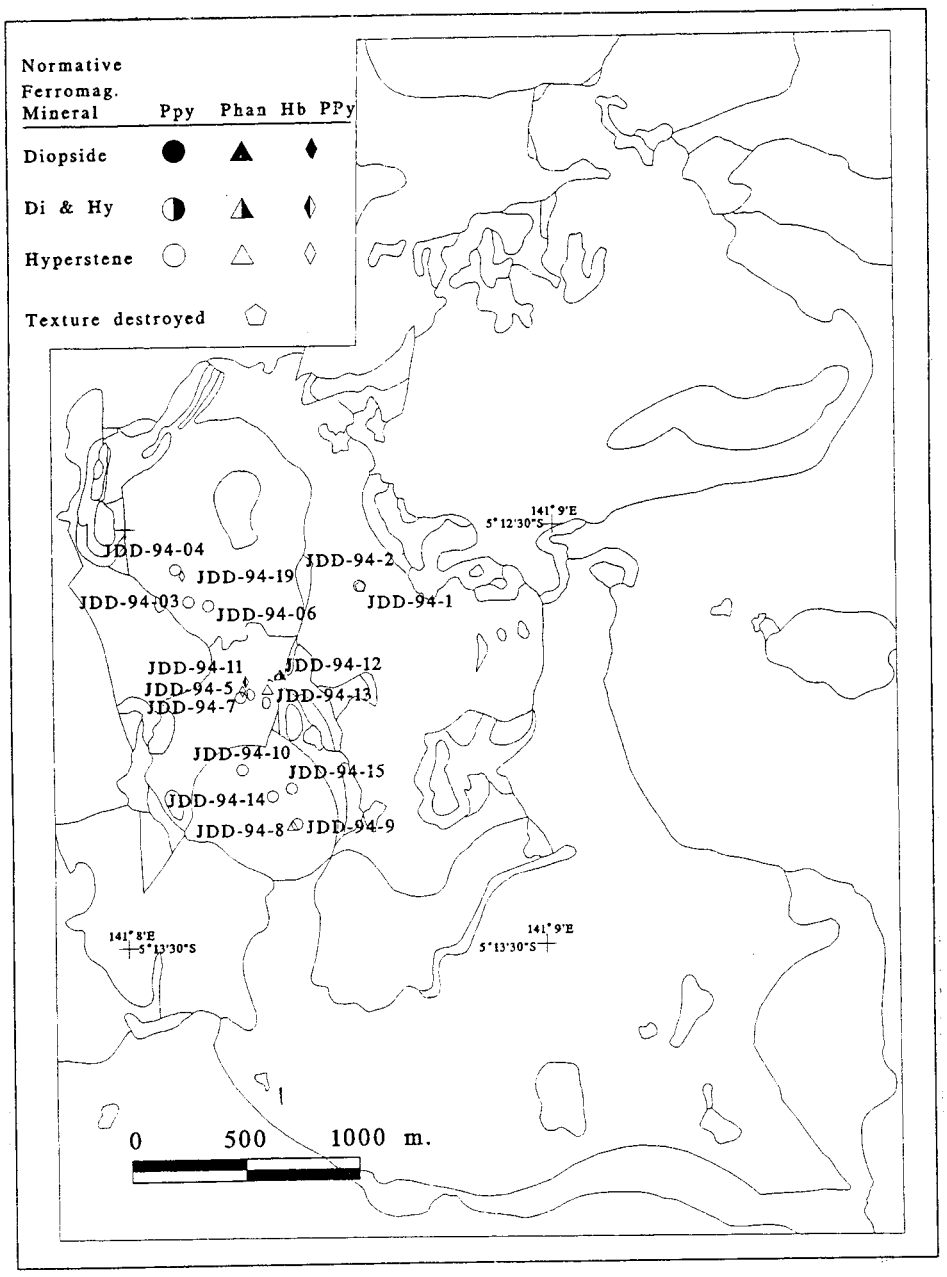

Figure 55: Location map for surface samples collected in 1994 (Suite 2). Also indicated by symbols are rock textures and normative ferromagnesian minerals.

Sydney Intrusion											
				Modal Minerals						Normative	
Sample	Texture	A/CNK	Biotite	Qtz	Pyx	Hbld	Ttn	Gar	Epi	An content Plag. Feld.	F-mag Mineral
331-047.8	phanerite	0.82	none	4.71	1.94	1.54	1.43		1.02	39.50	di&hy
331-218.5	porphyry	0.81	mag	3.27	4.09	0.10	0.31		1.23	37.55	di&wo
340-166.1	phanerite	0.82	mag	8.20	8.68		0.78		0.10	36.80	di&wo
342-084.5	phanerite	0.80	mag	8.37	9.06		0.98		0.10	35.38	di&wo
342-115.4	n.d.	0.81	n.d.	n.d.	n.d.	n.d.	n.d.	n.d.	n.d.	36.44	di&wo
342-141	phanerite	0.64	none	7.23	6.69		0.72	2.17		44.87	di&wo
344-016	phanerite	1.04	mag	5.89	7.76		0.98			45.55	hy
JDD-94-01	text. dest.	1.30	hyd	n.d.	n.d.	n.d.	n.d.	n.d.	n.d.	12.01	hy
Fubilan Intrusion											
				Modal Minerals						Normative	
Sample	Texture	A/CNK	Biotite	Qtz	Pyx	Hbld	Ttn	Gar	Epi	An content Plag. Feld.	F-mag Mineral
302-069	porphyry	1.05	hyd	3.33						1.16	hy
316-314.7	porphyry	1.00	hyd	1.34						3.34	hy
321-263.1	porphyry	1.24	hyd	1.97						5.41	hy
321-312.5	n.d.	1.00	n.d.	n.d.	n.d.	n.d.	n.d.	n.d.	n.d.	7.68	hy
321-368	porphyry	0.98	hyd	1.27						4.22	di&hy
323-308	porphyry	1.00	hyd	2.15	0.29					4.29	hy
334-216.2	porphyry	1.04	hyd	3.71						4.49	hy
345-489.5	n.d.	1.15	n.d.	n.d.	n.d.	n.d.	n.d.	n.d.	n.d.	10.31	hy
346-195.4	porphyry	1.13	hyd	4.19						12.56	hy
346-269.8	porphyry	1.09	hyd	3.06						14.61	hy
360-095	porphyry	1.06	hyd	3.56						4.50	hy
366-232.5	text. dest.	1.22	hyd							18.64	hy
367-089.8	porphyry	1.15	hyd	1.87							hy
401-158.8	n.d.	1.06	n.d.	n.d.	n.d.	n.d.	n.d.	n.d.	n.d.	8.34	hy
401-171.2	porphyry	1.03	hyd & mag	0.28						3.48	hy
401-218.3	phanerite	1.15	hyd	4.18						16.00	hy
455-023.1	n.d.	1.07	n.d.	n.d.	n.d.	n.d.	n.d.	n.d.	n.d.	8.06	hy
455-051.1	porphyry	1.02	hyd & mag	0.88						12.27	hy
JDD-94-02	porphyry	1.07	hyd & mag	1.56						4.57	hy
JDD-94-03	porphyry	1.01	hyd	0.3						3.51	hy
JDD-94-04	porphyry	1.08	hyd	1.36						1.04	hy
JDD-94-06	porphyry	1.02	hyd	1.37						2.18	hy
JDD-94-19	hbld ppy	1.10	hyd	0.35			0.35			15.17	hy

Table 16: Petrographic and chemical features of diamond drill core (DDH) and surface samples collected in 1994 (Suite 2).

Kalgoorlie Intrusion

Sample	Texture	A/CNK	Biotite	Modal Minerals Qtz	Pyx	Hbld	Ttn	Gar	Epi	Normative An content Plag. Feld.	F-mag Mineral
319-276.1	n.d.	0.84	n.d.	n.d.	n.d.	n.d.	n.d.	n.d.	n.d.	26.36	di&hy
383-157.6	phanerite	0.87	none				2.70	0.43	2.81		
389-271	phanerite	0.88	hyd & mag	1.58	1.29	0 89	0.69		0.99	21.42	di&hy
407-257.8	phanerite	1.09	hyd & mag	8.93			0.46			12.09	hy
411-045	porphyry	1.12	hyd	0.49	0.69	0.20	0.69			29.33	hy
458-151.8	porphyry	0.91	mag	1.90	5.19		0.70			25.02	di&hy
JDD-94-05	hbld ppy	1.09	hyd	2.35						7.75	hy
JDD-94-07	porphyry	1.06	hyd	0.39						3.61	hy
JDD-94-11	hbld ppy	0.97	hyd	3.08						5.17	di&ol
JDD-94-12	phanerite	0.98	hyd	3.60	3.11	0.88	0.88			31.47	di&hy
JDD-94-13	phanerite	1.22	none	1.82			0.51			22.29	hy

Ningi Intrusion

Sample	Texture	A/CNK	Biotite	Modal Minerals Qtz	Pyx	Hbld	Ttn	Gar	Epi	Normative Minerals An content Plag. Feld.	F-mag Mineral
351-313.2	phanerite	0.86	hyd	5.89	6.87	0.49	1.28		0.20	29.00	di&hy
356-166.5	phanerite	0.84	mag							19.64	di&hy
356-190	phanerite	0.93	mag							22.53	di&hy
386-075.4	porphyry	1.02	hyd & mag	3.52						18.50	hy
386-276.1	phanerite	0.85	hyd	1.98	2.48	4.56	1.39			23.35	di&hy
459-102.9	phanerite	0.70	none	8.83	8.73		0.98	1.86	2.16	28.90	di&wo
464-009	porphyry	1.14	mag	0.10	0.49	0.59			0.49	25.66	hy
464-355.5	phanerite	1.16	hyd & mag	6.11			0.22			20.16	hy
JDD-94-08	phanerite	1.07	hyd	0.72			0.45			17.14	hy
JDD-94-09	porphyry	1.07	hyd & mag	4.98						9.97	hy
JDD-94-10	porphyry	1.06	hyd & mag	0.68	4.28		0.39		0.19	27.93	hy
JDD-94-14	phanerite	1.13	hyd	16.04			-0.09			5.40	hy
JDD-94-15	porphyry	1.55	hyd & mag	2.18						13.11	hy

Abbreviations

n.d.	Not determined	hy	hypersthene	Qtz	quartz
text. dest.	Texture destroyed	di	diopside	Pyx	pyroxene
hyd	hydrothermal	wo	wollastonite	Hbld	hornblende
mag	magmatic	ol	olivine	Ttn	sphene
An	anorthite	ppy	porphyry	Epi	epidote
F-mag	Ferromagnesian				

Table 16 continued.

The sample most representative of pristine igneous phanerite is DDH 340-166.5 which comes from the Sydney Intrusion. Closely similar to this rock, and also from the Sydney intrusion are DDH 331-47.8 (phanerite), DDH 331-218.5 (porphyry), and DDH 342-84.5 (phanerite). The best example of extreme potassium feldspar-type alteration is DDH 302-69, which is from the Fubilan Intrusion.

The sample suites described above have been combined and regrouped into five categories for presentation and discussion: (1) Star Mountains region, (2) Fubilan intrusion, (3) Kalgoorlie intrusion, (4) Ningi intrusion, and (5) Sydney intrusion. The samples are characterized by the following features: 1) pyroxene is the dominant ferromagnesian mineral in all samples from the Sydney Intrusion and in most samples from the Kalgoorlie and Ningi intrusions; 2) hornblende is also present, but in lesser quantities than pyroxene, in some samples from the Sydney, Kalgoorlie, and Ningi Intrusions; and 3) biotite of magmatic origin is present in the Sydney intrusion, both hydrothermal and magmatic biotite are common in rocks from the Kalgoorlie and Ningi Intrusions, and hydrothermal biotite is the only ferromagnesian phase present in most samples from the Fubilan intrusion.

X-ray fluorescence spectrometry analyses were performed on more than 3000 samples of reverse-circulation drill cuttings from the Mt. Fubilan intrusion by the Folomian Laboratory, operated by Ok Tedi Mining Limited. The analyses performed on these samples did not include the complete list of oxides that are normally determined. In particular, Na_2O and P_2O_5 were not determined and TiO_2

was not done for all of the samples. These oxides are necessary for the calculation of normative minerals, for classification by the total-alkali-silica diagram, and for calculation of alumina indices. In addition it was impossible to eliminate samples from this set that had been contaminated by inclusion of siltstone, limestone, or massive ores. Nonetheless, the data are suitable for selective comparison with the more completely analyzed samples and are used as such for presentation on silica variation diagrams, for understanding the spatial variability of major oxides, for evaluation of sampling and laboratory consistency, and for illustrating of the effects of sample contamination. The collar locations of the drill holes from which the samples were taken are shown in Figure 56.

Normative Mineralogy

Normative minerals were calculated for all samples for which major oxide chemical data were available except those from reverse circulation drilling. The calculations were made using the CIPW module of NEWPET (Clarke, unpublished). The output obtained from NEWPET was compared to that of four other computer programs - PETCAL (Bingler and others, 1976), CIPW (Carr, unpublished), CIPWNORM (Mueller, unpublished), and CHEMPET (Yegorov, Korobeinikov, and Dubrovskii, 1998) - for consistency. All programs were found to produce similar results with the exception that many of the NEWPET norms

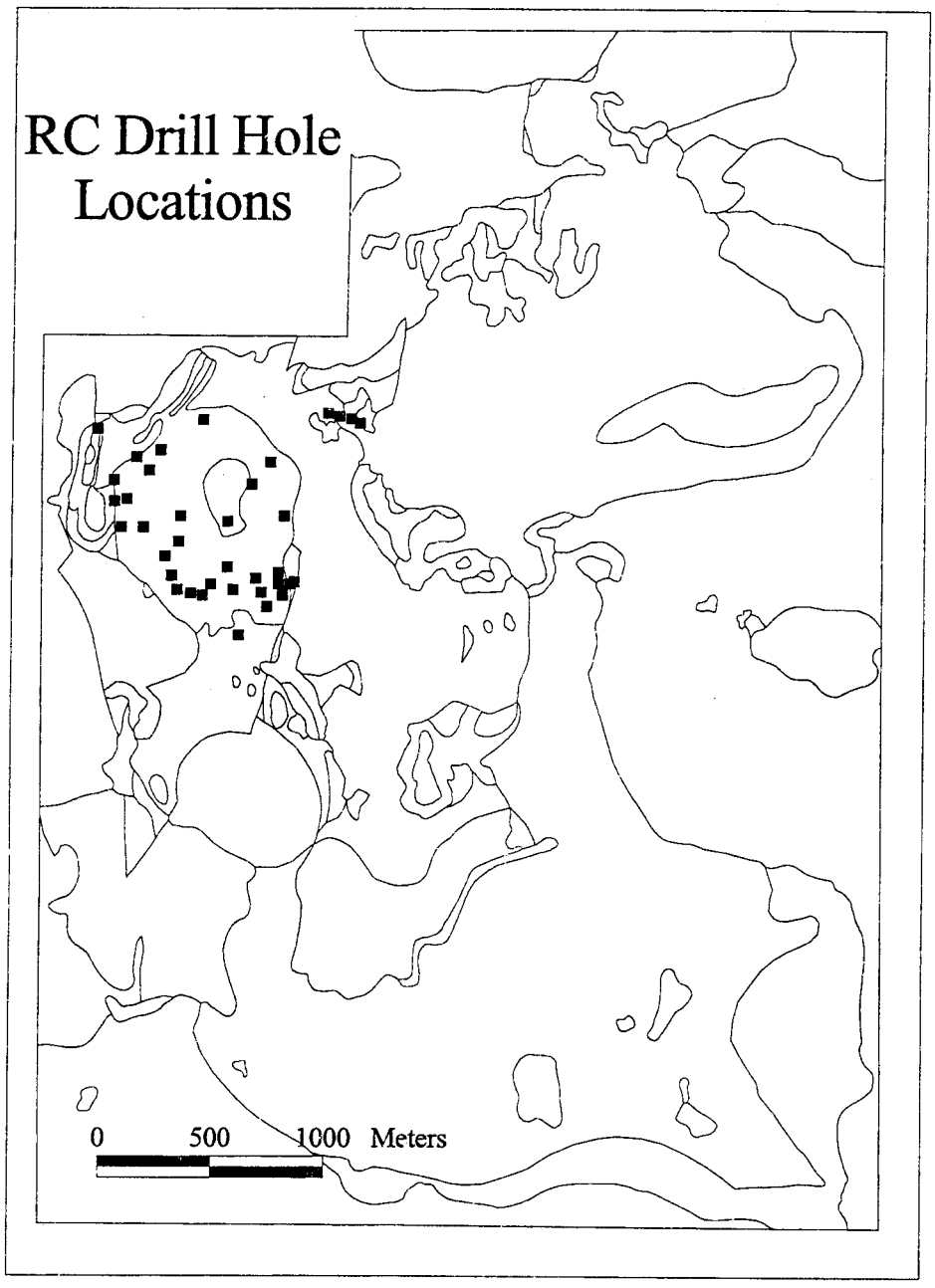

Figure 56: Collar locations of reverse-circulation drill hole samples.

include both nepheline (*ne*) and quartz (*q*), two incompatible phases (Ragland, 1989). Katchan (1982) also noted normative *ne* in two of his samples but these did not contain *q*. FeO^* (total iron as FeO) was adjusted for samples with appreciable amounts of sulfide in their mode by subtracting a molecular quantity of iron equal to the amount of molecular sulfur from total iron prior to final calculation.

The difference between samples with normative andesine and those with albite is perhaps the most striking feature of the normative mineralogy. Samples having anorthite contents of less than An_{10} come from rock that has undergone strong potassic alteration, whereas those with $An_{30\text{-}50}$ (andesine) have mineral assemblages of magmatic origin. Those samples having An content intermediate between albite and andesine cannot be characterized as magmatic or metasomatic without additional petrographic information. The average and range of normative An values in samples from the different intrusions are listed in Table 17. The spatial distribution of samples categorized by their anorthite content content (less than An_{10}, between An_{10} and An_{30}, and greater than An_{30}) is shown in Figure 57. Most samples from the Fubilan Intrusion have normative albite consistent with extremely altered nature of this intrusion. The least altered samples from the Kalgoorlie, and Ningi intrusions have oligoclase as their normative plagioclase feldspar. Altered samples from these intrusions have anorthite content as low as An_0 consistent with petrographic observations that hydrothermal alteration was not solely confined to the Fubilan intrusion. The Sydney Intrusion is characterized

Intrusion	Minimum An	Average An	Maximum An	Samples
Mt. Fubilan	0	5	19	84
Kalgoorlie	0	22	38	21
Ningi	0	17	29	21
Sydney	12	36	45	10

Table 17: Summary of the normative anorthite (An) contents of samples from the Sydney, Fubilan, Kalgoorlie, and Ningi Intrusions.

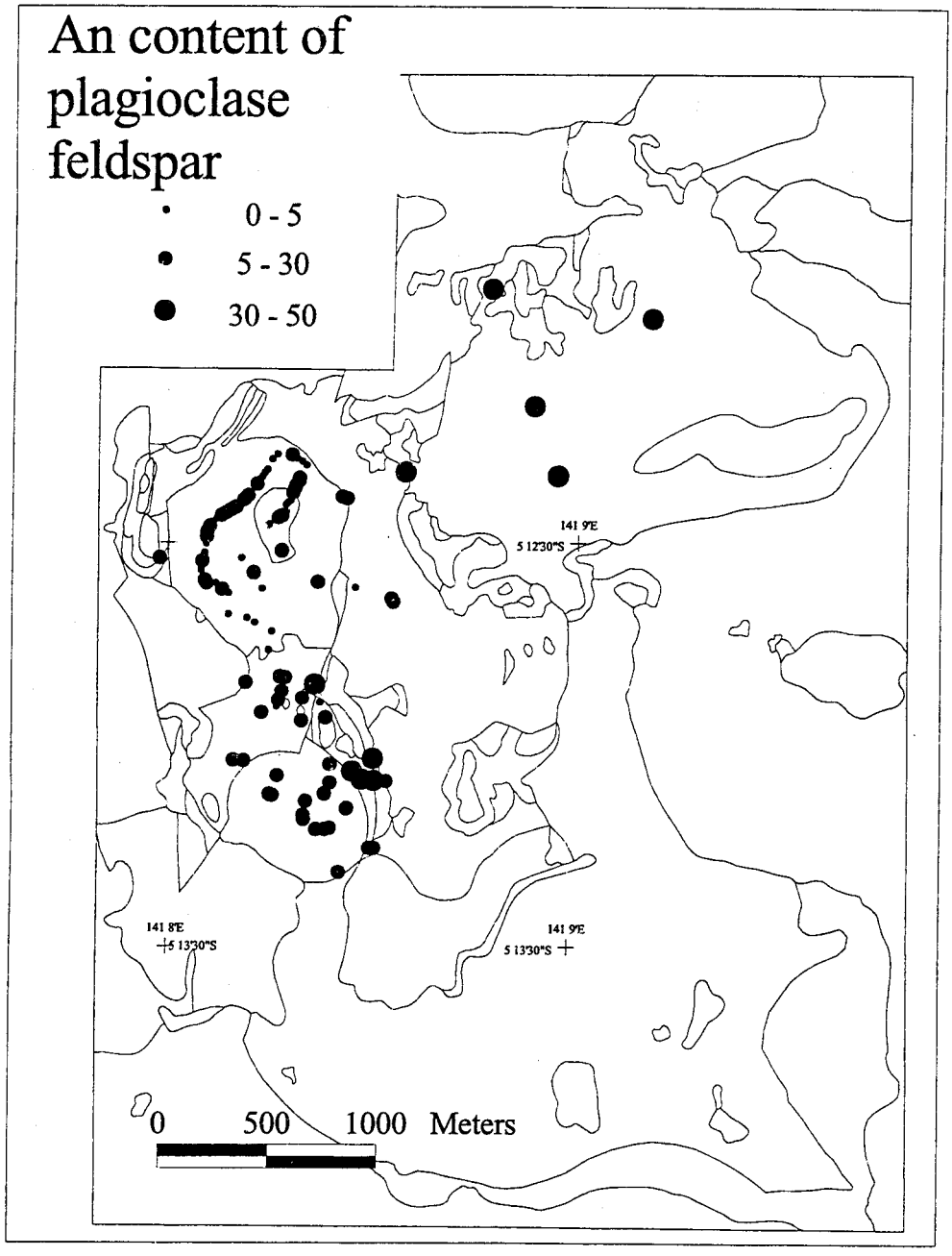

Figure 57: Map showing the spatial variation in normative anorthite content for samples of intrusive rock from the Ok Tedi Intrusive Complex.

by normative andesine. Only one of the samples assigned to the Sydney intrusion (JDD-94-01 - texturally destroyed phanerite?) has low anorthite content (An_{12}). The textural and chemical data for this sample suggests that hydrothermal alteration has affected part of the Sydney Intrusion, at least that part adjacent to the Fubilan intrusion.

All of the mafic minerals calculated in CIPW norms are anhydrous (olivine, wollastonite, diopside, and hypersthene), whereas many igneous rocks of intermediate composition, including those of the Ok Tedi Intrusive Complex, contain hydrous mafic silicates (typically hornblende and biotite). The amounts and types of mafic minerals identified in modal analyses cannot, therefore, be expected to be identical to their calculated normative counterparts. Certain inferences can be made, however, which allow the modal minerals in samples from the Ok Tedi Intrusive Complex to be predicted on the basis of calculated normative minerals. This is possible because the hydrous silicates can be considered to consist of combinations of anhydrous components. For example, modal hornblende may appear in the norm as some combination of *an*, *di*, *hy* and *ne* and similarly biotite may appear as some combination of *or, c* and *hy* (Williams, Turner, and Gilbert, 1982). Some normative components may not be present in the mode, but may be incorporated into other minerals that are present in the norm. For example, *ne* may be incorporated in pyroxene. Three generalizations appear well founded for samples of the Ok Tedi Intrusive Complex: 1) samples in which the normative

pyroxene is diopside come from rocks which are unaltered, or have only weak propylitic or weathering-related (supergene) alteration, and which contain pyroxene or hornblende in their modes; 2) samples with normative wollastonite are likely to contain modal garnet or epidote; and 3) samples with hypersthene and corundum in their norms are strongly altered to mineral assemblages consisting of potassium feldspar, albite, and hydrothermal biotite. These generalizations are supported by the fact that of 21 of 23 samples with normative *di* have modal pyroxene, that 10 out of 12 samples with normative *di* and *hy* have hornblende in their modes, and that 32 of 32 samples with normative *c* and *hy* have biotite in their modes (31 of 41 samples with modal biotite have normative *c*).

Silica Variation

Silica variation diagrams have been a popular method for illustrating the chemical evolution of suites of igneous rock ever since they were introduced by Powell (1891) and popularized by Harker (1909). They are prepared by plotting the weight percentages of the major-oxides against weight percent SiO_2. Samples collected from igneous rocks of a specific geologic province, and that show essentially linear trends on the diagrams, are considered to form consanguineous suites. Trends on these diagrams reflect the more or less orderly chemical evolution of magmas along a "liquid line of descent." During crystallization of a magma, the chemical components incorporated in the early-formed minerals

(compatible) become depleted in the residual magmas. In contrast, those components excluded from the early-formed minerals (incompatible) become enriched and subsequently enter the late-formed minerals. Successive fractions of residual magma formed by normal crystallization processes are characterized by increasing SiO_2 content that is accompanied by concomitant chemical trends of decreasing Al_2O_3, FeO and Fe_2O_3, CaO, TiO_2, and of increasing Na_2O and K_2O.

The oxide components of most samples from the Star Mountains plot along linear trends on silica variation diagrams as illustrated in Figure 58. Overall, the data document decreases in Al_2O_3, TiO_2, FeO^*, MgO, CaO, and P_2O_5 over a range from about 50 to 65 weight percent SiO_2. The decreases in the above oxides, with SiO_2, are also accompanied by increases in Na_2O and K_2O. Correlation coefficients and other regression parameters relating the various oxides to SiO_2 are listed in Table 18. Of these, trends for TiO_2, FeO^*, MgO, CaO, Na_2O, and P_2O_5 are strongly correlated to that of SiO_2. In contrast, K_2O is weakly correlated with SiO_2, and Al_2O_3 and H_2O show little correlation. The regression lines derived for this set of data are used throughout this study as the standard evolutionary trend for the region. As such, they will be plotted on all subsequent Harker diagrams used to depict the Ok Tedi Intrusive Complex. Three samples with SiO_2 lower than about 45 percent were excluded from trend lines drawn by Arnold, Griffin, and Hodge (1979) because they were considered to be anomalous. These samples are plotted

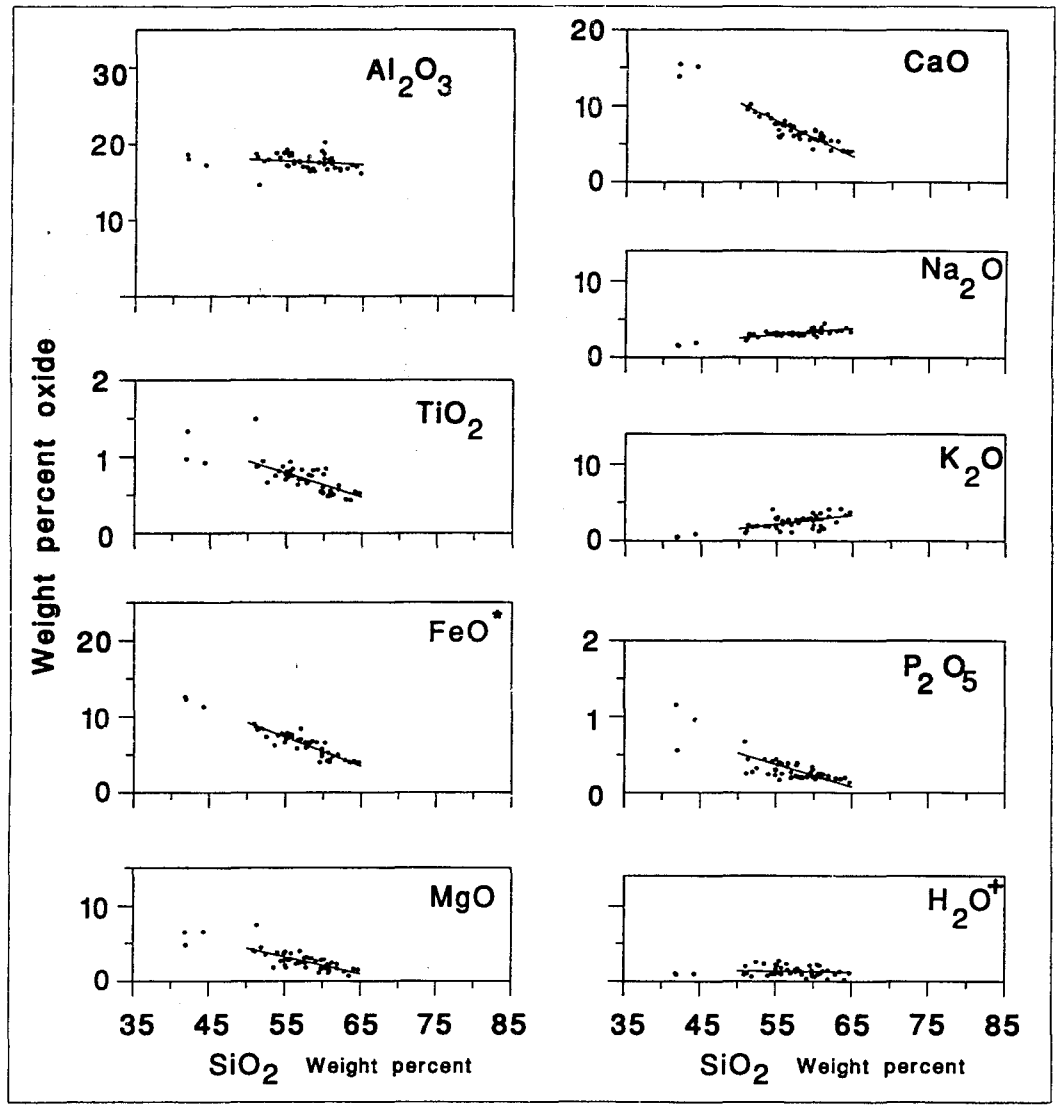

Figure 58: Silica variation diagrams for samples from the Star Mountains region.

	r	a	b
Al_2O_3	-0.26	-0.05	20.3
TiO_2	-0.77	-0.03	2.5
FeO^*	-0.95	-0.38	28.2
MgO	-0.81	-0.23	15.8
CaO	-0.94	-0.46	33.5
Na_2O	0.92	0.09	-1.9
K_2O	0.82	0.12	-4.6
P_2O_5	-0.79	-0.03	2.0

r = correlation coefficient
correlation trend lines calculated from the formula:

$$y = ax + b$$

where y = y axis value, a = slope of regression line
x = x axis value, and b = y axis intercept

Table 18: Regression equation and parameters for Star Mountains regional trend lines given in Figures 58 to 63.

on Figure 58 but were omitted from the calculation of trend lines used in this dissertation.

Samples from the Sydney Intrusion range from about 55 to 61 weight percent SiO_2 as shown in Figure 59. Most of the major-oxides plot near the regional regression trends. Significantly, the least altered samples plot as close to the regression trends as do the samples from which the trends are derived. K_2O values are somewhat higher than the regional trend. The sample with minor garnet in its mode (DDH 342-141) has higher CaO and lower FeO^* than the other samples. The sample of texturally destroyed rock (JDD-94-01) has higher Al_2O_3 and lower CaO than the regression trends; it also has high S when compared to the other samples that have virtually none of this chemical element, which reflects the presence of pyrite. The average values of TiO_2 and P_2O_5 for samples from the Sydney Intrusion are 0.59 and 0.27, respectively.

Most samples from the Fubilan Intrusion fall in a range from about 58 to 70 weight percent SiO_2 as shown in Figure 60. Those with quartz veins have SiO_2 values that range from 70 to 98 weight percent. Two samples (TS-42, and 43) are distinguished by high Al_2O_3 and low concentrations of SiO_2, FeO^*, and CaO. These are described as clay-altered by Mason (1993a,b,c). The sample of texture-destroyed rock has low SiO_2 accompanied by high sulfur reflecting the presence of the pyrite pseudomorphs. However, the most striking chemical features of the

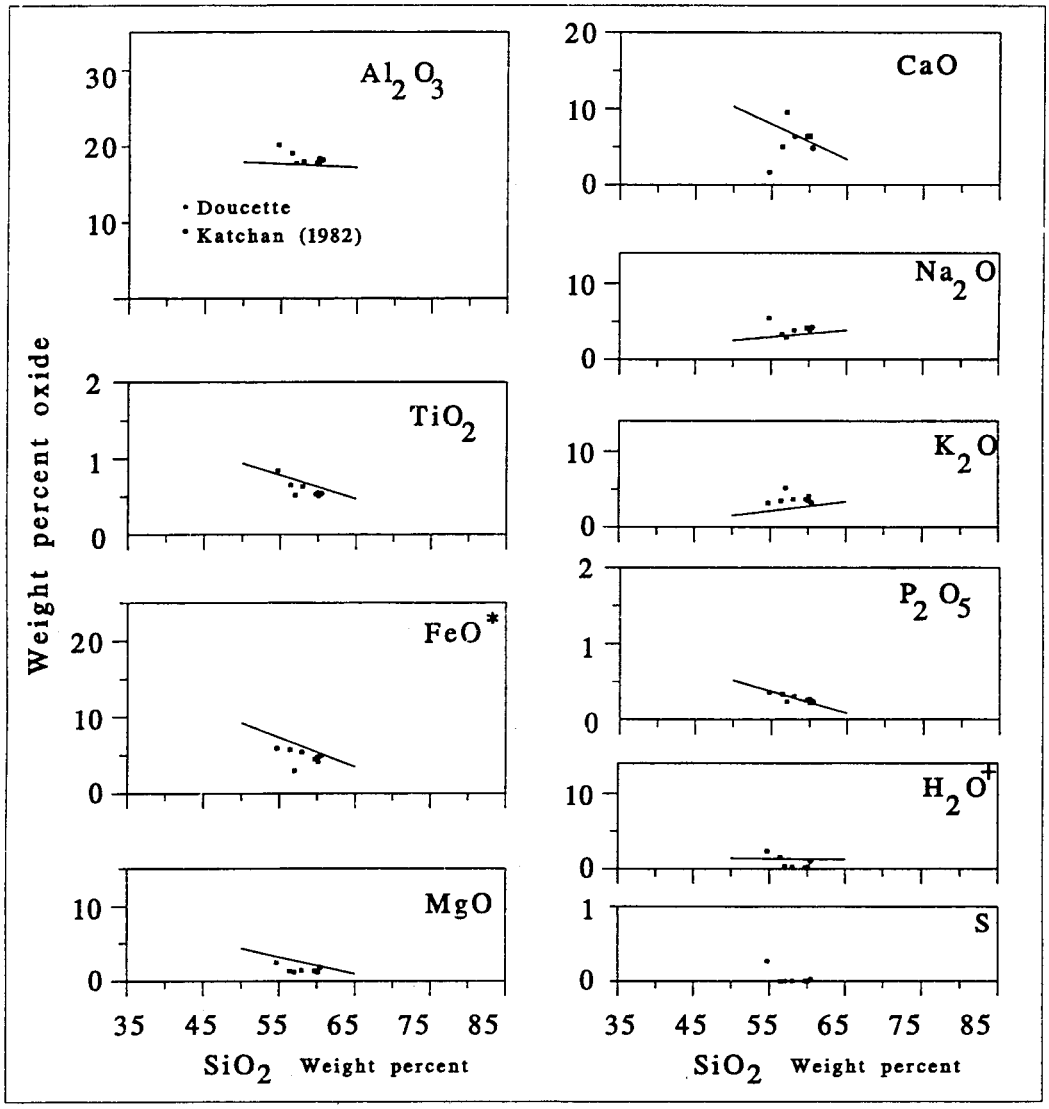

Figure 59: Silica variation diagrams for samples from the Sydney Intrusion. Trend lines based on regional variations.

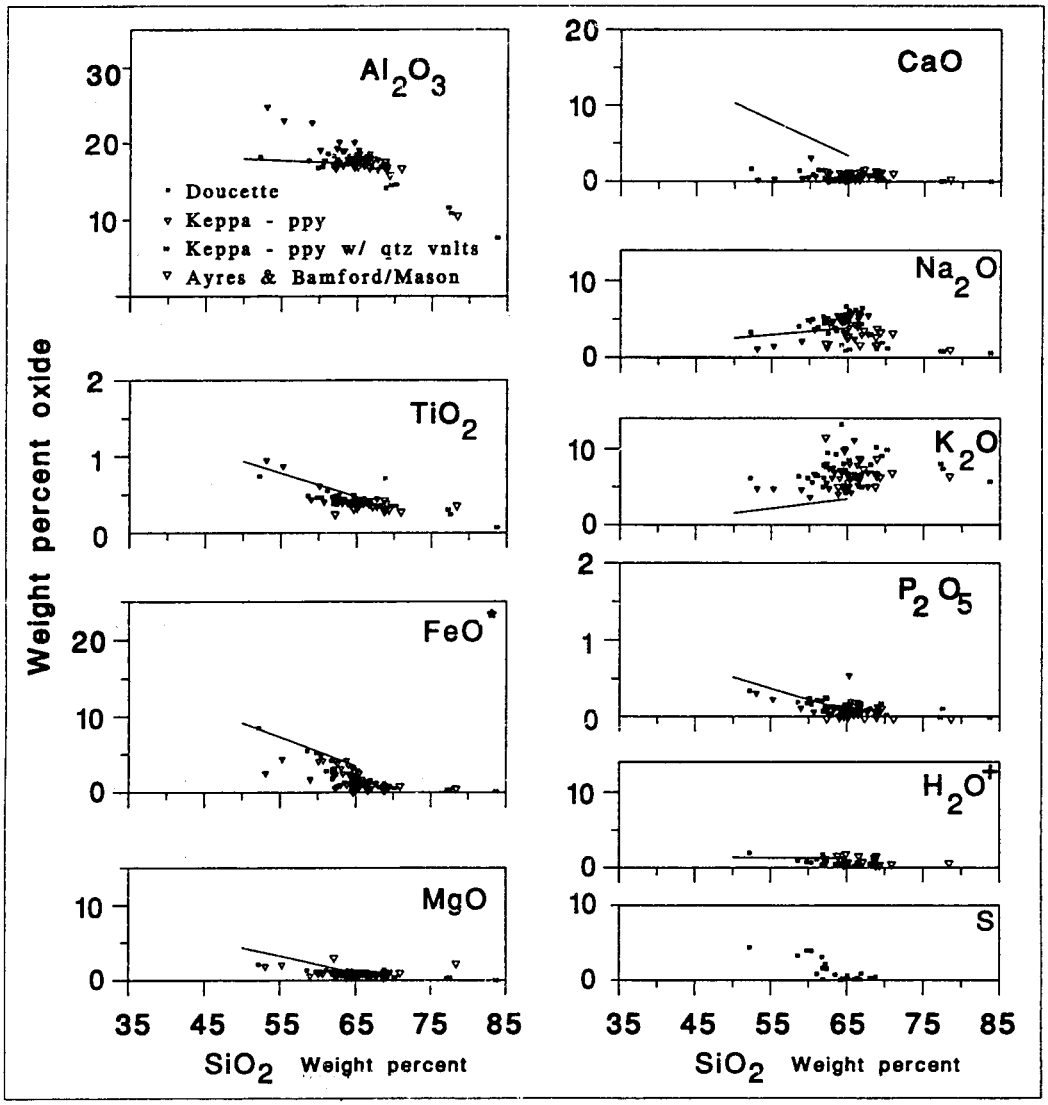

Figure 60: Silica variation diagrams for samples from the Fubilan Intrusion. Trend lines based on regional variations.

samples from the Fubilan Intrusion are the uniformly low values for CaO (range 0.01-1.60 weight percent -average 0.67) and uniformly high values for K_2O (range 4-13.2 weight percent - average 6.75). For comparison, the least-altered sample of the Sydney Intrusion (DDH 340-166.5) has 6.37 weight percent CaO and 3.48 weight percent K_2O. In addition many of the samples are characterized by low FeO^*. Concentrations of TiO_2, Al_2O_3, and P_2O_5 in most samples appear to fall on extensions of the regional trends to higher SiO_2. The average values of TiO_2 and P_2O_5 for samples from the Fubilan Intrusion are 0.43 and 0.25, respectively.

Most of the samples from the Kalgoorlie Intrusion range from 54 to 64 weight percent SiO_2 as shown in Figure 61. CaO ranges in abundance from 0.38 to 7.82 weight percent, K_2O from 2.30 to 9.02 percent, and FeO^* from 0.94 to 5.95 percent. Na_2O forms a trend that is parallel to the regression trend of regional data, but slightly higher, whereas MgO is somewhat lower. Values for TiO_2 and P_2O_5 plot along the regression trends and are indistinguishable from regional values. The samples, therefore, exhibit the chemical characteristics of both unaltered rock and of rock altered by potassium metasomatism. Three samples of endoskarn (not shown in Figure 61) have reduced amounts of SiO_2 that are accompanied by CaO contents varying from a low of 10.5 to a high of 18.7 weight percent. These three samples are also characterized by high iron content (13 to 34 weight percent FeO^*) reflecting the presence of magnetite veinlets.

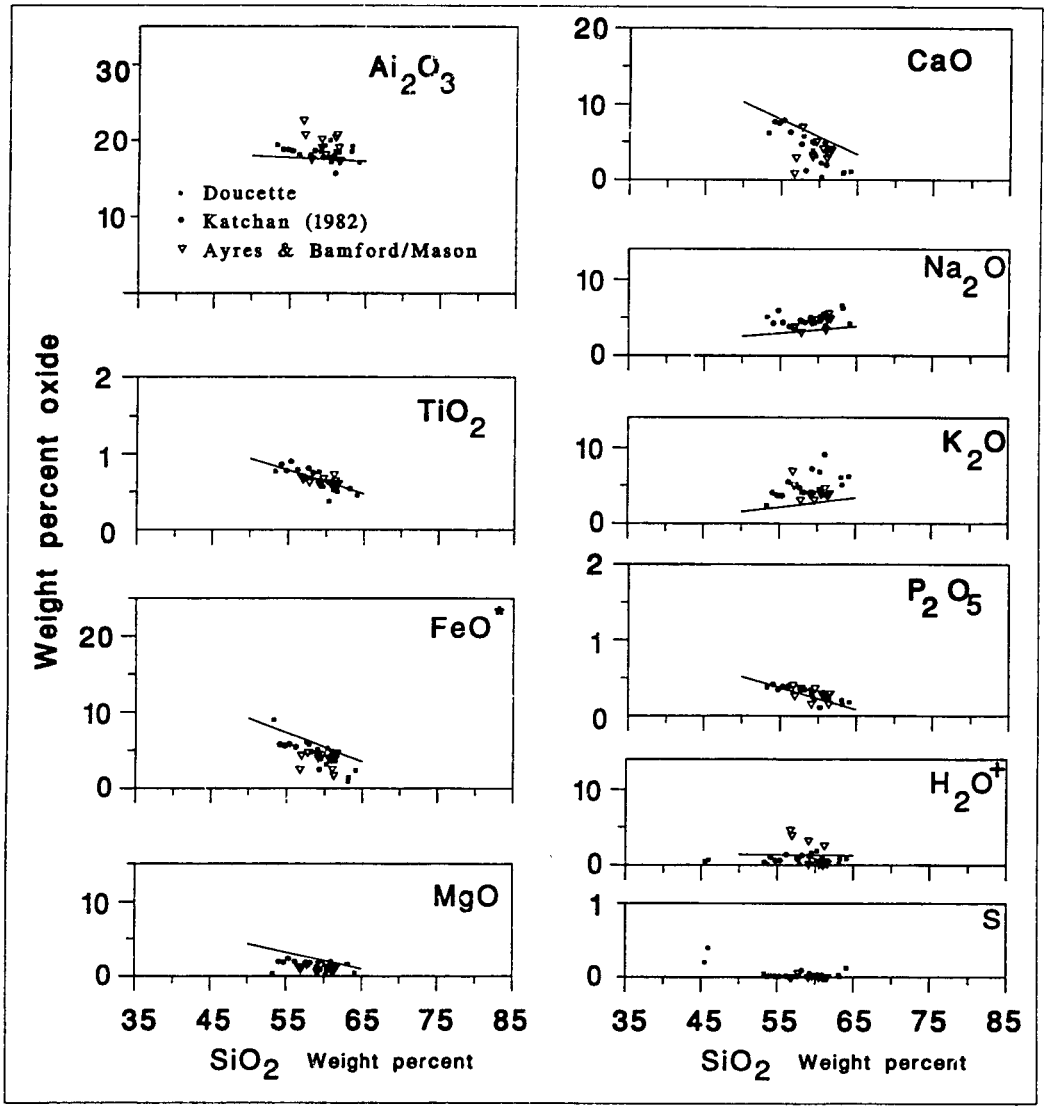

Figure 61: Silica variation diagrams for samples from the Kalgoorlie Intrusion. Trend lines based on regional variations.

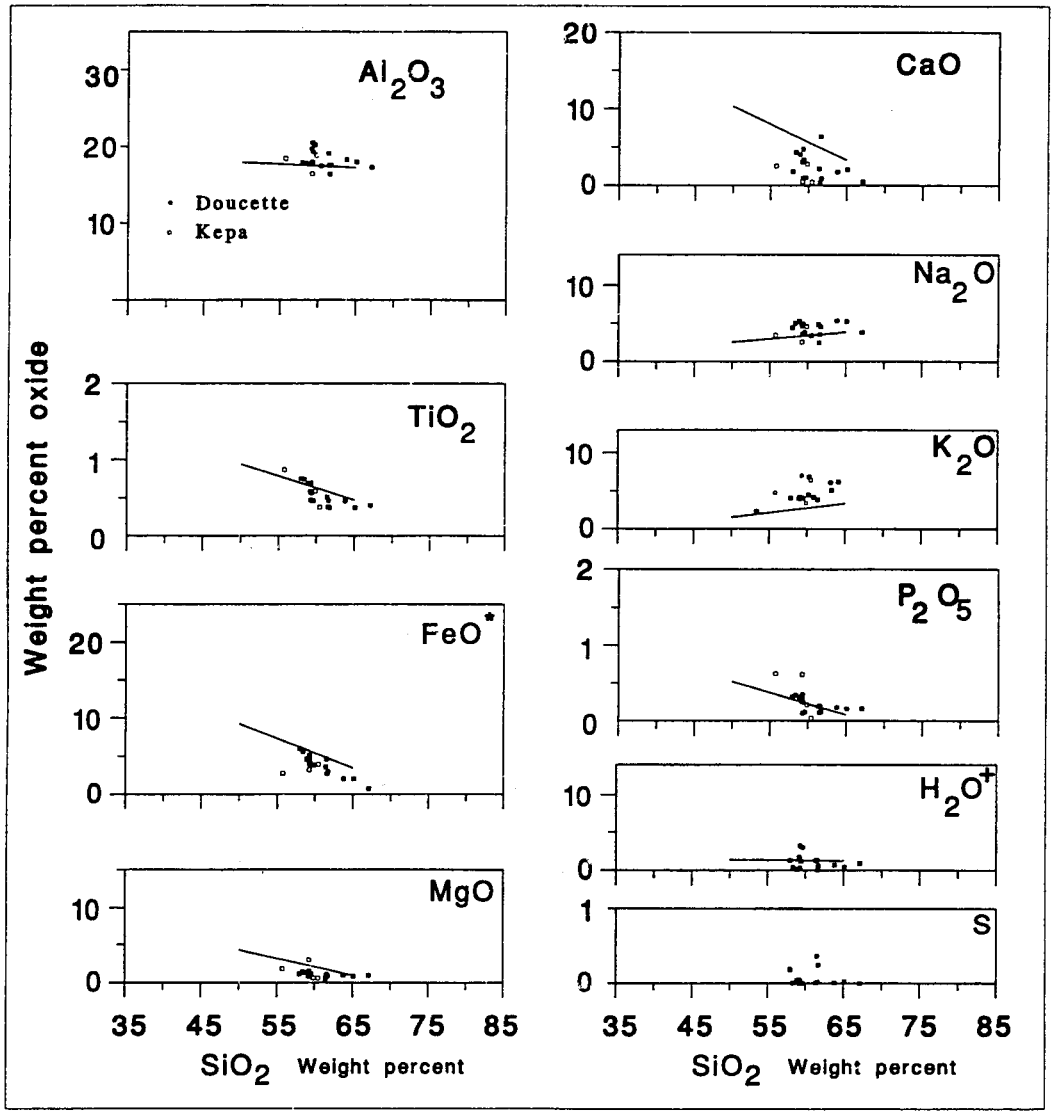

Figure 62: Silica variation diagrams for samples from the Ningi Intrusion. Trend lines based on regional variations.

Samples from the Ningi Intrusion range from 56 to 67 weight percent SiO_2 as shown in Figure 62. Most samples have CaO values that are depleted relative to the regional regression lines, whereas those of K_2O are higher. CaO ranges from 0.34 to 6.39 percent, K_2O from 3.30 to 7.91, and FeO^* from 0.71 to 5.97 weight percent. Concentrations of Na_2O, Al_2O_3, MgO, TiO_2, and P_2O_5 for most of the samples plot near those of the regional regression lines. These samples are chemically similar to those of the Kalgoorlie Intrusion and include both altered and unaltered rock.

The partial major oxide data from reverse circulation (RC) rotary drill cuttings from the Fubilan Intrusion form dense elliptical clouds on silica-variation diagrams (Figure 63) because of the large number of samples included in the data set. These clouds are surrounded by a scatter of more diffuse data points. The dense clouds of data reveal the fact that the total variation of SiO_2 and, to a lesser extent, that of the other major oxides within a single intrusive unit (the hydrothermally altered Fubilan Intrusion) can be large. Thus, individual intrusive rock units cannot be characterized by a single value or even a narrow range of values. The more diffuse data points represent contamination of samples of porphyry by other rock or minerals such as siltstone, limestone, quartz veinlets, metallic sulfides, magnetite, and limonite. The SiO_2 contents of the porphyries range from about 65 to 75 weight percent. Al_2O_3 values are aligned with their regional regression line and partly overlap the line. CaO amounts are very low and

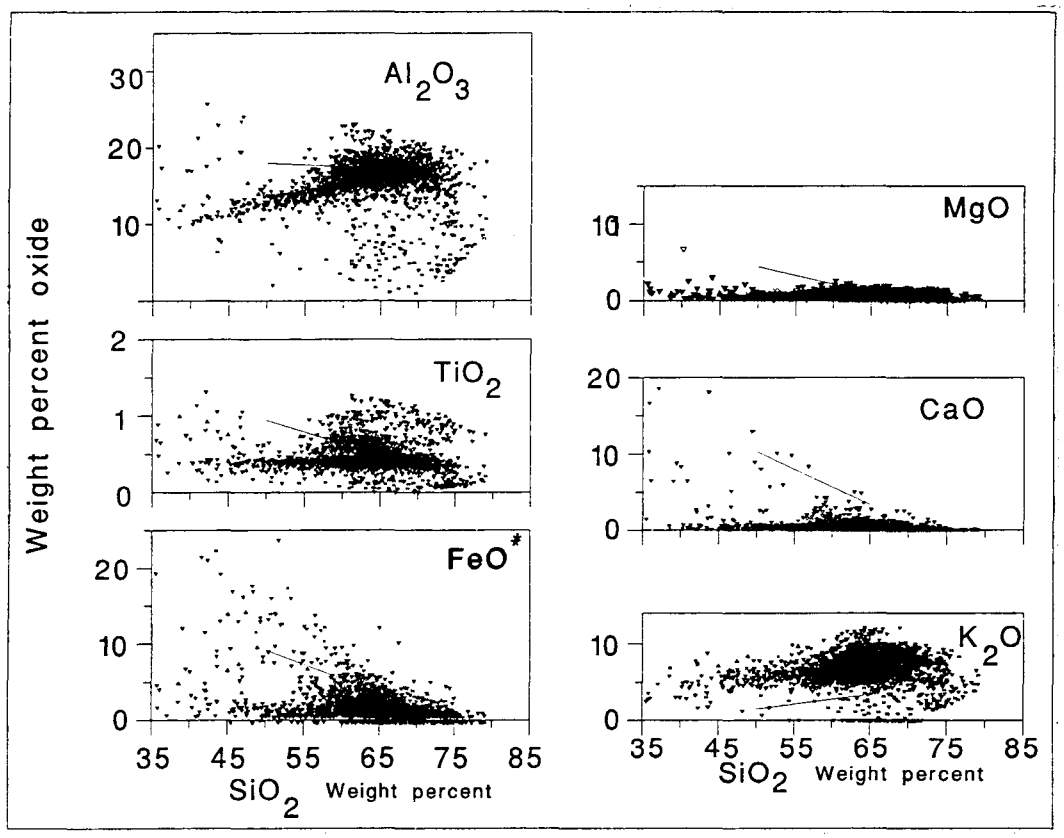

Figure 63: Silica variation diagrams for reverse-circulation drill cuttings from the Fubilan Intrusion. Trend lines based on regional variations.

lie below the regression line. In contrast, K_2O is uniformly higher than its regression line. FeO* abundances are aligned along, or lower than, their regression line. Analysis of the variation of MgO is equivocal with samples on the low end of the range of SiO_2 being below the regional regression line while those on the high end may have values above that line. TiO_2 appears to exhibit two trends; one is more or less coincident with the regional regression line for TiO_2 and the other is invariant with changes in SiO_2. Whether or not the two trends are separate is uncertain and, if they are separate, the reason is also unknown.

Alumina Variation

Alumina content is almost as important in the interpretation of igneous rocks as is the silica content (Shand, 1943; Ragland, 1989), especially for the felsic varieties. The concept of alumina saturation was first introduced by Shand (1943) who distinguished four groups of rocks based on the molecular ratio of Al_2O_3 to $CaO+Na_2O+K_2O$ (A/CNK) or to Na_2O+K_2O (NK). These are 1) peraluminous, 2) metaluminous, 3) subaluminous, and 4) peralkaline. *Peraluminous* rocks are characterized by values of A/CNK greater than one and by modal mica, corundum, tourmaline, topaz, Fe-Mn garnet, cordierite, or sillimanite. *Metaluminous* rocks are characterized by A/NK > 1 > A/CNK and by hornblende, aluminous augites, melillite, or by combinations of an aluminous phase (such as biotite) and a nonaluminous phase (pyroxene). *Subaluminous* rocks have A/NK ≈ 1 and

nonaluminous mafic minerals (diopside, olivine, or orthopyroxene). Finally, *peralkaline* rocks have A/NK < 1 and contain sodic-pyroxenes or sodic-amphiboles.

The method used herein to portray the variation in alumina is from an unpublished short course by S.R. Keith. It involves the use of a binary diagram on which molecular A/CNK ratios are plotted against the SiO_2 contents of a group of samples. Lines drawn parallel to the SiO_2 axis subdivide the diagram into fields of strongly metaluminous (A/CNK<0.65), metaluminous (0.65<A/CNK<1), peraluminous (1<A/CNK<1.1), and strongly peraluminous chemistry (A/CNK>1.1). Additional fields of unaltered and altered rock are based on empirical data derived from compilations of large numbers of samples of igneous rocks (Keith and others, 1991). A central field representing unaltered rock is bounded on either side by fields characterized by altered rock.

All but one of the samples from the regional data set are metaluminous (Figure 64). The sample that plots as peraluminous and two of the metaluminous samples fall in the field of altered rock. The three samples that were omitted from calculation by Arnold, Griffin, and Hodge are strongly metaluminous. The remaining samples form a trend (a-a' in Figure 64) approximately parallel to the boundary between altered and unaltered rock.

The least altered samples from the Sydney Intrusion plot well within the field of metaluminous rocks with A/CNK values of approximately 0.80 as depicted

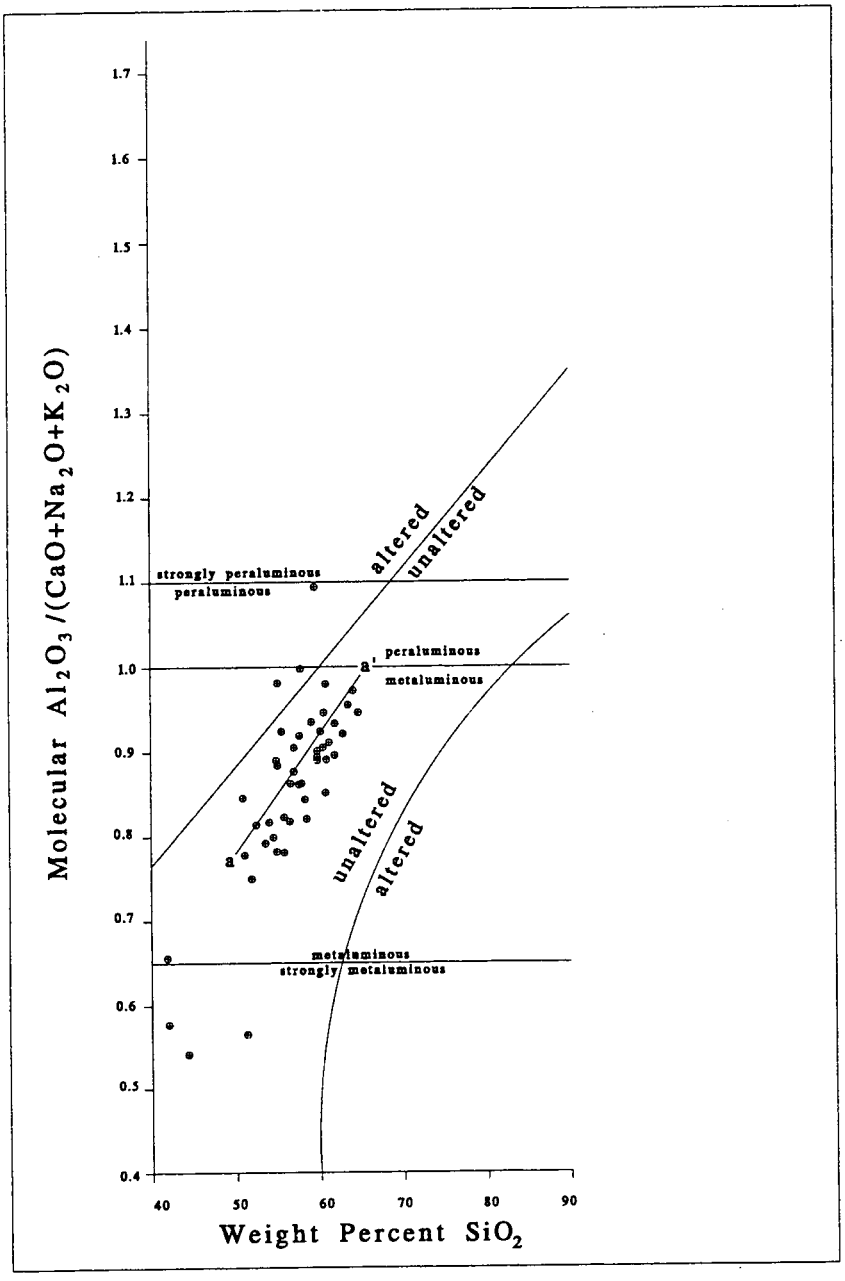

Figure 64: Alumina variation diagram for samples from the Star Mountains region. Line (a-a') is regression line calculated from the data portrayed.

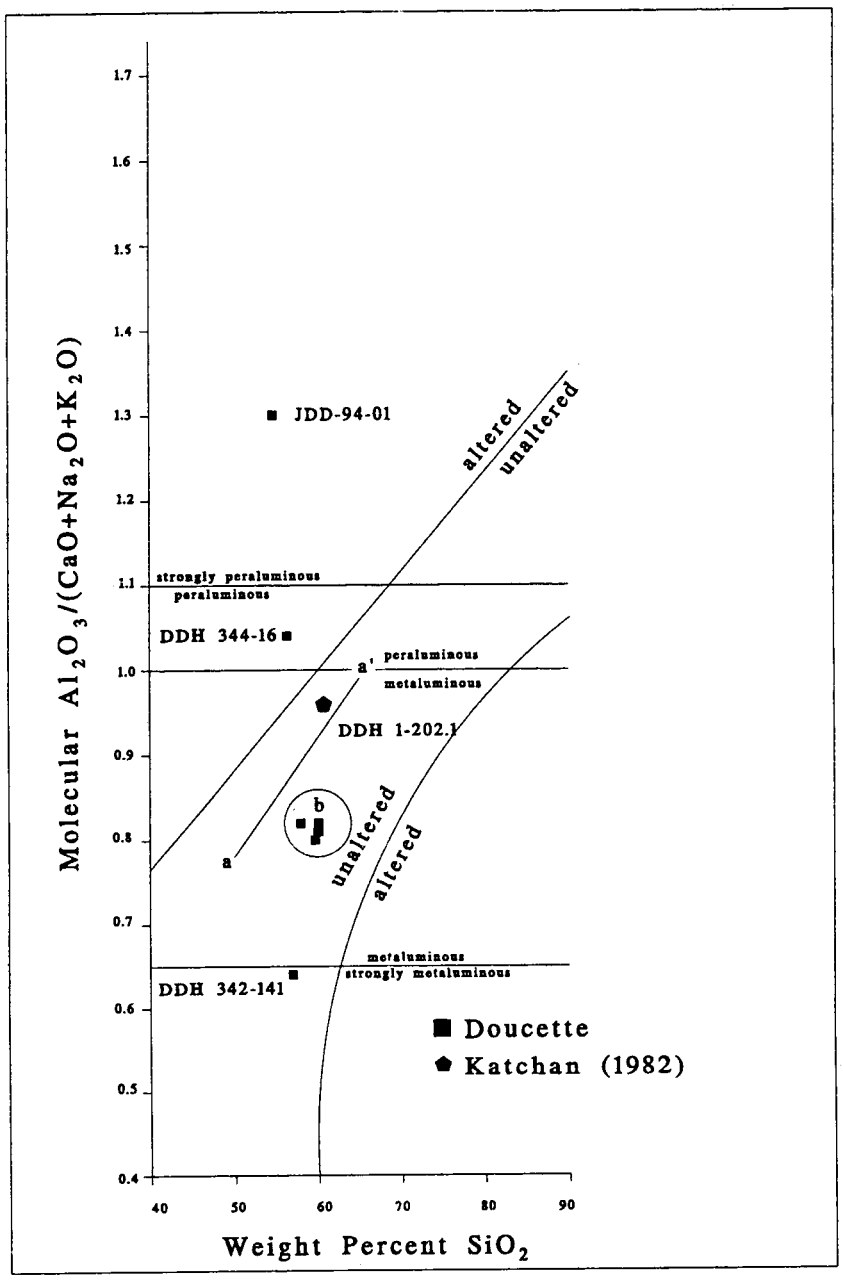

Figure 65: Alumina variation diagram for samples from the Sydney Intrusion. Line (a-a') is regression line for data from the Star Mountains region. Circle (b) is area of least-altered/unaltered rocks from the Ok Tedi Intrusive Complex.

by the circle (b) in Figure 65. The sample of texture-destroyed rock (JDD-94-01) plots as strong peraluminous reflecting the presence of substantial biotite and also may reflect the presence of significant amounts of clay. Sample DDH 344-016 plots as peraluminous-altered. This sample has weak clay alteration and shows weak to moderate weathering of pyroxene to limonite but is otherwise unaltered in appearance. Sample DDH 1-202.1, which contains hornblende and minor epidote, plots near the boundary between metaluminous and peraluminous. Whereas sample DDH 342-141, which contains minor garnet, plots near the boundary between strongly metaluminous and metaluminous.

Nearly all of the samples from the Fubilan Intrusion are confined to the fields of peraluminous or strongly peraluminous rock as shown in Figure 66 and most fall within the field of altered rock. In general, samples that contain quartz veinlets or that consist of silica-flooded porphyry have A/CNK values that are similar to those of unveined porphyry. Four samples of porphyry and two of veined porphyry have A/CNK values greater than 1.7 and thus cannot be shown on the diagram.

Samples from the Kalgoorlie Intrusion, as illustrated in Figure 67, consist of nearly equal numbers that plot as (strongly) peraluminous-altered and as metaluminous-unaltered. Four of the samples have A/CNK values (~0.84) near to those of the unaltered rocks of the Sydney Intrusion (b). These samples contain hornblende and pyroxene in their modes similar to those of the Sydney Intrusion,

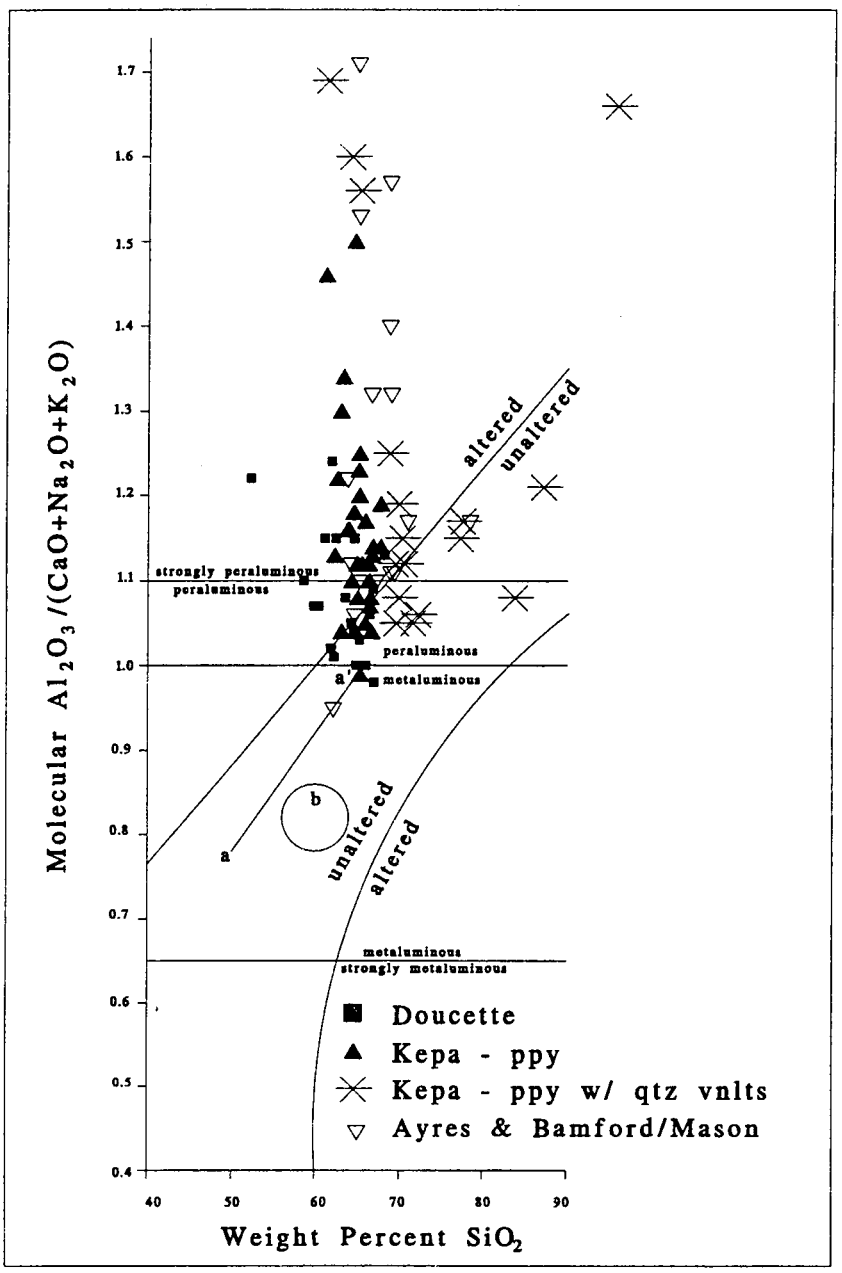

Figure 66: Alumina variation diagram for samples from the Fubilan Intrusion. Line (a-a') is regression line for data from the Star Mountains region. Circle (b) is area of least-altered and unaltered rocks from the Ok Tedi Intrusive Complex.

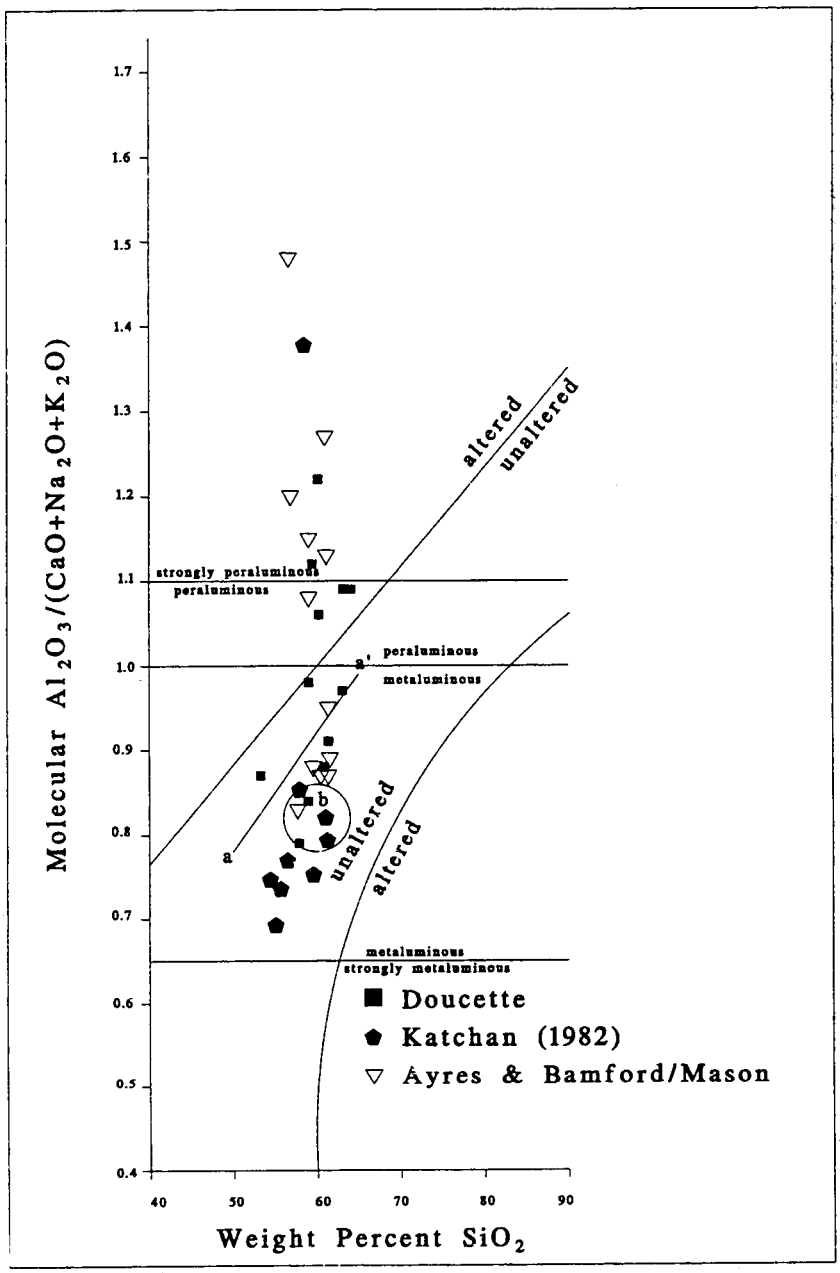

Figure 67: Alumina variation diagram for samples from the Kalgoorlie Intrusion. Line (a-a') is regression line for data from the Star Mountains region. Circle (b) is area of least-altered and unaltered rocks from the Ok Tedi Intrusive Complex.

but they also have normative oligoclase instead of andesine suggesting that they may be slightly altered or that they may come from a different magma batch.

Five samples from the Ningi Intrusion plot within the metaluminous field of Figure 68. Three of these have A/CNK values (~0.85) near to those of the unaltered rocks of the Sydney Intrusion (b). These samples contain pyroxene (±hornblende) in their modes and are thus similar to the unaltered rocks of the Sydney and Kalgoorlie Intrusions. They differ from those of the Sydney Intrusion by having normative oligoclase instead of andesine and as such are similar to those from the Kalgoorlie Intrusion. Sample DDH 459-102.9, which contains minor amounts of garnet, plots near the boundary between metaluminous and strongly metaluminous. Its position is similar to sample DDH-342-141 from the Sydney Intrusion and both samples contain garnet suggesting that propylitic (or endoskarn) alteration may result in a decrease in the ratio A/CNK. This could reflect a process in which Al_2O_3, Na_2O, and K_2O remain constant while CaO increases in concentration. The remaining 14 samples plot as altered and peraluminous or strongly peraluminous.

In summary, the samples of unaltered igneous rocks from the Ok Tedi Intrusive Complex are metaluminous. They have pyroxene, hornblende, and biotite in their modes and have A/CNK values less than 1. A/NK values are significantly greater than 1. Altered rocks have the chemical characteristics of peraluminous

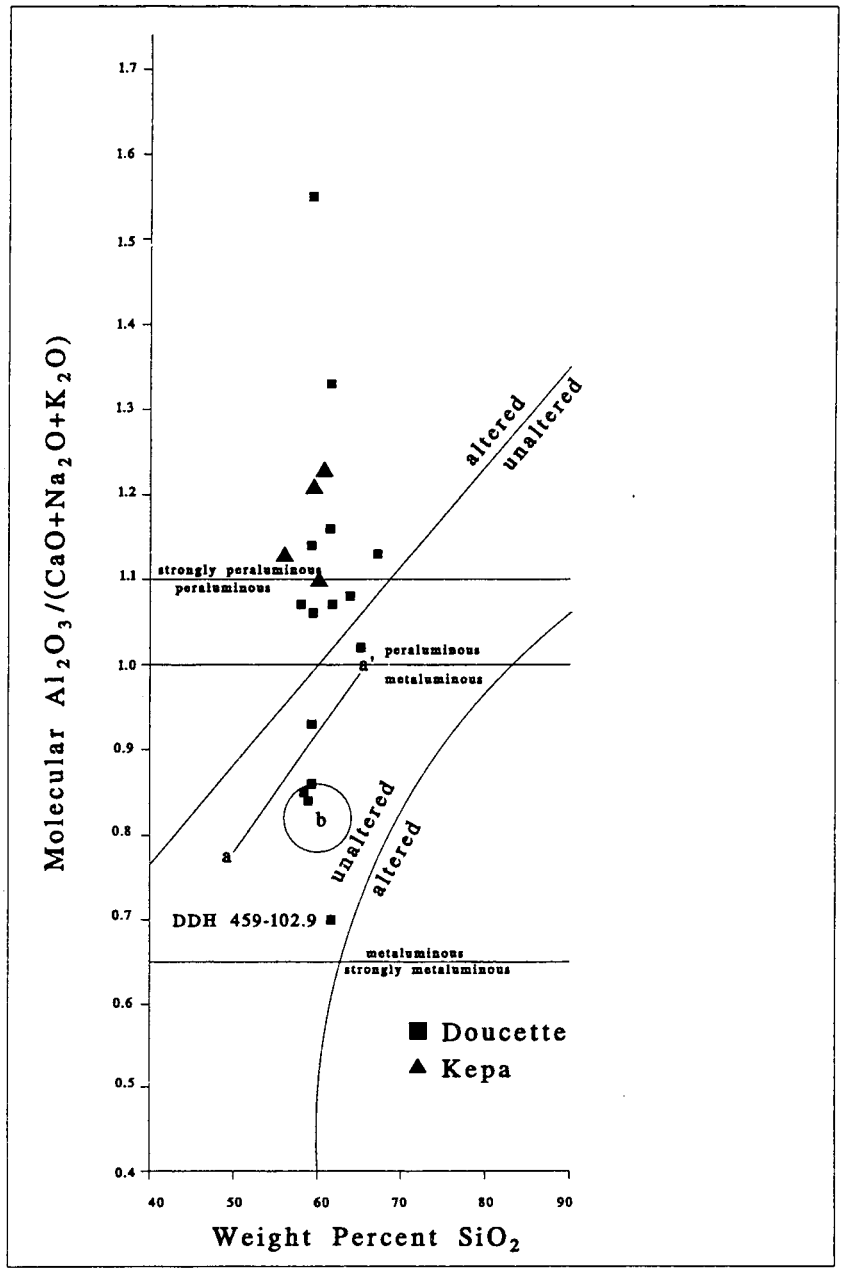

Figure 68: Alumina variation diagram for samples from the Ningi Intrusion. Line (a-a') is regression line for data from the Star Mountains region. Circle (b) is area of least-altered/unaltered rocks from the Ok Tedi Intrusive Complex.

and strongly peraluminous rocks and most contain hydrothermal biotite. The fact that the samples showing evidence of potassic alteration plot in peraluminous fields does not, however, make these rocks peraluminous. Shand (1943) noted that if corundum appears in the norm, without hypersthene, the rock is peraluminous, but that if corundum and hypersthene are present it is necessary to consider whether the ratio of Al_2O_3 (*c*) to (Mg, Fe)O+SiO_2 (hy) is about the same as in biotite. Most samples from the potassically altered rocks from the Ok Tedi complex were noted to contain both *c* and *hy* (see discussion of normative mineralogy) in sufficient concentrations to produce biotite. In addition, some of the excess Al is probably contained in clay minerals. Therefore, the plotted locations of the data in Figures 61-65 may actually reflect the chemical effects of hydrothermal alteration and not petrogenetic factors such as the source of the magmas or extreme magmatic differentiation. These alternative possibilities emphasize the necessity for petrographic observations to accompany interpretations made on the basis of chemistry alone. Samples that have undergone propylitic alteration are characterized by increased concentrations of CaO. Examples of rock with weak endoskarn alteration, those samples containing modal garnet in minor amounts, have lower A/CNK values than do unaltered rocks probably because of the increase in CaO. One sample containing epidote has a high value of A/CNK but most samples that contain this mineral are chemically similar to unaltered intrusive rock or rocks with weak endoskarn alteration.

Chemical Classification

Rock samples collected from the Ok Tedi Intrusive Complex have been divided into two categories based on texture and given names based on modal ratios of quartz, alkali feldspar, and plagioclase feldspar in an earlier chapter (Modal Classification). Samples with phaneritic texture were assigned plutonic names, whereas, samples with porphyritic texture and with aphanitic or aplitic groundmass were assigned volcanic names. This basic subdivision is also used in this chapter.

Several methods of classification of volcanic and plutonic rocks using chemical criteria have been put forth (e.g., Washington, 1918; Rittman, 1973; Le Maitre, 1976; Streckeisen, 1976; Le Bas and others, 1986). Two methods will be adopted in this chapter: (1) the Q'-ANOR method of Streckeisen and Le Maitre (1979) for rocks with phaneritic texture; and (2) the total alkali-silica method (TAS) of Le Bas and others (1986) and Le Maitre and others (1989) for rocks with porphyritic texture.

A discussion of the magma series to which the igneous rocks of the Star Mountains and the Ok Tedi Intrusive Complex belong follows the assignment of rock names to the petrographic samples. The igneous rock series is determined using the Peacock alkali lime index (Peacock, 1931). The effects of hydrothermal

alteration on the alkali oxide contents of altered samples are also considered in this section.

Q'-ANOR Method

Streckeisen and Le Maitre (1979) published a method for classification of igneous rocks designed to provide a nomenclature approximately equivalent to that of the modal QAPF (quartz-alkali feldspar-plagioclase-feldspathoid) diagram of the I.U.G.S. They used the method for classification of both volcanic and plutonic rocks even though their justification for the use of chemical criteria for naming igneous rocks applied mainly to volcanic rocks in which accurate determinations of the essential QAPF mineral phases could not be deduced because of fine grain size or the presence of volcanic glass. Their method is adapted here for classification of the igneous rocks of the Ok Tedi Intrusive Complex that have phaneritic texture. Only the portion of the diagram that includes quartz normative rocks is used herein because feldspathoid-bearing assemblages are not found at Ok Tedi.

The diagram used for this method of classification is based on normative mineralogy. Streckeisen and Le Maitre (1979) recommended the use of the Barth-Niggli molecular norm for calculation of Q (quartz), Ab (albite), An (anorthite), and Or(orthoclase). I used the CIPW norm because a computer program for calculation of the Barth-Niggli norm was unavailable, whereas such programs for the CIPW norm were readily available. Accordingly, these programs are likely to be used by

many students of igneous petrology and the results obtained will be readily compared with those of others. In addition, the CIPW norm is probably more commonly used outside of Europe than is the Barth-Niggli norm. Le Maitre (1976) notes that, fortunately, the difference between these two norms is negligible for most igneous rocks and of the same order of magnitude as errors involved in the chemical analyses.

The Q'-ANOR classification diagram is constructed by plotting values of Q' (Q/Q+Ab+An+Or) versus the ratio An/An+Or (ANOR) on a rectangular graph. The authors chose a rectangular graph rather than a triangular diagram to avoid confusion with the QAPF diagram of the I.U.G.S. Lines defining limits corresponding to the fields of the modal QAPF diagram are drawn based on information contained in a database of more than 2500 analyses of individual rocks, and of which many are accompanied by modal analyses. Streckeisen (1976) selected the ratio 100*(An/An+Or) based on the observation that Or decreases and An increases from granite to granodiorite and tonalite, from syenite to monzonite, diorite and gabbro, and from nepheline syenite to essexite and theralite.

The distribution of Q' and ANOR values in samples of volcanic and plutonic rocks from the Star Mountain region (Mason, 1975; Ayres and Bamford, 1976, revised 1987; and Arnold, Griffin, and Hodge, 1979) is portrayed in Figure 69. Unlike other sections of this chapter, a regression line is not calculated for

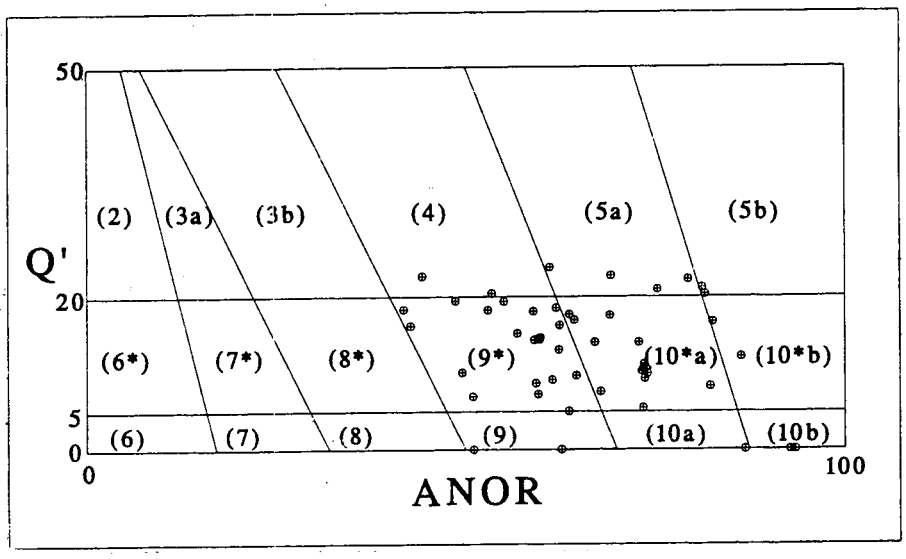

Figure 69: Q'-ANOR diagram for samples of volcanic and plutonic rocks (undifferentiated) from the Star Mountains region.

these values nor portrayed on the following diagrams because the regional data do not define a linear trend. Instead, they form a broad range in both Q' and ANOR. The samples occupy nine fields including 4, 5a, 5b, 9*, 10a*, 10b*, 9, 10a, and 10b.

Samples from the Sydney intrusion all contain modal pyroxene except for DDH 1-202.1 (Katchan, 1982), which has hornblende in its mode. All of these samples, except for DDH 342-141 plot in the field of quartz monzodiorite in Figure 70A). Sample DDH 342-141 plots in the field of monzonite, and is distinguished from the other samples from the Sydney Intrusion by having a minor amount of garnet in its mode.

The one sample from the area mapped as Fubilan Intrusion, DDH 401-218.5, is altered, contains neither pyroxene nor hornblende, and plots in the field of alkali-feldspar quartz syenite (Figure 70B).

Samples from the Kalgoorlie Intrusion occupy the fields of quartz monzonite, monzonite, alkali-feldspar quartz syenite, and alkali feldspar syenite (Figure 70C). All of the samples of Katchan (1982) contain either pyroxene, hornblende, or both. Two of my samples with phaneritic texture contain both pyroxene and hornblende and plot as (quartz) monzonite. Of the two samples that do not contain either of these minerals, one plots in the field of quartz monzonite and the other in the field of alkali-feldspar quartz syenite.

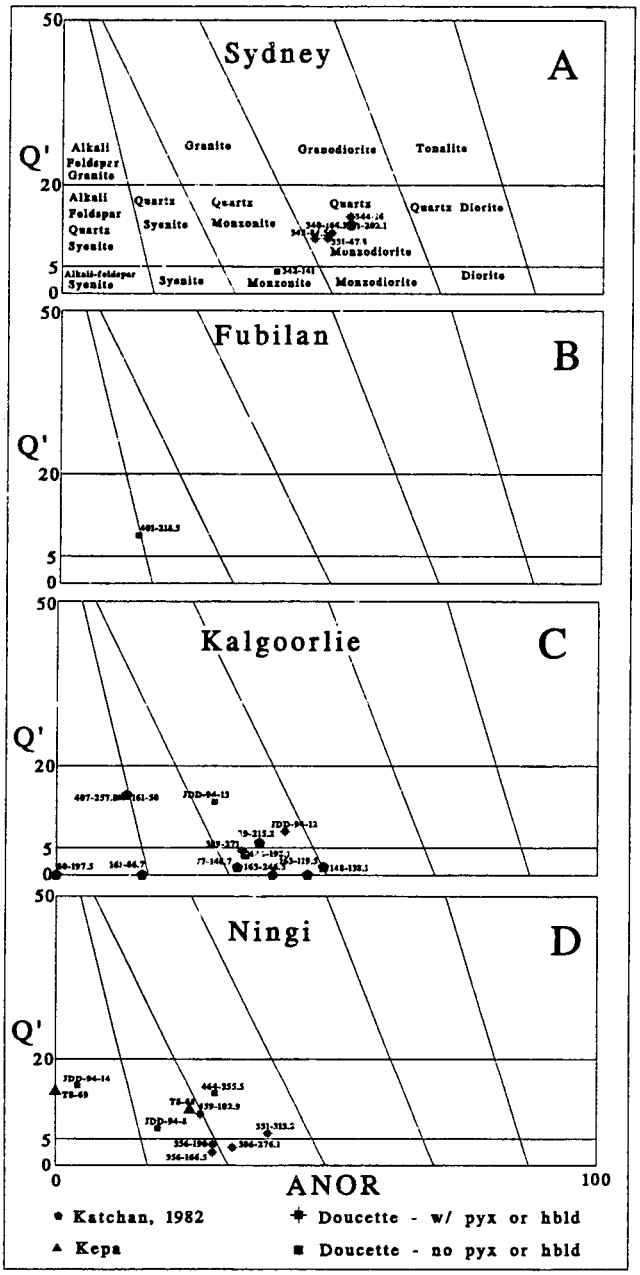

Figure 70: Q'-ANOR diagram for samples of phaneritic rocks from the Ok Tedi Intrusive Complex: (A) Sydney Intrusion, (B) Fubilan Intrusion, (C) Kalgoorlie Intrusion, (D) Ningi Intrusion.

Pyroxene and/or hornblende-bearing phanerites from the Ningi Intrusion fall in the fields of (quartz) monzonite and (quartz) syenite (Figure 70D). Samples of phanerite without these minerals fall in the fields of quartz monzonite, quartz syenite, and alkali-feldspar quartz syenite.

In summary, the least-altered rocks of the Sydney Intrusion according to the Q'/ANOR classification are quartz monzodiorites whereas similar rocks from the Kalgoorlie and Ningi intrusions are (quartz) monzonites. Altered samples from the Kalgoorlie and Ningi intrusions are classified as (quartz) syenites and (quartz) alkali-feldspar syenites.

Total Alkali-Silica Method

The total alkali-silica (TAS) method of classification was designed for use with volcanic rocks that cannot accurately be classified based on modal analyses because of fine grain size and/or the presence of glass (Le Bas and others, 1986; Le Maitre and others 1989). This problem is clearly relevant to samples with porphyritic texture from the Ok Tedi Intrusive Complex. They average about 40 volume percent aphanitic groundmass.

The binary TAS diagram includes 15 fields (see Figure 7). Two of these fields are further subdivided according to other chemical criteria giving a total of 17 root names. Three of the root names (trachybasalt, basaltic trachyandesite, and trachyandesite) are still further subdivided into two additional sub-root names based on the amount of Na_2O and K_2O contained in the rocks. The division of the field of

interest in relation to the rocks of the Ok Tedi Intrusive Complex. The sub-root names for basaltic trachyandesite and trachyandesite are shown in Figure 71A. The TAS diagram also carries information as to the degree of silica saturation of the volcanic rocks. Shand (1943) developed the concept of silica saturation. He divided igneous rocks into three different categories based on their SiO_2 content: (1) oversaturated rocks , containing modal quartz; (2) saturated rocks, containing only saturated minerals (feldspars, pyroxenes, amphiboles, micas, the iron-titanium oxide minerals, and several accessory minerals; and (3) undersaturated rocks, containing olivine, feldspathoids, and/or certain rare minerals. Le Bas and others (1986) assigned these groups to appropriate fields in Figure 71B where they are designated as $O_{1\text{-}3}$ (oversaturated), $S_{1\text{-}3}$ (saturated), or $U_{1\text{-}3}$ (undersaturated).

Le Bas and others (1986) and Le Maitre and others (1989) recommend that analyses with more than 2 weight percent H_2O^+ be considered with suspicion and that all analyses be recalculated to 100 percent free of H_2O and CO_2. They also suggested that the method was designed for unaltered volcanic rocks and should not be used for rocks that have "suffered" metasomatism. I choose to use the classification for both altered and unaltered samples and justify this misuse of the method as a means by which to demonstrate the effects of potassium metasomatism on the altered rocks of Ok Tedi.

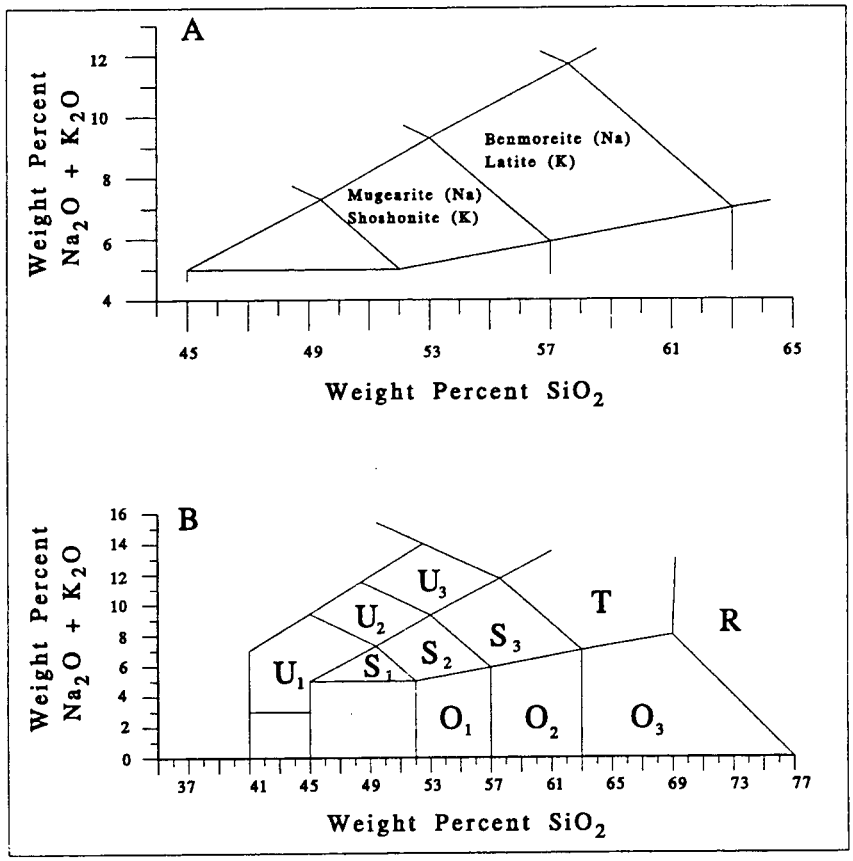

Figure 71: Total alkali-silica diagram: (A) Shows the subdivision of the root names basaltic trachyandesite and trachyandesite, (B) shows the designation of fields as silica-oversaturated (O), saturated (S), and undersaturated (U).

All samples of volcanic and plutonic rocks from the Star Mountains region (Mason, 1975; Ayres and Bamford, 1977; and Griffith, Arnold, and Hodge, 1979) are portrayed on a TAS diagram in Figure 72. These data are used to calculate a regional trend line (a-a') with which the samples from Ok Tedi can be compared. This trend line lies just below the boundary separating silica-oversaturated from silica-saturated rocks. The intrusive rocks of the Star Mountains region are, therefore, slightly oversaturated.

Total alkali-silica diagrams are given for samples of porphyry from the four units of the Ok Tedi Intrusive Complex in Figure 73. Also shown on each diagram is the trend line calculated from the volcanic and plutonic rocks of the Star Mountains Region. The samples from Ok Tedi Intrusive Complex, whether altered or unaltered, fall in fields of silica-saturated rock.

The only sample with porphyritic texture that comes from the area of the Sydney Intrusion is unaltered and occupies the field of trachyandesite (Figure 73A).

All but two of the samples from the Fubilan Intrusion that have not been contaminated by quartz veinlets occupy the field of trachyte (Figure 73B). Those samples that have been contaminated by quartz veinlets fall in the field of rhyolite indicating a general increase in the amount of SiO_2; the sum of Na_2O and K_2O decreases with increasing amounts of quartz as veinlets and as metasomatic replacements until nearly zero where the rocks consist essentially of monomineralic quartz.

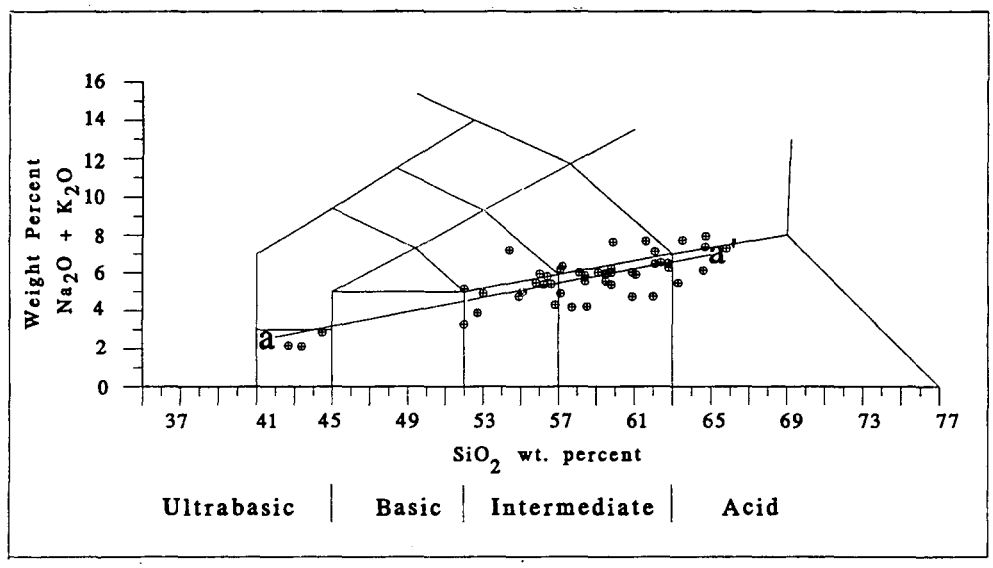

Fig 72: Total alkali-silica diagram with data from volcanic and plutonic rocks of the Star Mountains region. Also shown is a trend line (a-a') calculated from this data.

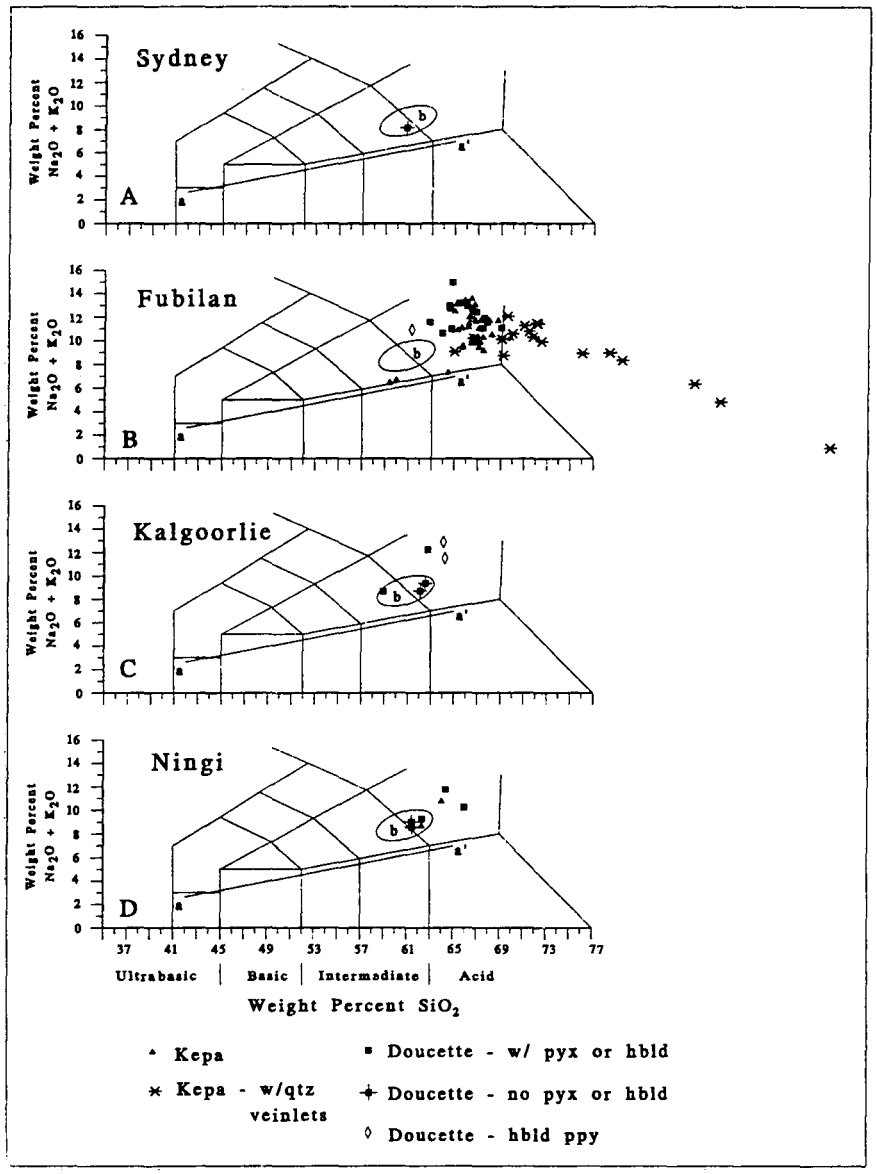

Figure 73: Total alkali-silica diagrams for the Ok Tedi Intrusive Complex. Each diagram also has the trend line (a-a') calculated from all volcanic and plutonic rocks of the Star Mountains region and an elliptical area (b) occupied by data from the least-altered samples.

The least-altered rock samples from the Kalgoorlie Intrusion plot within the field of trachyte near the boundary with trachyandesite (Figure 73C). The more intensely altered samples are centrally located in the field of trachyte. Samples from the Ningi Intrusion (Figure 73D) are similar in composition to those of the Kalgoorlie Intrusion.

In summary, the least-altered porphyries from the Ok Tedi Intrusive Complex plot adjacent to the boundary between trachyandesite and trachyte. The region occupied by these samples is shown as an ellipse in Figure 73 (b). Using the criterion that trachyandesites with Na_2O-2<K_2O are called latite, those samples that plot within field S_3 (Figure 71B) are, therefore, latites. Altered rocks plot in field T and have less than 20 normative percent of quartz in QAP; they are therefore, classified as trachytes. The overall effect of potassic metasomatism has been to increase the SiO_2 and Na_2O+K_2O contents of altered rocks relative to their unaltered equivalents. Samples from the Star Mountains region are slightly oversaturated in silica whereas those from the Ok Tedi Intrusive Complex are saturated. The classification of the samples from the Ok Tedi Intrusive complex is not consistent with the modal analyses of unaltered phaneritic rocks which contain up to nine percent quartz. This may be explained as a remnant of the fact that the assignment of the boundary between saturated and undersaturated rocks is on the basis of the amount of feldspathoids in rocks, whereas the assignment of the boundary between the saturated and oversaturated rocks is on the basis of a density minimum between

volcanics rock series that are alkaline and those that are calc-alkaline (LeMaitre, 1989). However, this inconsistency remains troubling.

Igneous Rock Series

Suites of compositionally different volcanic and plutonic rocks that are commonly associated in space and time have been grouped into igneous rock series (e.g., Peacock, 1931; Irvine and Baragar, 1971; Lamayre and Bowden, 1982; Batchelor and Bowden, 1985; Keith and others, 1991). These series are believed to be related by common source (the crust and mantle regions that were melted to produce magma), common process (anhydrous or hydrous melting, fractional crystallization, or magma mixing), and/or common tectonic environment (orogenic, post-orogenic, or anorogenic).

The alkali-lime index was introduced by Peacock (1931) to address the problem of fitting igneous rock series into the two groups, "alkalic and subalkalic (calc-alkalic, calcic)," that had long been recognized (Harker, 1909; Tyrrell, 1926). Peacock's method of classification distinguishes four igneous rock series (alkalic, alkali-calcic, calc-alkalic, and calcic.) The rock series to which a suite of igneous rocks is assigned is determined from a binary variation diagram in which values of CaO and the sum of the alkali oxides (Na_2O+K_2O) are plotted as ordinates against SiO_2. The point on the abscissa at which these curves cross determines the rock series. This type of diagram has been called the Peacock diagram and the SiO_2

value where CaO is equal to the sum of the alkali oxides is the alkali-lime index. The boundaries between the four rock series were determined by examination of mineral assemblages in naturally occurring suites of rocks. For example the boundary between alkalic and alkali calcic fields was chosen to represent the silica value at which feldspathoids cease to appear in appreciable amounts. The boundary between alkali-calcic and calc-alkalic series was chosen to divide two groups of igneous rocks that Peacock had studied in Iceland. His Iceland C suite (trachybasalt, trachyandesite, trachyte, trachyrhyolite) was the basis of alkali-calcic suite, whereas his Iceland B suite (olivine-basalt, quartz-hornblende diorite, hornblende granodiorite, granophyre, granite, aplite) was the basis of the calc-alkalic suite.

Peacock diagrams for the Star Mountains region and the least altered samples from each of the intrusions at Ok Tedi, except the Fubilan Intrusion, are given in Figure 74. Samples from the Fubilan Intrusion are not portrayed because none are considered to be sufficiently unaltered. The CaO and Na_2O+K_2O values for the Star Mountains region form continuous trends from about 50 to 65 percent SiO_2. Regression lines calculated from this data cross at 59.3 weight percent SiO_2. This suite of samples, therefore, has an alkali-lime index of 59.3 and is assigned to calc-alkalic igneous rock series according to the method of Peacock.

Samples of unaltered rock from the Ok Tedi intrusions are restricted in number and form loose clusters rather than linear (or curvilinear) trends. This

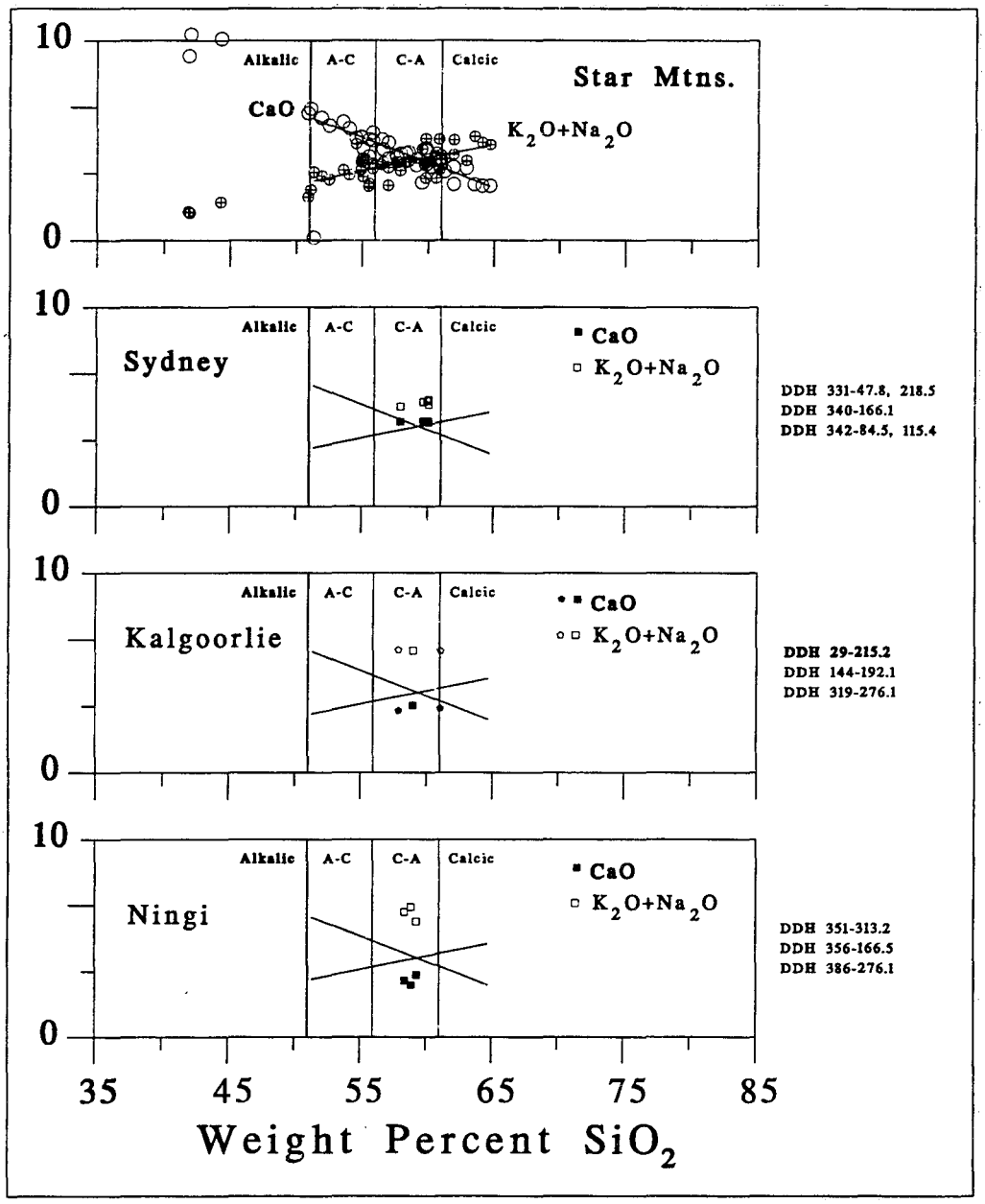

Figure 74: Peacock diagrams for data from: (A) Star Mountains region, (B) Sydney Intrusion, (C) Kalgoorlie Intrusion, and (D) Ningi Intrusion.

behavior is to be expected because the samples come from individual intrusions and igneous rock series are defined on the basis of suites of volcanic or plutonic rocks not on the basis of individual plutons or stocks. Nonetheless, it can be seen in Figure 74 that CaO values from the Sydney intrusion fall near to the regression lines defined by the regional data and that those from the Kalgoorlie and Ningi Intrusions are farther away from the regional values. Na_2O+K_2O values of unaltered rock from the three Ok Tedi intrusions are distinctly higher than those of the other igneous rocks of the Star Mountains. The Peacock diagram can be used to dramatically illustrate the effects of hydrothermal alteration. Samples from all of the intrusions at Ok Tedi are subdivided into four categories based on the An percent of their normative plagioclase feldspar in Figure 75. These four categories are considered to form a spectrum between unaltered (An > 30) and extremely altered rock (An < 5). The CaO and Na_2O+K_2O contents of many of the least-altered rocks plot near to the regression lines for the spatially adjacent igneous rocks of the Star Mountains. With a decrease in normative anorthite content (corresponding to an increase in alteration), CaO becomes progressively lower in value while the sum of Na_2O and K_2O increases. The increase in alkali oxides is accompanied by higher values of SiO_2. Samples with the lowest anorthite content ($<An_5$) have CaO values that approach zero while the sum of Na_2O and K_2O increases to greater than 10 weight percent and SiO_2 increases to approximately 70 percent.

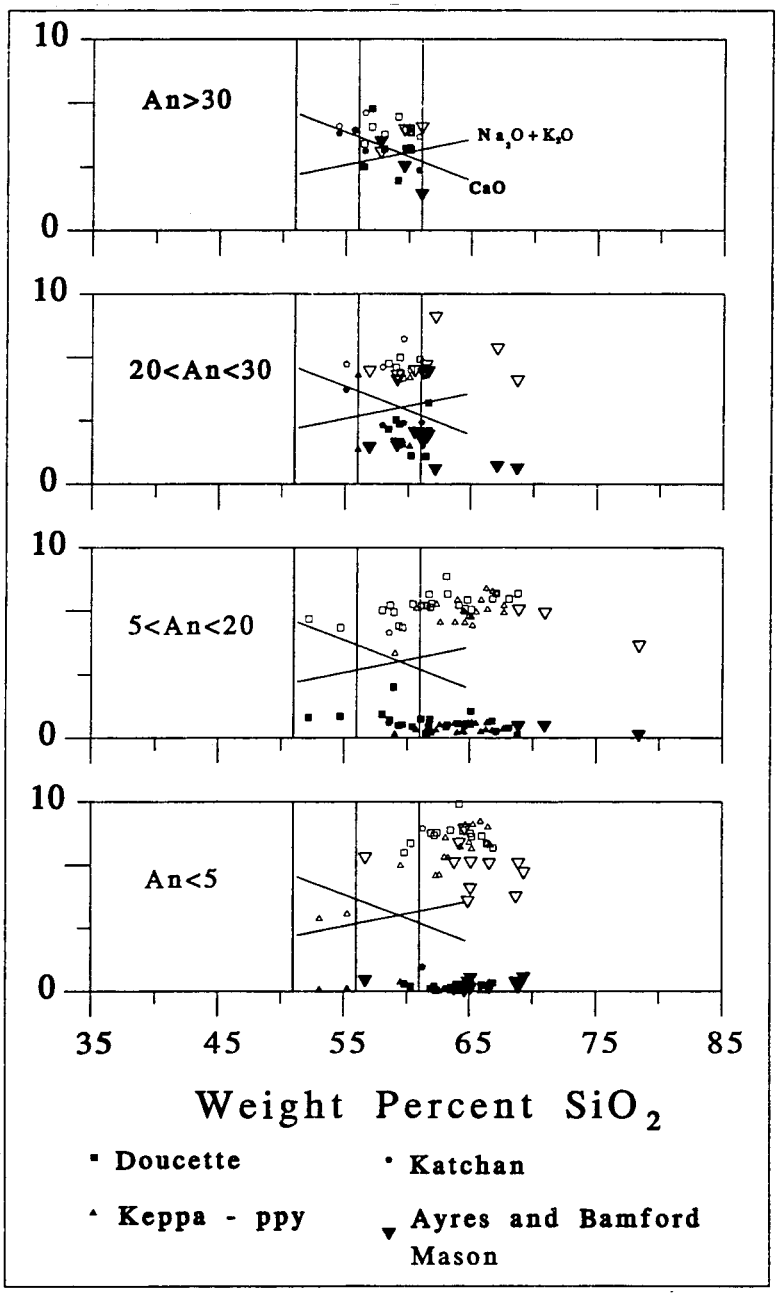

Figure 75: Peacock diagrams showing data for altered and unaltered samples from the Ok Tedi Intrusive Complex: (A) unaltered and least-altered, (B and C) intermediate alteration, and (D) extremely altered.

Irvine and Baragar (1971) present an alternative method of chemical classification for volcanic rocks. They divide the volcanic rocks into three groups based on chemistry: (1) subalkaline, (2) alkaline, and (3) peralkaline. The subalkaline category is subdivided into a tholeiitic basalt series and a calc-alkalic series; the alkaline category is subdivided into an alkali olivine basalt series and a group consisting of nephelinic, leucitic, and analcitic rocks. These authors present a five-step method of classification. Their first step is to determine whether a rock is peralkaline. The second step is to classify as subalkaline or alkaline using a binary plot of SiO_2 versus the sum of the alkali oxides. The third step is to determine whether subalkalic rocks are tholeiitic or calc-alkaline using the AFM ternary diagram ($A=Na_2O+K_2O$, $F=FeO^*$, and $M=MgO$) and to further classify as potassium-rich, average, or potassium-poor. The forth step is used to subdivide the alkalic category. The fifth step is to compare chemical analyses against appropriate samples from the literature and to check the results against the rock's petrographic character.

Samples of igneous rocks from the Star Mountains region and least-altered rocks from the Ok Tedi Intrusive complex are presented on the alkaline versus subalkaline classification diagram used in step two of Irvine and Baragar's classification scheme in Figure 76. The samples from the Star Mountains region are overwhelmingly subalkaline (Figure 76A) whereas those from the Sydney Intrusion (Figure 76B) fall along the boundary between subalkaline and alkaline

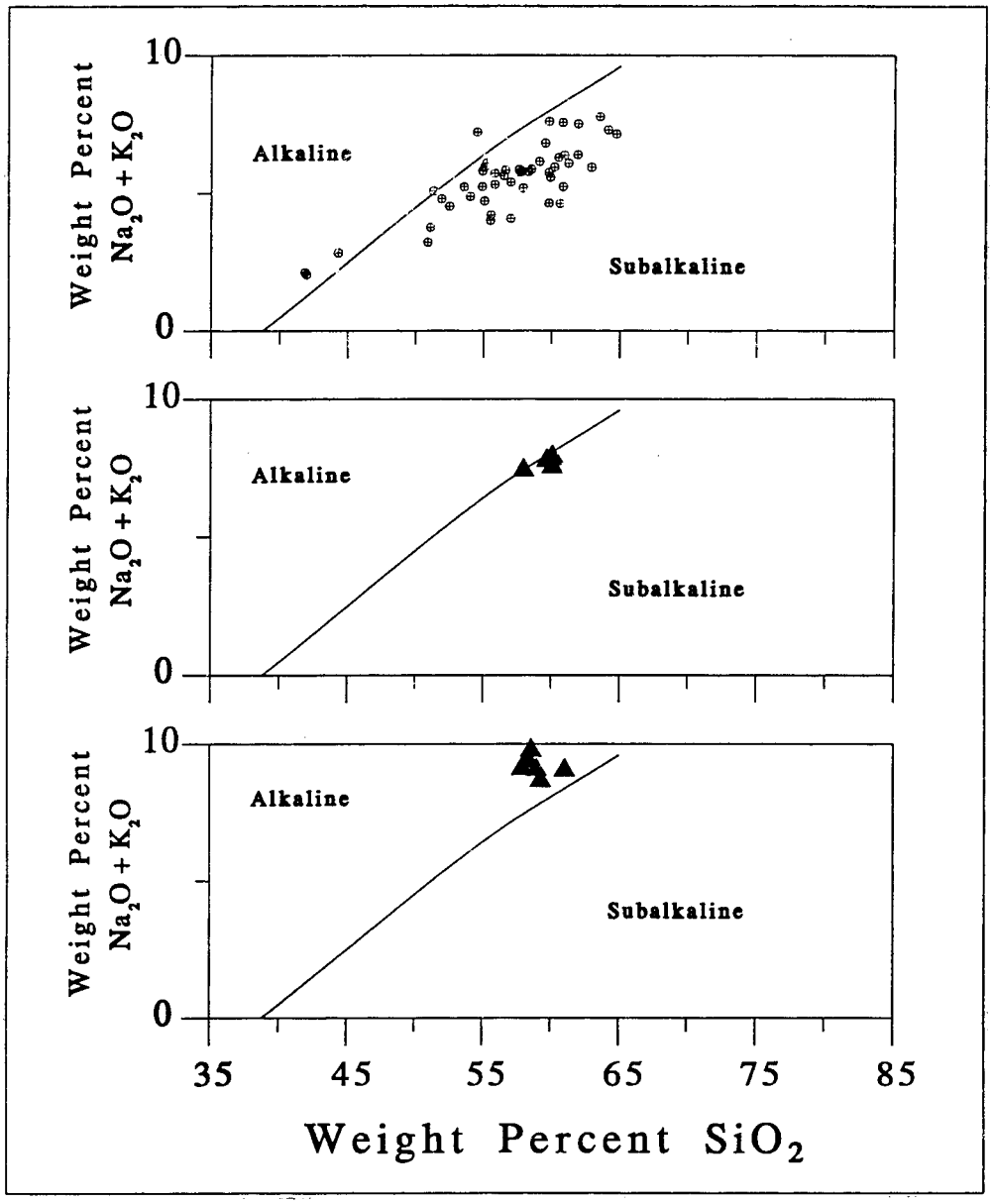

Figure 76: Irvine and Baragar classification diagram for alkaline and subalkaline volcanic rocks: (A) samples from Star Mountains region, (B) samples from Sydney Intrusion, and (C) samples from Kalgoorlie and Ningi Intrusions.

and those from the Kalgoorlie and Ningi Intrusions plot as alkaline. This same group of samples is plotted on AFM diagrams (step 3a of Irvine and Baragar's classification scheme) in Figure 77. All but a few of the samples from the Star Mountains region (Figure 77A) fall in the calc-alkaline field as do all of the unaltered rocks from the Sydney (Figure 77B), Kalgoorlie and Ningi (Figure 77C) Intrusions. A set of binary diagrams with fields for high, medium, and low potassium volcanic rocks (Le Maitre, 1989) is given as Figure 78. It can be seen from these diagrams that the samples from the Star Mountains region (Figure 78A) have medium to high K_2O and that all of the unaltered samples from the Ok Tedi Intrusive complex (Figures 78B and C) are high-K.

In summary, the unaltered igneous rocks of the Star Mountains regions are calc-alkaline by the classification methods of Peacock (1931) and Irvine and Baragar (1971). The samples range in composition from basalt to andesite (Figure 78A) and a few samples are as silicic as dacite and rhyolite. Those that have SiO_2 content between 57 and 68 weight percent can be termed high-K andesites. The least-altered samples from the Sydney, Kalgoorlie, and Ningi Intrusions differ from those of the remainder of the Star Mountains because they form clusters on Harker and Peacock alkali-lime diagrams rather than trends and by having consistently higher total alkalies and lower CaO. They may be part of the Star Mountains calc-alkaline series but they could also be related to a completely unrelated, and possibly alkali-calcic, suite of volcanic and plutonic rocks.

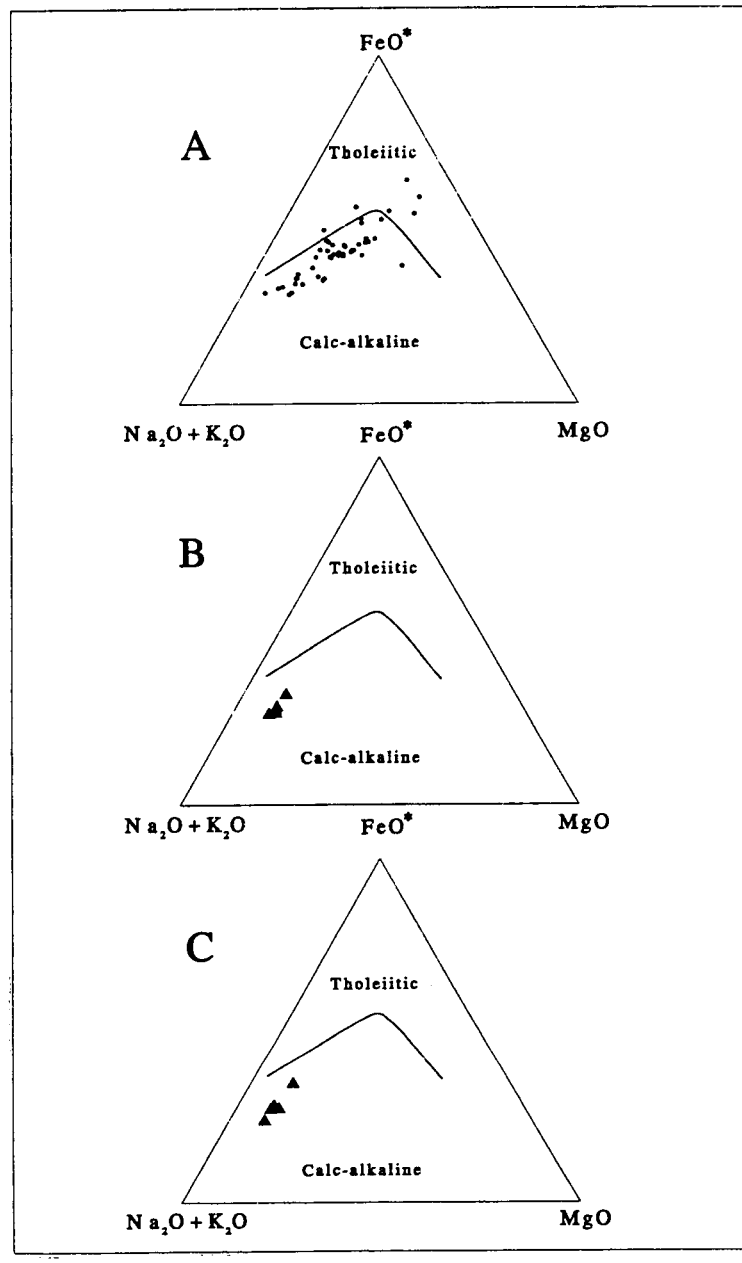

Figure 77: AFM diagrams with unaltered samples from: A. Star Mountains region, B. Sydney Intrusion, and C. Kalgoorlie and Ningi Intrusions. Also shown in each diagram is the curve used by Irvine and Baragar (1971) to separate fields of calc-alkaline from tholeiitic rocks.

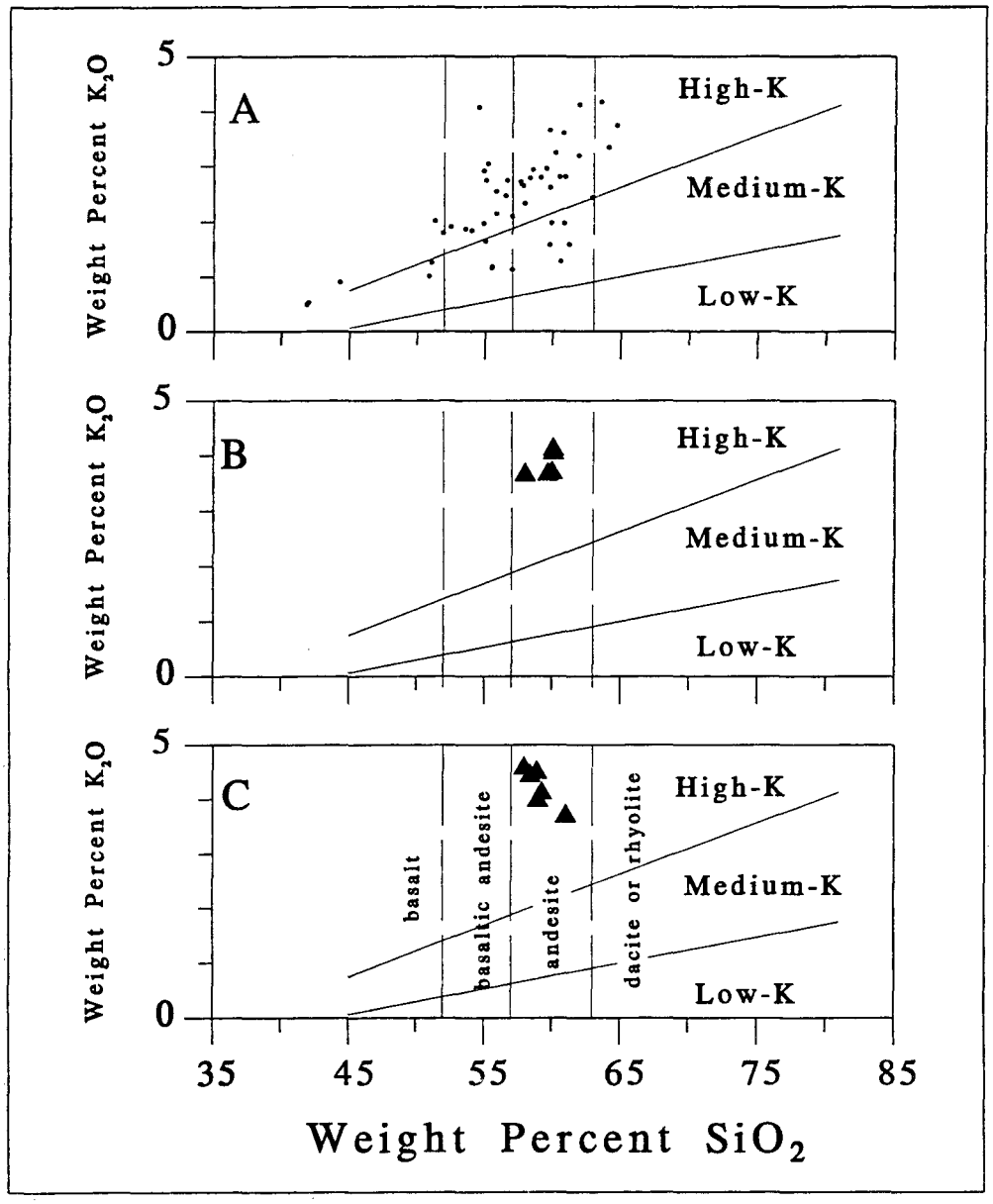

Figure 78: Binary plot of K_2O versus SiO_2 with fields of high, medium and low potassium volcanic rocks (LeMaitre, 1989). A. Star Mountains region, B. Sydney Intrusion, C. Kalgoorlie and Ningi Intrusions.

Iron Content and Oxidation State

The oxidation state of the rocks at Ok Tedi and of the magmas that crystallized to form these rocks are estimated in this section by reference to chemical analyses and to the presence of specific minerals in the modes of the rock samples.

Igneous rocks can be categorized as iron-poor or iron-rich by the ratio of their iron to magnesium oxide contents (Keith and others, 1991). These authors suggest that the amount of iron in a magma is more a function of the method by which a region of the crust or mantle is melted than a function of the composition of the source region. They attribute iron-poor magmas to hydrous melting and iron-rich magmas to adiabatic or thermal melting under anhydrous conditions. This topic will not be considered in detail in this dissertation, nonetheless, one of their diagrams is useful in characterizing the chemistry of the Ok Tedi intrusions. The iron contents of volcanic and plutonic rocks from the Star Mountains region are portrayed in Figure 79A, a binary plot on which the ratios of total iron (FeO^*) to MgO are plotted versus SiO_2 content. Curves drawn on this diagram separate fields of strongly iron-rich, moderately iron-rich, weakly iron-rich, moderately iron-poor, and strongly iron-poor rocks. Most samples from the Star Mountains plot near the boundary between weakly iron-rich and moderately iron-poor igneous rocks. Samples from the Ok Tedi Intrusive Complex are shown in Figure 79B using symbols that provide information on their texture and normative ferromagnesian

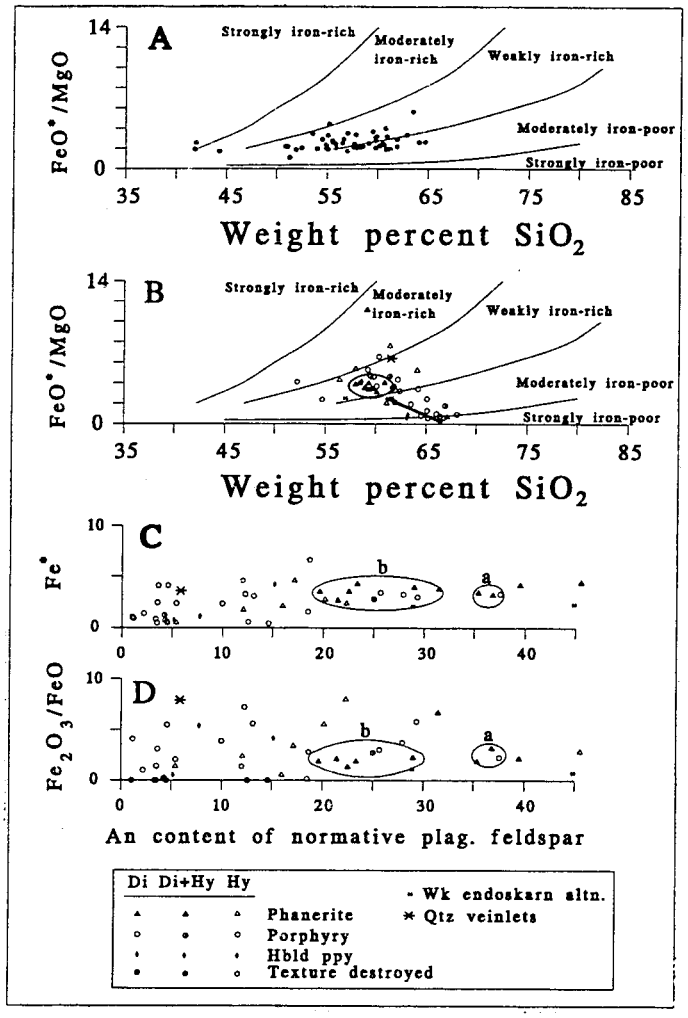

Figure 79: Diagrams illustrating the iron content and the ratio of ferric to ferrous iron in rocks of the Ok Tedi Intrusive Complex: (A) Plot of FeO^*/MgO versus SiO_2 for igneous rocks of the Star Mountains region (modified from Keith and others, 1991), (B) FeO^*/MgO versus SiO_2 for intrusive rocks of the Ok Tedi Intrusive Complex, (C) Total iron as Fe^* versus An content of normative plagioclase feldspar for rocks of the Ok Tedi Intrusive complex, (D) Plot of the ratio of ferric to ferrous iron versus An content of normative plagioclase feldspar for intrusive rocks of the Ok Tedi Intrusive complex. Ellipses a and b in C and D represent samples with normative andesine (a)or oligoclase (b).

mineral content. Most of those samples with diopside or diopside and hypersthene in their norms, the least-altered samples, fall in the field of weakly iron-rich rocks (area mineral content. Most of those samples with diopside or diopside and hypersthene in their norms, the least-altered samples, fall in the field of weakly iron-rich rocks (area enclosed by an ellipse in Figure 79B). Most of those with hypersthene as the only normative ferromagnesian mineral and with albite (or oligoclase) as their normative plagioclase feldspar, the potassically-altered rocks, are weakly iron-rich to strongly iron-poor (that is they are displaced in the direction of the arrow shown in Figure 79B). A few of the samples are moderately iron-rich; these have either andesine or oligoclase as their normative plagioclase feldspar. The deviation of iron content in altered rocks from the values of their unaltered equivalents can be attributed to redistribution of the metal during hydrothermal alteration and to dilution by increased SiO_2 and K_2O contents.

Two additional diagrams illustrating the iron content and the oxidation state of iron in rocks of the Ok Tedi Intrusive Complex are given in Figures 79C and D. Values of total iron (as Fe) are plotted against normative An content in Figure 79C. The three least-altered samples (areas a and b in Figure 79C) have similar total iron (about 3.25 percent). Total iron content remains approximately constant in almost all samples with anorthite content greater than about An_{20} and with normative diopside or with both diopside and hypersthene. The variance of the iron content of these samples is relatively low. Samples with normative

anorthite lower than An_{20} and with hypersthene as the only normative ferromagnesian mineral are much more variable in iron content.

A plot of Fe_2O_3/FeO versus normative anorthite is given in Figure 79D. The ferric/ferrous ratios of samples with normative diopside and with andesine as the normative plagioclase feldspar are close to 2.6. This ratio is somewhat lower (~2.3) in samples with normative diopside and hypersthene and with oligoclase as the normative plagioclase feldspar. The variance in the ferric/ferrous iron ratio is relatively high in samples with anorthite content below about An_{20} and with hypersthene as the only normative ferromagnesian mineral. The increased variance of Fe^* and Fe_2O_3/FeO at low anorthite contents also reflects the redistribution of iron and the dilution of the iron content by additions of SiO_2 and K_2O resulting from the metasomatic effects imposed on the rocks that have undergone potassic alteration.

Oxygen fugacity at the time of crystallization of the igneous rocks cannot be directly evaluated from the ferric/ferrous iron ratio of rock samples (Hall, 1996) because this ratio is dependant on bulk composition and is also affected by constituents other than iron and oxygen (Sack and Carmichael, 1980; Dickenson and Hess, 1986). Further, this ratio can be affected by subsolidus processes such as weathering which is usually an oxidation process and that generally leads to an increase in the ratio of ferric to ferrous iron. Instead, the presence of specific oxide or ferromagnesian silicate mineral assemblages are considered to more accurately

reflect the oxidation state of the magmas which form igneous rocks than is the ratio of ferric to ferrous iron. The minerals (or mineral assemblages) that define the oxidation state of magmas are called *buffers* after their use in experimental petrology to control oxygen fugacities. The most common minerals used as buffers in petrologic experiments are hematite, magnetite, and wustite. These minerals are considered to define the range of oxygen fugacity at which magmas form because the majority of magmas are not sufficiently oxygen-deficient to contain wustite and not sufficiently oxygen-rich as to contain hematite (Hall, 1996). The stability relations of wustite, magnetite, and hematite are shown in Figure 80, which is modified from Buddington and Lindsley (1964). The reaction boundaries between quartz +magnetite and fayalite (Buddington and Lindsley, 1964) and between quartz + magnetite + sphene and ilmenite + hedenbergite (Dilles, 1987) are also given in Figure 80. These reactions are useful in constraining the oxygen fugacity of magmas that formed under conditions between the magnetite-hematite and magnetite-wustite boundary curves. The assemblage quartz + magnetite + sphene is common in unaltered samples with plutonic and volcanic textures from the Ok Tedi Intrusive Complex, and this assemblage defines the magmas from which these rocks were formed as relatively oxidized (Dilles, 1987; Wones, 1989).

Several of the minerals that are present in the massive ores and skarns at Ok Tedi reinforce the hypothesis that the intrusive and hydrothermal processes that formed the ore deposit were oxidizing in character. Epidote and andradite are

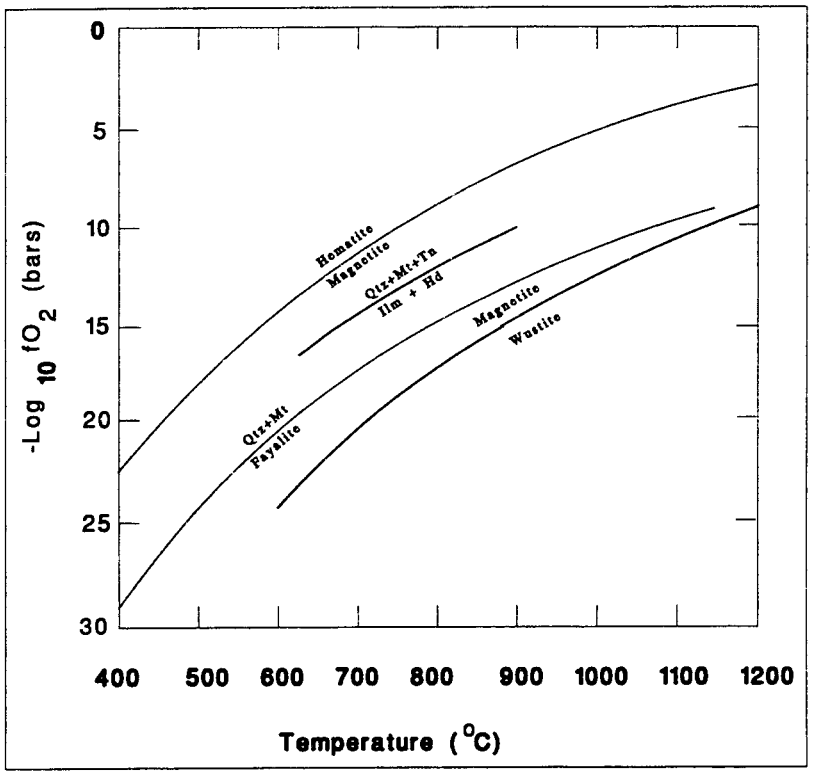

$$6\ Fe_2O_3 \rightleftharpoons 4\ Fe_3O_4 + O_2$$

hematite ⇌ magnetite + oxygen

$$3\ CaTiSiO_5 + 2\ Fe_3O_4 + 3\ SiO_2 \rightleftharpoons 3CaFeSi_2O_6 + 3\ FeTiO_3 + O_2$$

sphene + magnetite +quartz ⇌ hedenbergite + ilmenite + oxygen

$$2\ Fe_3O_4 + 3\ SiO_2 \rightleftharpoons 3\ Fe_2SiO_4 + O_2$$

magnetite + quartz ⇌ fayalite + oxygen

$$2\ Fe_3O_4 \rightleftharpoons 6\ FeO + O_2$$

magnetite ⇌ wustite + oxygen

Figure 80: Plot of log f_{O2} versus temperature for mineral assemblages commonly used as oxygen buffers in petrologic experiments. The equations for these reactions are also listed above. (Modified from Buddington and Lindsley, 1964; and Dilles, 1987).

minerals enriched in ferric iron and these are common in the endoskarns (and exoskarns?) at Ok Tedi. In addition magnetite, a relatively oxidized mineral, is the most abundant mineral in most of the massive ores.

The ratio of ferric to ferrous iron oxide can have a powerful influence on the nature and abundance of the normative minerals calculated for igneous rocks (Middlemost, 1989). Various authors have suggested different methods of assigning this ratio. Le Bas and others (1986) proposed that the Fe_2O_3/FeO ratio should be "taken as that assigned by the analyst." However, in chemical analyses where both oxides have not been determined as is commonly the case, they recommended that a method supplied by Le Maitre (1976) should be used to determine the ratio. Briefly, this method consists of adjusting the ratio of FeO to Fe_2O_3 to equal 0.93 - 0.0042 SiO_2 - 0.022 (Na_2O+ K_2O) for volcanic rocks and 0.88 - 0.0016 SiO_2 - 0.027 (Na_2O + K_2O) for plutonic rocks. Irvine and Baragar (1971) have suggested that the value of Fe_2O_3 should have an upper limit equal to the content of TiO_2 + 1.5 weight percent. Middlemost (1989) proposed a set of standard Fe_2O_3/FeO ratios for different volcanic rocks that he thought should be applicable to all normative mineral calculations (for example andesite and trachyandesite would be assigned the value of 0.35).

The normative minerals listed in Appendix 12 and the figures herein that are based on these minerals were calculated using the values of Fe_2O_3 and FeO that were supplied by Chemex Laboratories. Values for this ratio provided by direct

chemical analyses for these iron oxides obtained in this study range from 0 to 8.6. However, calculations were also performed on several samples of least-altered rock using the ratio suggested by Middlemost (0.35). The principal effects of changing the iron ratio are as follows: (1) normative diopside, magnetite, quartz, and apatite become lower in abundance, (2) hematite and wollastonite are eliminated from the norm, and (3) hypersthene increases in abundance. The normative feldspars (An, Ab, and Or) are virtually unchanged in abundance. Although hematite has not been recognized in microscopic or microprobe analyses and in spite of the fact that the abundance of apatite in the norms that were calculated using standardized iron ratios more closely match the modal abundances of this mineral, these changes are considered objectionable because of their effect on normative pyroxene. Decreasing the diopside and wollastonite components in favor of an increase in hypersthene content would be particularly misleading because the pyroxene in unaltered Ok Tedi intrusive rock is, in fact, diopside as predicted from the normative mineralogy and because the composition of the pyroxene is an important factor in the characterization of the intrusions at Ok Tedi. In addition, the use of a standard value for the ratio of ferric to ferrous iron would camouflage the oxidized nature of the igneous rocks at Ok Tedi.

Volatiles

Chemical analyses were carried out to determine the concentrations of water (H_2O^+ and H_2O^-), sulfur, and fluorine in all samples that I collected in 1994. These same samples were also analyzed for LOI (loss on ignition) which measures the change in weight of samples before and after heating in a furnace for one hour at 1010° C to drive off volatiles. Ideally, the value determined for LOI should equal the sum of the volatile constituents in a rock sample or should exceed this value if all contained volatile components were not analyzed. A plot of LOI versus $H_2O^+ + H_2O^- + S + F$ is given in Figure 81. A strong correlation exists between these variables ($r = 0.892$) but LOI values are lower than those of the sum of $H_2O^+ + H_2O^- + S + F$ for most samples. This is particularly true at higher values of LOI and total volatiles, and this discrepancy indicates that LOI underestimates the volatiles present in many of the rock samples. The inverse is true for many samples with low amounts of the volatile constituents. This effect is probably a result of weak propylitic alteration of these samples that includes trace to minor quantities of calcite and for which analyses of CO_2 were not performed.

The amount of H_2O^- (surficial moisture) in the intrusive rocks from Ok Tedi ranges from 0.03 to 1.43 weight percent with an average of 0.34. H_2O^+, which exists in mineral lattices as the H^+ or OH^- ion and which is referred to as *water of crystallizaion*, ranges from 0.1 to 3.23 weight percent and averages 0.73. The amount of H_2O^+ in the least-altered rocks from the Sydney, Kalgoorlie, and Ningi

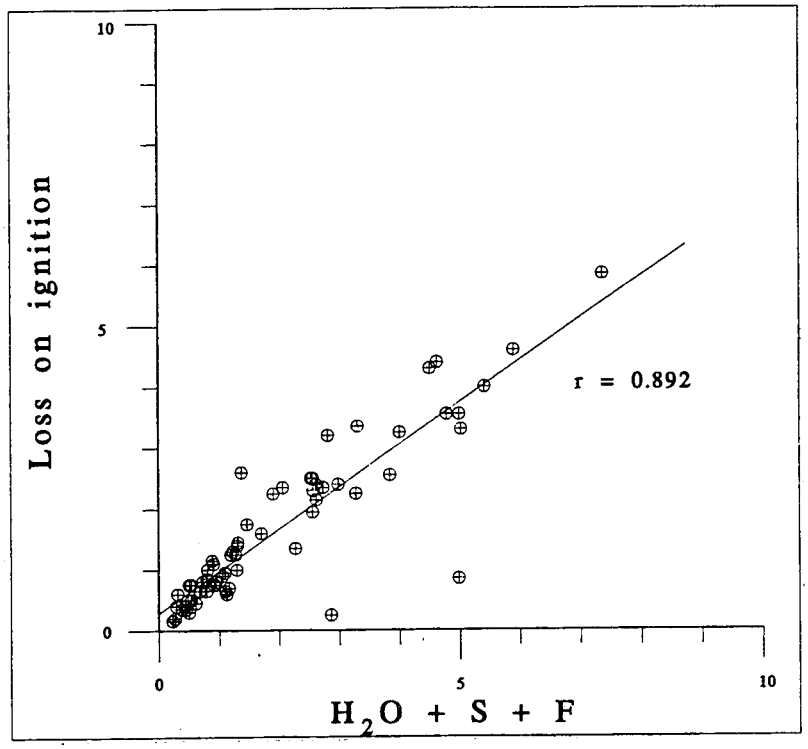

Figure 81: Plot of LOI (loss on ignition) versus the sum of the volatile phases H_2O, S, and F.

intrusions is less than 0.4 weight percent. Elevated H_2O^+ contents in some samples of the highly-altered host rocks reflect the presence of relatively abundant hydrothermal micas and clays.

The sulfur content of the least-altered rocks of the Ok Tedi Intrusive Complex is generally less than 0.05 weight percent. A few samples that show little or no hydrothermal alteration are nonetheless crosscut by pyrite veinlets and these samples have elevated sulfur contents. The average sulfur content in more than 2600 samples from the strongly mineralized Fubilan Intrusion is 1.14 weight percent. The locations of the reverse-circulation rotary drill holes from which these samples were collected are given in Figure 56. A plot illustrating the range of sulfur values versus SiO_2 is given in Figure 82. The sulfur content of these samples varies from less than the limit of detection (0.01) to 10 weight percent. Relatively high sulfur values (greater than about .5 weight percent) are present throughout the range of silica contents but the highest values are in samples with about 65 weight percent SiO_2.

Analyses of fluorine in samples from the Ok Tedi Intrusive Complex range from a low of 240 ppm to 7100 ppm. The lowest values are in the least-altered rocks and those highly altered samples that contain little if any hydrothermal biotite, such as DDH 302-69. A map illustrating the distribution of fluorine values at Ok Tedi is given as Figure 83. Samples from the Sydney Intrusion contain

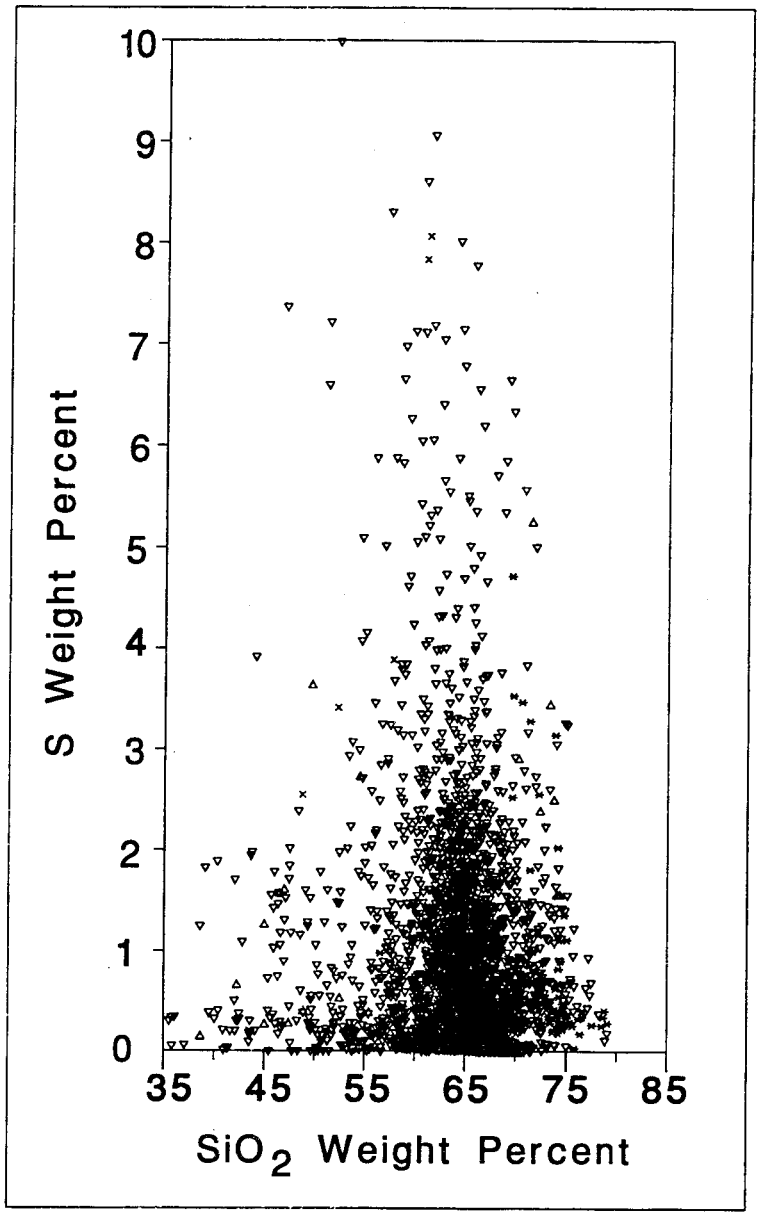

Figure 82: Plot of S versus SiO_2 for samples from reverse-circulation drill holes.

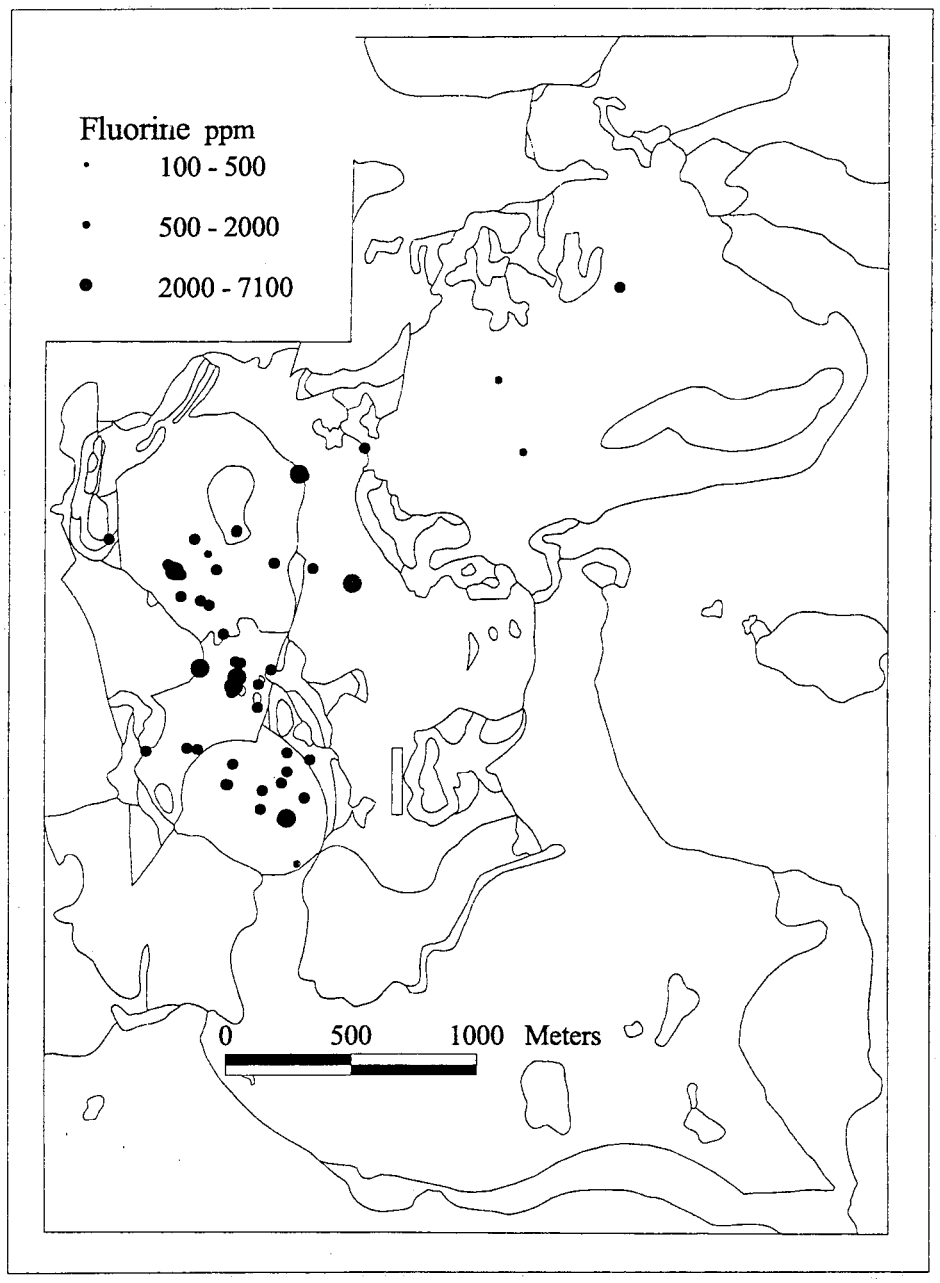

Figure 83: Map showing the distribution of fluorine values in the intrusive rocks of the Ok Tedi Intrusive Complex.

relatively low levels of fluorine. Those from the Kalgoorlie and Ningi Intrusions contain both high and low values, reflecting the variable distribution of hydrothermal alteration in these areas. All but one sample from the Fubilan Intrusion contain moderate to high concentrations of fluorine. The distribution of fluorine values in Figure 83 clearly suggests that enrichment of this volatile element is an important factor in hydrothermal alteration and ore deposition at Ok Tedi.

Trace Elements

The contents of selected trace and minor elements are discussed in this section. Rare earth element abundances of the least altered samples from the Ok Tedi Intrusive Complex are compared to samples from similar rocks from the Papua New Guinea area and to altered igneous rocks from Ok Tedi. Rubidium and strontium contents of unaltered and potassically altered rocks are contrasted.

Rare Earth Elements (REE)

Petrographic studies that include rare earth element determinations typically include *Masuda-Coryell* diagrams for interpretation of the data (Masuda, 1962; Coryell and others, 1963). Such diagrams are constructed by dividing the REE abundances of the samples being studied by the values of the same elements in a reference standard which is external to, or part of, the system under consideration (Henderson, 1984), and by plotting the logs of these results against the atomic

number (or more generally by element name). The process is known as *normalization* and the most common reference standard uses average values of REE in chondritic meteorites. Chondritic meteorites are chosen because they are believed to be similar in chemical composition to the primitive earth. Chondritic meteorites are not believed to show fractionation among the REE. Therefore, any variations from horizontal trends on diagrams using chondrite-normalized data can be considered to represent fractionation of the REE in the petrographic system under examination. In addition, abundance variations between elements with odd and even atomic numbers are eliminated by normalization thus smoothing the sawtooth-shaped curves that would otherwise be obtained. Normalizing factors used by a number of different researchers are listed in Table 19. The values used in NEWPET (Clarke, unpublished) are used herein. The values of Clarke are identical to those of Nakamura (1974) except for Pr, Tb, Ho, and Tm which do not appear in the Nakamura tabulation.

Johnson (1982) has described the chemical characteristics of andesites from Papua New Guinea and has included a figure with chondrite-normalized REE patterns of samples gathered from 10 locations where andesites had been identified. Their locations are shown in Figure 84. Two groups of andesite are distinguished and these correspond to two of three volcanic rock associations that have been identified in the arc and trench environments of Papua New Guinea.

	1	2 Avg. of 12 Chondrites	3 Chondrites	4 Avg. of 10 Chondrites	5 Avg. Chondrites	6 Leedy Chondrite
La	0.329	0.340	0.390	0.329	0.330	0.315
Ce	0.865	1.100	1.200	0.865	0.980	0.813
Pr	0.130	0.130	0.140		0.120	0.116
Nd	0.630	0.610	0.640	0.630	0.630	0.597
Sm	0.203	0.230	0.230	0.203	0.220	0.192
Eu	0.077	0.080	0.082	0.077	0.084	0.0722
Gd	0.276	0.340	0.340	0.276	0.340	0.259
Tb	0.050	0.052	0.051		0.051	0.049
Dy	0.343	0.340	0.330	0.343	0.370	0.325
Ho	0.077	0.080	0.076		0.075	0.073
Er	0.225	0.240	0.230	0.225	0.210	0.213
Tm	0.035	0.034	0.031		0.038	0.03
Yb	0.220	0.200	0.180	0.220	0.190	0.208
Lu	0.034	0.035	0.031	0.034	0.036	0.0323

1	Clarke	unpublished
2	Ahrens	1965
3	Ehmann	1968
4	Nakamura	1974
5	Coryell and others	1963
6	Taylor and Gorton	1977

Table 19: Comparison of the normalizing factors commonly used for REE plots by different researchers. Those of Clarke (unpublished) were used herein.

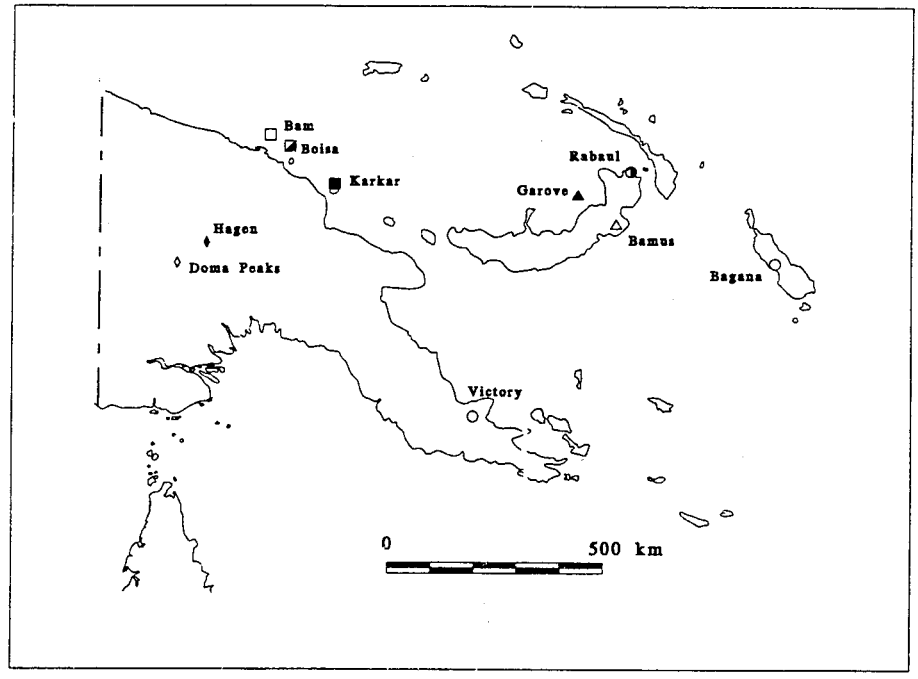

Figure 84: Map showing location of samples of Papua New Guinea andesites analyzed by Johnson, 1982.

Group one andesites, present in the Highlands, Eastern Papua, Rabaul (New Britain), and Bougainville, are characterized by higher concentrations of alkalis and incompatible elements than andesites of group two. They show fractionated REE patterns in which light REE (LREE) are moderately or strongly enriched relative to heavy REE (HREE) as shown in Figure 85A, and high initial $^{87}Sr/^{86}Sr$ values from 0.7039-0.7049. Group two andesites are present in the volcanic arcs of the Bismarck Sea (excluding the Rabaul province) and are characterized by REE patterns that show little enrichment of LREE elements (Figure 85B) or may be LREE-depleted (Bamus). They are characterized by alkali and incompatible elements and initial $^{87}Sr/^{86}Sr$ ratios that are low (from 0.7034-0.7037) relative to those of group one. Hornblende phenocrysts are present in many andesites of group one but are uncommon in samples from group two. Biotite is present in some samples of group one andesites, particularly in trachybasalts and trachyandesites (Johnson, 1982). The third volcanic rock association in the region is a chain of islands east of New Ireland that is characterized by alkaline rocks. This association does not include andesites.

The chondrite-normalized REE contents of the least-altered intrusive rocks from the Sydney and Ningi Intrusions are listed in Appendix 13 and plotted in Figure 86A. These samples show strong enrichment of LREE to HREE with $(La/Lu)_{cn}$ ratios of 14 to 17 and as such are similar to samples of Victory andesites (Eastern Papua) and Doma Peaks andesites (PNG Highlands) which have $(La/Lu)_{cn}$

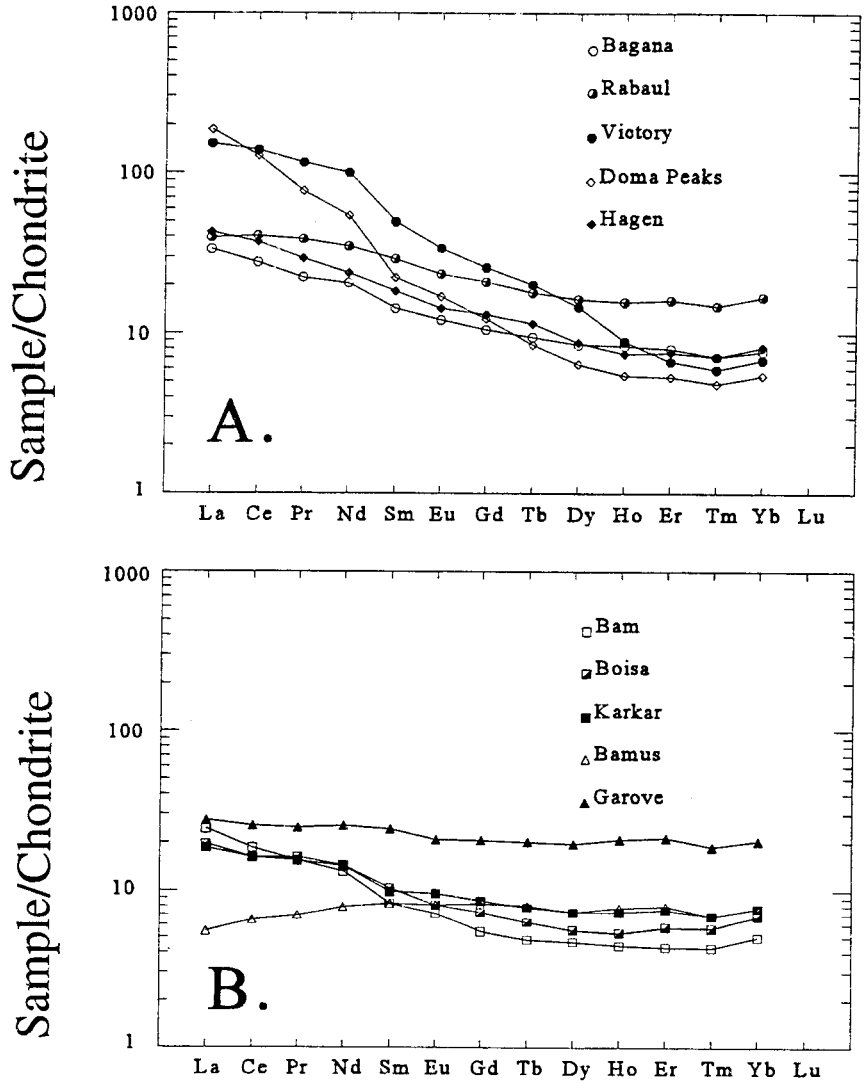

Figure 85: Rare-earth element plots for samples of andesite from the Papua New Guinea area (Johnson, 1982). (A) Group one. (B) Group two.

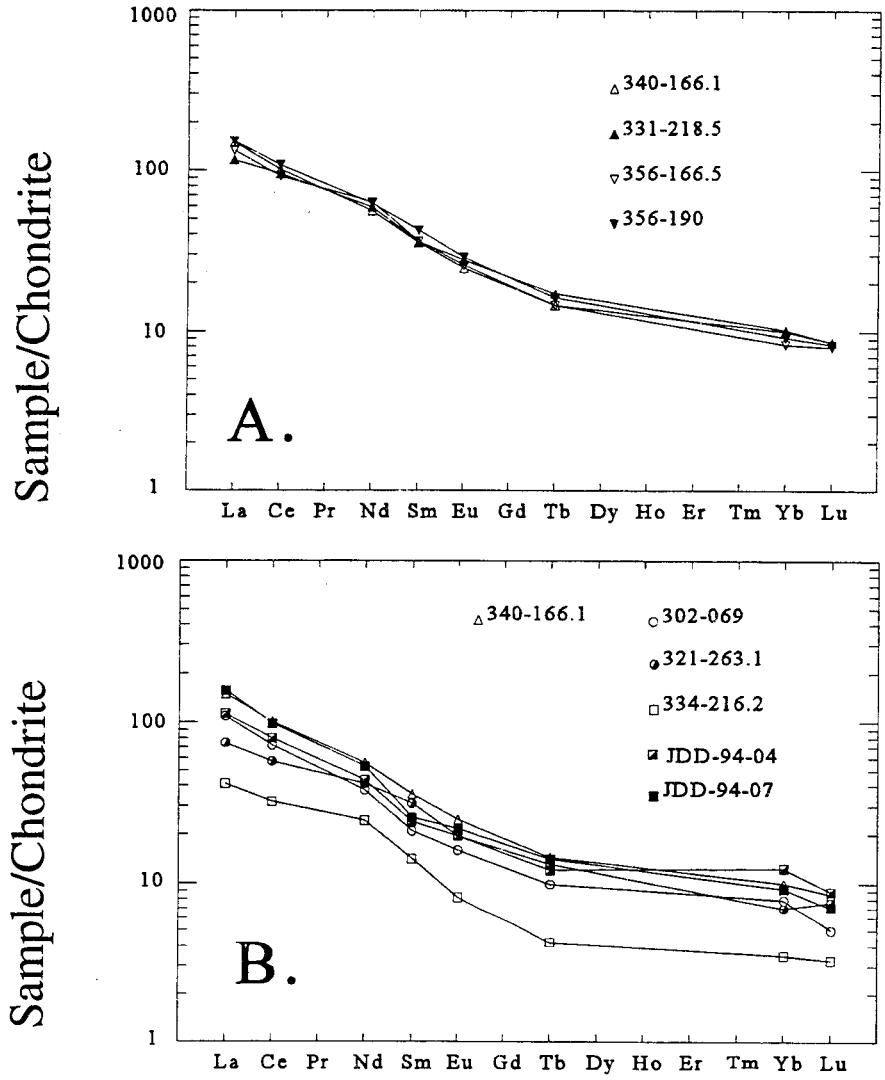

Figure 86: Rare-earth element plots for samples from the Ok Tedi Intrusive Complex: (A) Least-altered or unaltered, (B) Potassic alteration.

of 22 and 34 (Johnson, 1982). The patterns do not display Eu anomalies and therefore are similar to other rocks of andesitic composition (Henderson, 1984). The linear patterns of the four samples shown in Figure 86A form a tight bundle suggesting very little difference in the REE contents within or between the unaltered rocks of the Sydney and Ningi Intrusions.

The chondrite-normalized REE contents of altered intrusive rocks from the Ok Tedi Intrusive Complex are listed in Appendix 13 and plotted in Figure 86B. One sample of least-altered rock (DDH 340-166.1) is also included for comparison. All of the altered samples have normative anorthite contents that are less than An_6. All samples display the same LREE-enriched pattern as do their unaltered equivalents and all lack Eu anomalies. The REE patterns of all but one of these samples are depleted relative to DDH 340-166.1. The exception is JDD-94-07 which is similar in abundance to DDH 340-166.1 for most of the REE. The trend line representing sample DDH 334-216.2 shows the most displacement relative to DDH 340-166.1, even though this rock is not the most potassium-enriched or calcium-poor of the altered rocks shown in the diagram. These two factors suggest that although depletion of REE has occurred in the potassically-altered rocks at Ok Tedi, the degree of depletion cannot be simply related to the intensity of alteration.

Rubidium and Strontium

Rubidium and strontium are commonly present in trace to minor concentrations in intrusive rocks of intermediate to silicic composition. In samples from the Ok Tedi Intrusive Complex, rubidium ranges from 84 ppm in unaltered intrusive rocks to 280 ppm in samples with strong potassic alteration (Appendix 12). Values as low as 15 ppm characterize samples of endoskarn with significant quantities of calcite in their norms. Strontium ranges from 1200-1300 ppm in unaltered intrusive rock to as low as 230 ppm in samples with strong potassic alteration. The concentrations of these elements in samples with normative andesine, oligoclase, and albite are contrasted in Figure 87. In general the concentrations of these elements are consistent with and further reinforce interpretation of the trends of the major oxides. The behaviors of these elements reflect their position in the periodic table of elements. Potassium and rubidium are both group one elements and both are univalent. Calcium and strontium are both group two elements and both are divalent. Because they are similar in ionic radius and charge, rubidium commonly substitutes for potassium in the atomic structures of minerals, and strontium substitutes for calcium. Strontium is enriched in the least altered samples, which are also characterized by relatively high concentrations of calcium. Rubidium is enriched in samples having undergone strong potassium enrichment with potassic-alteration. Conversely, both strontium

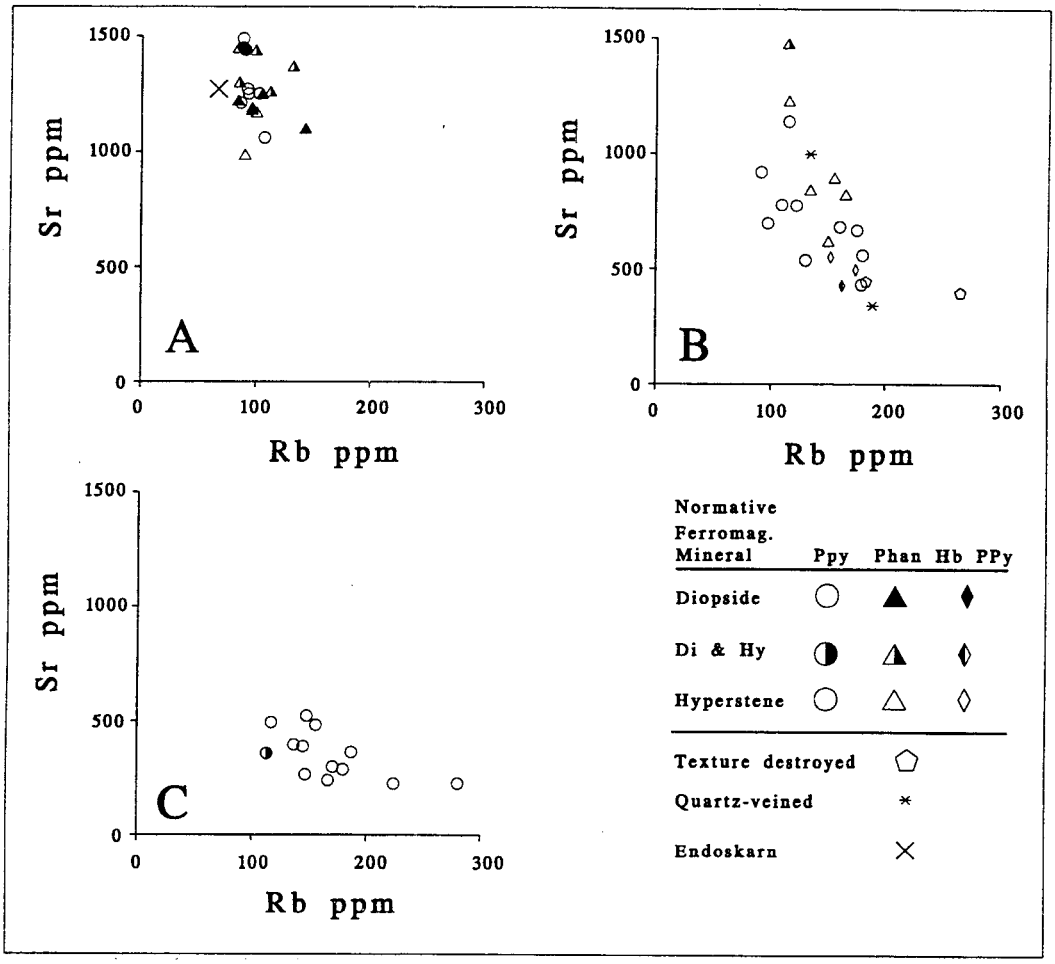

Figure 87: Plot of rubidium versus strontium in samples of Ok Tedi intrusive rock with: (A) normative andesine, (B) normative oligoclase, and (C) normative albite.

and calcium are strongly depleted in rocks that have undergone potassic alteration. The antipathetic relationship of K to Ca and Rb with respect to alteration-mineralization processes at Ok Tedi are expectable trends and consistent with those observed in porphyry systems elsewhere.

Gold and Copper

Although the Ok Tedi deposit contains local concentrations of molybdenum and other metals, copper and gold are the only elements that are credited by the companies that smelt the ore. For this reason, copper and gold are the only elements that are consistently listed in analyses of diamond drill hole, reverse-circulation, and blast hole samples. These two elements are also the only ones that will be discussed in detail in this dissertation.

The elemental abundances of gold, in parts per million (ppm), and copper, in weight percent, of the samples collected for this study in 1994 are listed in Table 20. Part of the samples were analyzed by the Folomian laboratory at Ok Tedi by atomic absorption spectroscopy. All of these samples consist of diamond drill core. The core had earlier been split into two portions. One half of the core had been crushed and submitted for analyses; the other half had been archived. Hand specimens, typically 10 to 20 cm in length, were collected from the archive boxes and used for the thin-section and XRF analyses of this dissertation. The crushed rock submitted for gold and copper analyses at Folomian laboratory

Sample	Au	Cu	Lab	Interval m.	Sample	Au	Cu	Lab	Interval m.
300-068.75	0.83	0.965	Folomian	0.6	**389-271**	0.07	0.086	Folomian	3.0
302-069	0.06	0.038	Folomian	3.0	**401-158.8**	0.90	0.790	Folomian	3.5
316-314.7	0.33	0.347	Folomian	2.0	**401-171.2**	0.25	0.165	Folomian	3.0
319-276.1	0.11	0.059	Folomian	3.0	**401-218.3**	0.20	0.093	Folomian	3.0
321-263.1	0.22	1.180	Folomian	3.0	**407-257.8**	0.30	0.151	Folomian	4.2
321-312.5	0.44	0.436	Folomian	3.0	**411-045**	0.09	0.176	Folomian	3.8
321-368	0.40	0.293	Folomian	3.0	**455-023.1**	0.05	0.224	Folomian	3.0
323-308	0.02	0.140	Folomian	3.0	**455-051.1**	0.30	0.104	Folomian	3.0
331-047.8	0.03	0.004	Folomian	2.7	**458-151.8**	<0.01	0.015	Chemex	
331-218.5	0.02	0.007	Folomian	3.0	**459-102.9**	0.10	0.053	Chemex	
334-216.2	0.24	0.228	Folomian	3.0	**464-009**	0.38	0.037	Folomian	3.0
340-166.1	<0.01	0.005	Chemex		**464-355.5**	0.10	0.104	Folomian	3.0
342-084.5	0.01	0.004	Chemex		**JDD-94-01**	0.24	0.317	Chemex	
342-115.4	<0.01	0.002	Chemex		**JDD-94-02**	0.08	0.309	Chemex	
342-141	0.01	0.002	Chemex		**JDD-94-03**	0.39	0.294	Chemex	
344-016	<0.01	0.001	Chemex		**JDD-94-04**	0.36	>1.0	Chemex	
345-489.5	0.10	0.217	Folomian	3.0	**JDD-94-05**	0.24	0.059	Chemex	
346-195.4	0.36	0.508	Folomian	3.0	**JDD-94-06**	0.40	>1.0	Chemex	
346-269.8	0.09	0.120	Folomian	3.7	**JDD-94-07**	0.07	0.175	Chemex	
351-313.2	0.17	0.152	Folomian	3.0	**JDD-94-08**	0.12	0.147	Chemex	
356-166.5	0.08	0.172	Folomian	3.0	**JDD-94-09**	0.05	0.186	Chemex	
356-190	0.48	0.164	Folomian	3.0	**JDD-94-09V**	0.04	0.129	Chemex	
360-095	0.53	0.946	Folomian	3.0	**JDD-94-10**	0.04	0.039	Chemex	
366-232.5	0.08	0.135	Folomian	3.0	**JDD-94-11**	0.04	0.081	Chemex	
367-089.8	0.13	0.485	Folomian	3.0	**JDD-94-12**	0.01	0.815	Chemex	
383-157.6	0.56	0.468	Folomian	3.0	**JDD-94-13**	0.98	0.056	Chemex	
383-170.6	0.83	0.477	Folomian	3.0	**JDD-94-14**	0.39	0.022	Chemex	
383-172	0.24	0.236	Folomian	2.9	**JDD-94-15**	0.11	0.051	Chemex	
383-173.5	do.	do.	Folomian	do.	**JDD-94-19**	0.23	0.285	Chemex	
386-075.4	0.15	0.134	Folomian	3.0	**P21-93-01**	3.92	>1.0	Chemex	
386-276.1	0.20	0.267	Folomian	3.0					

Folomian Laboratory - Au by Fire Assay, Cu by Atomic Absorption Spectroscopy
Chemex Laboratory - Au and Cu by Inductively-Coupled Plasma Spectroscopy

Table 20: Gold (in ppm) and copper (in weight percent) contents of samples of intrusive rock collected from the Ok Tedi Intrusive complex in 1994.

typically consisted of composites of two to three meters of core. The composite lengths for each of these samples are listed in Table 20. The metal values listed in Table 20 for these samples are representative of the intervals from which they were taken and are not necessarily representative of the hand samples used for thin-sections and major-oxide determinations. However, the hand samples were chosen to be representative of the intervals from which they were taken and, therefore, the composite value are considered to be suitable for presentation. The other samples in Table 20 were not analyzed at Folomian because they either came from unaltered drill core, which the geologic staff of the mine did not deem appropriate for analyses, or because they were collected as hand specimens in 1994. These samples were analyzed by ICP spectroscopy at Chemex Laboratories. They are considered to be representative of the hand specimens from which thin-sections and major-oxide determinations were taken.

Statistical distributions of major elements (or oxides) in rocks are characterized by histograms that are symmetrical about the mean values of sample populations. An example of such a normal distribution is given in Figure 88A. This plot illustrates the K_2O content of 2638 samples of reverse-circulation rotary drill cuttings from the Mt. Fubilan Intrusion. Curves derived by smoothing such histograms are bell-shaped, such as the one illustrated in Figure 88B, and they are considered to define normal distributions. The curves representing normal distributions can be converted to straight lines by plotting sample values versus

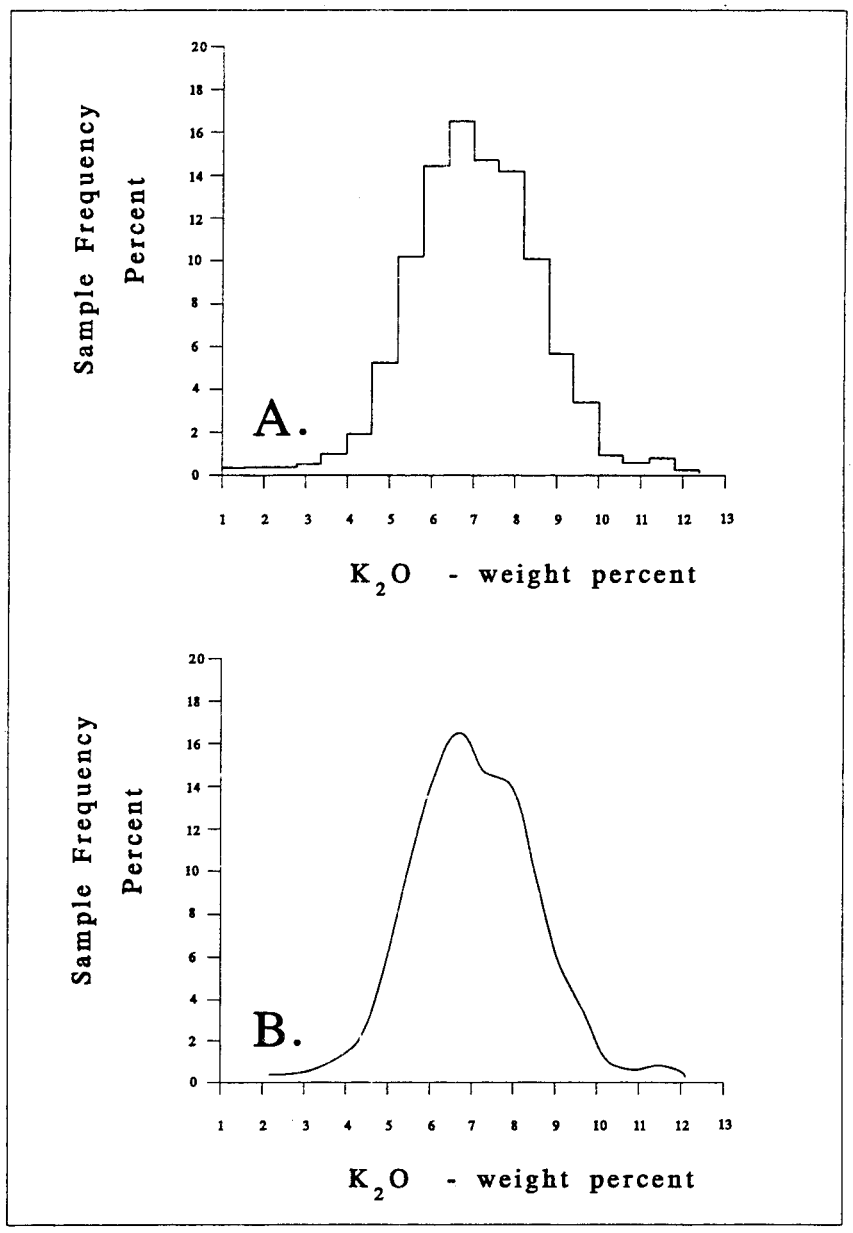

Figure 88: Example of a normal distribution - K_2O contents of samples from the potassically altered Mt. Fubilan Intrusion: (A) Histogram, (B) Curve derived from the histogram in A.

cumulative probability values (Tennant and White, 1959; LePeltier, 1969; and Sinclair, 1976). A normal-probability plot for the K_2O values portrayed in Figure 88 is given in Figure 89. In contrast to the behavior of the major oxides, statistical plots of trace elements typically display skewed histograms that result in curves that are displaced towards low values (Ahrens, 1954, 1957). Histograms having non-symmetrical shapes can commonly be modeled mathematically using logarithmic distribution statistics. Such distributions are made symmetrical by plotting sample frequency versus the logarithms of sample values rather than the sample values themselves. An example of a histogram for a log-normal distribution in which cumulative sample frequency is plotted against the logarithms of sample values is given in Figure 90A and the curve derived from this histogram appears as Figure 90B. This plot is of the gold content in samples of 4533 blast hole cuttings from the Fubilan Intrusion. The curve resulting from smoothing the histogram is approximately bell-shaped and its log-probability plot (Figure 91) approximates a straight line.

Several factors can affect the symmetry of histograms and can cause deviations from straight lines on probability plots. These factors include: 1) the inclusion of excessively large numbers of high (or low) values in a data set, 2) the presence of more than one population of sample values, and 3) sample populations that are neither arithmetic or logarithmic.

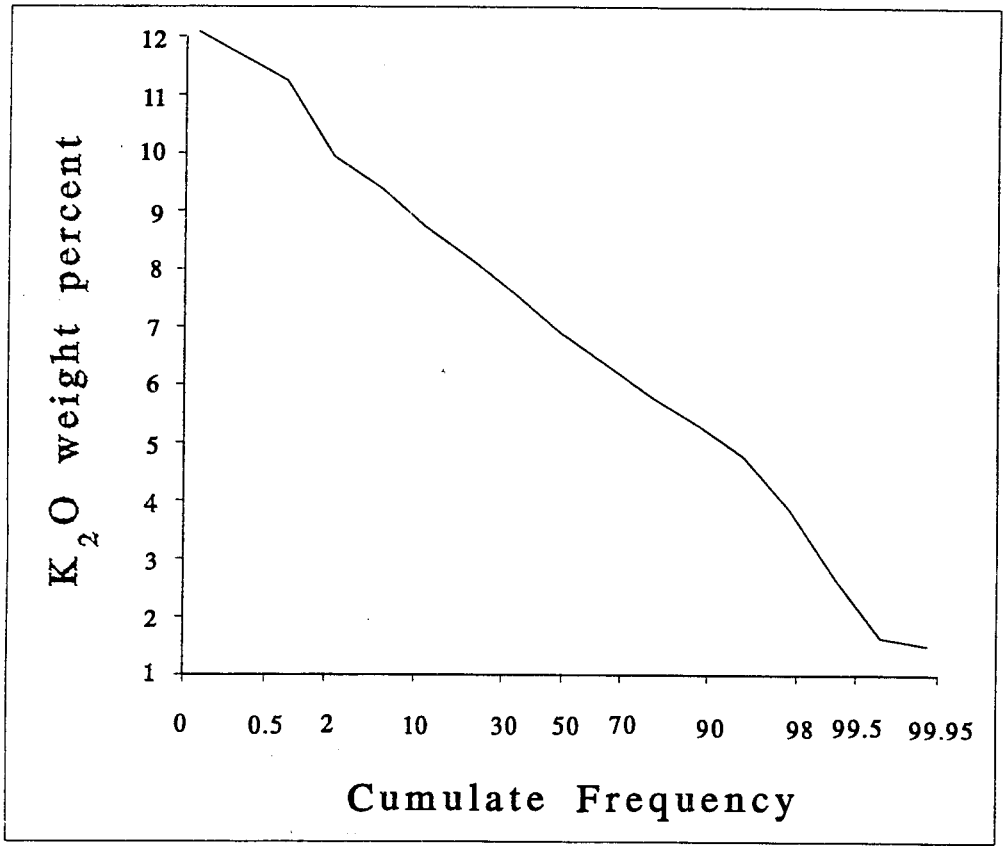

Figure 89: Normal-probability plot for K_2O contents of samples of rotary drill cuttings samples from the Mt. Fubilan Intrusion.

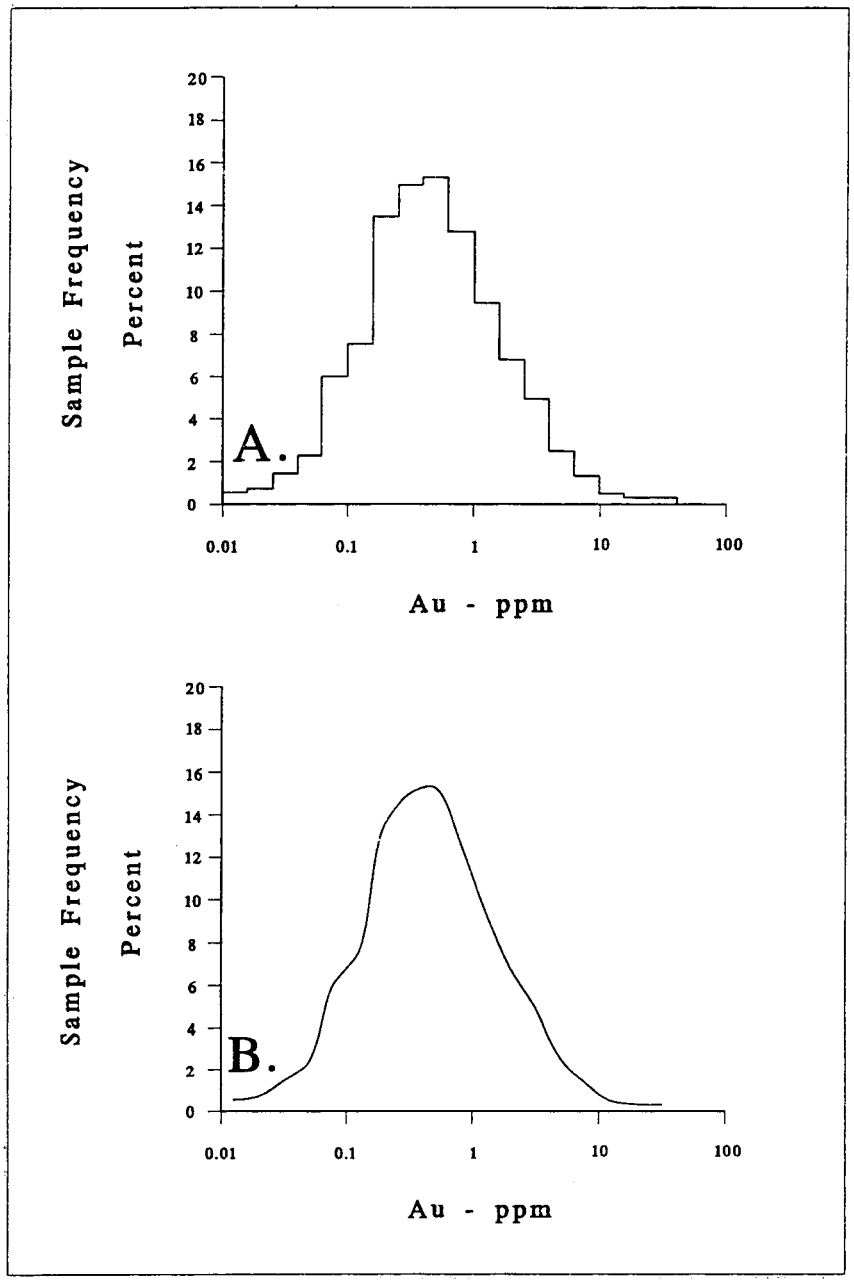

Figure 90: Example of a log-normal distribution - Au contents of samples from blast-hole drill cuttings: (A) Histogram, (B) Curve derived from the histogram in A.

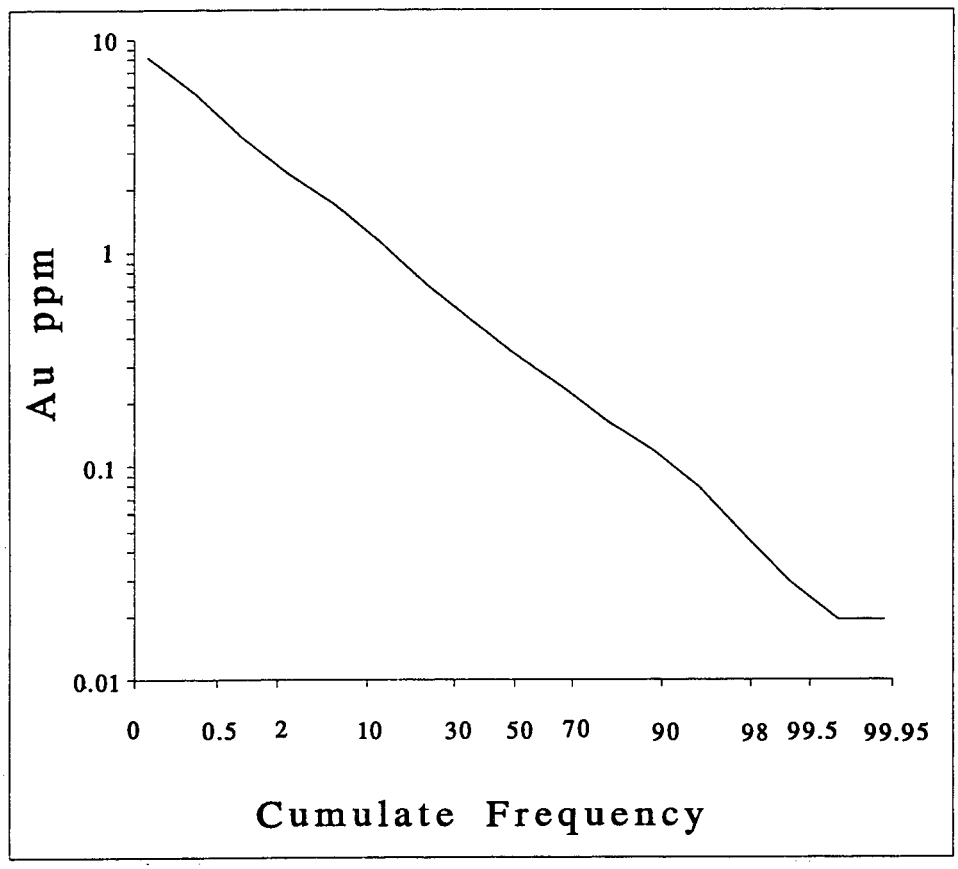

Figure 91: Log-probability plot for Au contents of samples from blast-hole drill cuttings

Average values and standard deviations of sample populations can be read directly from probability plots. The average values derived from normal-probability plots are referred to as arithmetic means and those from log-probability plots as geometric means.

The arithmetic and geometric means and their respective standard deviations of gold and copper values in the 1994 suite of samples together with similar statistics for 1000 samples of rotary drill cuttings, 2050 samples of drill core, and 4300 samples of blast hole cuttings are listed in Table 21. These statistics are graphically summarized in Figures 92-93.

The diamond drill core and hand samples collected in 1994 have an arithmetic mean of 0.30 ppm and a geometric mean of 0.19. About two percent have gold values larger than 0.9 ppm (or grams/tonne) and about one percent have values less than 0.015 ppm The mean values of this set of samples are similar to the means of gold in diamond drill core (0.33, 0.23) and about one-half of the means of rotary and blast hole drill cuttings (0,50-0.58, 0.33-0.36). The lower average values of the 1994 suite of samples and diamond drill core relative to those of rotary and blast drill cuttings are attributed to the fact that the former include substantial numbers of unaltered rocks from the Sydney, Kalgoorlie, and Ningi Intrusion whereas the latter are nearly all from the potassically-altered Fubilan Intrusion. The sample distributions of gold in rotary and diamond drill hole samples are portrayed on a log probability plot in Figure 92A. The gold values

		Gold - ppm			
		Arithmetic		Geometric	
	n	Mean	Std. Dev.	Mean	Std. Dev.
RC	1001	0.59	0.81	0.33	2.82
DDH	2049	0.33	0.33	0.23	2.41
BH Sulfide	987	0.58	0.76	0.36	2.55
BH Mixed	1307	0.50	0.60	0.33	2.44
BH Oxide	2052	0.56	0.67	0.36	2.61
Doucette 1994	54	0.30	0.31	0.19	2.82
		Copper - percent			
		Arithmetic		Geometric	
	n	Mean	Std. Dev.	Mean	Std. Dev.
RC	1001	0.32	0.64	0.15	3.24
DDH	2060	0.40	0.49	0.21	3.32
BH Sulfide	982	1.01	1.00	0.70	2.45
BH Mixed	1306	0.72	0.76	0.45	2.91
BH Oxide	2025	0.13	0.36	0.06	2.63
Doucette 1994	56	0.24	0.23	0.14	3.19

Table 21: Summary statistics for gold and copper data from diamond drill hole (DDH), reverse circulation (RC), and blast hole (BH) samples. Also includes statistical values for samples listed in Table 20.

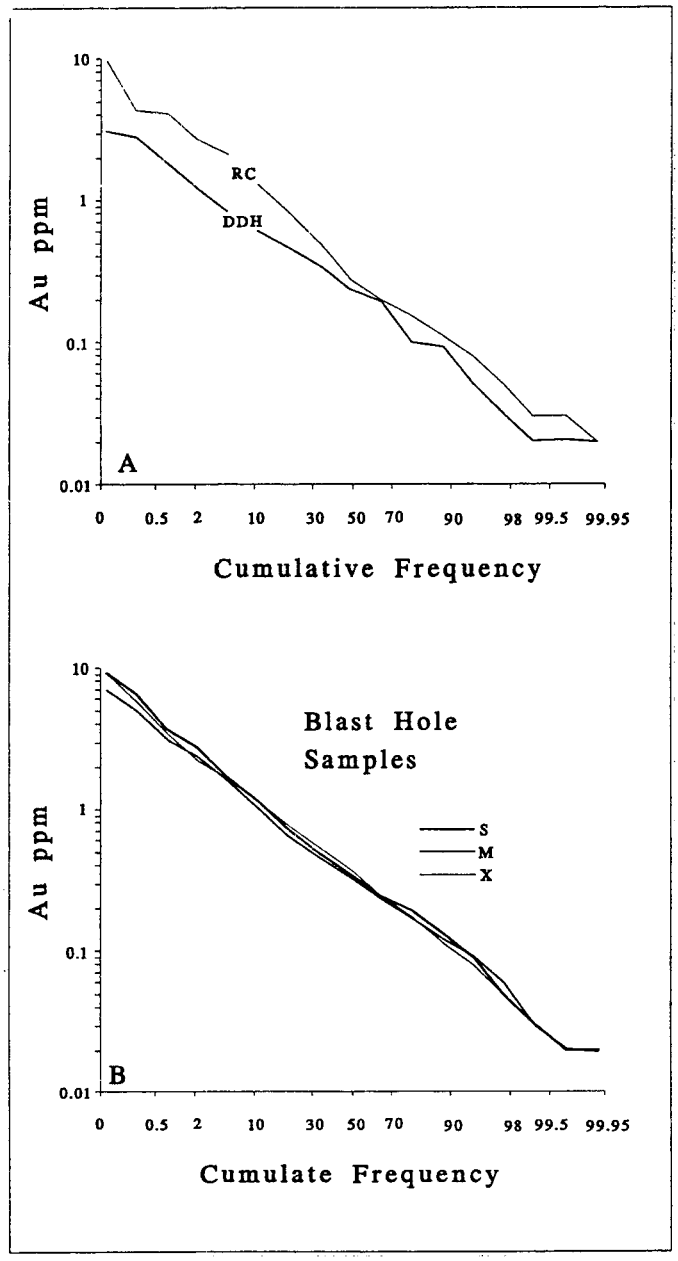

Figure 92: Log-probability plots of gold in: A. reverse circulation drill cuttings and diamond drill core, and B. blast hole cuttings grouped as to their content of sulfide minerals (S), limonite (X), or mixtures of sulfide minerals and limonite (M).

contained in samples of blast hole cuttings are summarized in Figure 92B. The data base of samples from blast hole drill cuttings includes details as to the presence, or absence, of sulfide minerals or limonites in the samples The average values and trends of sample sets containing sulfide minerals (S; chiefly pyrite, chalcopyrite, and chalcocite), limonite (X), and mixtures of sulfide minerals and limonite (M) are nearly identical (Figure 92B). The similarity of statistical values and trend lines for these samples on the log-probability plots suggest that the distribution of gold values has not been affected by supergene processes.

The arithmetic mean for copper in the 1994 suite of samples is 0.24 weight percent and the geometric mean is 0.14. About three percent of the samples have greater than one weight percent copper and approximately one percent have less than 0.015. The trends of copper content in diamond drill and rotary drill cuttings are approximately the same as one another in Figure 93A. The arithmetic and geometric means for the samples of diamond drill core are 0.40 and 0.21 and those of rotary drill cuttings are 0.32 and 0.15 weight percent. Data from samples of blast hole drill cuttings for samples containing sulfide minerals, limonite, and mixtures of sulfide minerals and limonite are plotted separately on log-probability diagrams in Figure 93B. These diagrams illustrate the fact that ore-grade copper is restricted to rock that contains sulfide minerals or mixtures of sulfides with limonite. The arithmetic and geometric means of copper in samples containing

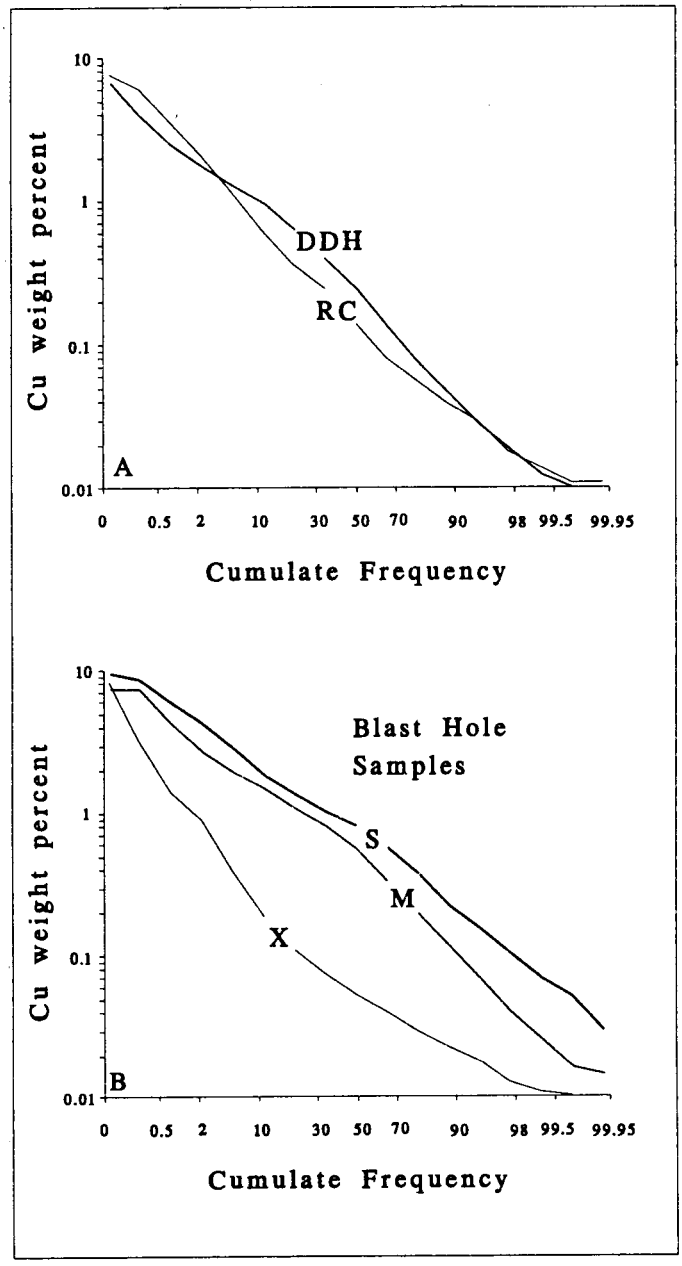

Figure 93: Log-probability plots of copper in: (A) reverse circulation drill cuttings and diamond drill core, and (B) blast hole cuttings grouped as to their content of sulfide minerals (S), limonite (X), or mixtures of sulfide minerals and limonite (M).

sulfide minerals with little if any limonite are 1.01 and 0.70 weight percent. The arithmetic and geometric means of samples containing both sulfide minerals and limonites are 0.72 and 0.45 weight percent. The rock samples with the highest grades come from areas where supergene chalcocite has replaced chalcopyrite and pyrite thus enriching the hypogene ore. Samples from rocks that have been so heavily oxidized as to destroy all sulfide minerals do not constitute an ore of copper. The arithmetic and geometric means for copper in "oxide" samples are 0.13 and 0.06 weight percent. Less than ten percent of oxide samples carry ore-grade concentrations of copper and most of this is contained in malachite, crysocolla, or cupiferous limonites. These minerals are not recovered in the flotation circuits at Ok Tedi and do not, therefore, constitute an economic asset.

Variations in the gold and copper contents of samples of rotary drill cuttings from the Fubilan intrusion with SiO_2 are illustrated in Figure 94. Samples that have SiO2 contents between about 55 and 70 weight percent consist entirely of altered intrusive rock whereas samples that have SiO_2 less than 55 weight percent have been contaminated with massive ores, limestone, or gossan and those with SiO_2 greater than 70 percent are contaminated by quartz veinlets. High values of gold and copper are present at nearly all levels of SiO_2 but are most plentiful in the range from about 60 to 70 weight percent SiO_2.

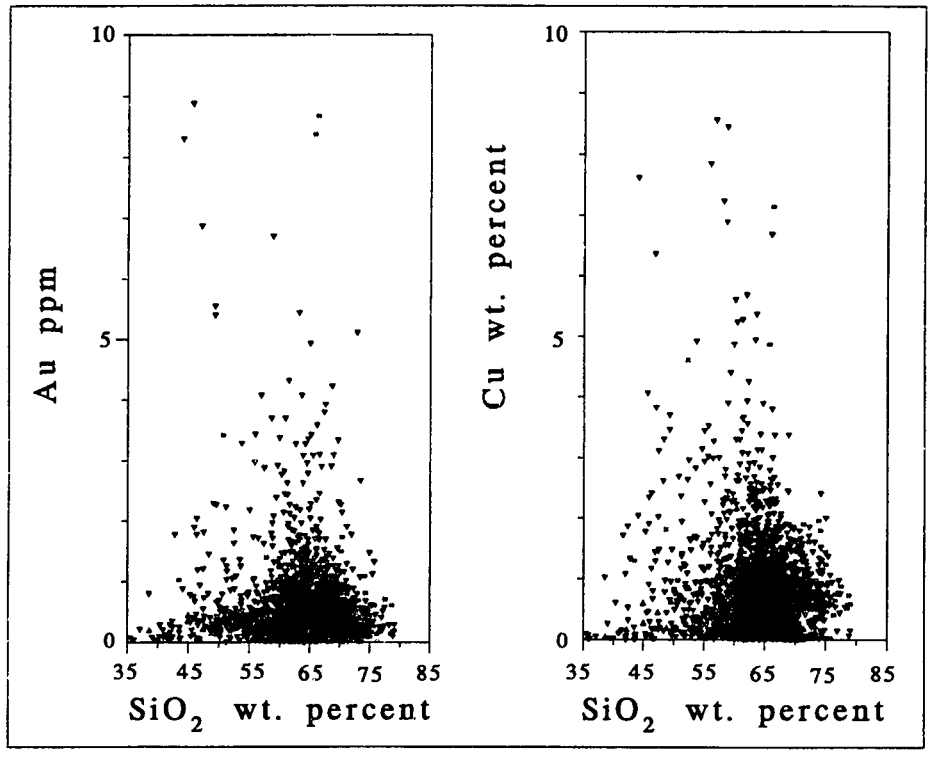

Figure 94: Silica-variation diagrams for gold and copper in samples of rotary drill cuttings from the Fubilan Intrusion.

Continuity of Alteration in Zone of Potassic Alteration

The purpose of the following discussion is to illustrate the extent and continuity of hydrothermal alteration and ore grade within the potassically altered and mineralized Mount Fubilan Intrusion using a contoured plan map and four drill-hole summary logs.

Porphyry-type deposits are characterized by widespread chemical alteration of host rocks by hydrothermal fluids. Titley (1982) described three general manifestations of alteration associated with porphyry-type mineral deposits. *Selectively pervasive* alteration is characterized by the replacement of specific minerals in host rocks leaving adjacent minerals undisturbed. The original texture of host rocks is often enhanced by this type of alteration. *Pervasive alteration* is defined by Titley (1982) as resulting in the destruction of original rock textures. *Vein-veinlet* alteration emanates from fractures and faults that were the conduits for hot aqueous fluids. Where fractures, or other conduits, are sparsely distributed or widely spaced, alteration is generally limited to narrow selvedges on, and surrounding, the fracture surfaces. Rock between fractures is generally unaffected by alteration in such instances. Where fractures are abundant in number and closely spaced, the alteration emanating from one fracture is likely to overlap that coming from its neighboring fractures and may cause whole-scale chemical replacement of host-rock minerals by alteration minerals. Veinlet alteration can, therefore, grade into pervasive alteration.

The Mt. Fubilan Intrusion is characterized by pervasive alteration throughout a minimum of several hundred meters laterally and vertically. The alteration differs from Titley's definition in that it has not totally destroyed the texture of the rock. The porphyritic texture of the intrusion is preserved at almost all locations although ferromagnesian minerals other than mica have been destroyed by hydrothermal alteration and are no longer visible. The most striking change in the hydrothermally altered rocks at Ok Tedi is the pseudomorphic replacement of phenocrysts of plagioclase feldspar by alkali feldspar but this type of alteration has not affected the macroscopic texture.

The hydrothermally altered intrusive rocks of Mt. Fubilan are also crosscut by veins and veinlets at most locations. These veinlets consist of fractures that are filled with quartz, hydrothermal biotite, metallic sulfide minerals, or magnetite. Bleached selvedges are common but often subdued in character because of masking by the effects of pervasive alteration.

Data from composite samples consisting of rock from reverse-circulation drill holes are used to illustrate the variation in chemical oxides. The composite samples are splits from two to three meter intervals. The data are not capable of discriminating small-scale differences in the chemistry adjacent to fine-veinlets, narrow zones of alteration, or selectively pervasive alteration because of their composite nature and their length. However, the intent of this discussion is not to examine small-scale variations but instead to demonstrate the fact that potassic

alteration of the Mt. Fubilan Intrusion is contiguous and pervasive over distances of hundreds of meters vertically and horizontally and for this task the data are well suited.

A plan map of part of the Mt. Fubilan Intrusion that has been contoured for the K_2O contents in reverse-circulation drill cuttings is given in Figure 95. Contour lines are drawn at 2 percent intervals from three to nine weight percent. For comparison with the contoured data, the abundance of K_2O in the least altered sample from the Sydney Intrusion (DDH 340-166.1) is 3.48 weight percent. The K_2O content of the Mt. Fubilan Intrusion, as shown in Figure 95, varies from 5 to more than 9 weight percent or 1.4 to 2.6 times the amount of this oxide in unaltered rock. The area falling within the 3-5 and less than 3 weight percent contours is anomalous and corresponds to the location of the quartz core. Samples from this area have had their K_2O, as well as other oxides, diluted by the SiO_2 content of quartz veinlets.

Graphic summary logs for three reverse circulation rotary drill holes are presented in the following pages. Each of the diagrams contains data for the major-oxides SiO_2, TiO_2, Al_2O_3, FeO^*, MgO, CaO, K_2O, the trace-elements Au and Cu, and lithology. The major oxide contents of a reference sample, DDH 340-166.5, of unaltered phanerite from the Sydney Intrusion are also shown for comparison. The locations of the three drill holes are given in Figure 96. The three drill holes selected for presentation were chosen because they have

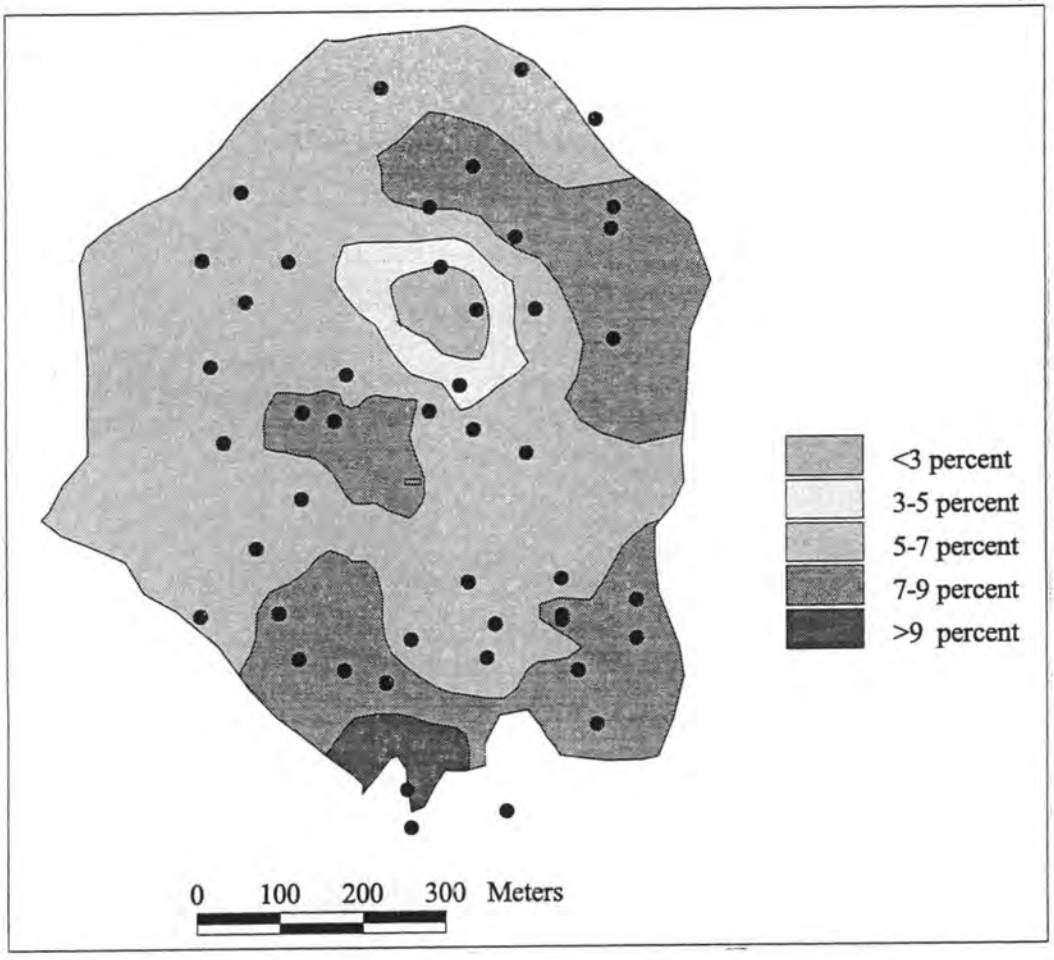

Figure 95: Plan view of part of the Mount Fubilan Intrusion contoured for K_2O content. The map is for a planned bench at 1753 meters elevation. Circle symbols show locations of composite samples.

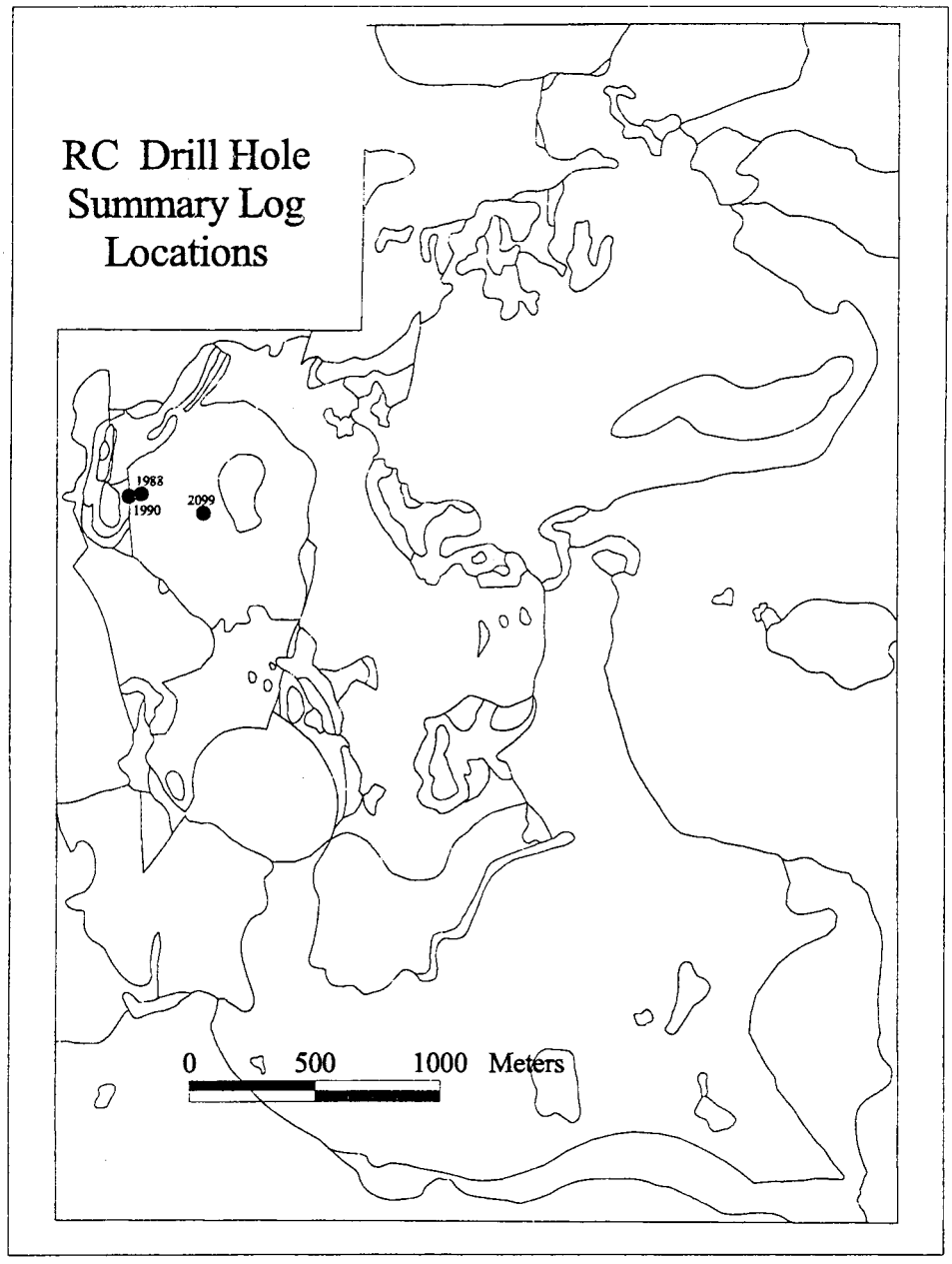

Figure 96: Map showing the locations of reverse-circulation rotary drill holes shown in Figures 97-99.

significant intersections of ore grade rock. They were not, however, chosen to show relationships between alteration and metallization.

A summary log of rotary drill hole RC-1990 is presented as Figure 97. The log summarizes data for 58 samples from drill cuttings. The hole was drilled from 1888 to 1657 meters elevation and remained in intrusive rock from top to bottom as shown in the lithic column on the right. Lines connecting the analytical values of CaO, TiO_2, and Al_2O_3 show little variation throughout the length of the hole and much of the variation is likely to be normal analytical error. CaO varies from 0.03 to 0.33 weight percent and is always less than 5 percent of the CaO content of the example of unaltered rock (DDH 340-166.1; 6.37 weight percent). TiO_2 ranges from 0.38 to 0.54 weight percent and averages 0.48 compared to 0.54 in the example of unaltered rock. Al_2O_3 ranges from 13 to 18 weight percent and is variably less or nearly the same as in the example of unaltered rock (18.1 weight percent) SiO_2 values are consistently higher than that of the reference sample (60.1 weight percent) and range from 60.0 to 67.8 weight percent with an average of 65.2. Variation in the abundance of MgO is limited and varies from 0.54 to 1.55 weight percent and averages 0.83 which is about 60 percent of the MgO content in DDH 340-166.1. Gaps in the line representing K_2O values are because of laboratory omissions or analytical problems. K_2O ranges from 5.38 to 9.94 weight percent, if the missing values are omitted from the calculation, and averages 7.99 which is more than twice the amount of K_2O in DDH 340-166.5. The range in K_2O

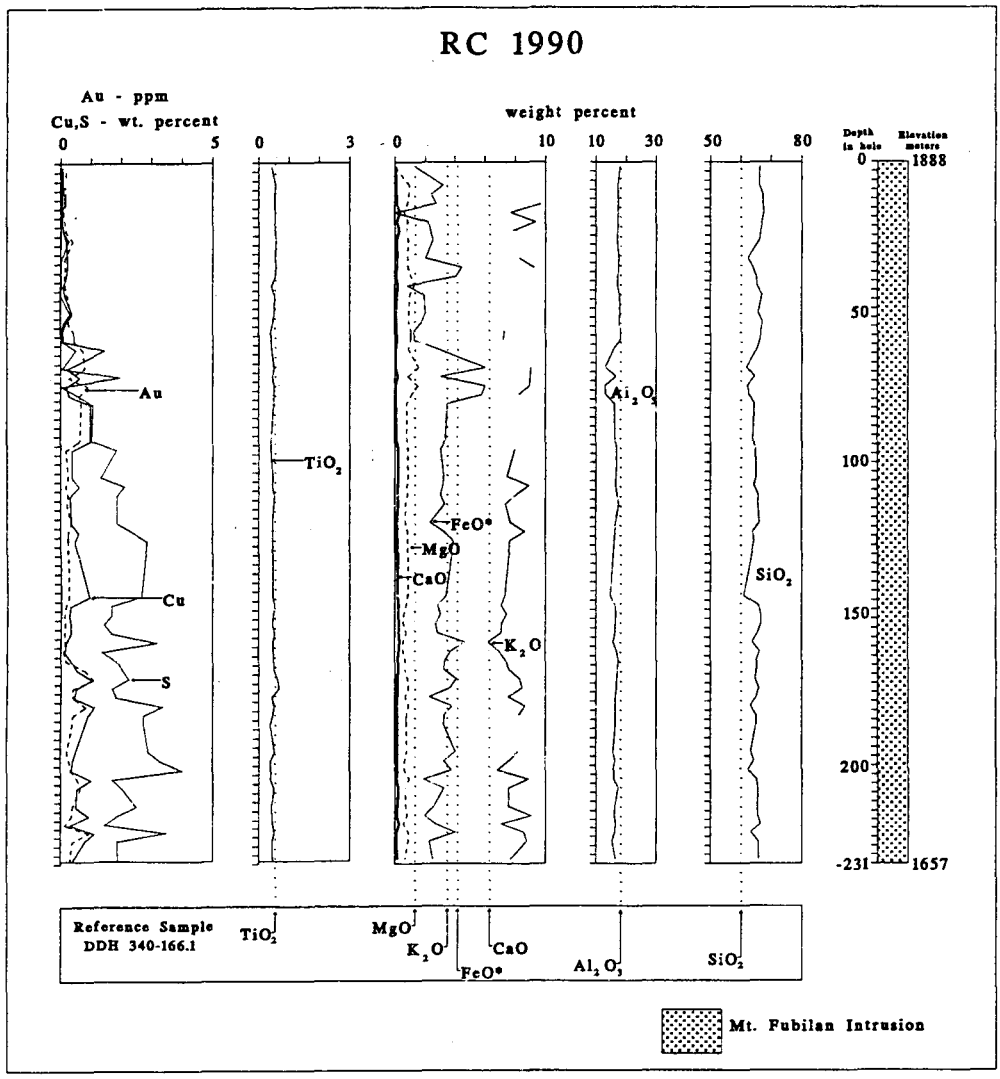

Figure 97: Lithic and selective chemical summary log of drill hole RC 1990.

shown by this drill hole is approximately the same as that displayed in the contoured plan map (Figure 95). The FeO* content is much lower than in the reference sample (4.18 weight percent) for the first 60 meters of the drill hole. It increases in abundance from about 2.3 weight percent to about 3.2 weight percent at 1844 meters and for the remainder of the hole is slightly less than that of the reference sample with a few peaks that exceed the FeO^* content of the reference sample. Gold, copper, and sulfur values increase at about the same depth as the increase in iron content probably reflecting the presence of metallic sulfide minerals. In contrast to the behavior of major oxides in Figure 97, gold, copper, and sulfur show strong deviations from linear behavior. Gold varies from less than the limit of detection (0.1 ppm) to 1.26 ppm and, in samples with values greater than 0.1 ppm, averages 0.35 ppm (grams/tonne). Copper ranges from 0.05 to 1.65 weight percent and averages 0.49. About one-half of the analyses of copper are above the cutoff grade of 0.4 weight percent used to define ore in 1989. Only two analyses of gold are greater than the cutoff grade of one gram/tonne. Much of the rock traversed by this drill hole is, therefore, copper ore, but not gold ore. Sulfur ranges from 0.01 to 4 weight percent.

A second example of a drill hole that also traverses only hydrothermally altered intrusive rock, RC-2099, is given in Figure 98. The abundance of SiO_2 in RC-2099 is mostly greater than that of the reference sample and varies from about 59 to 68 weight percent with an average of 63.5. TiO_2 ranges from 0.35 to 0.49

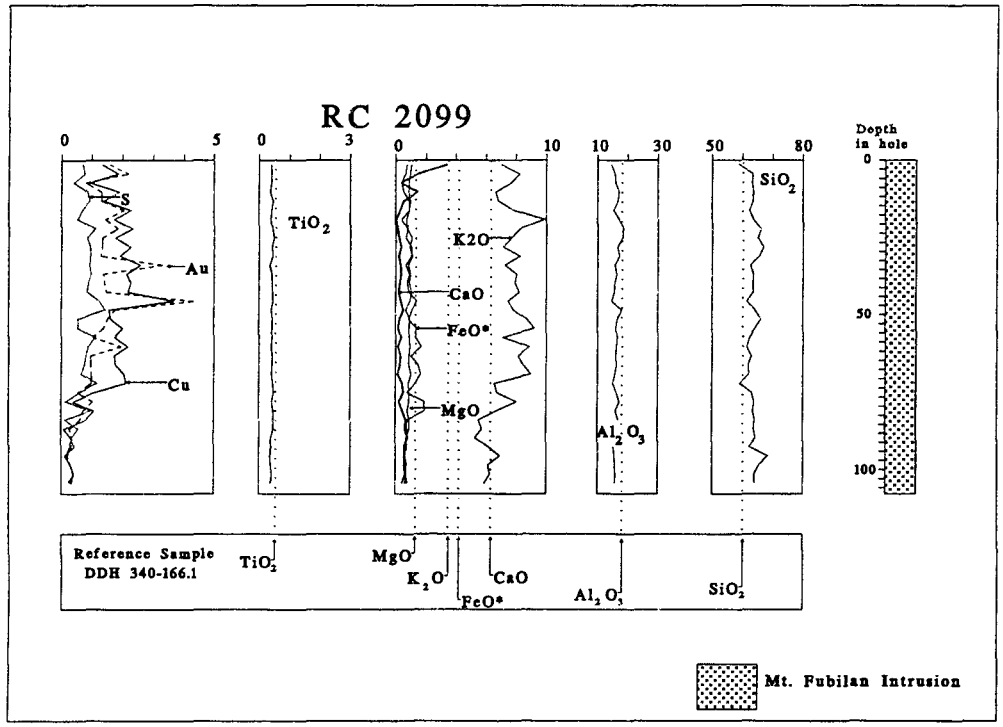

Figure 98: Lithic and selective chemical summary log of drill hole RC 2099.

weight percent and shows little variation with depth. Al_2O_3 is slightly lower than the reference sample throughout most of the drilled interval. It ranges from about 14.5 to 18.5 weight percent and averages 16.25. FeO^* varies from 0.41 to 1.92 weight percent and is strongly depleted with respect to the reference sample. MgO content shows little variation with depth in this drill hole. It ranges in abundance from 0.6 to about 1.1 weight percent and averages 0.86. CaO is fairly constant in abundance below a depth of 9 meters and ranges in abundance from 0.05 to 0.82 weight percent. It averages about 0.40 weight percent. The peaks in CaO near the top of the hole reflect contamination of the samples by limestone sheeting used to armor roads and drill benches. K_2O ranges from 5.2 to 9.9 weight percent. The range in K_2O displayed in this drill hole, like that of RC-1990, is approximately the same as that shown in the contoured plan map of Figure 95. Both gold and copper are of ore grade for about two-thirds of this drill hole; the averages for the entire hole are 1.23 ppm and 1.52 weight percent respectively. The variations in gold and copper displayed in the data from this drill are different from those of RC-1990 in that they are not accompanied by similar changes in FeO* content.

Drill hole RC-1988, which is collared in intrusive rock and bottoms in hornfels is portrayed in Figure 99. CaO, Al_2O_3, and FeO values are fairly constant in this drill hole and are similar in intrusive rock and hornfelsed siltstone suggesting that metasomatism in the zone of potassic alteration has produced a homogenization of the whole rock chemistry of intrusive rocks and

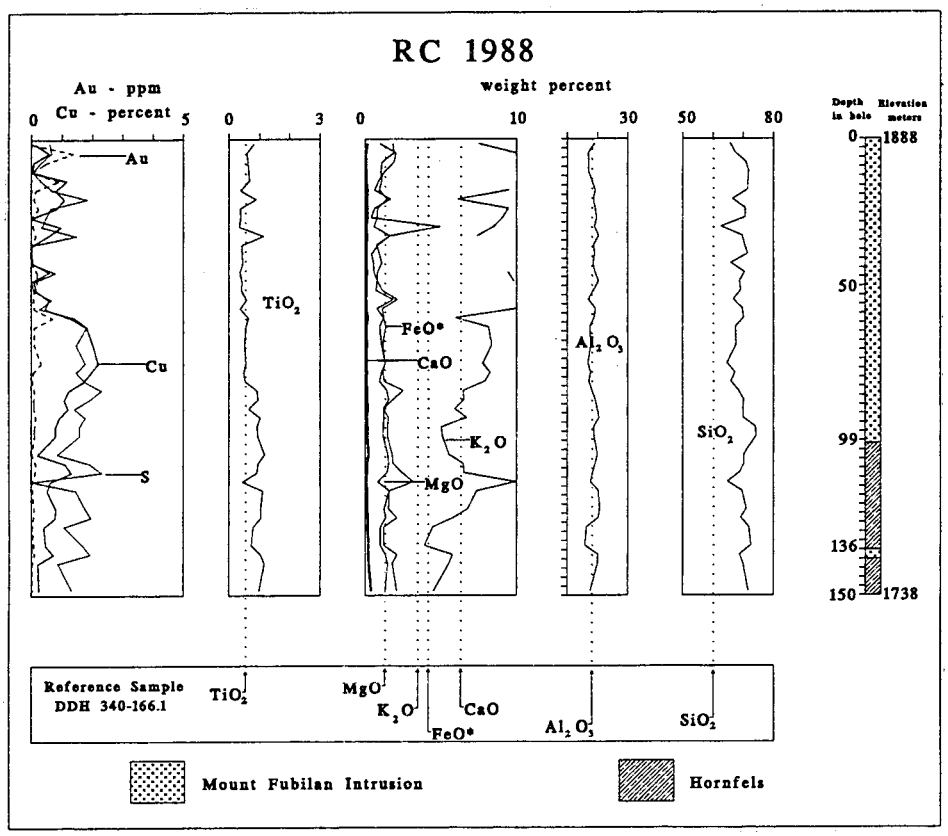

Figure 99: Lithic and selective chemical summary log of drill hole RC 1988.

metasedimentary siltstones alike. The SiO_2 ranges from content is consistently higher than in DDH 340-166.1. The TiO_2 content increases in abundance from an average of 0.58 in intrusive rock to 0.91 in hornfelsed siltstone. The average abundance of TiO_2 in the Fubilan Intrusion is about 0.44 weight percent and is about 0.71 in the Ieru Formation. Copper is of ore grade in the middle portion of the drill hole and remains elevated in the siltstone indicating that copper has been deposited in host rocks as well as in intrusive rocks.

The data portrayed in the contoured plan map and drill logs given in this chapter demonstrate a sustained and continuous increase in the K_2O content of the Mount Fubilan Intrusion compared to the unaltered rock of the Sydney intrusion. The increase in K_2O from about 3.9 weight percent in the reference samples to an average of 7.0 weight percent in the Mount Fubilan Intrusion is accompanied by a dramatic and continuous reduction in the CaO content (from 6.37 to 0.48). CaO shows an antipathetic relationship to K_2O. Hydrothermal alteration has virtually eliminated CaO from the Mount Fubilan intrusion while greatly increasing the abundance of K_2O. Less impressive but significant are the generally lower average values of FeO^* (1.89 wt. %) and MgO (0.75 wt. %) with respect to the reference specimen (4.89 wt. % FeO^* and 1.31 wt. % MgO). The striking geochemical feature shown in the drill hole summary is the near linear distribution of the major oxide data with respect to depth and lithology. Variations from average values are relatively small and much of the variation may be within the limits of analytical

error. This behavior demonstrates the pervasive nature of potassic hydrothermal alteration in the Mount Fubilan intrusion as opposed to selective or vein-veinlet alteration.

Metasomatic Gains and Losses

The metasomatic transformation of a parent rock of one chemical composition and mineral assemblage to form a daughter rock with a different chemical and mineral assemblage involves changes in the concentrations of the major oxide and trace element components of the rock, and may also alter density and volume. Some chemical elements remain immobile during alteration. Others are transported into the system where they may undergo reactions with pre-existing minerals or precipitate to form new minerals. Still other chemical components are liberated in the process of alteration. They become mobile upon dissolution into the hydrothermal fluids, where subsequently they will be reprecipitated nearby or transported out of the system entirely. The amount of matter that is added to a system is referred to as a *gain* and the amount removed from the system is referred to as a *loss*. Mathematical formulae devised to describe the mass transfer of components in a hydrothermal system have been proposed by Gresens (1967) and Grant (1986). Grant (1986) provided a graphical approach to Gresens' method, the

isocon diagram, that allows for the presentation of data and from which chemical differences can be estimated by measuring the distances between points on a graph.

The equation defined by Gresens is given below:

$$X_n = [f_v(\rho^B/\rho^A)C_n^B - C_n^A]a \qquad \text{Equation 1}$$

Where X_n is the gain or loss of component n with respect to a reference (unaltered) rock, ρ^A and ρ^B are the specific gravities of the assumed protolith and the altered rock, and the volume factor (f_v) is the amount by which the volume of solid reactants must be multiplied in order to obtain the volume occupied by the products (Gresens, 1967). Grant (1986) suggested that the term f_v in the Gresens equation relates to mass, not to volume. The values C_n^A and C_n^B refer to the concentrations of component n in the protolith and in the altered rock respectively, and a is the reference mass of the original sample (commonly assigned a value of 100 grams).

The first step in applying either the Gresens equation or the isocon method is to identify the pre-alteration composition of an altered rock (Grant, 1986). Ideally, this composition comes from an analysis of an unaltered sample, but if one is not available a least-altered sample indicates the direction of alteration. This is a very important step and is accomplished by careful consideration of the field relations and petrographic characteristics of the local geologic setting. The sample that I consider to be least-altered, DDH 340-166.1, is from the Sydney Intrusion. It

contains modal pyroxene, biotite, and sphene, and has diopside in its norm. Although the Sydney Intrusion exhibits weak propylitic alteration, areas of localized strong propylitic alteration, and endoskarn, this sample contains only a trace amount of the minerals that are characteristic of propylitic alteration (epidote, chlorite, actinolite). The sample is phaneritic in texture and is a quartz monzodiorite, based on modal analysis. The major oxide and trace element abundances of this sample and of the samples that will be compared to it in this chapter are given in Table 22.

The chemical analyses of an original and an altered rock cannot be directly compared to estimated gains and losses until a reference frame, or assumption, has been made (Potdevin, 1993). The assumptions commonly used in mass balance calculations are that either the overall volume or mass of a system is conserved, or that one or more components (such as Al_2O_3, TiO_2, the rare-earth elements, or Zr) have remained immobile throughout the alteration process.

Isocon diagrams are prepared by plotting the oxide and element values of a least-altered rock against the same values in a sample of altered rock. A line based on one of the above assumptions and plotted on the isocon diagram is referred to as an *isocon* or *line of equal concentrations*. The metasomatic gains and losses of an altered rock are calculated by determining the difference between a predicted value of each oxide or element based on the isocon versus their values in the altered

SAMPLE	340-166.1	331-218.5	356-166.5	319-276.1	319-339.3	321-263.1	JDD-94-04	302-069
Intrusion	Sydney	Sydney	Ningi	Kalgoorlie	Kalgoorlie	Fubilan	Fubilan	Fubilan
Texture	phanerite	porphyry	phanerite	phanerite	phanerite	porphyry	porphyry	porphyry
Alteration	least alt.	least alt.	least alt.	least alt.	least alt.	potassic	potassic	potassic
SiO_2	60.10	60.10	58.90	59.00	57.90	61.90	63.50	64.20
TiO_2	0.54	0.51	0.68	0.76	0.68	0.42	0.40	0.36
Al_2O_3	18.10	18.20	17.70	18.50	17.70	18.30	17.30	18.00
Fe_2O_3	3.46	3.14	3.24	3.86	3.94	2.20	0.00	1.02
FeO	1.07	1.39	1.67	1.64	2.21	1.07	1.37	0.25
MnO	0.10	0.12	0.08	0.06	0.08	0.03	0.02	0.02
MgO	1.31	1.14	1.29	1.24	1.43	0.92	0.68	0.34
CaO	6.37	6.30	4.01	5.06	5.78	0.43	0.14	0.08
Na_2O	4.16	3.93	5.33	5.14	4.49	4.44	3.49	1.61
K_2O	3.48	4.10	4.54	4.03	4.05	6.13	9.27	13.20
P_2O_5	0.25	0.22	0.31	0.35	0.35	0.07	0.11	0.08
H_2O^+	0.26	0.13	0.11	0.28	0.15	1.76	0.49	0.31
S	0.02	0.03	0.43	0.05	0.26	0.10	0.75	0.01
F in ppm	480	240	1130	1100	620	1840	1760	680
Sum	99.28	99.31	98.29	99.97	99.02	97.77	97.52	99.48
XRF-determined values								
Rb	84	92	114	90	88	130	187	280
Sr	1220	1270	1480	1440	1490	539	364	230
Ba	688	944	751	705	648	874	639	708
Nb	13	12	16	14	15	12	12	12
Zr	246	251	275	252	248	197	176	155
Y	29	27	23	27	25	22	25	26
S.G.	2.68	2.70	2.58	2.57	2.67	2.34	2.38	2.23
INAA-determined values								
Cr	75.10	66.30	2.20			6.00	65.60	61.80
Co	4.07	4.10	9.30			1.52	1.33	1.71
Ni	27	22	22			22	<57	<42
Zn	166	60	51			53	30	51
W	<6	<4.5	2.20			1.10	8.30	7.90
Cs	0.47	1.14	0.89			0.72	0.60	0.82
Sc	5.96	4.97	7.31			9.26	7.59	3.70
Ta	0.59	0.55	0.82			0.68	0.69	0.67
La	48.9	38.1	43.6			24.4	37.1	35.9
Ce	87.5	82.4	79.4			49.2	68.9	62.0
Nd	35.1	37.0	34.9			25.9	27.3	23.6
Sm	7.16	7.29	7.34			6.30	4.85	4.26
Eu	1.90	2.13	1.98			1.50	1.50	1.23
Tb	0.72	0.85	0.72			0.65	0.60	0.49
Yb	2.20	2.24	1.82			1.54	2.72	1.74
Lu	0.29	0.29	0.27			0.26	0.30	0.17
Hf	5.26	5.25	5.51			4.84	4.82	4.69
Th	8.19	7.76	11.60			8.80	8.19	7.70
U	2.40	1.70	2.78			2.99	5.00	2.70

Table 22: Geochemical data for the rock samples used to estimate hydrothermal gains and losses. Major oxides in weight percent, all other elements are listed in ppm.

sample. In general, all isocons are produced from linear equations in the form of:

$$y = bx + c \qquad \textbf{equation 2}$$

where y is a predicted value, b is the slope of the line, x is a known value, and c is the y-axis intercept. Grant (1986) derived a set of equations to calculate isocons for systems in which volume is constant, or a single oxide component, Al_2O_3, is assumed to be immobile. These equations are given below.

$$C^B=(\rho^A/\rho^B)C^A \qquad \text{constant volume} \qquad \textbf{equation 3}$$

$$C^B = (C^B_n/C^A_n)C^A \qquad \mathbf{n=Al_2O_3} \qquad \text{constant alumina} \qquad \textbf{equation 4}$$

The slope of these isocons is equal to (ρ^A/ρ^B) if volume is constant, and to (C^B_n/C^A_n) if a single constituent (Al_2O_3 in this example) is immobile. The isocon is usually drawn so that it passes through the origin of the diagram, therefore the value of the y-axis intercept (c) is usually zero. The major oxides or trace elements that plot on or near an isocon are considered to have been immobile during alteration, and those that do not are considered to have been mobile. Elements or oxides that plot above an isocon represent gains, whereas those that plot below it represent losses. The gains and losses of chemical constituents are estimated by determining the difference between the predicted concentration of an element or oxide in grams per 100 grams of rock, or ppm, taken from an isocon, and that of an altered sample. The differences can be determined either by measuring off the isocon diagram, or

mathematically by subtracting the expected value of each constituent from the actual value present in the altered rock.

The volumes of bodies of rock such as igneous plutons or zones of metasomatic alteration are commonly considered to remain constant before and after alteration in calculations involving altered rocks (Lindgren, 1918, 1924, 1933; Mackin, 1968). Lindgren proposed a "law of equal volumes" based on the measurement of stratigraphic units across a number of zones of alteration. His arguments were made in regard to the metamorphism and metasomatism of siliciclastic and carbonate rocks, but they should apply equally well to intrusive rocks. The constant volume assumption has been employed by many authors since Lindgren proposed the law of equal volumes, but changes in volume may occur nonetheless, and it is not uncommon today for researchers to assume that some other factor than volume has been conserved in a metasomatic event. An example of the calculation of an isocon based on the constant volume assumption along with representative differences of CaO (loss) and K2O (gain) of a altered sample (DDH 302-69) compared to an unaltered reference sample (DDH 340-166.1) is given below.

Example calculation using the constant volume assumption:

$C^B=(\rho^A/\rho^B)C^A$ constant volume **equation 3**

The densities of reference sample (DDH 340-166.5) and sample DDH 302-069 are 2.68 and 2.23 respectively. The predicted value for an example oxide taken from Table 22, CaO, is:

C^B = (2.68/2.23)*6.37 = 7.66 grams/100 grams

The actual measured value of C^B is 0.08 which is less than the predicted value therefore the rock has a calculated loss of: **actual value - predicted value** = 0.08 - 7.66 = -7.58 g/100 g as given in Table 23.

and for another example, the predicted value of K_2O is:

C^B = (2.68/2.23)*3.48 = = 4.18 grams/100 grams

The actual measured value of C^B is 13.2 which is greater than the predicted value therefore the rock has a calculated gain of: **actual value - predicted value** = 13.20 - 4.18 = 9.02 grams/100 grams as given in Table 23.

Metasomatic gains and losses for unaltered and potassically altered intrusive rocks from the Ok Tedi Intrusive Complex based on the constant volume assumption are given in Table 23.

The conservation of a single component such as Al_2O_3, TiO_2, or Zr is also a common assumption in studies of metasomatic alteration. These chemical components are only weakly soluble in most natural waters (Ellis and Mahon, 1977; Taylor and McLennen, 1985), and the choice of these elements as immobile components has yielded plausible results in the calculation of mass transfer in studies of altered rocks by several authors, including Zech and others (1988) and Kalsbeek (1992). This assumption has, however, been found invalid in other

Sample	331-218.5	356-166.5	319-276.1	319-339.3	321-263.1	JDD-94-04	302-069
Intrusion	Sydney	Ningi	Kalgoorlie	Kalgoorlie	Fubilan	Fubilan	Fubilan
Texture	porphyry	phanerite	phanerite	phanerite	porphyry	porphyry	porphyry
Alteration	least alt.	least alt.	least alt.	least alt.	potassic	potassic	potassic
				absolute gains and losses - grams/100 grams			
SiO_2	0.45	-3.53	-3.67	-2.43	-6.93	-4.18	-8.03
TiO_2	-0.03	0.12	0.2	0.14	-0.2	-0.21	-0.29
Al_2O_3	0.23	-1.1	-0.37	-0.47	-2.43	-3.08	-3.75
Fe_2O_3	-0.29	-0.35	0.25	0.47	-1.76	-3.9	-3.14
FeO	0.33	0.56	0.52	1.14	-0.16	0.17	-1.04
MnO	0.02	-0.02	-0.04	-0.02	-0.08	-0.09	-0.1
MgO	-0.16	-0.07	-0.13	0.12	-0.58	-0.8	-1.23
CaO	-0.02	-2.61	-1.58	-0.61	-6.87	-7.03	-7.58
Na_2O	-0.2	1.01	0.8	0.31	-0.32	-1.19	-3.39
K_2O	0.65	0.93	0.4	0.56	2.14	5.35	9.02
P_2O_5	-0.03	0.05	0.09	0.1	-0.22	-0.17	-0.22
H_2O^+	-0.13	-0.16	0.01	-0.11	1.46	0.2	0
S	0.01	0.41	0.03	0.24	0.08	0.73	-0.01
Sum of gains	1.7	3.1	2.3	3.1	3.7	6.5	9.0
Sum of losses	-0.9	-7.8	-5.8	-3.6	-19.6	-20.7	-28.8
				absolute gains and losses - ppm			
F	-236	631	599	138	1290	1219	103
Rb	9	27	2	4	34	92	179
Sr	59	213	168	265	-858	-1010	-1236
Ba	261	36	-12	-43	86	-136	-119
Nb	-0.9	2.5	0.0	2.0	-2.9	-3.0	-4.0
Zr	7	19	-5	1	-85	-101	-141
Y	-1.8	-7.1	-3.0	-4.0	-11.2	-8.0	-9.0
Cr	-8.2	-75.8			-80.0	-19.0	-28.5
Co	0.1	5.1			-3.1	-3.3	-3.2
Zn	-105	-121			-137	-157	-149
Cs	0.7	0.4			0.2	0.1	0.3
Sc	-1.0	1.1			2.4	0.9	-3.5
Ta	0.0	0.2			0.0	0.0	0.0
La	-10.4	-7.2			-31.6	-18.0	-22.9
Ce	-4.5	-11.5			-51.0	-29.6	-43.2
Nd	2.2	-1.6			-14.3	-12.2	-18.6
Sm	0.2	-0.1			-1.9	-3.2	-4.3
Eu	0.2	0.0			-0.7	-0.6	-1.1
Tb	0.1	0.0			-0.2	-0.2	-0.4
Yb	0.1	-0.5			-1.0	0.2	-0.9
Lu	0.0	0.0			-0.1	0.0	-0.2
Hf	0.0	0.1			-1.2	-1.1	-1.6
Th	-0.4	3.1			-0.6	-1.0	-2.1
U	-0.7	0.3			0.2	2.3	-0.2
Sum of gains	339	939			1413	1315	282
Sum of losses	-369	-225			-1280	-1503	-1787
slope of isocon	0.99	1.04	1.04	1.00	1.15	1.13	1.20
change in mass %	0.7	-3.7	-4.1	-0.4	-12.7	-11.2	-16.8
change in volume %	0	0	0	0	0	0	0

Table 23: Gains and losses of elements and oxides at constant volume in least-altered and altered samples compared to reference sample DDH 340-166.56.

studies (Dipple and others, 1990; Olsen and Grant, 1991; Rubin and others, 1993; and Marshall and Mancini, 1994). Metasomatic gains and losses for unaltered and potassically altered intrusive rocks from the Ok Tedi Intrusive Complex based on the assumption of constant alumina are given in Table 24.

Isocons based on several elements are also common in studies of metasomatic alteration. The usual practice is to choose an isocon based on a least squares equation that includes the most possible constituents, and that fits a straight line through the origin (Grant, 1986; Baumgartner and Olsen, 1995).

The lanthanides, or rare-earth elements (La, Ce, Pr, Nd, Sm, Eu, Gd, Tb, Dy, Ho, Er, Tm Yb, Lu), have been considered immobile in many petrographic studies. These inner transition metals all have essentially the same atomic radii and electrical charge, and their chemical properties are so similar, that, except for Eu, they are not easily separated or fractionated in the chemical reactions that occur in magmas and hydrothermal solutions.

In addition oxygen has also been considered as an immobile constituent by investigators such as Rubie (1982) and Potdevin (1993).

Several mineralogical and chemical factors noted in previous chapters provide constraints on the choice of the element or elements that can be used to define a reference frame for the altered intrusive rocks at Ok Tedi. Particularly obvious is the evidence for mobility of K_2O and CaO, shown by the replacement of andesine by potassium feldspar, and by the behavior of these oxides in Harker

Sample	331-218.5	356-166.5	319-276.1	319-339.3	321-263.1	JDD-94-04	302-069
Intrusion	Sydney	Ningi	Kalgoorlie	Kalgoorlie	Fubilan	Fubilan	Fubilan
Texture	porphyry	phanerite	phanerite	phanerite	porphyry	porphyry	porphyry
Alteration	least alt.	least alt.	least alt.	least alt.	potassic	potassic	potassic
				absolute gains and losses - grams/100 grams			
SiO_2	-0.33	0.13	-2.43	-0.87	1.14	6.06	4.43
TiO_2	-0.03	0.15	0.21	0.15	-0.13	-0.12	-0.18
Al_2O_3	0	0	0	0	0	0	0
Fe_2O_3	-0.34	-0.14	0.32	0.56	-1.3	-3.31	-2.42
FeO	0.31	0.62	0.55	1.16	-0.01	0.35	-0.81
MnO	0.02	-0.02	-0.04	-0.02	-0.07	-0.08	-0.08
MgO	-0.18	0.01	-0.1	0.15	-0.4	-0.57	-0.96
CaO	-0.11	-2.22	-1.45	-0.45	-6.01	-5.95	-6.25
Na_2O	-0.25	1.26	0.89	0.42	0.23	-0.49	-2.53
K_2O	0.6	1.14	0.47	0.65	2.61	5.94	9.74
P_2O_5	-0.03	0.07	0.09	0.11	-0.18	-0.13	-0.17
H_2O^+	-0.13	-0.14	0.01	-0.1	1.5	0.24	0.05
S	0.01	0.41	0.03	0.24	0.08	0.73	-0.01
Sum of Gains	0.9	3.8	2.6	3.4	5.6	13.3	14.2
Sum of Losses	-1.4	-2.5	-4.0	-1.4	-8.1	-10.7	-13.4
				absolute gains and losses - ppm			
F	-243	661	609	151	1355	1301	203
Rb	8	32	4	6	45	107	196
Sr	43	287	193	297	-694	-802	-983
Ba	252	78	2	-25	178	-19	24
Nb	-1.0	3.0	0.7	2.3	-1.0	0.0	-1.0
Zr	4	34	1	7	-52	-59	-90
Y	-2	-5	-3	-3	-7	-3	-3
Cr	-9.2	-71.2			-69.9	-6.2	-12.9
Co	0.0	5.3			-2.6	-2.6	-2.3
Zn	-107	-111			-115	-129	-114
Cs	0.7	0.4			0.2	0.2	0.4
Sc	-1.0	1.5			3.2	1.9	-2.2
Ta	0.0	0.2			0.1	0.1	0.1
La	-11.1	-4.2			-25.0	-9.6	-12.7
Ce	-5.6	-6.2			-39.3	-14.7	-25.0
Nd	1.7	0.6			-9.6	-6.3	-11.3
Sm	0.1	0.3			-0.9	-2.0	-2.9
Eu	0.2	0.1			-0.4	-0.3	-0.7
Tb	0.1	0.0			-0.1	-0.1	-0.2
Yb	0.0	-0.3			-0.7	0.6	-0.5
Lu	0.0	0.0			0.0	0.0	-0.1
Hf	0.0	0.4			-0.5	-0.2	-0.5
Th	-0.5	3.6			0.5	0.4	-0.4
U	-0.7	0.4			0.6	2.7	0.3
Sum of Gains	310	1108			1583	1414	424
Sum of Losses	-381	-199			-1018	-1054	-1263
slope of isocon	1.01	0.98	1.02	0.98	1.01	0.96	0.99
change in mass %	-0.5	2.3	-2.2	2.3	-1.1	4.6	0.6
change in volume %	-1	6	2	3	13	18	21

Table 24: Gains and losses of elements and oxides at constant Al_2O_3 in least-altered and altered samples compared to reference sample DDH 340-166.56.

variation and Peacock diagrams (Figures 59-62, and 75). The behavior of Rb and Sr, shown in Figure 87, provides evidence that one or both of these elements became mobile as would be expected because Rb behaves geochemically the same as K_2O and Sr the same as CaO. The presence of quartz veinlets at many locations throughout the zone of potassic alteration, particularly in the quartz core, may indicate that SiO_2 was added to the system from without, or may merely represent redistribution of the oxide within the system, but in either case documents the mobility of this oxide. Therefore, none of these oxides or elements can be expected to define an isocon. In contrast, TiO_2, which occurs principally as rutile pseudomorphs after sphene in altered samples, may have remained immobile and may be useful in defining an isocon. The amount of the mineral zircon in thin-sections of altered and unaltered samples is not greatly different, suggesting that Zr may also have been immobile.

The locations of the samples discussed in this chapter are given in Figure 100. Isocon diagrams constructed based on three different assumptions are given in Figures 101-106. The three assumptions are: (1) constant volume, (2) constant Al_2O_3, and (3) constant rare-earth elements (REE), TiO_2, Y, and Zr. The last set of constituents was chosen by visual examination of the isocon diagrams and for the mineralogical considerations discussed earlier. Calculations of gains and losses for altered and unaltered samples compared to the reference sample of unaltered rock

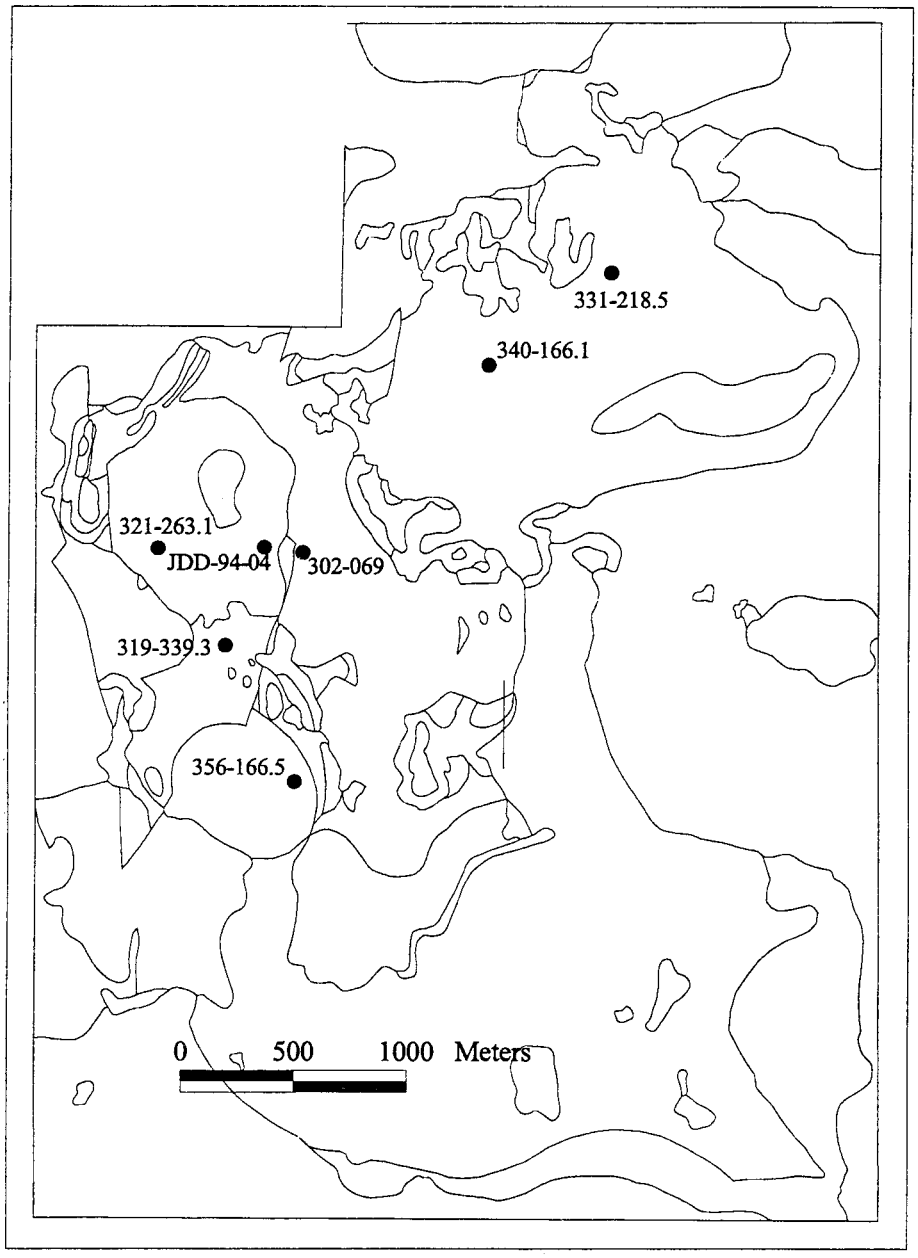

Figure 100: Approximate locations of the samples included in this discussion of hydrothermal gains and losses

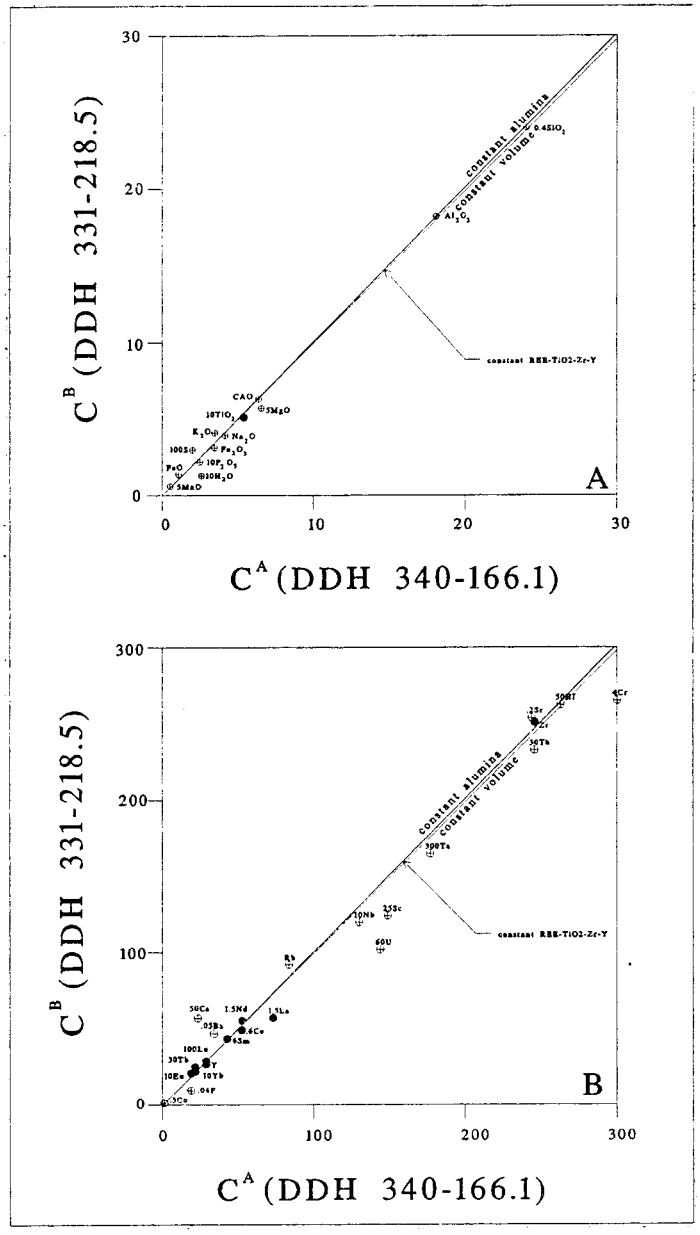

Figure 101: Isocon diagrams comparing major oxide (A) and trace-elements concentrations (B) of reference sample DDH 340-166.1, a phanerite from the Sydney Intrusion, and a sample of unaltered rock with porphyritic texture (DDH 331-218.5) from the Sydney Intrusion. Filled symbols comprise the rare-earth elements, TiO_2, Y, and Zr.

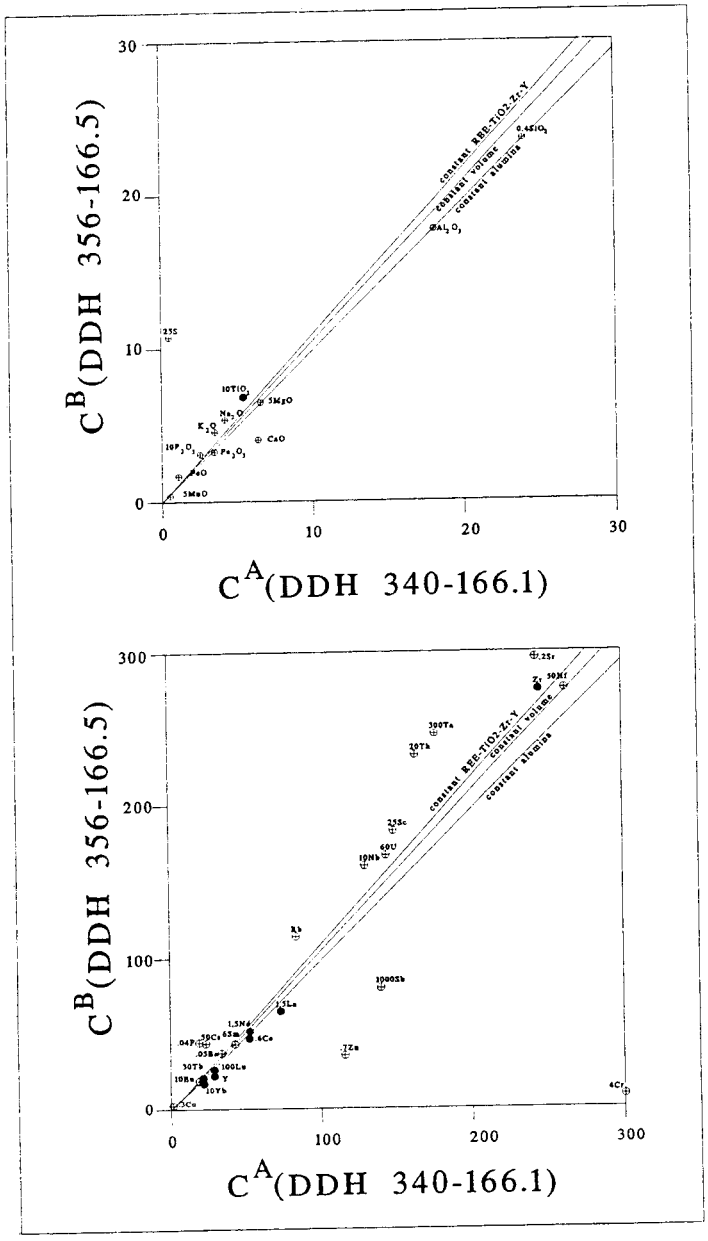

Figure 102: Isocon diagrams comparing major oxide (A) and trace-elements concentrations (B) of reference sample DDH 340-166.1, a phanerite from the Sydney Intrusion, and a sample of least-altered rock with phaneritic texture (DDH 356-166.5) from the Ningi Intrusion. Filled symbols comprise the rare-earth elements, TiO_2, Y, and Zr.

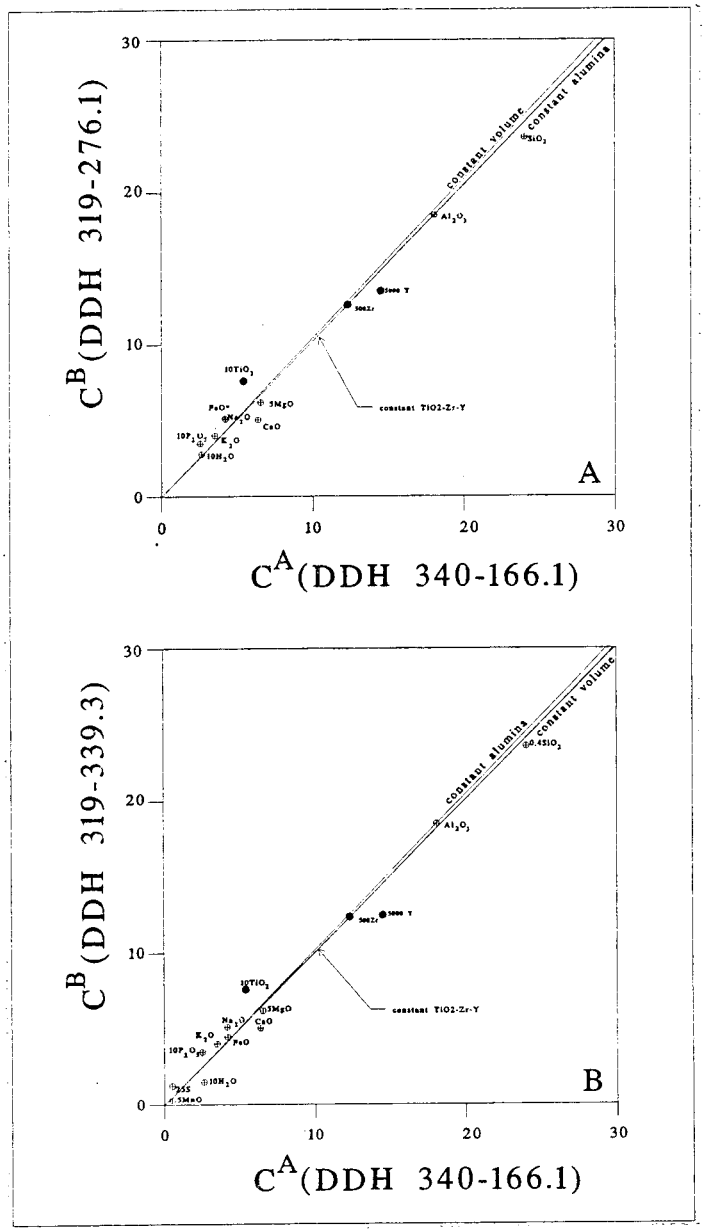

Figure 103: Isocon diagrams comparing major oxide concentrations and Y and Zr contents of reference sample DDH 340-166.1, a phanerite from the Sydney Intrusion, and two samples of least-altered rock with phaneritic texture from the Kalgoorlie Intrusion:
(A) DDH 319-276.1, and (B) DDH 319-339.3 Filled symbols comprise TiO_2, Y, and Zr.

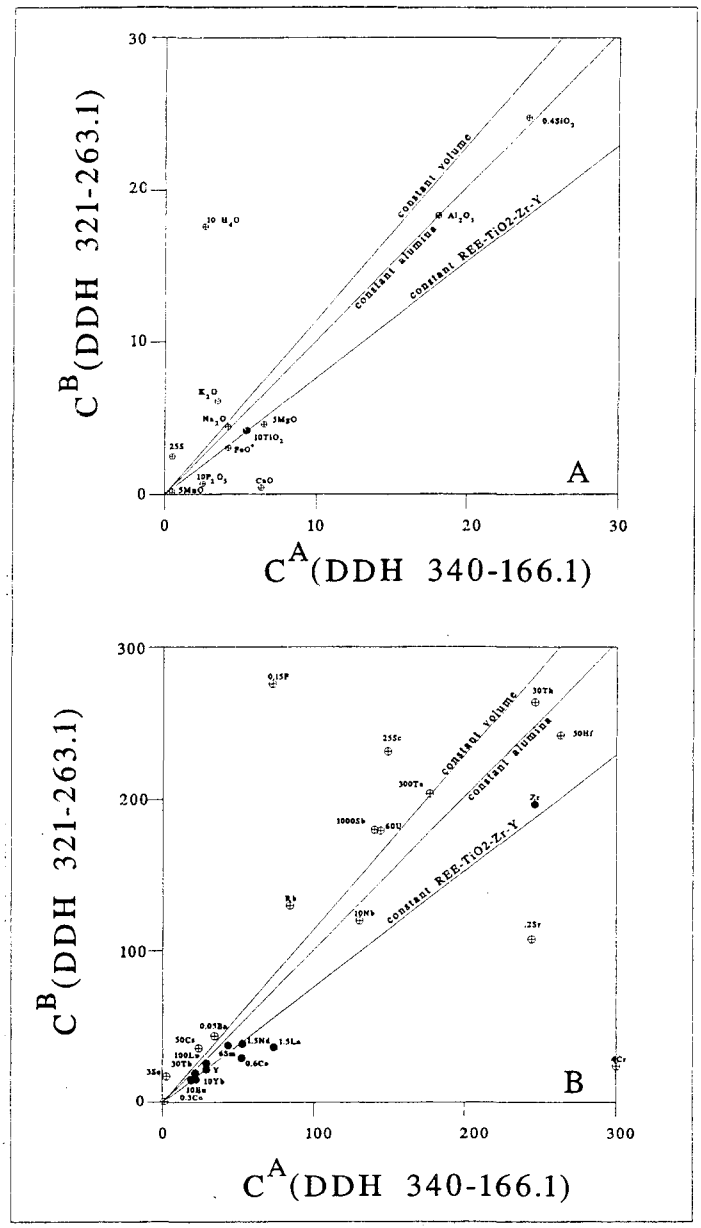

Figure 104: Isocon diagrams comparing major oxide (A) and trace-elements concentrations (B) of reference sample DDH 340-166.1, a phanerite from the Sydney Intrusion, and a sample of potassically-altered rock with porphyritic texture (DDH 321-263.1) from the Fubilan Intrusion. Filled symbols comprise the rare-earth elements, TiO_2, Y, and Zr.

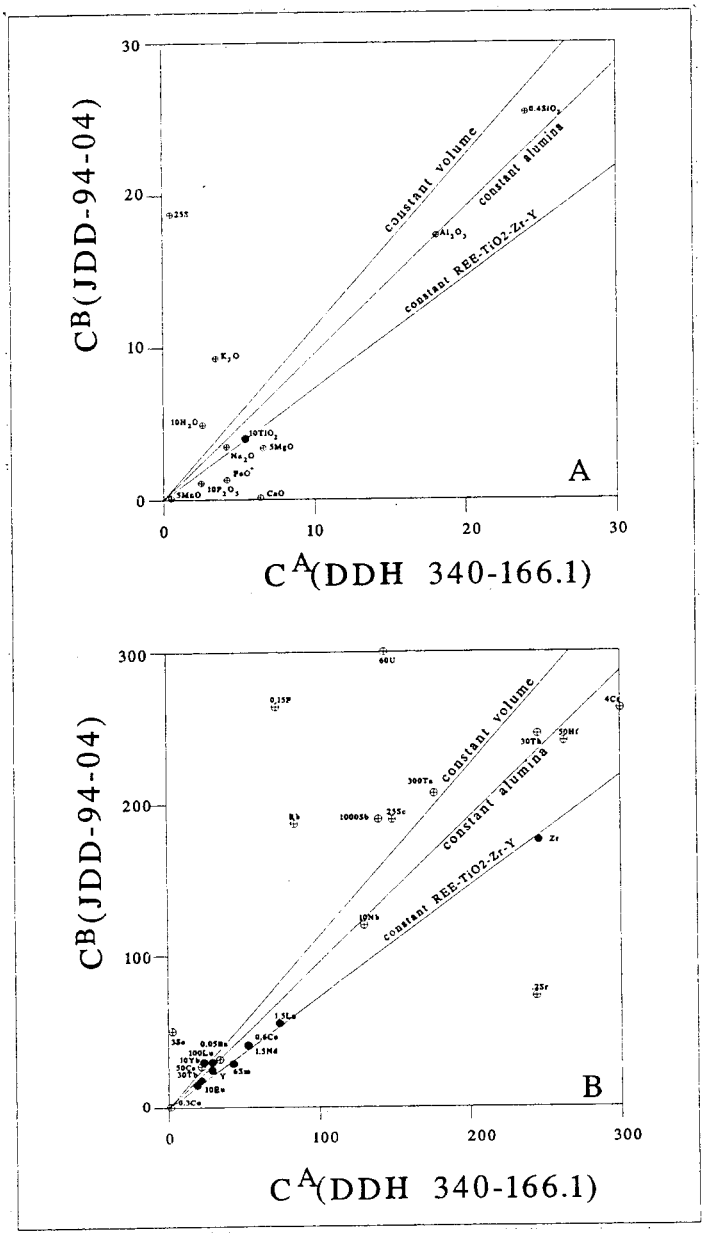

Figure 105: Isocon diagrams comparing major oxide (A) and trace-elements concentrations of reference sample DDH 340-166.5, a phanerite from the Sydney Intrusion, and a sample of potassically-altered rock with porphyritic texture (JDD-94-04) from the Fubilan Intrusion. Filled symbols comprise the rare-earth elements, TiO_2, Y, and Zr.

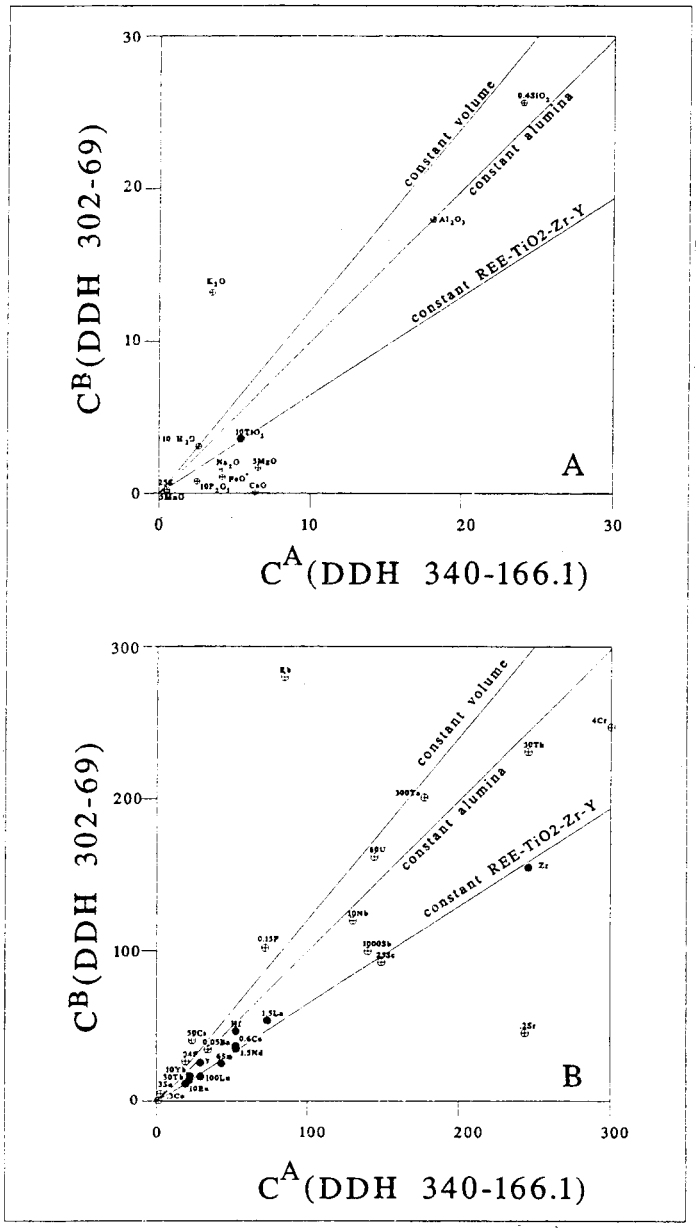

Figure 106: Isocon diagrams comparing major oxide (A) and trace-elements concentrations of reference sample DDH 340-166.1, a phanerite from the Sydney Intrusion, and a sample of extremely potassically-altered rock with porphyritic texture (DDH 302-69) from the Sydney Intrusion. Filled symbols comprise the rare-earth elements, TiO_2, Y, and Zr.

SAMPLE	331-218.5	356-166.5	319-276.1	319-339.3	321-263.1	JDD-94-04	302-69
Intrusion	Sydney	Ningi	Kalgoorlie	Kalgoorlie	Fubilan	Fubilan	Fubilan
Texture	porphyry	phanerite	phanerite	phanerite	porphyry	porphyry	porphyry
Alteration	least alt.	least alt.	least alt.	least alt.	potassic	potassic	potassic
absolute gains and losses - grams/100 grams							
SiO_2	-0.22	-6.15	-2.49	-2.57	15.95	19.77	25.36
TiO_2	-0.03	0.10	0.21	0.14	0.01	0.01	0.01
Al_2O_3	0.03	-1.89	-0.02	-0.51	4.46	4.13	6.30
Fe_2O_3	-0.33	-0.50	0.32	0.46	-0.45	-2.52	-1.22
FeO	0.32	0.51	0.55	1.13	0.25	0.59	-0.44
MnO	0.02	-0.03	-0.04	-0.02	-0.05	-0.05	-0.04
MgO	-0.17	-0.13	-0.10	0.11	-0.08	-0.27	-0.51
CaO	-0.09	-2.88	-1.46	-0.63	-4.44	-4.50	-4.04
Na_2O	-0.25	0.83	0.88	0.30	1.26	0.46	-1.08
K_2O	0.61	0.77	0.47	0.55	3.47	6.74	10.95
P_2O_5	-0.03	0.04	0.09	0.10	-0.12	-0.07	-0.08
H_2O^+	-0.13	-0.17	0.01	-0.11	1.56	0.30	0.14
S	0.01	0.41	0.03	0.24	0.08	0.74	0.00
Sum gains	0.99	2.66	2.56	3.03	27.04	32.74	42.76
Sum losses	-1.25	-11.75	-4.11	-3.84	-5.14	-7.41	-7.41
absolute gains and losses - ppm							
F	-242	610	609	137	1473	1411	370
Rb	8	23	4	3	66	126	226
Sr	46	160	192	263	-394	-524	-558
Ba	253	6	1	-44	348	138	263
Nb	-1.0	2.0	1.0	2.0	2.0	3.0	4.0
Zr	4	9	0	0	9	-3	-4
Y	-2.0	-8.0	-3.0	-4.0	0.0	4.0	7.0
Cr	-9.1	-79.1			-51.4	11.0	13.3
Co	0.0	4.9			-1.6	-1.6	-0.9
Zn	-107	-129			-74	-91	-56
Cs	0.7	0.4			0.4	0.3	0.5
Sc	-1.0	0.9			4.7	3.3	-0.2
Ta	0.0	0.2			0.2	0.3	0.3
La	-11.0	-9.3			-13.0	1.5	4.3
Ce	-5.4	-15.3			-17.7	5.2	5.5
Nd	1.8	-3.1			-0.9	1.8	0.9
Sm	0.1	-0.4			0.8	-0.4	-0.4
Eu	0.2	-0.1			0.1	0.1	0.0
Tb	0.1	-0.1			0.1	0.1	0.0
Yb	0.0	-0.6			-0.1	1.1	0.3
Lu	0.0	0.0			0.0	0.1	0.0
Hf	0.0	-0.2			0.8	1.0	1.3
Th	-0.5	2.7			2.5	2.2	2.4
U	-0.7	0.2			1.2	3.3	1.2
Sum gains	314	819			1909	1713	900
Sum losses	-379	-245			-553	-620	-620
slope of isocon	1.00	1.08	1.02	1.01	0.76	0.73	0.65
change in mass %	-0.4	-7.6	-2.3	-0.6	31	37	55
change in volume %	-1	-4	2	0	50	55	86

Table 25: Gains and losses of elements and oxides at constant REE, TiO_2, Zr, and Y in least-altered and altered samples compared to reference sample DDH 340-166.5.

(DDH 340-166.1) based on constant REE, TiO2, Y, and Zr are summarized in Table 25.

The isocon diagrams given in Figure 101-106 compare four examples of least-altered rocks from the Sydney, Kalgoorlie, and Ningi Intrusions and three samples of potassically-altered rock from the Fubilan Intrusion to a least-altered reference sample from the Sydney intrusion (DDH 340-166.1. The major and trace element concentrations are given in Table 22. Calculated absolute gains and losses based on each of the three assumptions are given in Tables 23-25. Absolute gains and losses are equal to value of each oxide or element in a sample compared to their predicted values based on isocons. Relative gains and losses (not listed in the tables) are equal to the absolute gains and losses divided by the value of each oxide or element in the reference sample. Data presented in the isocon diagrams in the figures of this chapter are scaled using the method of Grant (1986) in order to improve the clarity of graphical presentation by preventing the overlapping of data points. However, the numbers that appear in tables are calculated from data that have not been scaled. Some elements that are included in Table 22 have values less than the detection capability of the method used in analyses (W, Ni) or display erratic behavior (Cr, Zn), therefore these are not shown in the isocon diagrams.

Least-Altered Rocks of Sydney, Kalgoorlie, and Ningi Intrusions

Although, the isocon diagram was devised to compare changes in rocks that are different in composition, it is also an excellent method for comparing samples that are chemically similar because it provides a visual confirmation of this similarity for many oxide or element pairs on a single illustration.

Two hypotheses are tested in the following paragraphs using the isocon method. First, that the least-altered phaneritic and porphyritic rocks of the Sydney Intrusion are chemically identical, and second, that the least-altered rocks of the Kalgoorlie and Ningi Intrusions are chemically similar to those of the Sydney Intrusion.

A sample of pristine porphyry (DDH 331-218.5) is compared to the reference sample (DDH 340-166.1) in Figure 98. Major oxide contents are plotted in Figure 101A and trace element contents in Figure 101B. The three isocons (constant volume, constant alumina, and constant REE, TiO_2, Y, and Zr) are nearly coincident and the sums of gains and losses given in Tables 23-25 are small, the samples differing by less than 2.6 grams/100 grams regardless of which frame of reference is assumed. All of the major oxides except K_2O and MgO plot in contact with one or more of the isocons. Many of the trace elements also plot on or near the set of isocons. The variance of all the oxide and element components, including K_2O and MgO, can be attributed to routine error involved in sample selection, preparation, and analysis. The two intrusive rock samples are closely similar in

major oxides, trace elements, and specific gravity, despite the fact that one is porphyritic and the other phaneritic in texture. This chemical similarity supports a likely hypothesis that the two textural types of igneous rocks may have crystallized from a common magma. The textural variation between samples of these two rocks may relate to differences in cooling history, emplacement, and location of separate batches of a single magma, rather than to separate batches of two or more distinctly different magmas.

A sample of least-altered phaneritic intrusive rock (DDH 356-166.5) from diamond drill core taken from the Ningi Intrusion is plotted against the reference standard in Figure 102. This sample differs from that of the Sydney Intrusion by having edenite and biotite, rather than pyroxene and biotite, as ferromagnesian minerals. Its normative An content of 19.6 contrasts with a value of 36.8 in the reference sample. Sample DDH 356-166.5 also contains sparse, thin veinlets of pyrite. The three isocons are closely adjacent, but farther apart than those of the unaltered samples plotted in Figure 101. The major oxide contents of SiO_2, MgO, Fe_2O_3, FeO, and FeO^* plot on or near the line representing constant Al_2O_3. The K_2O, NaO_2, and TiO_2 contents of DDH 356-166.5 are slightly elevated with respect to the assumed isocons, whereas CaO is somewhat depleted. Most of the trace elements also plot on or nearby the isocons, but several (Rb and Sr, Nb, U, Sc, Th, and Ta) are slightly enriched relative to the reference sample. It is uncertain whether these variations represent analytical error, random variations, or

fundamental differences between the rocks. It is noteworthy that both Rb and Sr are enriched relative to the isocons, whereas these elements have antipathetic behavior in potassically altered samples from the Fubilan Intrusion. It is possible that Sr is enriched because of the presence of edenite in hornblende. The presence of pyrite is reflected by a S value that is enriched relative to the isocons. Fluorine is also elevated with respect to the reference sample (Table 22). This volatile element is likely present as a component of biotite and hornblende, where it substitutes for OH^-.

The major oxide and trace-element contents of two samples (DDH 319-276.1 and DDH 319-339.3) of least-altered phaneritic rock from the Kalgoorlie Intrusion are compared to the reference sample (DDH 340-166.1) in Figure 103. These samples have normative An contents of 26.3 and 30 respectively. Pyroxene is the ferromagnesian mineral of sample DDH 319-339.3 and probably is present in DDH 319-339.3 (which was not examined petrographically), although the fluorine content is high and may indicate the presence of hornblende. The isocons for constant volume and Al_2O_3 were prepared in the same manner as in the previous and subsequent diagrams, but the third isocon in Figure 103 includes only TiO_2-Y-Zr. The rare-earth elements are not included because instrumental neutron activation analyses (INAA) were not performed on any samples from the Kalgoorlie area. The constant volume, alumina, and TiO_2-Zr-Y isocons are virtually indistinguishable from one another and most of the major oxides plot reasonably

close to these isocons. However, CaO is moderately depleted with respect to the isocons and TiO_2 is moderately enriched.

The least-altered samples from the Kalgoorlie Intrusion are closely similar to the reference sample of unaltered rock from the Sydney Intrusion, suggesting that these two intrusions may have formed from a common batch of magma and that they may, in fact, constitute a single intrusion. The sample from the Ningi Intrusion shows small but significant differences in major-oxide and trace element contents compared to the reference sample. It is clear that the Ningi Intrusion is close in composition to the Sydney and Kalgoorlie Intrusions, but it is unclear as to whether or not it is unequivocally of the same composition. The Ningi Intrusion may instead represent a different batch of magma, the same magma that differentiated prior to solidification, or intrusive rocks formed from the same magma, but affected by weak hydrothermal alteration.

Potassically-Altered Rocks

Metasomatic gains and losses for three hydrothermally altered samples (DDH 321-263.1, JDD-94-04, and DDH 302-69) from the Fubilan Intrusion are listed in Tables 23-25. These three samples were selected for discussion in this chapter because each is representative of one of the K_2O intervals on the contour diagram given by Figure 95. All three of the samples are characterized by the presence of corundum and hypersthene in their norms, by a predominance of

potassium feldspar, and by having albite as their plagioclase feldspar. In thin-section they display partial or complete pseudomorphs of orthoclase after plagioclase feldspar; hydrothermal biotite is the only ferromagnesian mineral present, and all magmatic sphene has been altered to rutile. The K_2O content of sample DDH 302-69 at 13.2 weight percent is the highest of any of the grab, DDH, or RC samples, and it typifies extreme potassium feldspar alteration.

Isocon diagrams for each of the three samples are presented in Figures 104-106 in the same manner as in the previous discussion concerning unaltered rocks. The most striking features of these diagrams are the distinctly different slopes of the isocons representing constant volume, Al_2O3, the rare-earth elements, TiO_2-Zr-Y, and the progressive changes in FeO^*, CaO, Na_2O, K_2O, Rb, and Sr.

If any one of the three reference frames is assumed valid, then considerable change in rock chemistry must have taken place, which negates the validity of the other two reference frames. If volume was constant during alteration, then Al_2O_3, the rare-earth elements, TiO_2, Zr, and Y must have been mobile and transported out of the system. If Al_2O_3 remained immobile and constant, then the rare-earth elements, TiO_2, Zr, and Y must have been removed from the system, and both the volume and overall mass of the altered sample must have changed during hydrothermal alteration. And finally, if the rare-earth elements, TiO_2, Zr, and Y remained constant, then Al_2O_3 had to have been added to the system, and its mass and volume must have increased drastically.

Changes in the total mass and volume of a rock after alteration, compared to the mass and volume before alteration, are defined by Grant (1986) as:

change of mass = (1/slope of isocon) - 1 **equation 5**

change of volume = (1/slope of isocon)*(ρ^A/ρ^B) - 1 **equation 6**

Solutions of these equations for the three samples from the Fubilan Intrusion using the assumption that the rare-earth elements, TiO_2, Zr, and Y (Tables 25) remained immobile suggest that mass gains of 31, 37, and 55 percent, and volume gains of 50, 55, and 86 percent, respectively, would be required to convert a protolith such as DDH 340-166.5 to produce samples DDH 321-263.1, JDD-94-04, and DDH 302-69 (Table 25). Such extreme changes in mass and volume are geologically unlikely, and imply that rather than being conserved, these commonly assumed immobile oxides and elements must have become mobile and were removed by hydrothermal fluids.

If volume is considered constant, then losses in mass of 13, 11, and 17 percent are implied for the three samples (Table 23), whereas if Al_2O_3 was immobile and unchanged during alteration, then smaller changes in mass (1, 5, and 1 percent) are required (Table 24), but volumes must have increased by 13, 18, and 21 percent.

Large gains in K_2O and Rb and large losses of CaO and Sr are indicated regardless of which of these three frames of reference, if any, is appropriate. Lesser, but significant losses in FeO^*, MgO, and P_2O_5 are indicated by the isocon

diagrams (Figures 104-106) and the calculations summarized in Tables 23-25. The Na_2O contents of the samples decrease progressively with increasing K_2O content. Changes in all other oxide and trace element components are equivocal or dependent on which assumption is accepted. The Al_2O_3 content of all three rocks has been depleted if volume was unchanged by alteration. The SiO_2 content of the three samples shows gains if the alumina content remained constant, but underwent losses if volume was constant. Fluorine is strongly enriched in samples DDH 321-263.1 and JDD-94-04 relative to sample DDH 340-166.1, whereas it is only weakly enriched in the most potassically-altered sample, DDH 302-069. This reversal in trend for fluorine abundance results from the progressive replacement of all mineral species, including hydrothermal biotite, by potassium feldspar with increasing potassium metasomatism and is also reflected in a progressive loss of MgO.

The conclusions drawn from the discussion in this chapter are: 1) the Sydney and Kalgoorlie Intrusions may have formed from the same batch of magma, 2 The Ningi Intrusion is compositionally different from the Sydney and Kalgoorlie Intrusions as shown in Figure 102 because of either fractionation of the same batch of magma or incipient hydrothermal alteration; 3) the Fubilan Intrusion has undergone extensive potassic alteration involving an inward flux of potassium rich hydrothermal fluids, which has caused the metasomatic dissolution and removal of significant quantities of Ca, Fe, Mg, and Sr, and the precipitation of K and Rb in

potassium feldspar; and 4) the commonly assumed immobile constituents TiO_2, Zr, and the rare-earth elements must have been removed from the system, therefore, they were not immobile.

Discussion

Classification of Intrusive Rocks

Although the classification of igneous rocks is, in many cases, a simple and straightforward exercise, this has not proven to be true for the unaltered rocks of the Ok Tedi Intrusive Complex. I originally considered it essential that the classification scheme used herein be compatible with the recommendations of the IUGS and that the names applied based on chemical classifications should agree with names derived from modal criteria. This has proven more difficult than anticipated because the Ok Tedi samples fall in between latite and andesite and between alkalic and subalkalic compositions (76B and C). Another reason for the difficulty is that the classification of igneous rocks is still evolving and the currently available schemes are not entirely consistent from one to the other.

The igneous rocks of the Ok Tedi Intrusive Complex have been tentatively classified in previous chapters using several different methods. These include: the modal QAP diagram(Figure 50), the total alkali-silica (TAS) method (Figure 73) of Le Bas and others (1986) , and the normative Q'-ANOR method (Figure 70) of Streckeisen and LeMaitre (1979) for rock names and the alkali-lime index (Figure 75) after Peacock (1931) for igneous rock series. Particular care has been given to the classification of the least-altered rocks because the nomenclature used in

descriptions of the igneous host rocks form an important part of the criteria for the subdivision of porphyry copper deposits.

The least-altered phaneritic igneous rocks from the Sydney Intrusion are plotted on four different classification diagrams in Figure 107. Two of the three samples plot as quartz monzodiorite (field 9*) on the modal QAP plot. All three plot as quartz monzodiorite on the normative Q'A'P' and Q'-ANOR diagrams. In contrast, they are monzonite based on the TAS diagram of Middlemost (1994). The IUGS recommends that classification be done, wherever possible, from modes and on this rationale the term quartz monzodiorite is considered most appropriate for these samples.

The least-altered igneous rock with porphyritic texture is plotted on three classification diagrams in Figure 108. The sample is andesite on the Q'A'P' and Q'-ANOR whereas it is latite on the TAS diagram (Figure 73) of Le Bas and others (1986). The IUGS recommends that fine-grained igneous rocks be classified using the TAS diagram and on this basis the term latite is considered most appropriate for this sample.

The major oxides, trace elements, and modal and normative mineralogies of samples 331-218.5 (a phanerite) and 340-166.1 (a porphyry) shown in Figures 107 and 108 are compared in Table 26. The two samples exhibit nearly identical chemistry and mostly similar mineralogy. Nonetheless, and in accordance with preferred classification schemes for igneous rocks, the term quartz monzodiorite is

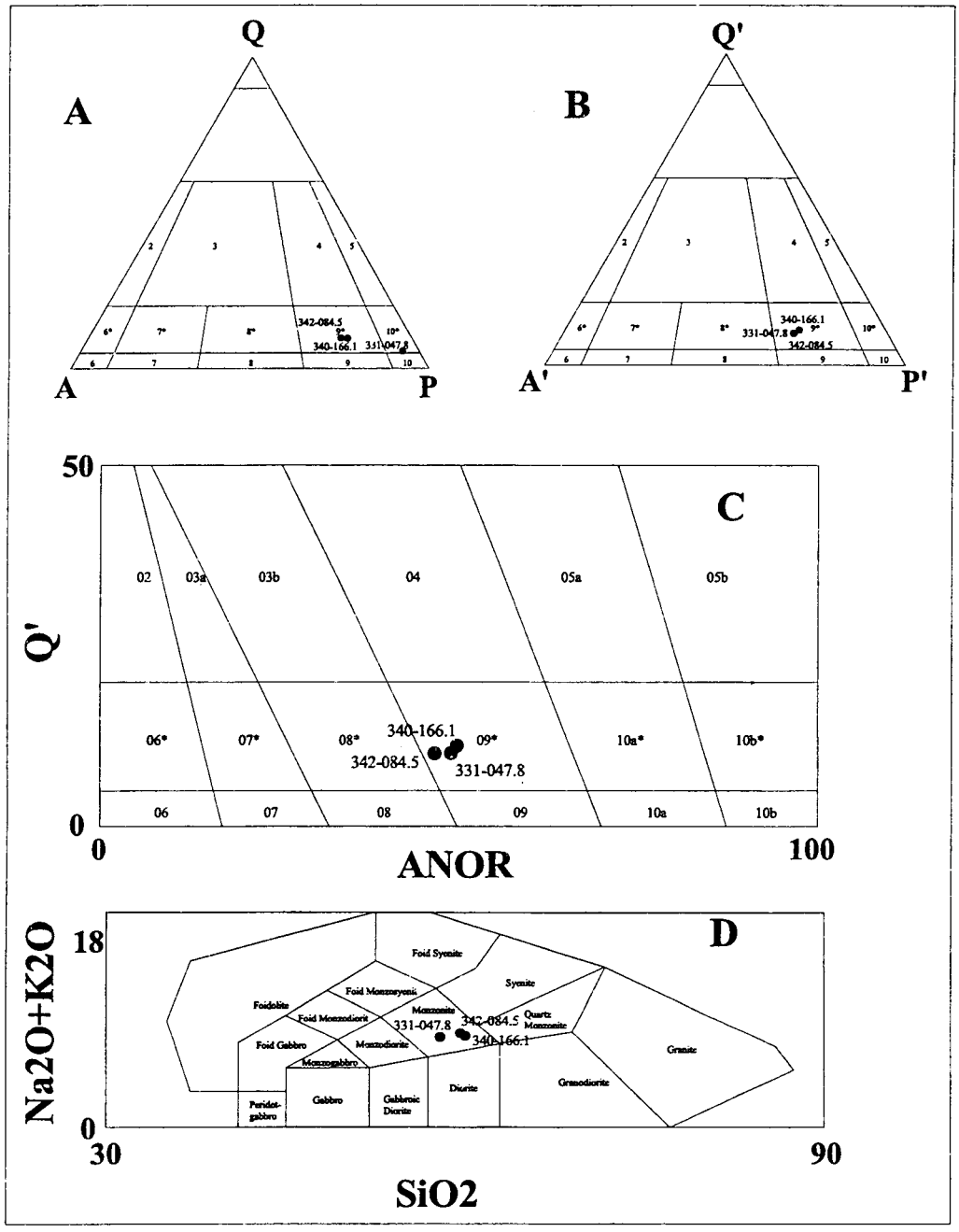

Figure 107: Classification diagrams for the least-altered phanerites from the Sydney intrusion: (A) modal QAP, (B) normative Q'A'P' , (C) Q'-ANOR diagram of Streckeisen and Le Maitre (1979), and (D) TAS diagram of Middlemost (1994).

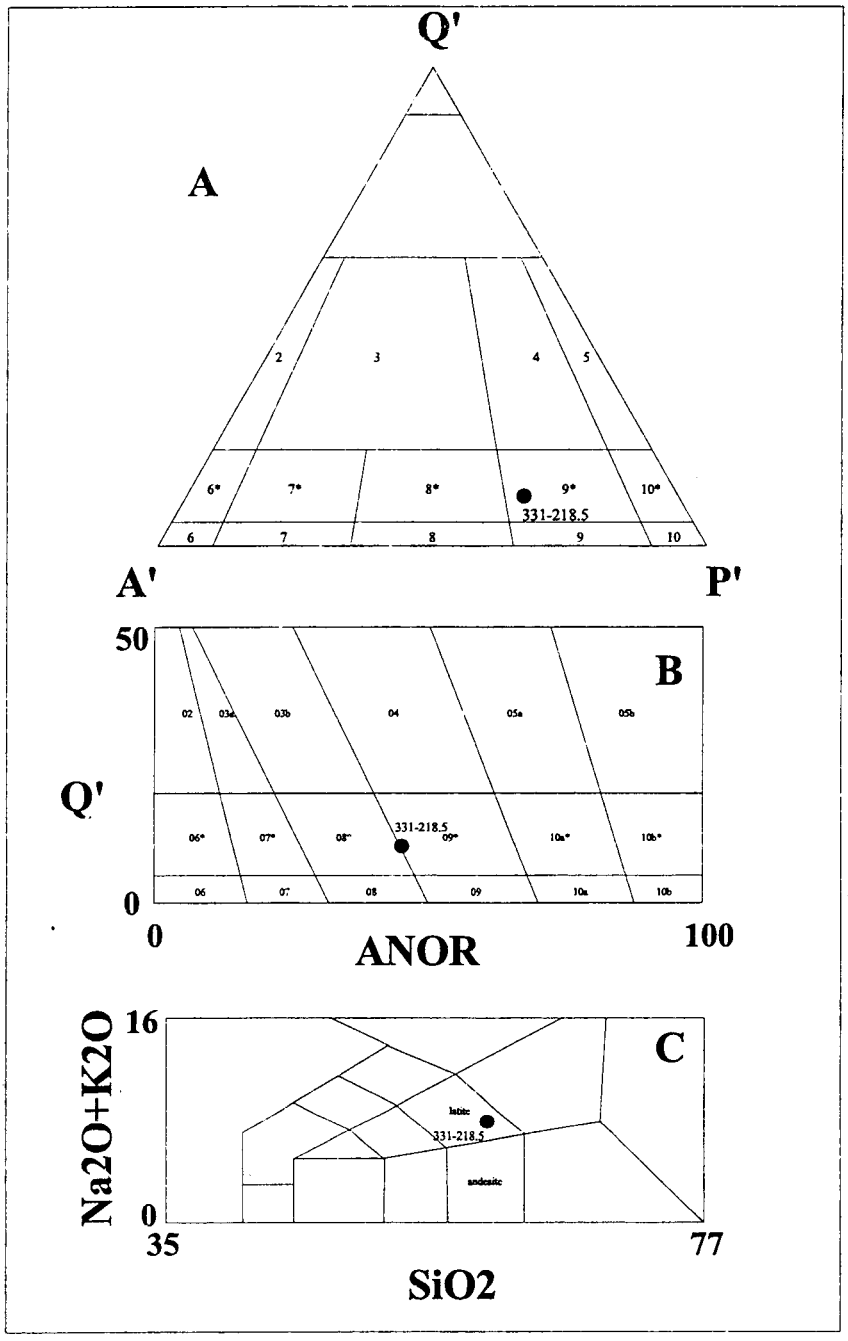

Figure 108: Classification diagrams for a sample of least-altered porphyry from the Sydney intrusion. (A) normative Q'A'P', (B) Q'-ANOR diagram of Streckeisen and Le Maitre (1979), and (C) TAS diagram of Le Bas and others (1986).

Major Oxides

Sample	331-218.5	340-166.1
Texture	Porphyry	Phanerite
SiO2	60.1	60.1
TiO2	0.5	0.5
Al2O3	18.2	18.1
Fe2O3	3.1	3.5
FeO	1.4	1.1
MnO	0.12	0.10
MgO	1.1	1.3
CaO	6.3	6.4
Na2O	3.9	4.2
K2O	4.1	3.5
P2O5	0.22	0.25
Cr2O3	< 0.1	< 0.01
H2O+	0.13	0.26
H2O	<0.05	0.12

Norm

Sample	331-218.5	340-166.1
Q	8.9	9.6
An	20.0	20.5
Ab	33.3	35.2
Or	24.3	20.6
C	0.0	0.0
Z	0.1	0.1
Di	6.2	7.1
Wo	1.2	0.5
Mt	3.4	2.2
Hm	0.8	1.9
Ilm	1.0	1.0
Ap	0.5	0.6
S.G	2.7	2.7

Trace Elements

Sample	331-218.5	340-166.1
Sc	4.97	5.96
Cr	66.3	75.1
Co	4.1	4.07
Ni	22	27
Rb	93	96
Cs	1.14	0.47
Sr	1040	1060
Ba	1170	889
La	38.1	48.9
Ce	82.4	87.5
Nd	37	35.1
Sm	7.29	7.16
Eu	2.13	1.9
Tb	0.85	0.72
Yb	2.24	2.2
Lu	0.29	0.29
Hf	5.25	5.26
Ta	0.55	0.59
Th	7.76	8.19
U	1.7	2.4

Mode

Sample	331-218.5	340-166.1
Quartz	3.3	8.2
Plagioclase	45.7	61.7
K-Feldspar	0.6	15.7
Groundmass	38.1	0.0
Biotite	0.5	1.7
Pyroxene	4.1	8.7
Hornblende	0.1	0.0
Opaques	2.7	2.3
Sphene	0.3	0.8
Apatite	0.2	0.3

Table 26: Major and trace element compositions, and normative and modal mineral assemblages of a sample with phaneritic texture compared to a sample with porphyritic texture. The two samples are nearly identical in chemical composition despite having different textures.

appropriate for the phanerite and latite for the porphyry. Thus, a problem is obvious because neither of these two terms occupy the same field on any of the common classification diagrams.

In order to illustrate the how igneous rock names pertinent to the Ok Tedi intrusions are actually used in the geologic literature and how the term "latite" can be equivalent to "quartz monzodiorite" I examined two data bases of chemical analyses taken the geologic publications. One of these, the 19,516 sample IGBA database, is described by Brändle and Nagy (1995); it includes analyses of 2023 samples of andesite and 83 of (quartz) latite. I constructed the second database, that consists of analyses of 509 samples of (quartz) monzodiorites and other igneous rocks that are geographically and genetically associated with (quartz) monzodiorite. The second database was constructed because the IGBA database has few analyses of (quartz) monzodiorites..

The names applied to the IGBA samples by the original authors of source references were retained by the researchers who compiled the database in order to avoid biasing the data. The spread of the data for each rock type on the classification diagrams can, therefore, be considered to represent the amount of variation in chemical composition of rocks bearing that name. Analytical data for andesites and (quartz) latites from the IGBA database are plotted on the Q'A'P', Q'-ANOR, and TAS (Le Bas and others, 1986) classification diagrams in Figure 109.

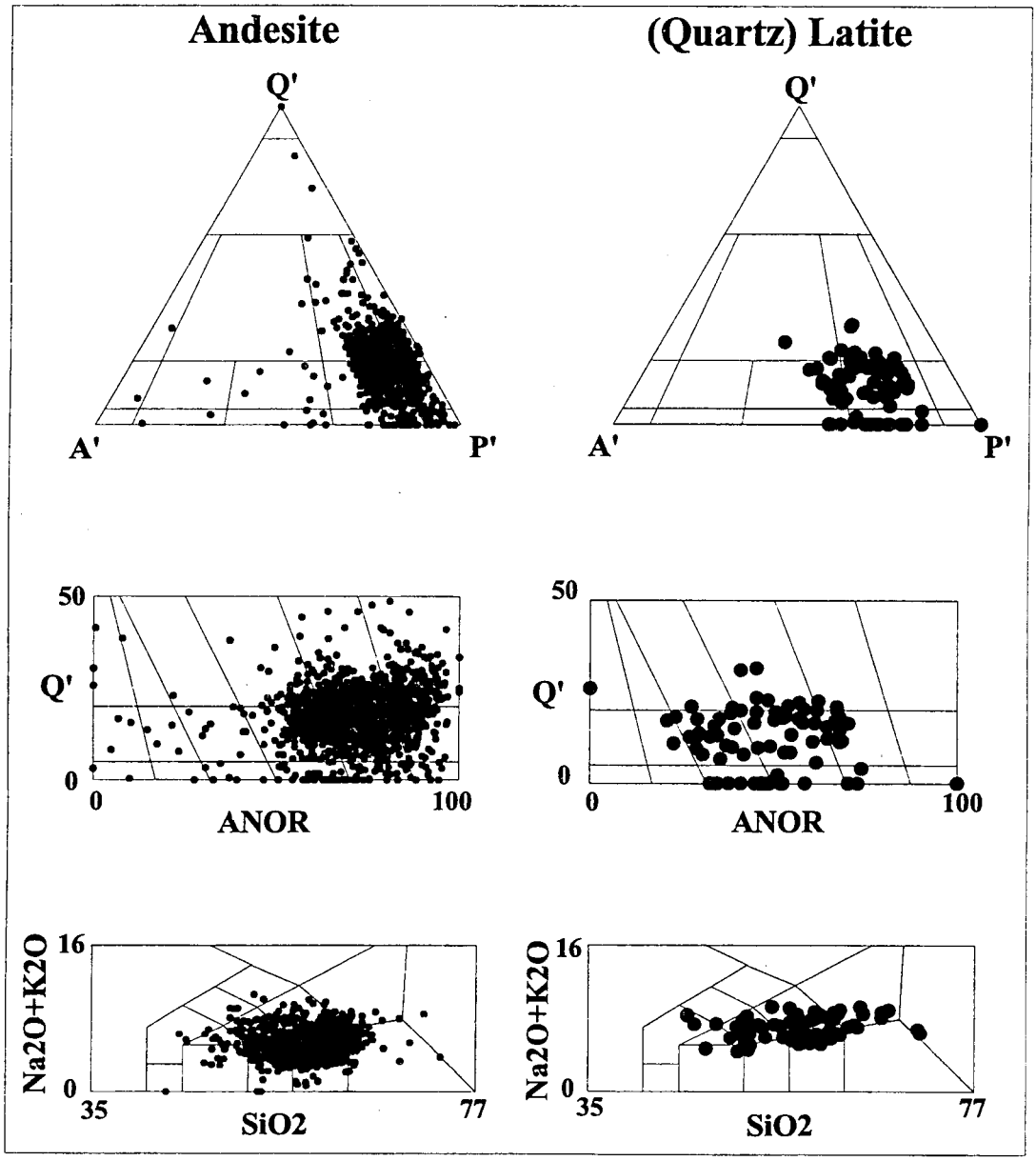

Figure 109: Comparison of 2023 samples of andesite and 83 of (quartz) latite from the IGBA database of Brändle and Nagy (1995) on the (A) Q'A'P', (B) Q'-ANOR (Streckeisen, and Le Maitre, 1979), and (C) TAS (Le Bas and others, 1986) classification diagrams.

Points representing andesites form a cluster in the left-hand portion of field 10* and right-hand part of field 9* in the normative Q'A'P' diagram (Figure 109A). Samples with greater amounts of normative quartz plot in the lower parts of fields 4 and 5. These same samples form a cluster extending from fields 5b* and 10b to the middle of fields 4 and 9* on the Q'-ANOR diagram (Figure 109B). The majority of andesites plot in the fields of quartz over-saturated rocks (basaltic andesite, and andesite) on the TAS diagram (Figure 109C) although many other samples plot in adjacent fields.

Points representing samples of latite plot in the right one-third of field 8* and the left two-thirds of field 9* on the Q'A'P' diagram (Figure 109A). Distributions of these same samples extend from the left side of field 10a* to the left side of field 8* in the Q'-ANOR diagram (Figure 109B). The majority of latites plot in the fields of quartz-saturated rocks (basaltic trachyandesite and trachyandesite) on TAS diagram (Figure 109C) although other samples plot nearby in adjacent fields.

The data presented in these diagrams illustrate the fact that andesites, as the term is used in the geological literature, are mainly restricted to the right-hand section of field 9* and to field 10* of the normative Q'A'P' and Q'-ANOR diagrams and that (quartz) latites are nearly as likely to plot in the left-hand portion of field 9 and 9* as they are to plot in fields 8 and 8*. The distribution of the two

rock types on these diagrams suggest that the boundary between fields of andesite and latite, as they are drawn, may represent an artificial rather than a natural break.

Analytical data for 25 samples of (quartz) monzodiorite that have SiO_2 values less than 65 weight percent are presented in Figure 110. All but two of the samples plot as monzodiorite or quartz-monzodiorite on the Q'A'P' diagram (Figure 110A). The samples are about evenly distributed between (quartz) monzodiorite and (quartz) monzonite on the Q'-ANOR diagram (Figure 110B). They plot in the fields monzodiorite, monzonite, and quartz monzonite on the TAS diagram (Figure 110C) of Middlemost (1994). It can be seen from Figure 110 that approximately half of the samples that have been named (quartz) monzodiorite by various authors plot as (quartz) monzonite on the Q'-ANOR diagram and that nearly all plot in the fields of quartz-saturated rocks and not in the fields of quartz-oversaturated rocks. Just as in the case of the samples from Ok Tedi, interpretation of the data from these samples implies that rocks with identical chemistry but different texture can be classified as (quartz) monzodiorite or latite. The fact that samples of quartz monzodiorite from the Ok Tedi deposit, and from other locations throughout the world, show similar distributions on the common classification diagrams suggests that the problems that I experienced in applying the petrographic nomenclature to the least-altered rocks at Ok Tedi are not unique to this investigation.

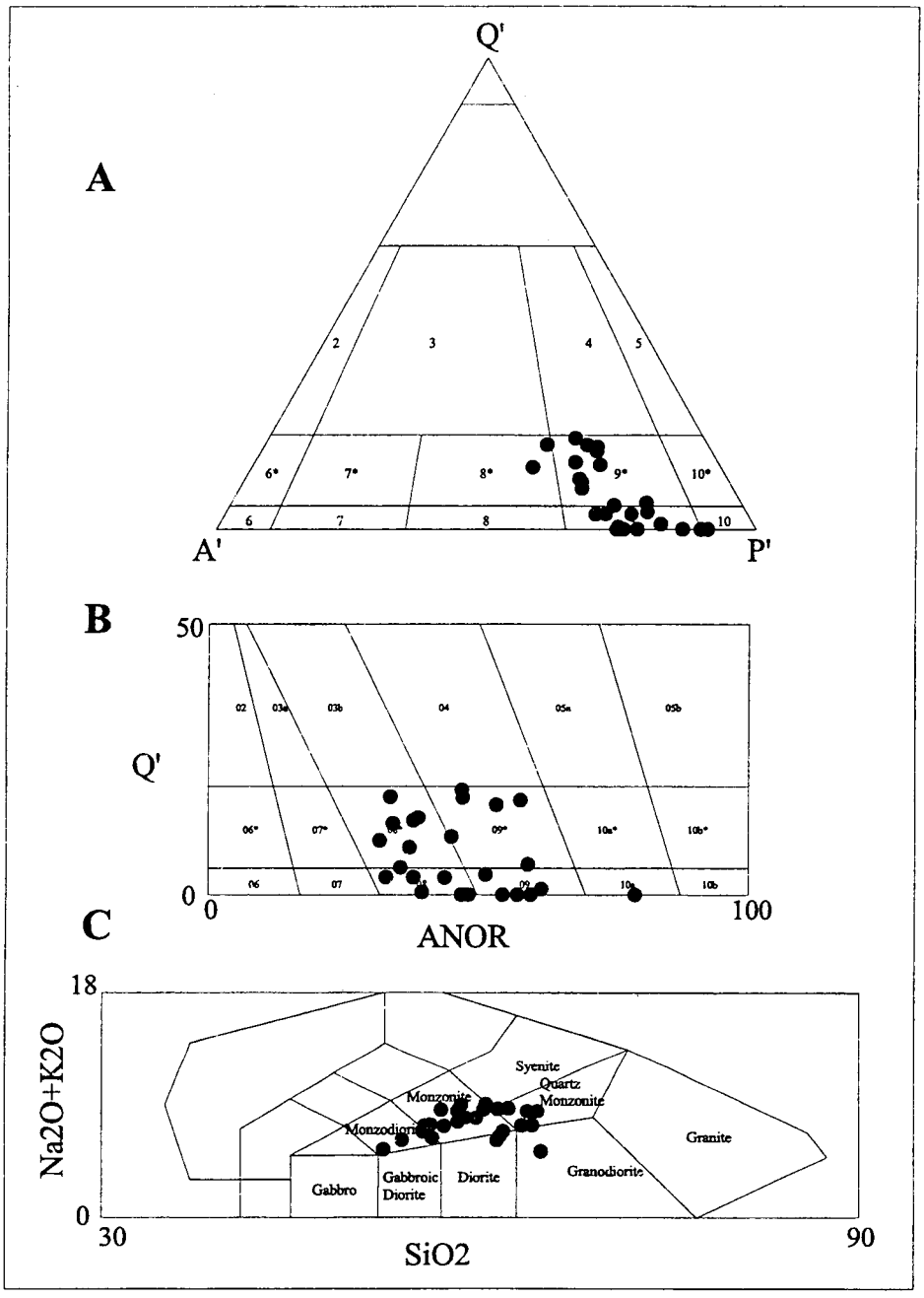

Figure 110: Comparison of 25 samples of (quartz) monzodiorite on the (A) Q'A'P', (B) Q'-ANOR (Streckeisen, and Le Maitre, 1979), and (C) TAS (Middlemost 1994). classification diagrams.

In summary, the least-altered rocks with phaneritic texture from the Sydney Intrusion are quartz monzodiorite and those with porphyritic texture are quartz latite in spite of the fact that they are chemically equivalent. The problem in nomenclature is caused by differences in current chemical and modal classification schemes. I suggest that criteria for the classification of rocks intermediate between andesite and latite may require clarification.

The altered intrusive rocks of the Mt. Fubilan, Kalgoorlie, and Ningi Intrusions have been modified from their original pristine igneous compositions. They are metasomatic rocks consisting of mineral assemblages formed by the hydrothermal replacement of the original igneous minerals. Therefore, the IUGS terminology is not appropriate for classifying them and they are best described as altered-quartz monzodiorites (those with phaneritic texture) and altered-latites (those with porphyritic texture). The IUGS names and ternary QAP diagrams such as Figure 51 or binary Q'-ANOR diagrams such as Figure 70, although inappropriate for classification purposes, can be useful in illustrating the direction, gross chemistry, and extent of hydrothermal alteration. It is important to note, however, that these rocks demonstrate the problems involved in classifying rocks strictly on their chemical composition. It is unlikely that the hydrothermal nature of these rocks would be recognized from chemical criteria alone without microscopic examination and that an automated geochemical sampling program that was not accompanied by petrographic studies would result in incorrect classification.

Conditions of Magmatic Crystallization and Hydrothermal Mineralization

The petrochemical data contained in the figures, tables, and appendices herein can be used to constrain some of the extensive and intensive variables that prevailed during the magmatic emplacement of the Ok Tedi Intrusive complex and during the hydrothermal and supergene alteration processes that followed. However, it is important to bear in mind that igneous minerals and their hydrothermal daughter minerals form over a wide range of temperatures, pressures, and chemical environments. Estimations of environmental parameters represent only moments in time in a series of events that occurred over the duration of a hundred thousand, or more, years and that entailed many discrete intervals of magma injection, earthquakes, hydrothermal explosions, heating, cooling, and bathing in fluids with widely varying temperatures, fluid pressures, and dissolved chemical species.

Subsolidus re-equilibration of minerals that originally formed as phenocrysts in magmas may produce compositional changes at high, but sub-magmatic, temperatures through diffusion, exsolution, pseudomorphic replacement, and other processes. Hydrothermal fluids from several different sources may produce overlapping or overprinted mineral assemblages at intermediate temperatures. And, at the lowest temperatures ground waters, particularly in areas of torrential rainfall such as Ok Tedi, gain access to near surface rocks where they

cause oxidation of magnetite and sulfides to form limonites, cause hydration of feldspars to form clays, and cause the conversion of iron-magnesium silicate minerals to mixtures of clay and limonite. Any of these processes may reset or obliterate geologic thermometers and barometers. Additionally, equilibrium must be assumed in many or all geothermometers and barometers, but textural features such as oscillatory zones in plagioclase feldspar and exsolution textures of ilmenite in magnetite, as in the least-altered igneous rocks of the Ok Tedi Intrusive Complex, suggest that equilibrium may not have been attained in these minerals even under the conditions of initial magmatic crystallization.

Burnham (1979, 1981) has discussed seven major constraints that control mineral stabilities in magmatic and hydrothermal systems and they are: H_2O content, temperature or heat content, oxidation state (f_{O2}), metal content, chlorine content, sulfur content, and the ratio of NaCl to KCl. Anderson (1996) has reviewed the status of thermobarometry in granitic batholiths and discussed several methods that have been used to learn about the intensive parameters that controlled the formation and emplacement of granitic rocks.

Several of the methods described by Anderson (1996) are applicable for estimates of the conditions under which the igneous and metasomatic rocks of the Ok Tedi Intrusive complex formed. These include the two-feldspar (Ghiorso, 1984; Fuhrman and Lindsley, 1988; Wen and Nekvasil, 1994) and ilmenite-magnetite thermometers (Anderson and others, 1993), the aluminum-in-hornblende

barometer (Hammarstrom and Zen, 1986), and the sphene (titanite)-magnetite-quartz assemblage (Wones, 1989) that is an estimator of oxygen fugacity (f_{O2}). In addition to the methods discussed by Anderson, temperature is estimated from the isotherms for clinopyroxenes given in Kretz (1982); the relative chemical activities of Na, K, and H^+ in the zone of potassic alteration are estimated using activity-activity diagrams as described by Meyer and Hemley (1967), Helgeson (1974), and Montoya and Hemley (1974), and Bowers and others (1984); sulfur fugacity is assessed from the presence of pyrite and magnetite in the massive magnetite, magnetite-sulfide, and sulfide metasomatic bodies in, and peripheral to, the zone of potassic alteration; and the salinity of hydrothermal fluids is estimated from the presence of cubes of halite in, or the freezing point depression of, fluid inclusions.

Some of the available methods for estimating intensive and extensive parameters are more robust than others; they retain clues to the physical parameters under which they originated even though later conditions may change greatly. The hornblende-plagioclase feldspar and hornblende-pyroxene thermometers are examples of robust estimators. The two-feldspar and ilmenite-magnetite thermometers are examples of less robust estimators (Anderson, 1996). In order to combat the problems involved with single estimators, Anderson stresses that petrologists should use as many different thermometers and barometers as possible to access the temperatures, pressures, and other environmental conditions involved in the formation of igneous rocks.

The temperature of formation for crystals of pyroxene in the least-altered intrusive rocks can be estimated from isotherms on the clinopyroxene slope of the solvus surface derived by Kretz (1982) as shown in Figure 111. Microprobe-determined compositions of diopside crystals in samples from the Ok Tedi Intrusive Complex are also plotted on Figure 111. Formations of the pyroxene crystals in the least-altered samples are assigned temperatures of 700°C, or less from the plotted positions of the compositions relative to the isotherms of Kretz. This temperature is also within the range of temperatures obtained from calculations of coexisting potassium and plagioclase feldspar as shown in Figure 23. The positions and shapes of solvus curves for 400, 500, and 800°C that are drawn on ternary diagrams in Figures 23 and 24 were calculated by the program SOLVCALC (Wen and Nekvasil, 1994). Calculations using microprobe-determined compositions of potassium and plagioclase feldspars from the least altered rock samples and equations given by Elkins and Grove (1990) yielded temperatures of about 800 to 600°C. In contrast, the weakly or moderately altered rocks yielded temperatures from about 550 to 400°C (the lower limit of the method). Temperatures below 400°C require a different thermometer. The temperatures obtained for individual samples are summarized in Table 27.

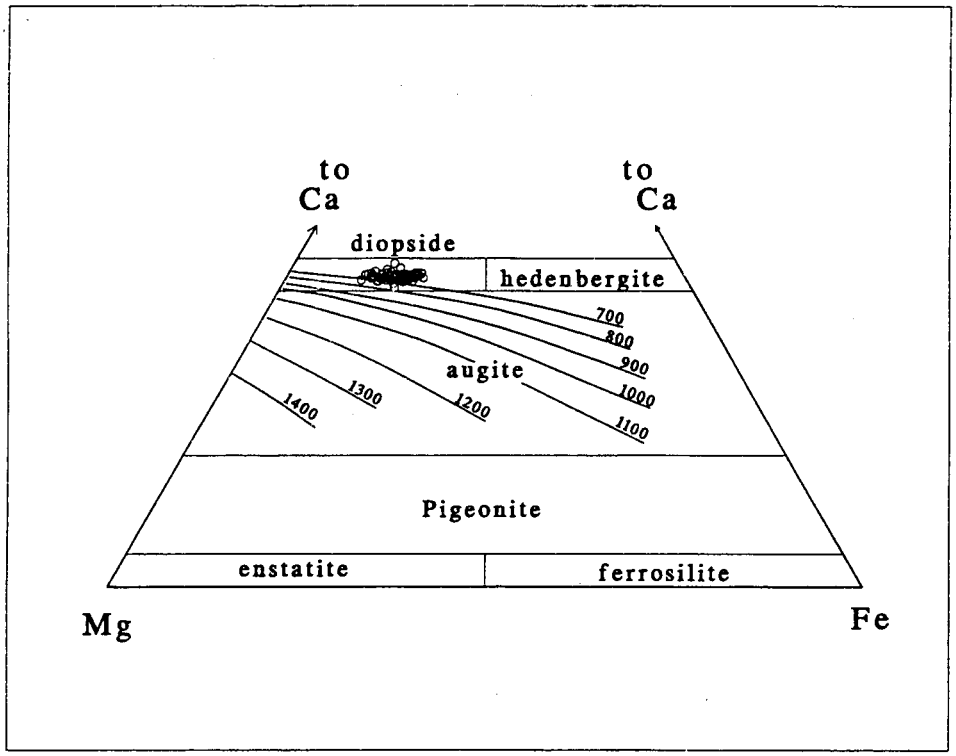

Figure 111: Isotherms (°C) on the Ca pyroxene solvus surface projected onto the pyroxene quadrilateral (Kretz, 1982). Microprobe-determined compositions for the magmatic pyroxenes of the Ok Tedi Intrusive Complex form a cluster near, and on, the 700°C isotherm.

Sample	Estimated T_{low}	Estimated T_{high}	Intrusion	Texture	A/CNK	Biotite	Normative An
JDD-94-03	400	420	Fubilan	porphyry	1.01	hyd	3.51
DDH-407 257.8	400	700	Kalgoorlie	phanerite	1.09	hyd & mag	12.09
JDD-94-11	330	340	Kalgoorlie	hbld ppy	0.97	hyd	5.17
DDH-356 166.5	480	500	Ningi	phanerite	0.84	mag	19.64
DDH-356 190	650	800	Ningi	phanerite	0.93	mag	22.53
JDD-94-14	350	560	Ningi	phanerite	1.13	hyd	5.40
DDH-331 218.5	600	800	Sydney	porphyry	0.81	mag	37.55
DDH-340 166.1	500	800	Sydney	phanerite	0.82	mag	36.80
DDH-342 84.5	600	850	Sydney	phanerite	0.80	mag	35.38
DDH-344 16	550	850	Sydney	phanerite	1.04	mag	45.55
DDH-351 313.2	650	750	Sydney	phanerite	0.86	hyd	29.00

Table 27: Calculated temperatures (°C) of formation of coexisting plagioclase and potassium feldspars in selected samples from the Sydney, Kalgoorlie, Ningi, and Fubilan Intrusions. The temperatures were calculated using equations from Elkins and Grove (1990).

Three microprobe analyses of exsolution lamellae of ilmenite and host magnetite were made on polished thin-sections DDH 342-84.5 (Sydney Intrusion), DDH 331-218.5 (Sydney), and DDH 458-151.8 (Kalgoorlie). The compositions of the ilmenite and magnetite were entered into the program QUILF (Anderson, Lindsley, and Davidson, 1993) for calculation of temperature and oxygen fugacity. The temperatures obtained range from 380 to 505 °C and are compatible with subsolidus exsolution of ilmenite from magnetite. Values for oxygen fugacity obtained from the QUILF calculations range from 10^{-17} to 10^{-20} and plot near the magnetite-hematite buffer as shown in Figure 112.

Crystallization pressures of igneous rocks are commonly estimated from metamorphic mineral assemblages in the intruded wall rocks but the best way to approach the problem is to estimate the equilibration P directly from coexisting mineral assemblages of the granitic rocks themselves (Ague, 1997). Hammarstrom and Zen (1986) presented evidence that pressure could be evaluated from the total aluminum (Al^{tot}) content of hornblende. The theoretical basis of the "Al-in-hornblende" barometer is the Gibbs phase rule P = C-F+2 where P is the maximum number of independent phases, C is the number of independent components, and F is the number of independent degrees of freedom. Any amphibole-bearing igneous rock that can be described by the ten component system (SiO_2-TiO_2-Al_2O_3-Fe_2O_3-FeO-MgO-CaO-Na_2O-K_2O-H_2O) and that contains the nine phase assemblage of plagioclase feldspar + hornblende + quartz + potassium feldspar + biotite + sphene

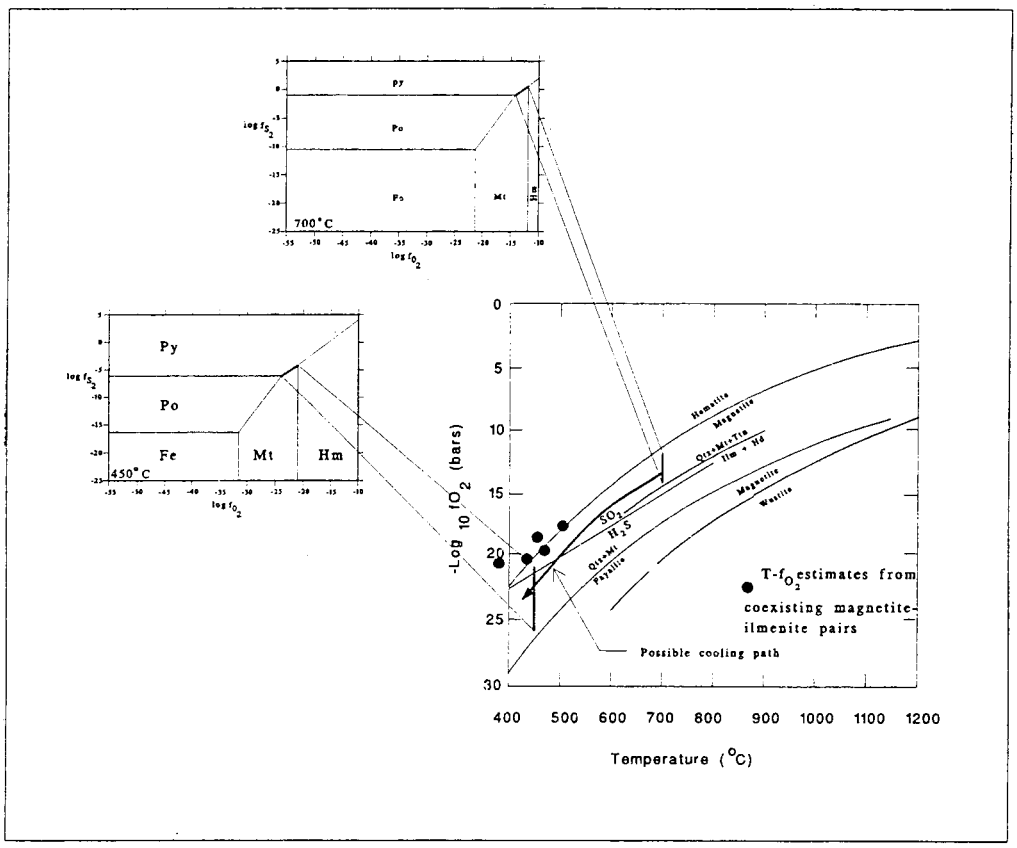

Figure 112: Diagram summarizing possible oxygen and sulfur fugacities during magmatic crystallization and hydrothermal alteration at Ok Tedi. Included are projections from f_{O2} versus f_{S2} at 450 and 700°C into a temperature versus f_{O2} diagram, f_{O2} and temperature estimates of the exsolution of ilmenite from magnetite, oxygen buffers, and a line representing the stability of H_2S versus SO_2.

+ a FeTi oxide + melt + a fluid phase is trivarient. The three degrees of freedom that are possible according to the phase rule can be expressed as oxygen fugacity, temperature, and pressure. If oxygen fugacity is buffered by a second iron-titanium oxide mineral and the temperature of formation is near the solidus then pressure is the only unconstrained variable. Hammarstrom and Zen (1986) proposed that the content of Al_2O_3 is directly related to pressure in systems that comply with the above requirements (ten component system, nine phase mineral assemblage) and they proposed an equation by which pressure could be estimated. Since the publication of Hammarstrom and Zen's paper several authors have proposed modifications of the original equation. Two samples from the Ningi Intrusion contain hornblende and all of the other minerals of the required assemblage and have had their total alumina content measured by microprobe analyses. These can therefore be used for pressure estimation. The values of total alumina in multiple analyses of hornblende crystals from the two samples are listed in Table 28 along with the equations given by Hammarstrom and Zen (1986), Hollister and others (1987), Johnson and Rutherford (1989), and Schmidt (1990) and estimated pressures calculated from each of the calibrations. Pressure estimates were calculated from the maximum, average, and minimum alumina content in each sample. The minimum pressure at which hornblende is stable as a crystallizing phase is 500 bars (Burnham, 1979) to one kilobar (Ague, 1997). If values less than 500 bars are eliminated from Table 28 than the calculated pressures obtained for

DDH 356-166.5 Ningi Intrusion 1662 m. elevation			DDH 351-313.2 Ningi Intruson 1497 m. elevation		
Run No.	**Mineral**	**Al^{total}**	**Run No.**	**Mineral**	**Al^{total}**
601	edenite	1.01	**19004**	edenite	1.03
602	edenite	0.89	**19005**	edenite	1.06
606	edenite	0.90	**19006**	edenite	1.06
607	edenite	0.94	**19010**	edenite	1.03
608	edenite	0.83	**19013**	edenite	0.96
609	edenite	0.99	**19014**	edenite	1.07
610	edenite	0.91	**19015**	edenite	0.99
615	edenite	0.88	**19016**	edenite	1.04
617	edenite	0.88	**19017**	edenite	1.05
618	edenite	0.87	**19018**	edenite	1.09
620	edenite	0.87	**19020**	edenite	1.03
621	edenite	0.88	**19021**	edenite	1.13
631	edenite	0.94	**19022**	edenite	1.02
632	edenite	0.94	**19023**	edenite	1.06
636	edenite	1.01	**19024**	edenite	1.01
637	edenite	0.89	**19027**	edenite	0.97
639	edenite	0.90	**19028**	edenite	1.00
647	edenite	0.81	**19029**	edenite	1.06
648	edenite	0.83	**19030**	edenite	1.07
649	edenite	0.83	**19031**	edenite	0.99
650	edenite	0.90	**19032**	edenite	0.92
652	edenite	0.92	**19033**	edenite	1.05
653	edenite	0.93	**19035**	edenite	1.05
654	edenite	0.89	**19036**	edenite	1.04
655	edenite	0.88	**19037**	edenite	1.03
657	edenite	0.89	**22024**	edenite	1.08
658	edenite	0.88			
	Maximum	1.01	Maximum		1.13
	Average	0.90	Average		1.03
	Minimum	0.81	Minimum		0.92
Schmidt, 1992			**P (+/- 0.6 kbar) = 4.76 Al^{Tot}-3.01)**		
Maximum		1.8			2.4
Average		1.3			1.9
Minimum		0.9			1.4
Hollister and others, 1987			**P (+/- 1 kbar) = + 5.64 Al^{Tot}-4.76**		
Maximum		1.0			1.6
Average		0.3			1.1
Minimum		-0.2			0.4
Hammarstron and Zen, 1986			**P = 5.03 Al^{Tot} -3.92**		
Maximum		1.2			1.8
Average		0.6			1.3
Minimum		0.2			0.7
Johnson and Rutherford, 1988			**P=4.28Al^{Tot} -3.54**		
Maximum		0.80			1.30
Average		0.32			0.89
Minimum		-0.06			0.39

Table 28: Total aluminum (Al^{tot}) cations per 23 oxygen atoms from microprobe analyses of crystals of hornblende in samples DDH 356-166.5 and DDH 351-313.2 and estimates of crystallization pressures in kilobars.

the samples of the Ningi Intrusion range from 0.6 to 2.4 kilobars. The calculated pressures of DDH 356-166.5 are consistently about 0.6 kilobars less than those obtained from DDH 351-313.2 regardless of the calibration equation used. The important point is that all values obtains yield relatively low pressures and, therefore, a relatively shallow depth of emplacement (~3 to 5 kilometers).

The minimum water content in the magma(s) that crystallized to form the Ok Tedi Intrusive Complex is constrained by the presence of biotite in most of the unaltered rocks and hornblende in a few of the samples. Burnham (1979) states that the water content of magma must be 2-4 weight percent and pressure must be greater than 500 bars for hornblende or biotite to stabilize as phenocryst phases. Naney (1983) determined that about 4 weight percent of water at 2 kilobars is necessary for hornblende whereas biotite may be stable in melts containing as little as 0.5 weight percent water. The presence of biotite as an early formed phenocryst phase and of hornblende in only a few samples, where it undoubtably formed late in the crystallization of the magmas at Ok Tedi, documents an increase in water content with increasing crystallinity.

Additionally, magmas that contain less that 2 weight percent water are incapable of releasing sufficient mechanical energy through second boiling to produce the extensive fracture systems that are required to provide the conduits through which hydrothermal fluids can flow, cause alteration of silicate and oxide minerals, and deposit metal sulfides and gold (Burnham, 1981, Anthony, 1983).

The presence of fluid inclusions in quartz crystals in the least-altered phanerites of the intrusions at Ok Tedi also demonstrate the presence of an aqueous phase late in the crystallization process.

Additional constraints on the water content and solidification temperatures of igneous melts can be obtained from experimental studies. Holtz and Johannes (1994) have summarized the liquidus and solidus phase relations for the hypothetical system Qz-Or-Ab (eutectic melts or haplogranites). Temperatures for the melting and solidification of igneous rocks such as those at Ok Tedi are undoubtably higher than those obtained for the hypothetical system because of the presence of additional phases such as anorthite in plagioclase feldspar and the iron and magnesium contents of ferromagnesian minerals. Nonetheless consideration of experimental data from study of these eutectic compositions does provide lower boundaries on the solidification temperature of igneous melts and on the amount of water that can be contained in magmas. Burnham (1979) has shown that the solubility of water is about the same in melts of a variety of compositions (andesite, albite, and Li pegmatite) for the range of pressures, 1 to 2 kilobars, likely to have prevailed at the crustal level in which the Ok Tedi Intrusive Complex was emplaced as shown in Figure 113. A curve delimiting the water-saturated solidus of eutectic or minimum granitic compositions (redrawn from Holtz and Johannes, 1994), liquidus curves for given amounts of H_2O (solid lines), and H_2O solubility curves (dashed lines) are illustrated in Figure 114. It can be seen from the position

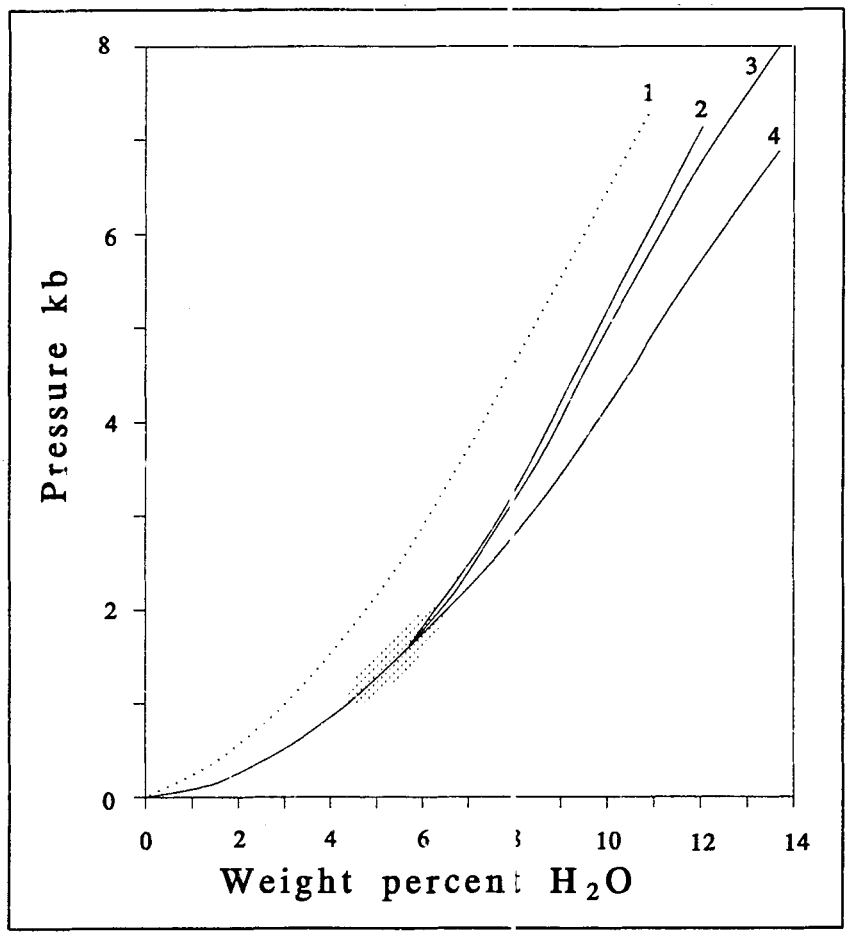

Figure 113: Diagram showing the equimolal solubility of H_2O as a function of pressure in four types of silicate melts: (1) basalt (1100°C), (2) andesite (1100°C), (3) albite, (700-870°C), and (4) Li-pegmatite (660-720°C). Redrawn from Burnham (1979). The stippled area indicates the range of pressures inferred for the crystallization of the Ok Tedi magmas.

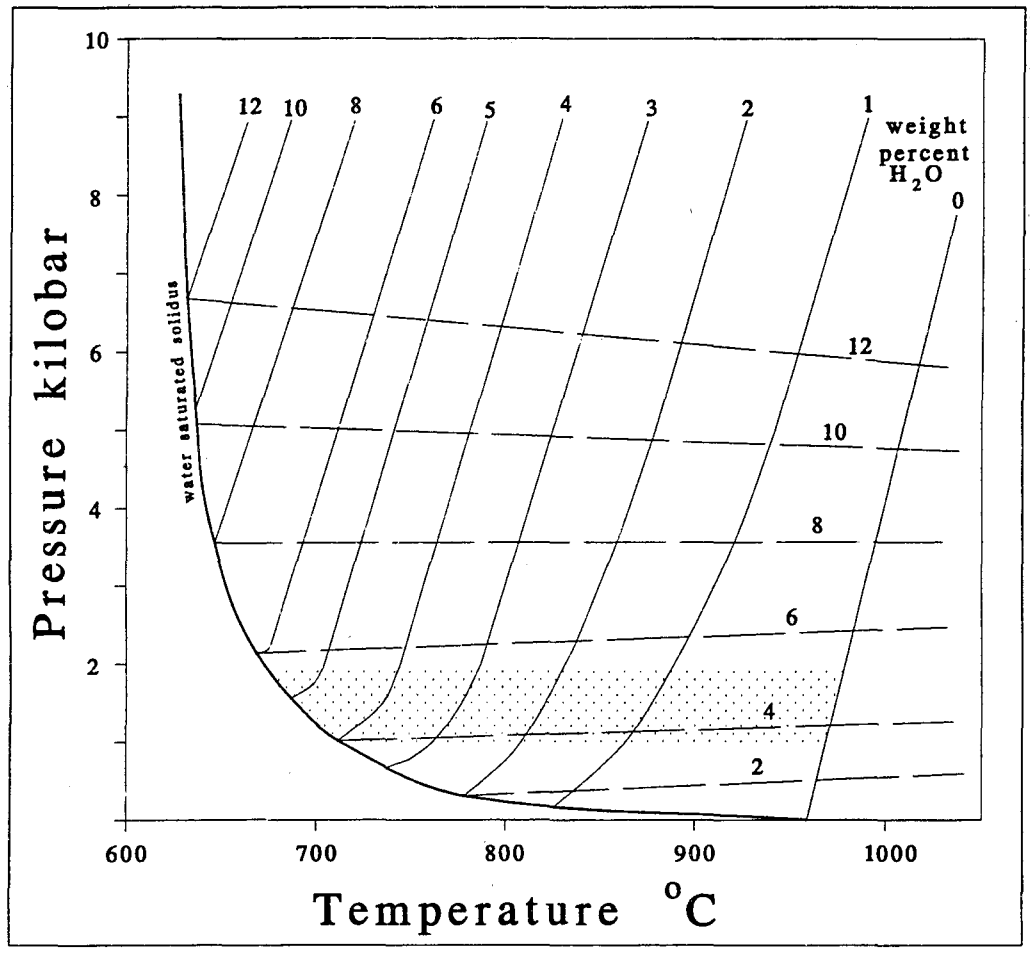

Figure 114: Temperature versus pressure plot showing the liquidus curves for given amounts of H_2O (solid lines), H_2O solubility curves (broadly dashed lines), and the water-saturated solidus for the system Qz-Ab-Or-H_2O (eutectic and minimum granitic compositions). Redrawn from Holtz and Johannes (1994). The stippled are indicates the range of pressure inferred for the crystallization of the Ok Tedi magmas.

of the water saturated solidus curve that, regardless of water content, granitic magmas can be expected to have solidified by 630°C which suggests that the temperatures less than this value that were calculated using two-feldspar thermometry represent subsolidus re-equilibration. The maximum solubility of water at pressures of 1-2 kilobars is 4 to 6 weight percent. In order to have produced a fluid phase it is necessary that the magmas at Ok Tedi must have been oversaturated with respect to water. It is likely that the magmas did not become oversaturated until some critical percentage of phenocrysts had crystallized. The average groundmass content of the igneous rocks with porphyritic texture at Ok Tedi is about 38 volume percent. The groundmass can be equated to liquid content in a crystal mush. If part or all of fluids responsible for hydrothermal alteration at Ok Tedi originated from the porphyritic magmas, it is possible that water did not become supersaturated with respect to the melt phase until greater than 50 volume percent of these magmas solidified as a result of crystallization.

The stability fields of iron oxide and sulfide minerals are commonly depicted on binary plots of the activity, or fugacity, of oxygen versus sulfur (Barton and Skinner, 1979) and these diagrams are used to describe and interpret phase relations in geologic systems. The stability of single minerals and coexisting two and three mineral assemblages are dependant on temperature as well as oxygen and sulfur fugacity. Two log f_{O2}-f_{S2} diagrams for 700 and 450°C are given in Figure 112. These temperatures were chosen because they provide reasonable upper and

lower bounds on the transition from magmatic to hydrothermal conditions. The boundaries between pyrite and magnetite on these diagrams set limits on oxygen and sulfur fugacity at a particular temperature. The upper and lower values of oxygen fugacity defined by the two mineral assemblage magnetite-pyrite are projected from the log f_{O_2}-f_{S_2} diagrams for 700 and 450°C into a binary diagram of temperature versus log f_{O_2} in Figure 109. The values of oxygen fugacity at 700°C ($\sim 10^{-12}$ to 10^{-14}) and at 450°C (10^{-21} to 10^{-26}) are above the quartz + magnetite ⇌ fayalite (QFM) buffer and as such are indicative of strongly oxidizing conditions. The values of f_{O_2} implied by the presence of the pyrite-magnetite assemblage are consistent with the presence of quartz and sphene in the magmatic assemblage and the high oxygen fugacity suggested by the compositions of coexisting magnetite and exsolved ilmenite. The sulfide minerals, pyrite and chalcopyrite, are ubiquitous phases throughout the zone of potassic alteration whereas massive, hydrothermal, magnetite is rare in the center of porphyry mineralization. Most bodies of massive magnetite (± pyrite and chalcopyrite) at Ok Tedi are concentrated near the outer fringe of the potassic zone although a few pods of massive ore were exposed near the center of the potassic zone. The distribution of magnetite and the sulfide minerals in porphyry and massive ore bodies probably records fluctuations in the ratio of sulfur to oxygen as the hydrothermal fluids and gases evolved. Sulfur fugacity may have been higher than the pyrite-magnetite boundary in zones of normal porphyry ore, lower than this boundary in areas of massive magnetite, and at

the boundary in areas of massive magnetite-pyrite±chalcopyrite. The fluctuations were likely related to both structural position within the hydrothermal system and time. Crosscutting relations and other textural features in all of the massive replacement ore bodies that I observed at Ok Tedi indicate that where both are present, magnetite preceded pyrite (±chalcopyrite). Clark and Aranciba (unpublished) argue that the strongly oxidized nature of the hydrothermal fluids in systems that contain early magnetite-rich veins is definable as a preponderance of SO_2 over reduced sulfur species, including H_2S; that under such conditions magnetite and gold can readily participate; and that copper and other chloride-complexed base metals remain in solution until later in the hydrothermal process. If the model of Clark and Aranciba can be extended to the massive replacement ore bodies at Ok Tedi, it provides an explanation for the textural relations of pyrite±chalcopyrite and magnetite and may imply that the massive bodies of magnetite formed prior to the deposition of sulfide minerals in the porphyry ore bodies. It also may indicate that the change from magnetite to pyrite and chalcopyrite deposition was due to cooling through the boundary between SO_2 and H_2S as shown at a temperature of about 500°C for the cooling path shown in Figure 112. This tentative interpretation is consistent with thermodynamic data (Robie and others, 1978 and 1979) that demonstrate that H_2S becomes increasingly stable relative to SO_2 with diminishing temperature and at constant f_{O2}.

Relevant to this discussion are related sulfur isotope studies that are currently being conducted on sulfide concentrates from the Ok Tedi deposit (Field and others, 1999, unpublished data). The $\delta^{34}S$ per mil values of 49 sulfide concentrates, excluding those of two anomalously depleted chalcocites of supergene origin, range from -3.4 to +2.2 per mil. This range is entirely compatible with those published for other major porphyry Cu-Mo deposits such as Bingham, Utah (Field, 1966), Butte, Montana (Zhang and others, 1999), and El Salvador, Chile (Field and Gustafson, 1976). Moreover, this narrow range about the zero per mil value of the meteorite standard is consistent with that of a deep-seated "magmatic" source of sulfur (Ohmoto and Rye, 1979). Most of the different sulfide minerals from Ok Tedi exhibit reasonable approximations to isotopic equilibrium, and using the fractionation equations of Ohmoto and Rye (1979) provide isotopic estimates of depositional temperatures. These include temperatures of 470°C for one molybdenite-chalcopyrite mineral pair, 380° to 420°C for two molybdenite-chalcocite pairs, 365° to 595° C for four pyrite-chalcopyrite pairs, and 360° to 545°C for two chalcopyrite- bornite pairs. Thus, the sulfur isotope data suggest a general temperature range of about 450° to 550°C for hydrothermal mineralization at Ok Tedi. The presence of fluid inclusions containing cubes of halite demonstrates that the fluids that evolved in the hydrothermal stage of magmatism were characterized by very high salinities, at least 35 weight percent NaCl equivalent (Roedder, 1971; Nash, 1976), through at least part of their evolution.

Halite-bearing inclusions were observed in interstitial crystals of quartz, but not earlier formed minerals, in intrusive rocks with phaneritic texture suggesting that the saturation of the Ok Tedi magmas with respect to water and the separation of a hydrous phase did not occur until late in their sequence of crystallization. Homogenization temperatures from halite-bearing inclusions were reported as 650 to 450°C (Wilkins, unpublished). Nedachi (1992) reported the presence of multiphase fluid inclusions in phlogopite-quartz-apatite veinlets of the Fubilan Intrusion that have filling temperatures of 380 to 470°C. Separation of a fluid phase from the magmas at Ok Tedi is likely, based on the fluid inclusion data, to have occurred at temperatures of 650°C or below.

The stabilities of most of the silicate gangue minerals of the potassic, phyllic, and argillic zones of porphyry deposits can be represented in the system Na_2O-K_2O-Al_2O_3-SiO_2-HCl-H_2O. Boundaries between the common hydrothermal phases are delineated on mineral stability diagrams in terms of the logarithm of the activities (or ratios of activities) of the dissolved species that control mineral-solution equilibria. The dissolved substances that play important roles in the hydrothermal fluids that produce porphyry deposits include H^+, K^+, and Na^+. In addition, Ca^{2+}, Mg^{2+}, and iron (Fe^{2+} and Fe^{3+}) are also important particularly in zones of propylitic alteration. However, calcium is not a major constituent in the samples of altered rock collected and analyzed as part of this study as has been shown earlier in Harker (Figure 60), Peacock (Figure 75B) and isocon (Figure 106-

108) diagrams for potassically altered rocks. Accordingly, the stability of minerals containing CaO and their relations to other hydrothermal phases will not be included here. Mineral stability diagrams have been constructed from experimental and thermodynamic data by several authors including Hemley and others, (1961), Garrels and Christ, 1965, and Bowers and others (1984). Four mineral stability diagrams covering the likely range of hydrothermal temperatures (500-300°C) experienced by the intrusive rocks of the Ok Tedi Intrusive Complex are redrawn from Bowers and others (1984) in Figure 115. The diagrams are for 1 kilobar pressure. The dominant aluminosilicate minerals in the potassic zone at Ok Tedi are potassium feldspar and subordinate albite. These two minerals can coexist throughout the range of temperatures shown in Figure 115, but only if the activities of K^+ and Na^+ are very much greater than the activity of H^+. The stippled areas in Figure 115 show the likely compositions of the hydrothermal fluids that formed the potassic zone at Ok Tedi. In areas where potassic alteration was particularly strong, fluid compositions must have moved from the boundary between albite and potassium feldspar into the field of potassium feldspar because albite is not a major mineral phase in samples with greater than about 10 weight percent K_2O.

The temperature estimates made in this chapter are combined with inferences drawn from petrographic observations to construct the paragenesis

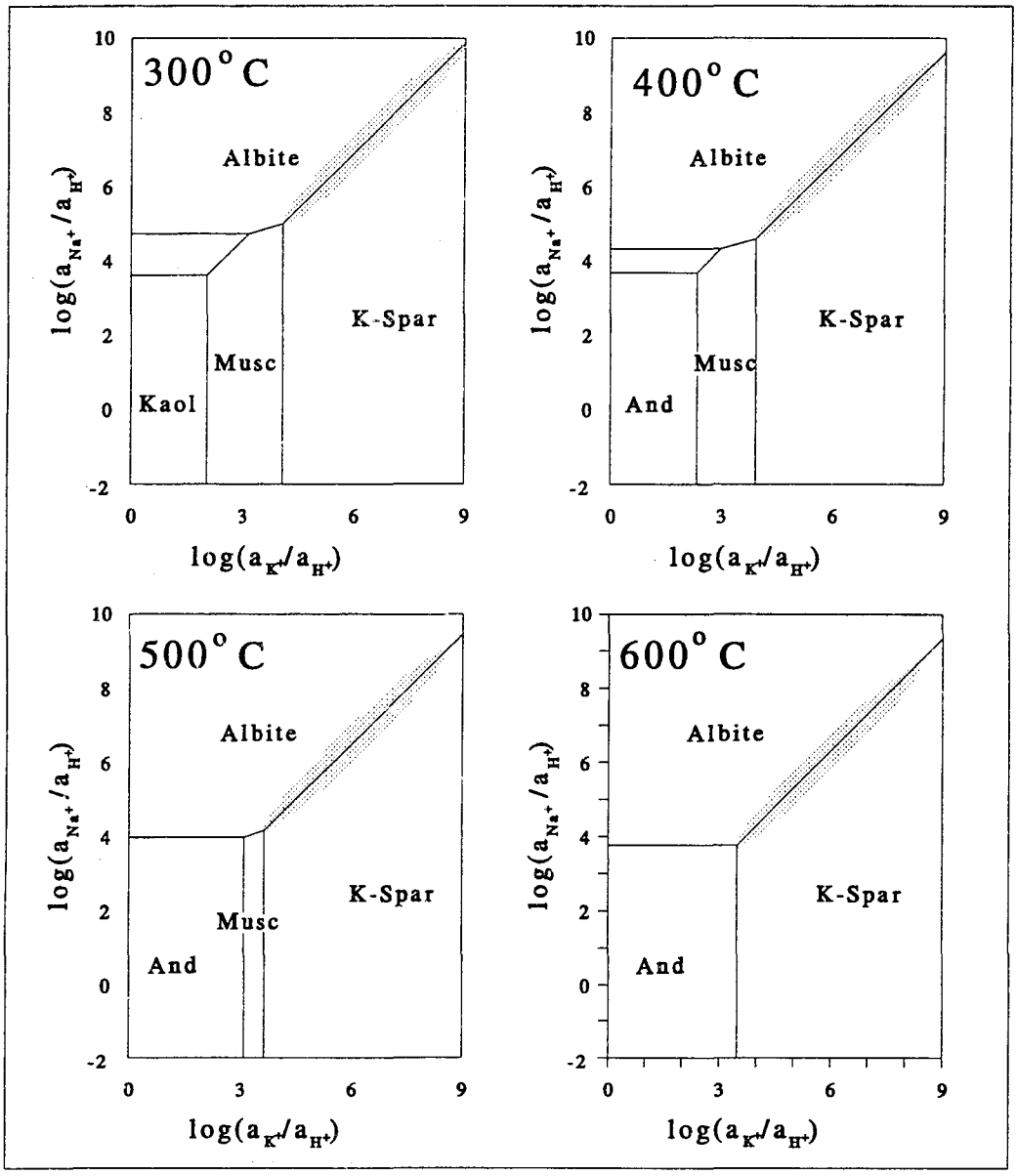

Figure 115: Activity-activity diagrams showing the fields of stability of silicate minerals as a function of the ratios of potassium to hydrogen versus sodium to hydrogen for the range of temperatures that may have prevailed during potassic alteration at Ok Tedi. Redrawn from Bowers and others, 1984).

diagram of Figure 116. It must be reemphasized that the temperatures assigned are rough approximations. Only a few of the mineral phases have had temperature estimated by geologic thermometers and these values are likely to represent minimum or re-equilibration temperatures. Calculated temperature intervals are represented by solid line segments; dashed line segments represent mineral relations from microscopic examinations; and dotted lines are inferred from intuition. Crystallization of the earliest formed magmatic minerals, apatite and plagioclase feldspar, are inferred to have begun just below a liquidus temperature calculated from the composition of DDH 340-166.5 by the computer program PELE (Boudreau, 1999). Crystallization of quartz, the last magmatic mineral formed in most samples with phaneritic texture at Ok Tedi, is assigned a temperature of about 650°C estimated from the water-saturated solidus at about 1.5 kilobars pressure (Figure 114). The crystallization of hornblende is assigned so as to straddle the location of the solidus temperature (~650°C) because the full buffering assemblage necessary for the successful application of the "Al-in-hornblende" barometer, that is present in some phanerites at Ok Tedi, is reported to only become stable near the solidus (Ague and Brandon, 1996). The high temperature ends of the lines representing the formation of hydrothermal feldspars are from the two-feldspar thermometer; the low temperature ends are unconstrained. The transition in stability from hydrothermal magnetite to pyrite is taken as the approximate point where the hypothetical cooling path of Figure 113

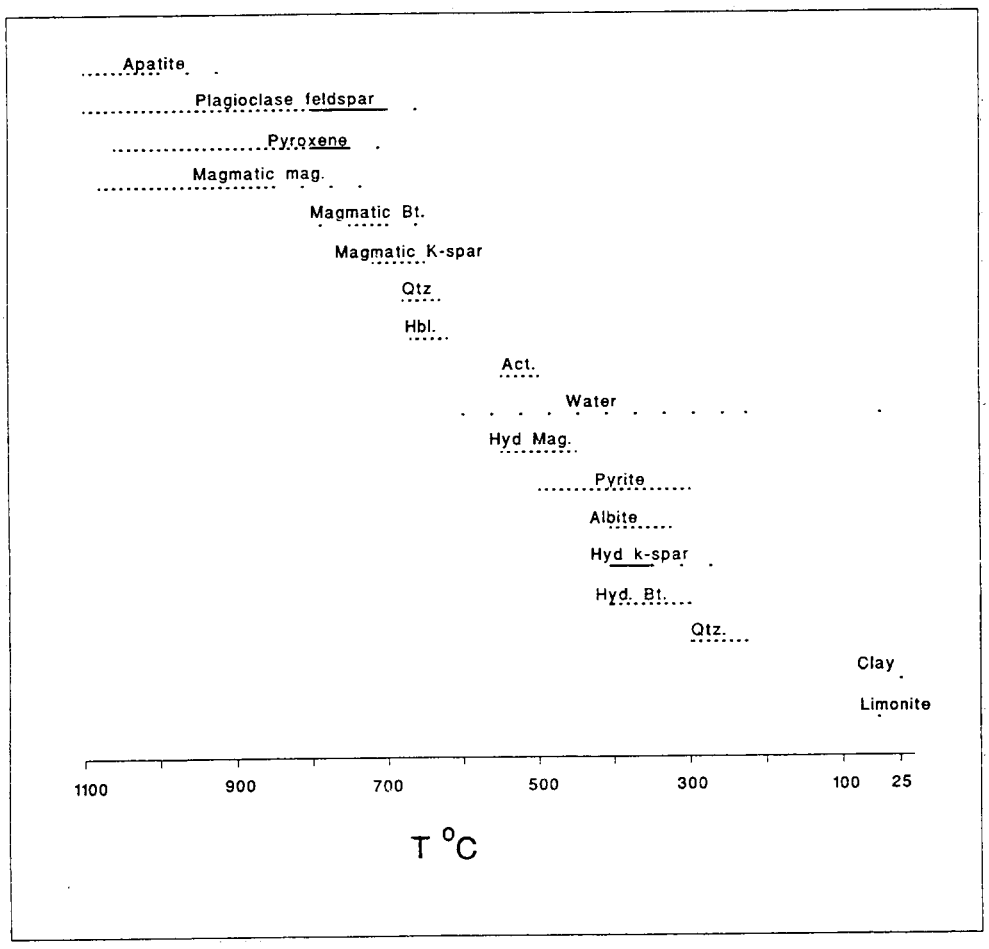

Figure 116: Paragenetic diagram summarizing the inferred sequence of formation of magmatic and hydrothermal minerals and water in the Ok Tedi Intrusive Complex. Solid lines - temperatures calculated from geothermometers. Dashed lines - temperatures inferred from the relationships of individual minerals to coexisting phases in thin-sections. Dotted lines - speculative and projections from better constrained relationships.

crosses the line separating SO_2 from H_2S. Water is assumed to have been present as a fluid phase throughout the process of formation of quartz, hornblende, albite, potassium feldspar, hydrothermal biotite, magnetite, and pyrite in the zone of potassic alteration. The lack of superimposed zones of quartz-sericite or advanced argillic alteration suggests that lower temperature magmatic or meteoric waters may not have had contact with the rocks of the potassic zone again until they were uplifted into the zone of weathering and supergene alteration. The formation of clays and limonites are inferred to have occurred in the zone of weathering and thus are assigned to the lowest temperature range on Figure 116.

Summary and Conclusions

Magma intermediate in composition between andesite and quartz latite was intruded into sedimentary host rocks of the New Guinea Fold Belt between 2 and 3 millions year ago at a depth 3 to 5 kilometers below the paleosurface. The magma crystallized to form hypabyssal intrusive rocks with phaneritic and porphyritic textures. Subsequently, hydrothermal fluids, derived at least in part from this magma, interacted with the consolidated igneous rocks and their siliciclastic and carbonate host rocks to produce rocks with potassic and propylitic mineral assemblages, massive replacement bodies of magnetite and sulfide minerals, and endoskarn. In the process of alteration the fluids deposited economic quantities of copper and gold.

My purpose in beginning this dissertation was to sample and characterize as many of the lithologic components of the Ok Tedi ore deposit as possible. Practical considerations, including sample accessibility, limited the study to two components: (1) the most pristine possible samples of igneous rock, and (2) metasomatized rock from the zone of potassic alteration. Least-altered samples were sought out and sampled because the validity of any study of the alteration of one rock to form another is limited to the extent the parent is known. The zone of potassic alteration was sampled because it is the principal host of gold and copper ore in the giant Ok Tedi deposit and, because exploration and active mining have

been preferentially directed to this rock type, it is the best exposed and sampled rock type in this area of steep topography, deep soils, and heavy forest. Areas of propylitic alteration and endoskarn are present at Ok Tedi but outcrops of this rock type were not readily available during my time there. Furthermore, samples that can be classified as propylites or endoskarns include such a wide variety of mineral assemblages and textures that they deserve separate studies, such as that of Katchan (1982), and further research is warranted. Phyllic (quartz-sericite) alteration, which is common in most porphyry copper deposits, is subdued to absent at Ok Tedi.

Petrographic examinations revealed that andesine or oligoclase, and potassium feldspar, pyroxene, and quartz were the most abundant minerals in the least altered intrusive rocks, whereas orthoclase, albite, and quartz predominate in rocks that have undergone potassic alteration. Potassic alteration, where pervasive, is nearly a monomineralic assemblage consisting predominantly of orthoclase with only trace amounts of minerals. The characteristic accessory mineral assemblage of the least-altered rocks is biotite, magnetite, sphene, and apatite. Hornblende is present locally and has formed, at least in part, by replacement of pyroxene. The characteristic accessory mineral assemblage in potassically-altered samples is rutile, biotite, pyrite, and chalcopyrite. Trace amounts of zircon are present in both altered and unaltered rock.

The detailed petrographic analyses, consisting of point counter estimates of the various minerals present in the least-altered igneous rocks, revealed that

samples with porphyritic texture are similar in mineralogy to those with phaneritic texture and major and trace element analyses demonstrated that they are identical chemically. The porphyritic rocks at Ok Tedi average about 65 percent phenocrysts and 35 percent microcrystalline groundmass The textural differences between phanerites and porphyries represent differences in cooling history at the same level in the crust rather than different differences in primary mineral chemistry. Phaneritic texture is commonly considered to be evidence for slow cooling over an extended period of time and is associated with relatively deep environments, whereas porphyritic texture is associated with rapid cooling in shallow subvolcanic environments. The phanerites and porphyries of the Ok Tedi Intrusive Complex, that are currently exposed at the surface, crystallized at the same crustal depth of 3 to 5 kilometers. Porphyritic texture developed in periods of time and in portions of the magma where pressure was released as overlying magma breached the surface causing eruptions or steam blasts, whereas phaneritic textures represent early cooled parts of the intrusive complex and areas of the complex where magmas did not communicate with the surface. The presence of breccias represent additional geologic evidence of periods of rapid pressure release.

The major oxide chemistry documented in the tables and appendices indicates that the unaltered rocks of the Ok Tedi Intrusive Complex are silica-saturated, metaluminous, and weakly iron-rich. Nearby intrusions of the Star Mountains Province clearly are calc-alkaline, whereas it is uncertain as to whether

or not those of the Ok Tedi Complex are calc-alkaline or alkali-calcic. The Ok Tedi intrusions plot on the line separating alkalic and subalkalic compositions, and this borderline trait may also be reflected in borderline calc-alkaline and alkali-calcic character. The intrusions were strongly oxidized and likely to have been saturated with water. The phanerites are correctly classified as quartz monzodiorites using I.U.G.S. criteria, and the porphyries as trachyandesite or latite, although they are chemically identical. The contradiction of different compositional names for rocks of identical chemistry arises because classification criteria for magmas intermediate in composition between andesite and latite require clarification beyond that available in the current geologic literature.

Data obtained from microprobe analyses indicate that the pyroxenes of the unaltered intrusive rocks are salite in composition. Salite was converted to actinolite and actinolitic hornblende in areas of weak propylitic alteration but is absent in potassically altered rock. Pseudomorphs of hydrothermal biotite after pyroxene are common in samples with moderate potassium feldspar metasomatism and samples with nearly pure three phase assemblages of potassium feldspar-quartz-albite, and with only traces of hydrothermal biotite as the only ferromagnesian mineral, are approached in areas of extreme potassic alteration. The hornblende in least-altered rock is calcic edenite in composition. Igneous biotite is more annitic in composition than hydrothermal biotite which is more phlogopitic.

Potassium and silica metasomatism produced extreme changes in the chemistry of the intrusive rocks of Mt. Fubilan as is documented by the use of isocon diagram. These changes were so extreme that it is likely that no single chemical element or oxide, including those elements that are commonly considered to be immobile during hydrothermal alteration, was unaffected. The K_2O contents of the most potassically-altered rocks have increased from about 3.5 weight percent in least-altered samples to a maximum of about 13.2 weight percent in those with the maximum identified degree of potassic alteration, a gain of about 380 percent, while CaO contents have decreased from about 6.4 weight percent to a minimum of less than 0.1 weight percent, a loss of nearly 99 percent. Major-oxide data from blast hole drill samples plotted as summary down hole logs demonstrate that the chemical changes brought about by potassium metasomatism are pervasive in character. The principal mineralogical manifestations of the changes in chemical composition are the conversion of andesite to orthoclase and albite, of pyroxene and hornblende to biotite, sphene to rutile, magnetite to chalcopyrite and pyrite, and the formation of quartz veinlets and areas of pervasive quartz flooding (as in the quartz core). The zone of potassic alteration is extensive, continuous, and pervasive. The chemical changes cause by this potassic alteration have been imposed, at minimum, on a volume of rock equal to a cylinder 1 kilometer in diameter and 500 meters in height. This metasomatism has involved the leaching and outward flux of immense quantities of calcium, iron, and other chemical

constituents, of which some proportion was redeposited in massive replacement bodies and endoskarn, concomitantly with the simultaneous influx of enormous amounts of potassium. The source of the potassium is unknown, but possibly was derived from outside the system now exposed at Ok Tedi, perhaps from deeper parts of the intrusive complex or from other as yet unexposed nearby intrusive systems.

Bamford and others (1972) were uncertain as to whether the Ok Tedi deposit formed by magmatic or hydrothermal processes. They presented arguments in favor of a hydrothermal origin and in favor of magmatic origin, and concluded that the deposit had formed by a combined magmatic-hydrothermal process in a single intrusive unit, the Mt. Fubilan Intrusion, that differed in mineralogy and chemistry from the surrounding igneous components of the Ok Tedi Complex (the Sydney, Kalgoorlie, and Ningi Intrusions) and that the presence of ore minerals in the Mt. Fubilan was the result of a compositional differences in the magma from which it was derived relative to the other intrusive bodies. Geologic evidence gathered subsequent to their work, and documented in the preceding chapters of this dissertation, has strengthened the case for hydrothermal alteration and weakened the case for magmatic formation of the ore minerals, and suggests that the Mt. Fubilan Intrusion was not substantially different in composition from the others.

The principal evidence supporting a hydrothermal, and thus metasomatic, origin for the alteration and metallization at Ok Tedi is the presence of pseudomorphic relations between minerals. The presence of pseudomorphs of albite and orthoclase after andesine, hydrothermal biotite after magmatic ferromagnesian minerals, rutile after sphene, and pyrite and chalcopyrite after magnetite all point to a replacement origin. Temperature estimates based on coexisting alkali-and plagioclase feldspar demonstrate magmatic temperatures (800-600°C) for samples of least-altered rock whereas the temperatures obtained for those samples that contain the above pseudomorphic mineral assemblages yield temperatures that are clearly submagmatic (500-300°C), and these in turn are largely consistent with sulfur isotope temperature estimates based on sulfide-sulfide mineral pairs.

The Sydney, Kalgoorlie, and Ningi Intrusions, that are spatially associated with the Mt. Fubilan Intrusion, have been demonstrated to be similar, if not identical, in mineralogy and chemistry based on petrographic examinations, major and trace element analyses, and microprobe analyses of constituent mineral phases. The Mt. Fubilan Intrusion is inferred to have been similar, or identical, to the other intrusive bodies prior to the onset of hydrothermal alteration. The differences in composition and mineralogy that now exist were imposed by the hydrothermal alteration. Ore minerals that are localized in the Mt. Fubilan Intrusion, and in potassically-altered portions of the other intrusions, were deposited simultaneously with the conversion of masses of igneous rock from latitic (quartz monzodioritic)

composition to quartz-alkali feldspar trachyte (quartz-alkali feldspar syenite) composition.

Bibliography

Abers, Geoffrey, and McCaffrey, Robert, 1988, Active deformation in the New Guinea fold-and-thrust belt; seismological evidence for strike-slip faulting and basement-involved thrusting: Journal of Geophysical Research, B, Solid Earth and Planets. 93; 11, Pages 13,332-13,354.

Ahrens, L.H., 1954, The lognormal distribution of the elements: Geochimica et Cosmochimica Acta., v. 5, p. 49-73.

Ahrens, L.H.,, 1957, Lognormal-type distributions - III: Geochim. et Cosmochim. Acta., v. 11, p. 205-212.

Ahrens, L.H., 1965, Distribution of the Elements in Our Planet: McGraw-Hill Book Company, New York, 110 p.

Ague, Jay J., and Brandon, Mark T., 1996, Regional tilt of the Mount Stuart batholith, Washington, determined using aluminum-in-hornblende barometry: Geological Society of America Bulletin, v. 108, p. 471-488.

Ague, Jay J., 1997, Thermodynamic calculation of emplacement pressures for batholithic rocks, California: implications for the aluminum-in-hornblende barometer. Geology, v. 25, p. 563-566

Andersen, D.J., Lindsley, D.H., and Davidson, P.M., 1993, QUILF: a PASCAL program to assess equilibria among Fe-Mg-Mn-Ti oxides, pyroxenes, olivine, and quartz: Computers & Geosciences, v. 19, p. 1333-1350.

Anderson, G.M., and Burnham, C. W., 1983, Feldspar solubility and the transport of aluminum under metamorphic conditions: American Journal of Science, v. 283-A, p. 283-297.

Anderson, J Lawford 1996, Status of thermobarometry in granitic batholiths. Transactions of the Royal Society of Edinburgh: Earth Sciences, v. 87, p. 125-138.

Anderson, D.J., Lindsley, D. H., and Davidson, P. M., 1993, QUILF: A Pascal program to access equilibria among Fe-Mg-Mn-Ti oxides, pyroxenes, olivine, and quartz: Computers and Geosciences, v. 19, p. 1333-1350.

Anthony, Elizabeth Youngblood, 1983, The milieu of porphyry copper deposits: [in] The milieu of porphyry copper deposits, Boardman-Shelby-J [editor], Kendall/Hunt Publ. Co.. Dubuque, IA, United States, p. 317-325.

Arnold, G. O, and Fitzgerald, F., 1977, Igneous rock types and their alteration, Mt Fubilan porphyry copper deposit: Geological Survey of Papua New Guinea, Report 77/5, 10 p.

Arnold, G. O., and Griffin, T. ., 1978, Intrusions and porphyry copper prospects of the Star Mountains, Papua New Guinea: [in] Porphyry copper deposits of the southwestern Pacific islands and Australia: Gustafson, L. B., Titley-S-R (editors, Economic Geology and the Bulletin of the Society of Economic Geologists. v. 73, pages 785-795.

Arnold, G. O., Griffin, T. J., and Hodge, C. C., 1979, Geology of the Ok Tedi and southern Atbalmin 1:100000 sheet: Part 3 Igneous rocks and structure: Geological Survey Papua New Guinea, Report 79/3, 98 pages.

Ayers and Bamford, 1976, revised 1987, The Mt. Fubilan (Ok Tedi) porphyry copper deposit: geology, geochemistry and origin: unpublished manuscript.

Bain, J. H. C, 1973, A Summary of the main structural elements of Papua New Guinea: [in] The western Pacific; island arcs, marginal seas, geochemistry, pages 147-161.

Bamford and others, 1972, The Mt. Fubilan (Ok Tedi) porphyry copper deposit, Territory of Papua and New Guinea: Economic Geology, v. 67, p. 1019-1033.

Barr, D.A., Fox, P.E., Northcote, K.E., Preto, V.A., 1976, The alkaline suite porphyry deposits - a summary: CIM Special Volume 15, p. 359-367.

Barton, M., and Skinner, Brian J., 1979, Sulfide mineral stabilities: [in] Barnes, H.L. [ed.] Geochemistry of Hydrothermal Ore Deposits, John Wiley & Sons, New York, p. 278-403.

Baumgartner, L. P, and Olsen, S.N., 1995, A least-squares approach to mass transport calculations using the isocon method: Economic Geology, v. 90, p. 1261-1270.

Batchelor, R.A., and Bowden, Peter, 1985, Petrogenetic interpretation of granitoid rock series using multi-cationic parameters: Chemical Geology, v. 48, p. 43-55.

Bateman, Paul, C., Clark, Lorin, D., Huber, N. King, Moore, James, G, Rinehart, C. Dean, 1963, The Sierra Nevada Batholith; a synthesis of recent work across the central part.: U. S. Geological Survey Professional Paper 414, pages D1-D46.

Bingler, E.C., Trexler, D.T., Kemp, W.R., and Bonham, H. F., Jr., 1976, PETCAL, a BASIC language computer program for petrologic calculations: Nevada Bureau of Mines and Geology Report 28, 27 pages.

Boudreau, A. E., 1999, PELE - a version of the MELTS software program for the PC platform: Computers & Geosciences, v. 25, p. 201-203.

Bowers, T.S., Jackson, K. J., and Helgeson, H.C., 1984, Equilibrium activity diagrams: Springer-Verlag, New York, 397 p.

Brändle, J. L., Nagy, G., 1995, The state of the 5th version of IGBA; igneous petrological data base: Computers & Geosciences. 21; 3, . 425-432.

Buddington, A.F., and Lindsley, D.H., 1964, Iron-titanium oxide minerals and synthetic equivalents: Journal of Petrology, v. 5, pages 310-357.

Burnham, C. W., 1979, Magmas and hydrothermal fluids: [in] Barnes, H. L., [ed.] Geochemistry of Hydrothermal Ore Deposits: 2nd edition, John Wiley and Sons, New York, p. 71-136.

Burnham, C. W., 1981, Physicochemical constraints on porphyry mineralization: [in] W.R. Dickinson, W.R., and W.D. Payne [eds.], Relations of Tectonics to Ore Deposits in the Southern Cordillera: Arizona Geolical Society Digest, v. 14, p. 71-77.

Cassidy, K. F., Groves, D. I., and McNaughton, N.J., 1998, Late-Archaen granitoid-hosted lode-gold deposits, Yilgarn Craton, Western Australia: Deposit Characteristics, crustal architecture and implications for ore genesis: Ore Geology Reviews, v. 13, p. 65-102.

Coryell, C.G., Chase, J. W., and Winchester, J. W., 1963, A procedure for geochemical interpretation of terrestrial rare-earth abundance patterns: Journal of Geophysical Research, v. 68, p. 559-566.

Creasey, S.C. 1966, Hydrothermal alteration: [in] Titley, S. R. [ed.], Geology of the porphyry copper deposits of southwest North America; University of Arizona Press, Tucson, p. 51-

Davies, H.L. and Norvick, M., 1974, Blucher Range, Papua New Guinea: Australian Bureau Mineral Resources, Geology and Geophysics , 1:250, 000 Geologic Map Series, Explanatory Notes.

Dickenson, M., and Hess, C., 1986, The structural role and homogenous redox equilibria of iron in peraluminous, metaluminous and peralkaline silicate melts: Contributions to Mineralogy and Petrology. v. 92; pages 207-217. 1986.

Dilles, John H., 1987, Petrology of the Yerington Batholith, Nevada: Evidence for evolution of porphyry copper ore fluids: Economic Geology, v. 82, p. 1750-1789.

Dipple, GM; Wintsch, R P; Andrews, MS 1990, Identification of the scales of differential element mobility in a ductile fault zone. Journal of Metamorphic Geology, v. 8, p. 645-661.

Duncan, Ian, 1972, Skarn genesis at the Ok Tedi porphyry copper deposit and the stability relations of aluminous calc-silicates: Honors thesis, Macquarie University, Sydney, Australia, unpublished.

Ehmann, W. D, 1968, Encyclopedia of the Chemical Elements: Hampel, C. A. [ed.], Van Nostrand Reinhold, New York, p. 568-570.

Elkins, Linda T., Grove, Timothy L., 1990, Ternary feldspar experiments and thermodynamic models: American Mineralogist, v. 75, p. 544-559.

Ellis, A. J., and Mahon, W. A. J., 1977, Chemistry and Geothermal Systems: Academic Press, New York, 392 pages.

Emmons, W. J. 1927, Relations of the disseminated copper ores in porphyry to igneous intrusions: American Inst. Mining Metall. Engineers Transactions, v. 75, p. 797-815.

Evans, Anthony M 1993, Ore Geology and Industrial Minerals An Introduction: Third edition, Blackwell Scientific Publications, Boston, 389 pages.

Ewart, A., 1982, The mineralogy and petrology of Tertiary-Recent orogenic volcanic rocks: with special reference to the andesitic-basaltic compositional range: [in] Andesites, Thorpe, R. S. [ed.], John Wiley & Sons, New York, p. 25-95.

Field, C. W., 1966, Sulfur isotope abundance data, Bingham District, Utah: Economic Geology, v. 61, p. 850-871.

Field, C. W., and Gustafson, L. B., 1976, Sulfur isotopes in the porphyry copper deposit at El Salvador, Chile: Economic Geology, v. 71, p. 1533-1548.

Field, C. W., McCulla, M.S., Wangu, Adam, and Doucette, J.D., 1999, unpublished sulfur isotope data for the Ok Tedi deposit, Papua New Guinea.

Fookes, Peter G.; Dale, Simon G.; Land, J. M., 1991, Some observations on a comparative aerial photography interpretation of a landslipped area: Quarterly Journal of Engineering Geology 24, p. 249-265.

Fuhrman, Miriam L; Lindsley, Donald H 1988, Ternary-feldspar modeling and thermometry. American Mineralogist 73, p. 201-215.

Garrels, Robert M., and Christ, Charles L., 1965, Solutions, minerals, and equilibria: Freeman, Cooper & Company, San Francisco, 450 pages.

Ghiorso, Mark S 1984, Activity/composition relations in the ternary feldspars. Contrib. Mineral. Petrol., v. 87, p. 282-296.

Goode, A. D. T., and Gilbert, D. J., 1976, Some petrographic observations, Ok Tedi porphyry copper deposit, Papua New Guinea: Broken Hill Proprietary Petrographic Division Report Number MRL-164.

Grant, J. A., 1986, The isocon diagram - a simple solution to Gresens' equation for metasomatic alteration: Economic Geology, v. 81, p. 1976-1982.

Gresens, R. L., 1967, Composition-volume relationships of metasomatism: Chemical Geology, v. 2, p. 47-65.

Griffin, T. J., 1983, Granitoids of the Tertiary continent; island arc collision zone, Papua New Guinea: [in] Circum-Pacific plutonic terranes: Roddick, J. A., Geological Society of America Memoir 159, p. 61-76.

Guidotti, C.V., 1984, Micas in metamorphic rocks: [in] Micas: Bailey, S. W. [ed], Reviews in Mineralogy, 13, p. 357-467.

Gustafson, L. B. and Hunt, J. P, 1975, The porphyry copper deposit at El Salvador, Chile: Economic Geology, v. 70, p. 859-912.

Hall, Anthony, 1996, Igneous Petrology: second edition, Harlow, England, 551 pages.

Hammarstrom, J. M., and Zen, E-an, 1986, Aluminum in hornblende: an empirical igneous geobarometer: Amer. Mineralogist, v. 71, p. 1297-1313.

Harayama, Satoru, 1992, Youngest exposed granitoid pluton on Earth: cooling and rapid uplift of the Pliocene-Quaternary Takidani granodiorite in the Japan Alps, central Japan. Geology, v. 20, p. 657-660.

Harker-Alfred, 1900, Igneous rock series and mixed igneous rocks: Journal of Geology, p. 389-399.

Harker, Alfred, 1909, The natural history of igneous rocks: Macmillan, New York, 384 pages.

Hearn, G. J., 1995, Landslide and erosion hazard mapping at Ok Tedi copper mine, Papua New Guinea: The Quarterly Journal of Engineering Geology, v. 28, p. 47-90.

Helgeson, H. C., 1974, Chemical interaction of feldspars and aqueous solutions: in The Feldspars, W. S. MacKenzie and J. Zussman, eds., Manchester: Manchester University Press, p. 184-215.

Hemley, Julian, Meyer, Charles, and Richter, D.H., 1961, Some alteration reactions in the system Na2O-Al2O3-SiO2-H2O: U.S. Geological Survey Professional Paper 424-D, p. 338-340.

Henderson, Paul, 1984, General geochemical properties and abundances of the rare earth elements: [in] Rare earth element geochemistry: Henderson-Paul

(editor). Developments in geochemistry: Elsevier Sci. Publ. Co.. Amsterdam, Netherlands, p. 1-32,

Hill, K.C. 1989, The Muller Anticline, Papua New Guinea; basement-cored, inverted extensional fault structures with opposite vergence: Tectonophysics, v. 158, p. 227-245.

Hollister, L. S., Grissom, G. C., Peters, E. K., Stowell, H. H., and Sisson, V. B., 1987, Confirmation of the empirical correlation of Al in hornblende with pressure of solidification of calc-alkaline plutons: American Mineralogist, v. 72, p. 231-239.

Holtz, François, and Johannes, Wilhelm, 1994, Maximum and minimum water contents of granitic melts: implications for chemical and physical properties of ascending magmas: Lithos, v. 32, p. 149-159.

Irvine, T. N., and Baragar, W. R. A., 1971, A guide to the chemical classification of the common volcanic rocks: Canadian Journal Earth Science, v. 8, p. 523-548.

Jacques, A. L., and Robinson, G. P, 1977, The continent/island-arc collision in northern Papua New Guinea: BMR Journal of Australian Geology and Geophysics, v. 2, p. 289-303.

Johannsen, A., 1931, A descriptive petrography of the igneous rocks: University of Chicago Press, 4 v.

Johnson, M. C., and Rutherford, M. J., 1989, Experimental calibration of the aluminum-in-hornblende geobarometer with application to Long Valley Caldera (California) volcanic rocks: Geology, v. 17, p. 837-841.

Johnson, R.W., 1982, Papua New Guinea: [in] Andesites; Orogenic Andesites and Related Rocks: Thorpe, R.S. [ed.], John Wiley & Sons. Chichester, United Kingdom, p. 225-244.

Kalsbeek, Feiko, 1992, Large-scale albitization of siltstones on Qeqertakavsak island, northeast Disko Bugt, west Greenland: Chemical Geology, v. 95, p. 213-233.

Katchan, George, 1982, Mineralogy and geochemistry of the Ertsberg (Gunung Bijih) and Ertsberg East (Gunung Bijih Timur) skarns, Irian Jaya Indonesia

and the Ok Tedi skarn, Papua New Guinea: Ph.D. dissertation, University of Sydney.

Keith, S.B., Laux, D., Pages, Maughan, Gerald, Schwab, Karen, Ruff, Steven, Swan, M.M., Abbott, E. W., Friberg, Steve and others, 1991, Magma series and metallogeny; a case study from Nevada and environs: [in] Geology and ore deposits of the Great Basin; field trip guidebook compendium, Buffa, R.H., and Conyer, A.R. [eds.], Geological Society of Nevada. Reno, NV, p. 404-493.

Kretz, Ralph, 1982, Transfer and exchange equilibria in a portion of the pyroxene quadrilateral as deduced from natural and experimental data: Geochimica et Cosmochimica Acta, v. 46, p 411 to 421.

Lameyre, Jean, Bowden, Peter, 1982, Plutonic rock types series; discrimination of various granitoid series and related rocks: Journal of Volcanology and Geothermal Research, v. 14; p. 169-186.

Lang, J. R., Stanley, C.R., and Thompson, J. F. H., 1995, Porphyry copper-gold deposits related to alkalic igneous rocks in the Triassic-Jurassic arc terranes of British Columbia: [in] Pierce, Francis Wahl, and Bohm, John G., [eds.] Porphyry Copper Deposits of the North American Cordillera, Arizona Geological Society, Arizona, p. 219-236.

Lanier, George, Raab, W. J., Folsom, R. B., and Cone, S., 1978, Alteration of equigranular monzonite, Bingham mining district, Utah: Economic Geology, v. 73, p. 1270-1286.

Le Bas, M. J., Le Maitre, R. W., Streckeisen, A., and Zanettin, B., 1986, A chemical classification of volcanic rocks based on the total alkali-silica diagram: Journal Petrology, v. 27, p. 745-750.

Le Maitre, R.W., 1976, Some problems of the projection of chemical data into mineralogical classifications: Contrib. Mineral. Petrol., v. 56, p. 181-189.

Le Maitre, R. W.; Bateman, P.; Dudek, A.; Keller, J.; Lameyre, J.; Le Bas ,M. J.; Sabine ,P. A; Schmid, R.; Sorensen, H.; Streckeisen, A.; Woolley, A.R.; Zanettin, B. (eds.), 1989, A Classification of Igneous Rocks and Glossary of Terms. Blackwell Scientific Publications, Boston. 193 p..

Leake, B.E., 1978, Nomenclature of amphiboles: Amer. Mineralogist, v. 63, p. 1023-1052.

Lepeltier, Claude, 1969, A simplified statistical treatment of geochemical data by graphical representation: Economic Geology, v. 64, p. 538-550.

Lindgren, Waldemar, 1918, Volume changes in metamorphism: Journal of Geology, v. 26, p. 542-554.

Lindgren, Waldemar, 1924, Contact metamorphism at Bingham, Utah: Bulletin of the Geological Society of America, v. 35, p. 507-534.

Lindgren, Waldemar, 1933, Mineral deposits: New York and London, McGraw-Hill book company, 930 p.

Lloyd, Alan, 1987, Ok Tedi starts up copper concentrator and new gold plant: Engineering & Mining Journal, p. 48-53.

Lowell, J.D., and Guilbert, J. M., 1970, Lateral and vertical alteration mineralization zoning in porphyry ore deposits: Economic Geology, v. 65, p. 373-408.

Mackin, J. H., 1968, Iron ore deposits of the Iron Springs District, southwestern Utah: [in] Ore deposits of the United States, 1933-1967 (Graton-Sales Volume), v. 2, p. 992-1019.

Marshall, Brian, and Mancini, Franco, 1994, Major and minor-element mobilization, with implications for Ni-Cu-Fe-sulphide re-mobilization during retrograde metasomatism at the Vammala Mine, southwest Finland: Chemical Geology, v. 116, p. 203-227.

Mason, Douglas R., 1975, Subdivision and geochemistry of Tertiary intrusive complexes from part of the New Guinea mobile belt: Australian Society of Exploration Geophysicists. v. 6; First Southwest Pacific workshop-symposium, p. 69-70.

Mason, Douglas R., and McDonald, J. A., 1978, Intrusive rocks and porphyry copper occurrences of the Papua New Guinea-Solomon Islands region; a reconnaissance study: [in]: Porphyry copper deposits of the southwestern Pacific islands and Australia, Gustafson, L. B., and Titley, S. R. [eds.]

Economic Geology and the Bulletin of the Society of Economic Geologists, v. 73, p. 857-877.

Mason, Douglas R., 1993a, Petrographic Studies of a Suite of Twenty Five Rock Samples From The Ok Tedi Mine, Papua New Guinea: Amdel Laboratories, Australia, Report G698300GI93.

Mason, Douglas R., 1993b, Petrological Studies of Seven Drill Core Rock Samples Ok Tedi Mine, Papua New Guinea Part II: Whole-rock Analyses and Mineral Analyses (Including Some Pit Samples, Amdel Laboratories, Australia, Report G807000G/94.

Mason, Douglas R., 1993c, Petrological Studies of a Suite of Rock Samples From The Ok Tedi Mine, Papua New Guinea Part II - Biotite Analyses And Clay Identifications: Amdel Laboratories, Report G69230OG/93.

Masuda, A., 1962, Regularities in variation of relative abundances of lanthanide elements and an attempt to analyze separation-index patterns of some minerals: Journal Earth Science, Nagoya University, v. 10, 173-187.

Meyer, C. and Hemley, J. J., 1967, Wall rock alteration: in Geochemistry of Hydrothermal Ore Deposits, H. L. Barnes, [ed]., New York: Holt, Rinehart, and Winston, p. 166-235.

Middlemost, E. A. K., 1989, Iron oxidation ratios, norms and the classification of volcanic rocks: Chemical Geology, v. 77, ages 19-26.

Middlemost, Eric, A. K., 1994, Naming materials in the magma/igneous rock system: Earth Science Reviews, v. 37, p. 215-224.

Montoya, J. W., and Hemley, J. J., 1975, Activity relations and stabilities in alkali feldspar and mica alteration reactions: Economic Geology, v. 70, p. 577-594.

Morimoto, Nobuo; Fabries, J.; Ferguson, A. K.; Ginzburg, I. V.; Ross, M.; Seifert, F.A.; Zussman, J.; Aoki, K.; Gottardi, G., 1988, Nomenclature of pyroxenes: American Mineralogist 73, 1123-1133.

Mueller, Daniel, and Groves, David I., 1995, Potassic Igneous Rocks and Associated Copper-Gold Mineralization: Springer-Verlag, Berlin.

Nakamura, Noboru, 1974, Determination of REE, Ba, Fe, Mg, Na and K in carbonaceous and ordinary chondrites: Geochimica et Cosmochimica Acta. 38, p. 757-775.

Naney, M.T., 1983, Phase relations of rock-forming ferromagnesian silicates in granitic melts: American Journal of Science, v. 283, p. 993-1033.

Nash, J. Thomas, 1976, Fluid-inclusion petrology — data from porphyry copper deposits and applications to exploration: U.S. Geological Survey, Professional Paper 907-D, p. D1-D16.

Nedachi, Munetomo, 1992, Composition of fluids related to Ok Tedi Mineralization, Papua New Guinea: Report Geological Survey of Japan, v. 279, p. 127-130.

Nockolds, S. R., 1947, The relation between chemical composition and paragenesis in the biotite micas of igneous rocks: American Journal of Science 245, 401-420.

Nordstrom, Darrell Kirk, and Munoz, James L., 1994, Geochemical thermodynamics: Blackwell Scientific Publications, Boston, 493 pages.

Olsen, S. N.; Grant, JA 1991, Isocon analysis of migmatization in the Front Range, Colorado, USA. Journal of Metamorphic Geology 9, 151-164

Ohmoto, Hiroshi, and Rye, R. O., 1979, Isotopes of sulfur and carbon, in Barnes, H.L., ed., Geochemistry of hydrothermal ore deposits (2d ed., New York, John Wiley & Sons, p. 509-567.

Page, R.W., and McDougall, Ian, 1972, Ages of Mineralization of Gold and Porphyry Copper Deposits in the New Guinea Highlands: [in] An Issue on Australia and Adjacent Islands: Economic Geology, v. 67, p. 1034-1048.

Page, R.W., 1975, Geochronology of late Tertiary and Quaternary mineralized intrusive porphyries in the Star Mountains of Papua New Guinea and Irian Jaya: Economic Geology, v. 70, p. 928-936.

Pe-Piper, Georgia, 1984, Zoned pyroxenes from shoshonite lavas of Lesbos, Greece; inferences concerning shoshonite petrogenesis: Journal of Petrology, v. 25, p. 453-472.

Peacock, M.A., 1931, Classification of igneous rock series: Journal of Geology, v. 39, p. 54-67.

Pigram, C.J., and Davies, H.L., 1987, Terranes and the accretion history of the New Guinea orogen: BMR Journal of Australian Geology and Geophysics. 10, p. 193-211.

Potdevin, J. L., 1993, Gresens 92: A simple Macintosh program of the Gresens method: Computers & Geosciences, v. 19, p. 1229-1238.

Powell, J. W., 1891, The eruptive rocks of Electric Peak and Sepulchre Mountain, Yellowstone National Park: Twelfth Annual Report of the United States Geological Survey, Part I - Geology, p. 577-590.

Ragland, Paul, 1989, Basic Analytical Petrology: Oxford University Press, New York, 384 pages.

Richard, Linda R; Clarke, D. B, 1990, AMPHIBOL: A program for calculating structural formulae and for classifying and plotting chemical analyses of amphiboles. American Mineralogist 75, p. 421-423.

Rittman, 1973, Stable mineral assemblages of igneous rocks: Springer Verlag, New York, 262 pages.

Robie, Richard A., Hemingway, Bruce S., and Fisher, James R., 1978, 1979 [revised], Thermodynamic properties of minerals and related substances at 2918.15K and 1 bar (10^5 Pascals) pressure and at higher temperatures: United States Geological Survey Bulletin 1452, 456 pages.

Roedder, Edwin, 1971, Fluid inclusion studies on the porphyry-type ore deposits at Bingham, Utah, Butte, Montana, and Climax, Colorado: Economic Geology, v. 66, p. 98-120.

Rose, A.W., 1970, Zonal relations of wallrock alteration and sulfide distribution at porphyry copper deposits: Economic Geology, v. 63, p. 920-936.

Rubie, David C 1982, Mass transfer and volume change during alkali metasomatism at Kisingiri, Western Kenya. Lithos 15, 99-109.

Rubin, Jeffrey, Henry, Christopher D., and Price, Jonathan G., 1993, The mobility of zirconium and other "immobile" elements during hydrothermal alteration: Chemical Geology, v. 110, p. 29-47.

Rush, P. M., and Seegers, H. J., 1990, Ok Tedi copper-gold deposits of Papua New Guinea, [in] Hughes, F. E [ed], Geology of the Mineral Deposits of Papua New Guinea, Australasian Institute of Mining and Metallurgy Monograph 14, v. 2, p. 1747-1754.

Sack, R. O., and Carmichael, I. S. E., 1980, Ferric-ferrous equilibrium in silicate liquids at 1 bar: Eos, Transactions, American Geophysical Union, v. 61, page 1152.

Schmidt, Max W, 1992, Amphibole composition in tonalite as a function of pressure: an experimental calibration of the Al-in-hornblende barometer. Contributions to Mineralogy and Petrology, v. 110, 304-310.

Shand, S. J., 1943, Eruptive rocks: their genesis, composition, classification, and their relation to ore deposits, with a chapter on meteorites: London, T. Murby, New York, J. Wiley, 488 pages.

Sillitoe, R.H., 1997, Characteristics and controls of the largest porphyry copper-gold and epithermal gold deposits in the circum-Pacific region: Australian Journal of Earth Sciences, v. 44, p. 373-388.

Sinclair, A. J., 1976, Applications of probability graphs in mineral exploration: Association of Exploration Geochemists, Special Volume No. 4, Richmond, B.C., Canada, 95 p.

Speer, J. A, .1984, Micas in igneous rocks: [in] Micas, Bailey, S. W. [ed.], Reviews in Mineralogy, Mineralogical Society of America, p.. 299-356.

Streckeisen, A., 1976, To each plutonic rock its proper name: Earth-Science Reviews. 12; 1, p. 1-33. 1976.

Streckeisen, A, 1976, Classification of the common igneous rocks by means of their chemical composition; a provisional attempt: Neues Jahrbuch fuer Mineralogie. Monatshefte. 1, p. 1-15. 1976.

Streckeisen, A., and Le Maitre, R.W., 1979, A chemical approximation to the modal QAPF classification of the igneous rocks: Neues Jahrbuch fuer Mineralogie. Abhandlungen. 136; 2, P. 169-206.

Sun, Shen Su, 1982, Chemical composition and origin of the Earth's primitive mantle: Geochimica et Cosmochimica Acta, vol.46, pp.179-192.

Taylor, S. R., and Gorton, M. P., 1977, Geochemical application of spark source mass spectrography - III. Element sensitivity, precision and accuracy: Geochimica et Cosmochimica Acta, v. 41, p. 1375-1380.

Taylor, S. R., and McLennan, S. M., 1985, The Continental Crust: Its Composition and Evolution: Blackwell, Oxford, 312 pages.

Tennant, C.B., and White, M.L., 1959, study of the distribution of some geochemical data: Economic Geology, v. 54, p. 1281-1290.

Titley, S. R., 1982, The style and progress of mineralization and alteration in porphyry copper systems; American southwest: [in] Advances in geology of porphyry copper deposits; southwest North America: Titley, S. R. [ed], University of Arizona Press, Tucson, Arizona, p. 93-116.

Tyrrell, G. W., 1926, The Principles of Petrology: Methuen & Co., Ltd., London, 349 pages.

Vance, J. A., 1969, On synneusis: Contributions to Mineralogy and Petrology, v 24, p. 7-29.

Vogt, Johan Herman Lie, 1921, The physical chemistry of the crystallization and magmatic differentiation of igneous rocks: Journal of Geology. 29, v. 4, p. 318-350.

Washington, Henry Stephens, 1918, A description of the quantitative classification of igneous rocks, with tables for the calculation of the norm: U. S. Geological Survey Professional Paper, p. 1-7..

Wen, Shaoxiong; Nekvasil, Hanna, 1994, Ideal associated solutions: application to the system albite-quartz-H_2O. American Mineralogist 79, 316-331.

Williams, Howell, Turner, F. J., and Gilbert, C.M., 1982, Petrography: an introduction to the study of rocks in thin sections: second edition, W. H. Freeman, New York, 626 pages.

Williams, S. A., and Forrester, J. D., 1995, Characteristics of porphyry copper deposits: [in] Pierce, F. W., and Bolm, J. G., [eds.} Porphyry copper deposits of the American Cordillera, Arizona Geological Society Digest, v. 20, p. 21-34.

Wones, D. R., 1989, Significance of the assemblage titanite+magnetite+quartz: American Mineralogist, v. 74, p. 744-749.

Yegorov, D. G, Korobeinikov, A.N.,and Dubrovskii, M. I., 1998, CHEMPET; calculation for the chemical systematics of igneous rocks based on the CIPW norm: Computers & Geosciences. 24; 1, p. 1-5.

Zanettin, B., 1984. Proposed new chemical classification of volcanic rocks. Episodes, v. 7, p. 19-20.

Zeck, H.P., Ottensen, C., and Toft, J., 1988, Volume effect of a gabbro-amphibole transition: Chemical Geology 67, 141-153.

Zhang, Lihua, Field, C. W., Dilles, J. H., and Reed, M. H., 1999, Sulfur isotope record of deep porphyry Cu-Mo mineralization, Butte District, Montana [abs.]: Geological Society of America Abstracts with Programs, v. 31, no. 7, p. A381-382.